VILNIUS GEDIMINAS TECHNICAL UNIVERSITY

Lina KISEŽAUSKIENĖ

EXPLORING THE POSSIBILITY TO ASSESS AND REDUCE THE RISK DUE TO HAZARDOUS MATERIALS TRANSPORTATION BY DEPLOYING ROADSIDE SAFETY BARRIERS

DOCTORAL DISSERTATION

TECHNOLOGICAL SCIENCES,
CIVIL ENGINEERING (02T)

Vilnius TECHNIKA 2014

Doctoral dissertation was prepared at Vilnius Gediminas Technical University in 2010–2014.

Supervisor

Prof Dr Egidijus Rytas VAIDOGAS (Vilnius Gediminas Technical University, Civil Engineering – 02T).

The Dissertation Defense Council of Scientific Field of Civil Engineering of Vilnius Gediminas Technical University:

Chairman

Prof Dr Donatas ČYGAS (Vilnius Gediminas Technical University, Civil Engineering – 02T).

Members:

Prof Dr Habil Juozas ATKOČIŪNAS (Vilnius Gediminas Technical University, Civil Engineering – 02T),

Dr Raimondas BLIŪDŽIUS (Kaunas University of Technology, Civil Engineering – 02T),

Prof Dr Juris SMIRNOVS (Riga Technical University, Civil Engineering – 02T),

Prof Dr Zenonas TURSKIS (Vilnius Gediminas Technical University, Civil Engineering – 02T).

The dissertation will be defended at the public meeting of the Dissertation Defense Council of Civil Engineering in the Senate Hall of Vilnius Gediminas Technical University at **2 p. m. on 11 December 2014**.

Address: Saulėtekio al. 11, LT-10223 Vilnius, Lithuania.
Tel.: +370 5 274 4956; fax +370 5 270 0112; e-mail: doktor@vgtu.lt

A notification on the intend defending of the dissertation was send on 10 November 2014.

A copy of the doctoral dissertation is available for review at the Internet website http://dspace.vgtu.lt/ and at the Library of Vilnius Gediminas Technical University (Saulėtekio al. 14, LT-10223 Vilnius, Lithuania).

VILNIAUS GEDIMINO TECHNIKOS UNIVERSITETAS

Lina KISEŽAUSKIENĖ

TRANSPORTUOJAMŲ PAVOJINGŲJŲ MEDŽIAGŲ KELIAMOS RIZIKOS TYRIMAS IR MAŽINIMAS ĮRENGIANT SAUGOS BARJERUS

MOKSLO DAKTARO DISERTACIJA

TECHNOLOGIJOS MOKSLAI,
STATYBOS INŽINERIJA (02T)

Disertacija rengta 2010–2014 metais Vilniaus Gedimino technikos universitete.

Vadovas

prof. dr. Egidijus Rytas VAIDOGAS (Vilniaus Gedimino technikos universitetas, statybos inžinerija – 02T).

Vilniaus Gedimino technikos universiteto Statybos inžinerijos mokslo krypties disertacijos gynimo taryba:

Pirmininkas

prof. dr. Donatas ČYGAS (Vilniaus Gedimino technikos universitetas, statybos inžinerija – 02T).

Nariai:

prof. habil. dr. Juozas ATKOČIŪNAS (Vilnaus Gedimino technikos universitetas, statybos inžinerija – 02T),
dr. Raimondas BLIŪDŽIUS (Kauno technologijos universitetas, statybos inžinerija – 02T),
prof. dr. Juris SMIRNOVS (Rygos technikos universitetas, statybos inžinerija – 02T),
prof. dr. Zenonas TURSKIS (Vilniaus Gedimino technikos universitetas, statybos inžinerija – 02T).

Disertacija bus ginama viešame Statybos inžinerijos mokslo krypties disertacijos gynimo tarybos posėdyje **2014 m. gruodžio 11 d. 14 val.** Vilniaus Gedimino technikos universiteto senato posėdžių salėje.

Adresas: Saulėtekio al. 11, LT-10223 Vilnius, Lietuva.
Tel.: (8 5) 274 4956; faksas (8 5) 270 0112; el. paštas doktor@vgtu.lt

Pranešimai apie numatomą ginti disertaciją išsiųsti 2014 m. lapkričio 10 d.

Disertaciją galima peržiūrėti interneto svetainėje http://dspace.vgtu.lt/ ir Vilniaus Gedimino technikos universiteto bibliotekoje (Saulėtekio al. 14, LT-10223 Vilnius, Lietuva).

Abstract

The dissertation presents an approach to decreasing the risk of transportation of hazardous materials (hazmat transportation) by applying construction-related solutions. They consist in deploying safety barriers between transportation routes and vulnerable property built in the roadside territory. The attention is focussed on the hazmat transportation accidents known as boiling liquid expanding vapour explosions (BLEVEs). It is considered how to predict thermal and mechanical effects of BLEVEs on potential barriers or roadside property. It is suggested to interlink results of this prediction with the conventional structural response techniques used for estimating the susceptibility of safety barriers to the effects of BLEVEs. The dissertation consists of introduction, three chapters, conclusions, list of references and papers published by the author as well as four annexes.

The first chapter presents a review and evaluation of the published work on the risk posed by the hazmat transportation. In addition, existing approaches to the design of safety barriers suitable to protect roadside property against fires and explosions on road and rail are discussed.

In the second chapter, BLEVEs are recognised as relatively frequent and highly damaging accidents on road and rail. The attention is focussed on predicting two main effects by BLEVE: thermal radiation and projectile impact. Three computational procedures are proposed for assessing thermal and mechanical effects generated of BLEVEs. The first procedure was developed to predict the position of road tanker vessel sustaining a BLEVE with respect to a potential target. The second procedure deals with assessing the thermal radiation of a BLEVE fireball. The third procedure was developed for forecasting the impact of road tanker vessel fragments on roadside object or possible safety barrier.

The third chapter formulates a series of proposals to the design of safety barriers aimed at protection of roadside objects against thermal and mechanical effects of BLEVEs on road and rail. The first proposal considers the sitting of barriers in the area of potential deployment. The second proposal deals with a design of a steel barrier intended for a protection of blast loading from a railway tanker BLEVE. The third proposal consists in recommendations of how to design a reinforced concrete barrier capable to sustain impact by fragments from a tanker vessel. All proposals have the form of preliminary, conceptual designs.

The main statements of the dissertation were published in twelve scientific articles: four articles – in the Thomson ISI Web of Science register.

Reziumė

Disertacijoje pateikiamas originalus būdas mažinti pavojingųjų medžiagų vežimo riziką taikant statybinio pobūdžio priemones. Tos priemonės – saugos barjerai, kurie yra statomi tarp transporto linijų ir pažeidžiamų pakelės objektų. Didžiausias dėmesys telkiamas į transporto avarijas, kurios vadinamos besiplečiančių verdančio skysčio garų sprogimais (BLEVE) (angl. boiling liquid expanding vapour explosions). Nagrinėjama, kaip prognozuoti šiluminius ir mechaninius tokių sprogimų poveikius. Jie gali pažeisti pakelėse esančius statinius ir juos turi sumažinti saugos barjerai. BLEVE poveikių prognozavimą siūloma susieti su konstrukcijų skaičiavimo metodais, kuriais vertinama barjerų reakcija į šiuos poveikius. Disertaciją sudaro įvadas, trys skyriai, išvados, literatūros šaltiniai, autorės publikacijų sąrašas ir keturi priedai.

Pirmajame skyriuje apžvelgiama mokslinė literatūra, kurioje nagrinėjama, kaip vertinti pavojingųjų medžiagų vežimo riziką. Tai pat nagrinėjami iki šiol sukurti saugos barjerų projektavimo metodai. Vertinamas tų barjerų tinkamumas apsaugoti pažeidžiamus pakelės objektus.

Antrajame disertacijos skyriuje sprendžiama BLEVE poveikių prognozavimo problema. Nustatyta, kad BLEVE sprogimai yra santykinai dažnos avarijos, vykstančios transportuojant pavojingąsias medžiagas. Dėmesys telkiamas į tokių sprogimų sukeliamų cisternos skeveldrų smūgių ir šiluminės spinduliuotės vertinimą. Siūloma procedūra, skirta prognozuoti sprogimą patiriančios cisternos padėtį pažeidžiamo pakelės objekto atžvilgiu. Taip pat siūlomos procedūros, kurių pagalba galima vertinti pakelės objektą ir (arba) saugos barjerą veiksiančius cisternos skeveldrų smūgius ir šiluminę spinduliuotę.

Trečiajame skyriuje pateikiami siūlymai, kaip projektuoti barjerus, kurie gali apsaugoti pakelės objektus nuo terminio ir mechaninio BLEVE sprogimų poveikio. Siūloma, kaip išdėstyti barjerus galimoje jų statybos vietoje. Taip pat siūloma, kaip projektuoti plieninį barjerą, galintį apsaugoti nuo sprogimo bangos, sukeliamos BLEVE būdu sprogstančios geležinkelio cisternos. Pateiktos rekomendacijos, kaip projektuoti gelžbetoninį barjerą, kuris turėtų atlaikyti cisternos skeveldrų smūgius. Barjerų projektavimo siūlymai turi išankstinių, techninių projektų pavidalą.

Darbo rezultatai publikuoti dvylikoje mokslo straipsnių, iš kurių keturi išspausdinti mokslo žurnaluose, įtrauktuose į *Thomson ISI Web of Science* duomenų bazę.

Notations

Symbols

Latin

A	–	random event of a road accident;
B	–	random event of BLEVE;
D	–	specific random damage event;
D_M	–	mechanical damage;
D_T	–	thermal damage;
E_k	–	kinetic energy of generated fragment;
$E(x)$	–	emissive power of a fireball surface;
$f(.)$	–	probability density function;
$f_{NU}(.)$	–	non-uniform density probability density function;
$f_{Uk}(.)$		uniform density probability density function;
$F(.)$	–	distribution function;
$F^{-1}(.)$	–	inverse distribution function;
$F_r(.)$	–	frequency;
h_{arv}	–	height of an impact point;
I	–	impact point;
l_{cvl}	–	length of the undamaged cylindrical part of the vessel;
l_k	–	length of the zone k;
$m_{e\text{-}c}$	–	mass of end-cap;
$m_{cyl,\,1}$	–	linear mass of the cylinder;
O	–	the origin point position;
$P(A \mid T)$	–	the conditional probability of traffic accident (event A);
$P(D \mid B)$	–	the conditional damage probability;
$P(D \mid B, \varDelta)$	–	the damage probability for different values of $\varDelta$;
P_{max}	–	peak overpressure;
p_k	–	probability weights;
R	–	the radius of fireball;
v_{arv}	–	arrival (impact) velocity;
v_{dep}	–	departure velocity;
$\boldsymbol{x}$	–	vector characteristic of BLEVE accident;
x_1	–	coordinate of tank centre across the road;
x_2	–	coordinate of tank centre along the road;
x_3	–	angle of the tank axis in relation to the road axis;

y_1	–	transverse rest position of the tank centre;
y_2	–	departure angle;
y_3	–	longitudinal rest position;

Greek

Δ	–	the distance from the explosion to a target; safety distance;
ξ_{cyl}	–	the length of the cylindrical part between the end-cap and circumferential crack;
$\xi_{cyl,\,j}$	–	value of the cylindrical part between the end-cap and circumferential crack sampled from a uniform distribution over the interval $]0, \xi_{cyl}[$;
ξ_{frg}	–	the random mass of fragment;
ξ_{front}	–	the length of the cylindrical part of the oblong end-cap;
$\xi_{front,j}$	–	the value of length of the oblong end-cap which will be ejected towards the line b_1–b_5;
ξ_{uni}	–	the uniformly distributed random crack position;
π	–	traveling frequency;
ς_{ground}	–	the inclination angle;
ς_{inc}	–	incidence angle;
ς_1	–	horizontal departure angle;
ς_2	–	vertical departure angle;
$\tau_a(x)$	–	the atmospheric transitivity;
$\boldsymbol{\psi}(.)$	–	vector-function;
$\varphi(.)$	–	the probability density function of the transverse rest position;
φ	–	ricochet angle;
$\boldsymbol{\Omega}$	–	unsafe distance around the target object.

Abbreviations

BLEVE	–	boiling liquid expanding vapour explosion;
CL	–	centreline;
FE	–	finite element;
hazmat	–	hazardous material;
HMIRS	–	hazardous materials incident reporting system;
LG	–	liquefied gas;
LNG	–	liquefied natural gas;
LPG	–	liquefied petroleum gas;
p.d.f.	–	probability density function;
QRA	–	quantitative risk assessment;
SC	–	sacrificial cladding;
SRA	–	structural reliability analysis;
TNO	–	the abbreviated name of a Dutch organisation for applied scientific research, in Dutch "Toegepast Natuurwetenschappelijk Onderzoek";
TRA	–	transportation risk assessment;
VCE	–	vapour cloud explosion;
VRS	–	vehicle restraint system.

Contents

Introduction

Problem formulation

The work considers in the broad sense the phenomenon of accidents during the transportation of hazardous materials or, in brief, hazmat transportation. These accidents are toxic releases from and explosions and fires of goods shipped by trucks and trains. Such accidents are well known for their severity and major losses which sometimes involve the loss of human lives. Losses caused by accidents during hazmat transportation on road and rail involve also thermal and/or mechanical damage to the property built in the vicinity of transportation routes.

The present work is devoted to protection of the built roadside property against fires and explosions on road and rail. The protection is achieved by a deployment of safety barriers between transportation routes and vulnerable roadside property. The key problems of design of such barriers are uncertainties related to thermal and mechanical effects induced by fires and explosions on road and rail and configuration of safety barriers by taking into account these uncertainties.

Relevance of the thesis

The relevance of this work consists in the burning actuality of severe accidents which occur during the hazmat transportation. Despite the progress in the field of transportation safety, accidents involving fires and explosions of goods shipped by trucks and trains are still everyday phenomenon on the world-wide scale and almost monthly phenomenon on the nationwide scale of large coun-

tries. Some accidents occurred in congested urban and industrial areas and were particularly severe. They are known even to the general public. History of severe hazmat transportation accidents includes, among others, explosions of railway tankers in Vioreggio (Italy, 2009) and Bialystok (Poland, 2010), explosions of road tankers in Spain in 1978, 2002, 2011. A protection of people, property and environment against such accidents remains the problem of great concern.

Research object

The object of research is assessment and minimisation of the risk posed by fires and explosions on road and rail to built roadside property. The research is focused on a minimisation of this risk by deploying safety barriers between transportation routes and vulnerable roadside property.

Aim of the thesis

The aim of this work is to prepare proposals for sitting and design of barriers aimed at protection of built roadside property against fires and explosions on road and rail. These proposals include recommendations for predicting effects of fires and explosions as well as recommendations for preliminary, conceptual design of safety barriers.

Objectives of the thesis

1. To determine hazmat transportation accidents which can cause the greatest damage to built roadside objects.
2. To investigate road traffic accidents with the aim of predicting potential positions of road tanker explosions and effects of these explosions on roadside objects.
3. To investigate, how to estimate thermal effect of road tanker explosions on roadside objects with respect to uncertainties related to this effect.
4. To develop a procedure suitable to a quantitative risk assessment (QRA) and allowing to predict impacts of fragments resulting from bursting of a road tanker vessel on a potential safety barrier.
5. To explore sitting and layout of safety barriers to be deployed alongside traffic routes.
6. To give provisions for the design of a safety barrier with sacrificial cladding (SC) used to resist blast loading generated by an explosion of a railway tanker vessel.
7. To give provisions for the design of a safety barrier made of reinforced concrete segments. The barrier must be aimed at protecting vulnerable

roadside property against an impact of fragments generated by an explosion of a tanker vessel.

Research methodology

The research methodology was formed by a combination of methods developed and widely used in the fields of QRA, statistics and data processing, stochastic simulation and structural reliability analysis (SRA). The methodological core of the research was quantification and propagation of uncertainties related to effects of fires and explosions in transportation and applying this uncertainty modelling to the design of safety barriers. Stochastic (Monte Carlo) simulation was applied to the propagation of uncertainties. The uncertainty modelling was combined with deterministic models of design of barrier structures.

Scientific novelty of the thesis

The main scientific novelty consists in the idea to apply principles of QRA to a design of safety barriers capable to protect built roadside property against fires and explosions on roads and railways used for transportation of hazardous materials. Until now similar barriers were deployed only by military for security reasons. Another novel elements are the following:

1. An application of probabilistic methods to modelling uncertainties related to effects of fires and explosions on road and rail.
2. A simulation-based propagation of uncertainties related to the effects of fires and explosions through mathematical models of these physical phenomena and mechanical models of barrier structures.
3. A utilisation of a small-size sample of effects of an explosion to the reliability-based design of a barrier.
4. Proposals for the design of a sacrificial steel barrier aimed at reduction of blast loading from an explosion and reinforced concrete barrier capable to stop fragments of a road or railway tanker vessel sustaining an explosion.

Practical value of research findings

The practical significance of the results achieved in this work is a possibility to design and deploy protective structures which will reduce the risk of hazmat transportation. A relatively small investment in the safety barriers will allow to avoid potentially huge losses in case of a major accident on road and rail. Meth-

odological procedures developed in this work will help in designing safety barriers which will adequately protect roadside objects. The practical importance of these procedures consists in the possibility to design safety barriers by taking into account considerable uncertainties related to the effects induced by fires and explosions on road and rail. Uncertainties related to the response of roadside objects to the effects generated by the fires and explosions can also be taken into consideration by means of the computational procedures proposed in the present work. The research findings presented in this dissertation can be applied by structural and safety engineers who want to reduce the risk to built property posed by transportation of hazardous materials.

Defended statements

1. The main hazards posed by the hazmat transportation to the roadside property are explosions known as BLEVEs and VCEs. A rough assessment of post-mortem accidents implies that BLEVEs are more likely to occur than VCEs. BLEVEs can be considered as the hazmat transportation accidents which pose the greatest hazard to the built roadside objects.

2. A prediction of thermal and mechanical effects of BLEVEs on the roadside objects will face considerable uncertainties. These uncertainties can be quantified and propagated by a combined application of probabilistic modelling and stochastic simulation. An application of these methods will yield simulated statistical samples which can be applied to the design of safety barriers capable to protect roadside property against fires and explosions on road and rail.

3. The safety barrier can be designed by applying a small-size statistical sample containing values of effects induced by fires and explosions. This sample can be obtained by experiment or from post-mortem investigation of accidents. The barrier can be designed by combining methods of SRA and statistical resampling procedure (bootstrap). An application of these approaches will yield an estimate of a barrier failure probability. This probability can be used for making design decisions.

4. The design of safety barriers provides a variety of structural solutions. Steel, reinforced concrete and soil can be applied to the design and construction of barriers. However, this design should be based on an application of QRA and SRA methods. They will allow to take proper account of uncertainties related to the effects generated by fires and explosions on road and rail.

Approval of research results

The main statements of the thesis were published in seven scientific articles: four articles – in the Thomson ISI Web of Science register (Vaidogas *et al.* 2012ab, Vaidogas and Linkutė 2012, Linkutė *et al.* 2013), three articles in other journals (Vaidogas and Kisežauskienė 2012, Vaidogas *et al.* 2013ab).

The main statements of the thesis were discussed during three national scientific conferences:

- in the 16th International Conference "Mechanika 2011", held in Kaunas, 2011;
- in the 11th International Conference " International Conference "Environmental Engineering", held in Vilnius, 2011;
- in the 8th International Conference "Transbaltica 2013", held in Vilnius, 2013.

Structure of the thesis

The thesis consists of introduction, 3 chapters, conclusions, list of references and the author's publications, six annexes. The structure of the thesis is presented in Figure 1.

The volume of the thesis is 169 pages, excluding annexes, 49 numbered formulas are used, 62 pictures and 20 tables. The list of references consist of 170 items.

Introduction
Problem formulation; Relevance of the thesis; Research object; Aim of the thesis; Objectives of the thesis; Research methodology; Scientific novelty of thesis; Practical values of research findings; Defended statements; Approval of research results; Structure of thesis

Chapter 1 RISK POSED BY HAZMAT TRANSPORTATION: A REVIEW FROM THE STANDPOINT OF STRUCTURAL ENGINEERING
• The problem of transportation risk assessment • Approaches to design safety barries of roadside property • Structural consideration of protective barriers • First chapter conclusions

Chapter 2 PREDICTING THE EFFECTS FROM HAZMAT TRANSPORTATION ACCIDENTS CAPABLE TO DAMAGE ROADSIDE PROPERTY
• Main hazards of materials transportation to roadside property • Risk related to road tank explosion • Thermal effects from road tank explosion • Second chapter conclusions

Chapter 3 PROPOSALS FOR THE DESIGN OF SAFETY BARIERS AIMED AT PROTECTION OF ROADSIDE PROPERTY
• The scope of barrier design • Safety barrier pre-optimisation stage • The design of barrier with sacrificial cladding • Proposals to design of reinforced concrete barrier • Third chapter conclusions

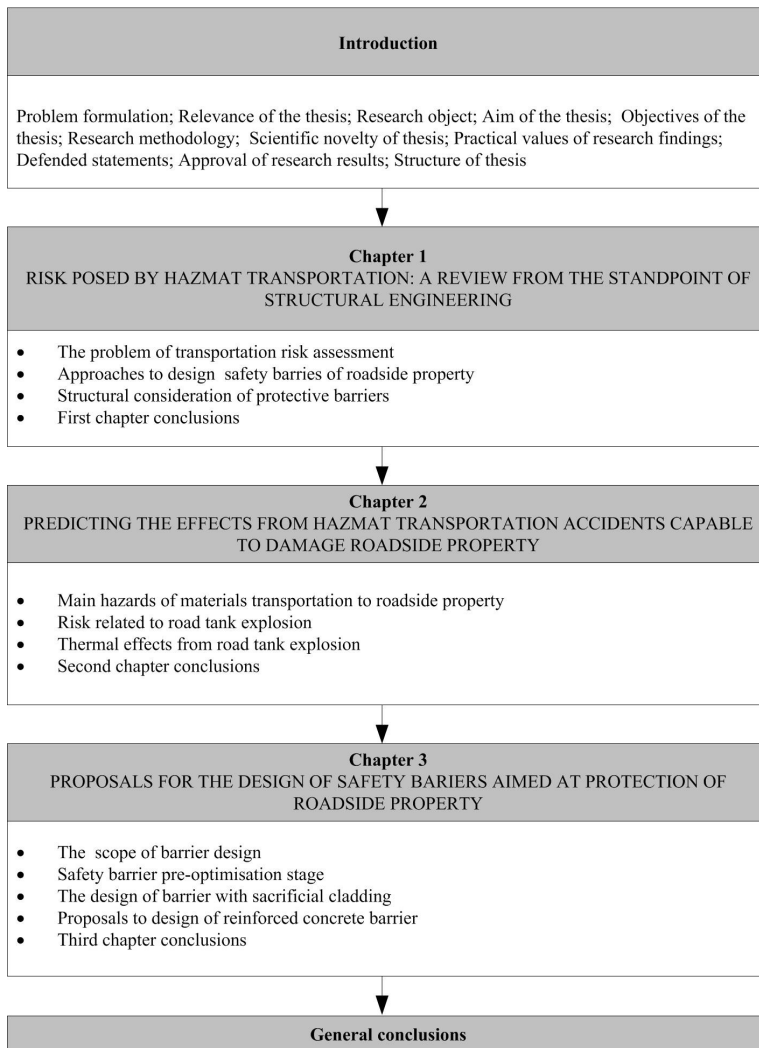| **General conclusions** |
|---|

Fig. 1. The structure of the dissertation

1

Risk posed by hazmat transportation: a review from the standpoint of structural engineering

The first chapter presents a review and evaluation of the published work on risk posed by transportation of hazardous materials (hazmat transportation). In addition, existing approaches to the design of safety barriers suitable to protect roadside property against fires and explosions on road and rail are discussed. The review covers general aspects of a transportation risk analysis (TRA), possible damaging events, structural aspects of TRA, consideration on the design of safety barriers. In particular, design of sacrificial and non-sacrificial blast walls. The review was partially presented in the papers published by Vaidogas et al. (2012ab) and Linkutė et al. (2013).

1.1. A review of approaches to transportation risk assessment

Every day large amounts of hazardous materials are transported by trucks and railway cars. Accidents of these vehicles pose serious risk to traffic and roadside territory (Planas-Cuchi *et al.* 2004; Oggero *et al.* 2006). Such accidents can escalate into toxic releases, major fires and explosions. In an extreme case a road or railway tanker accident can end up in severe explosions known as BLEVE and VCE (T. Abassi and S. A. Abassi 2007; Taveau 2010). BLEVE or VCE on road or rail can be a stand-alone accidents or, alternatively, cause secondary or

"knock-on" accidents in the roadside territory (Abdolhamidzadeh *et al.* 2010, 2011).

Predicting effects of such phenomena as BLEVE on roadside property is possible by means of mathematical modelling. The models of BLEVE effects cover blast, fireballs and projection of fragments (projectiles) (e.g., CCPS 1994; Casal 2008). Most of these models are strictly deterministic; some models include probabilistic elements (Hauptmanns 2001; Vaidogas 2006a; Mébarki *et al.* 2009; Nguyen *et al.* 2009). The key input information of them is of geometric nature. The prediction of BLEVE effects requires to know distance and orientation of the tanker in relation to potential targets (e.g., Birk 1996; Casal 2008). The identification of the position and orientation is particularly important when the potential distance between tank and target is relatively small.

As BLEVEs road tankers are relatively rare and unexpected events influenced by many random factors, the prediction of the tank position and orientation at the instant of BLEVE will have to deal with considerable uncertainties. Methods of QRA are naturally suited to quantify and propagate such uncertainties. Quantitative measures of uncertainties in position and orientation of exploding tank can serve as input into a QRA problem which will relate BLEVE to its risk profile.

There is a history of applications of QRA to transportation of hazardous materials or TRA (CCPS 1995; CPD 1999; Fabiano *et al.* 2002; Bubbico *et al.* 2004ab; Gheorghe *et al.* 2005; Grislis 2010). The common features of these applications are as follows:

1. Large traffic fragments are considered and divided into smaller route segments, for which risk is estimated. Methods of route disaggregation vary in different applications.

2. Methods used for the estimation of risk related to individual route segments are in most cases suitable for fixed installations.

3. Most applications deal with individual and societal risk to exposed population. Risk to built roadside property (buildings, objects of traffic infrastructure, industrial installations) is mentioned but not considered in detail.

4. The accident scenario prevailing in the applications of TRA is release of toxic materials and subsequent intoxication of population. Fires and explosions are not considered in detail, especially in the context of risk to fixed roadside objects.

5. When it comes to a fire and/or explosion accident on road and rail, authors often simply refer to models proposed in the literature for the prediction of effects of these phenomena, for instance, to the "coloured" books issued by the Dutch organisation TNO (CPD 1992, 2005). At-

tempts to relate in detail characteristics of traffic accidents to fires and explosions on road and rail are not known to us.

6. Methodological aspects of QRA applications to TRA look "suspiciously flat". Applications of TRA have few if any considerations on the uncertainty of risk assessments, quality and relevance of data, formal separation of experts' opinions and hard historical data.

In summary one can say that TRA is a widely developed extension of QRA; however, applications of TRA lack "attention to detail", where fires and explosions on road and rail are of concern. A BLEVE-related example of this state of investigations is the assessment of individual and societal risk due to LPG transportation done by Paltrinieri *et al.* (2009).

The idea that explosions and fires on road and rail may require an in-depth consideration of the risk to a specific object built in the vicinity of the route with the hazard of fire and explosion accidents is not new. Gheorghe *et al.* (2005) and Vaidogas (2007b) considered specific situation of exposure of roadside objects to fires and explosions on road and rail. The present study can be viewed as a refining of these approaches.

We think that the assessment of risk to specific roadside property posed by road tanker explosions requires a detailed simulation of the road accident preceding the BLEVE event. Results of such simulation will yield input information for the simulation-based prediction of BLEVE effects and eventually potential damage to roadside objects. The simulation results can be useful for a risk-based design of barriers which could provide protection against BLEVEs. The present study focuses on a stochastic (Monte Carlo) simulation of position and orientation of road tankers before they sustain an explosion.

This study comprised of two parts. The first part contains a description of a data on the rest position of road tankers involved in traffic accidents. Probabilistic models fitted to this data are presented as well. Finally, the first part presents considerations on the stochastic simulation of the accident position. The second part describes a case study used to illustrate the simulation procedure (Vaidogas *et al.* 2012b).

1.2. Approaches to design of safety barriers able to protect roadside property

The transport of flammable and explosive materials by road and rail has an increasing trend. The quantities of hazardous materials shipped by rail are larger than ones routed by road. Therefore the railway transportation has a higher potential of fires and explosions (e.g., Pontigia *et al.* 2011). However, the damage caused by fires and explosions on road can be larger, because roads often pass

populated areas or run in dangerous vicinity of or even inside industrial facilities (e.g., Lozano *et al.* 2010). Fires are the most often accidents suffered during the transportation of hazardous materials, followed by explosions and gas releases (Darbra *et al*. 2010).

The risk posed by potential fires and explosions on road can be controlled by providing adequate separation distances between road and facility site or individual roadside objects (process units, say). An employment of separation distances is a part of wider safety strategies known as facility sitting and land use planning (CCPS 2005; Cahen 2006; Cozzani *et al.* 2006; Taveau 2010, Nagashima *et al.* 2011). However, the cost of land acquisition for a provision of future road-to-facility separation distances can be unacceptably high. An employment of adequate separation distances can be impossible where existing roads adjoin existing facilities or where the space available for constructing a future road (facility) near an existing facility (road) is limited.

A compensation for less than desired separation distances includes options available on both transportation side and endangered facility side. Safeguards can be built into truck vehicles and safer routing applied (Paltrinieri *et al.* 2009; Förster and Günther 2009). However, the owner (designer) of the endangered facility may have little influence, if any, on the routing of flammable and explosive materials over an adjacent public road. The transportation of such materials over access and on-site roads can be vital to running the facility. The presence of congested vulnerable areas adjoined by on-site roads can make the on-site transportation more hazardous than the transportation over off-site, public roads (e.g., Bakke *et al.* 2010; Johnson 2010; Boudet *et al.* 2011).

Safety barriers built alongside on-site and off-site roads can compensate for separation distances. If designed properly, the safety barriers will provide protection allowing not to modify roadside objects or to reduce the costs of their strengthening (shielding). Safety barriers are similar to structures known as blast or barrier walls and used to protect against military weapons and improvised explosive devises (e.g., Smith 2010). A design of safety barriers and blast walls will have much in common; however, they will not be identical. Wilful military and terrorist explosions are generally less predictable than unintentional explosions of civilian vehicles carrying hazardous goods by road. Blast walls are normally not designed to resist effects of fireballs and large projectiles from road tanker explosions or to influence, in a way, a spread of flammable gases and liquids accidentally released from tank vehicles. The disadvantage of blast walls in terms of assuring security is that they prohibit observation of activities occurring on other side (Krauthammer 2008). A reduction of visibility by safety barriers should not be a problem as long as it does not impair road safety or prohibit a warning to personnel about an imminent fire or explosion on road.

A design of safety barriers will be governed by the specific effects of an accidental fire and/or explosion on road. A comprehensive review of such accidents is not known to us, although data on some specific accidents was examined (Ronza *et al.* 2007). It is reasonably safe to suggest that the largest potential of major fires and explosions on road has an intense transportation of flammable liquids, particularly, liquefied gases. Road accidents of tank vehicles carrying liquefied gases can escalate into BLEVEs (Planas-Cuchi *et al.* 2004; Tauseef *et al.* 2010).

The design of a safety barrier aimed at protecting against such explosions as BLEVE will include estimation of thermal and mechanical effects to be resisted or attenuated as well as determination of an optimal barrier structure. The barrier can be optimised by means of conventional deterministic or reliability-based methods as well as methods of multi-criteria decision making (MCDM) (Vaidogas 2007b; Zavadskas and Vaidogas 2009; Vaidogas and Šakėnaitė 2010, 2011). However, the optimal design of the barrier should be preceded by making several decisions concerning sitting the barrier: determination of the area available for its construction; positioning the barrier between road and roadside object(s); and configuring the barrier in plan. Making such decisions can be seen as a pre-optimisation stage of the barrier design. The present study seeks to highlight several problems which may arise in this design stage. The further text refers mainly to explosions on road, whereas fires are mentioned where necessary.

1.3. Some structural considerations related to the design of safety barriers

1.3.1. Sacrificial and non-sacrificial blast walls

A blast wall is a physical barrier separating a vulnerable object from a potential explosion which produces a blast loading capable to damage the object (Smith 2010). Blast walls are normally deployed to provide structural protection against military weapons or improvised explosive devices. However, blast walls are in principle suitable to mitigate the level of blast loading generated by accidental explosions occurring in industrial facilities and during a transportation of hazardous goods. Such blast loading is sometimes accompanied by impact of projectiles and spread thermal radiation. A typical example of such an explosion is BLEVE (e.g., Vaidogas and Juocevičius 2007).

A rigid, non-deforming blast wall will reflect blast energy back towards the explosive source and this energy will not be available to damage the protected object. However, the blast energy can be additionally absorbed by the wall when it undergoes permanent, damaging deformation. Blast wall can be relatively lightweight and weak and still offer some degree of protection because a high

level of deformation can absorb a significant amount of the blast wave energy. The cost of rigid, non-destructible walls is often prohibitive and a significant mitigation of blast can be achieved using relatively lightweight frangible or sacrificial walls (Smith 2010; Bogosian and Piepenburg 2002). The energy of blast loading can be absorbed by lightweight systems used as sacrificial cladding or, in brief, SC. They can be mounted on the front of a non-sacrificial structure to be protected or serve as a component of a blast wall (Guruprasad and Mukherjee 2000ab; Hanssen *et al.* 2002; Su *et al.* 2008).

Studies concerned with the performance of blast walls in providing protection against the damaging effect of blast loading deal, almost exceptionally, with two problems: (i) developing deterministic models of blast-wall interaction and wall behaviour under the blast loading; and (ii) verification of blast wall designs in highly specific experimental set-ups. In either case, characteristics of blast loading and structure subjected to it are (assumed to be) known in advance. It is a paradox that in fact no attention was paid to uncertainties related to this type of loading and structures exposed to it. In other words, the field remains almost fully deterministic.

It is obvious that blast loading generated by attack weapons, terrorist devices and industrial accidents is uncertain to a large measure. Uncertainties of certain degree will be always inherent in mechanical models describing behaviour of blast walls. A consistent quantification of the uncertainties related to blast loading and protective structures subjected to it is possible by a combined application of SRA and methodological tools developed in the field of QRA (Vaidogas 2003, 2006a, 2007a).

The problem of uncertainty quantification in the case of blast loading generated during industrial accidents is that such accidents are unique and unexpected events, to a large margin. Post mortem statistical data on blast loading characteristics can be either unavailable or not representative. However, a design of a blast wall can be based on an experimental simulation of an accident, in which blast loading to be mitigated by the wall will be imitated either physically or numerically. A series of such experiments may yield a statistical sample of blast loading characteristics. This sample will contain information on the variability of these characteristics and, indirectly, variability of potential damage to the wall and effects on the object to be protected. With such a sample, a design of blast wall will be possible even in the case when the size of the sample will be small from the standpoint of the classical statistics (Vaidogas 2009; Vaidogas and Juocevičius 2009; Juocevičius 2011). In addition, elements of this sample can be the so-called uncertain data, that is, data represented by probability distributions and not fixed, crisp values.

1.3.2. Amenability of sacrificial cladding of blast walls to mathematical modelling

SC is generally designed as a multi-layered structure attached to a non-sacrificial frame (Guruprasad and Mukherjee 2000ab; Hanssen *et al.* 2002; Su *et al.* 2008; Ma and Ye 2007). A building wall to be protected by SC serves as a typical support. A certain degree of energy absorption and dissipation can be achieved also by cladding built as a part of blast walls and supported along some contours, where cladding is attached to the frame of a blast wall (Karagiozova *et al.* 2010; Pellissetti and Schueller 2006). The frame can provide support over most of the cladding area or, alternatively, the support can be reduced to the minimum and be provided by vertical non-sacrificial or less frangible posts (Fig. 1.1). The configuration of a non-continuous support may influence a production projectiles which after an SC failure may damage the object protected by the wall.
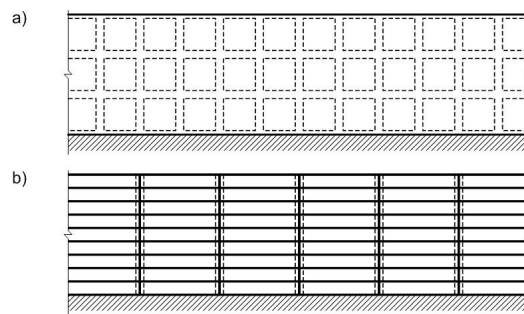
Fig. 1.1. Non-sacrificial frames supporting sacrificial cladding: a) densely distributed support; b) cladding supported by cantilever posts

The possibility to predict the behaviour of SC subjected to blast loading will depend on the presence of mathematical models which allow to obtain a deformation-time relationship and formally express a criterion for SC failure (cessation to accomplish the protective function in the course of blast loading). Studies of SCs and their components published in the recent two decades provide different possibilities of a mathematical modelling of SC behaviour. These studies can be subdivided into four groups:

1. Experimental measurements of SC deformations which do not contain any attempts to carry out a parallel analytical or numerical modelling (Straub and Der Kiureghian 2008; Vaidogas and Juocevičius 2008a).
2. Experimental studies with a parallel numerical, finite element (FE) modelling (e.g., Kelly and Smith 2009).

3. Studies containing an FE analysis only (Pellissetti and Schueller 2006; Lemaire 2009).
4. Studies which develop analytical models only or in addition to experimental measurements and/or FE computations (Guruprasad and Mukherjee 2000ab; Hanssen *et al.* 2002; Karagiozova *et al.* 2010; Ma and Ye 2007; Aven and Zio 2011; Vaidogas *et al.* 2012ab).

Most studies deal with the sandwich cladding which responds to blast loading by a compaction perpendicularly to the continuous base (Fig. 1.2a). A closer look at the analytical models allows to conclude that the most of them are based on a single-degree of freedom (SDOF) elastic or elastic-plastic idealisation of an SC fragment which deforms axially along the blast action (Ma and Ye 2007; Pellissetti and Schueller 2006; Lemaire 2009; Aven and Zio 2011; Vaidogas *et al.* 2012a). Louca *et al.* (2004) apply an SDOF idealisation to a blast wall cladding consisting of profiled steel sections which act as one-way slabs (Fig. 1.2b). Bahei-El-Din *et al.* (2006) used an FE analysis to study blast-tolerant sandwich plates which are also idealised as beam elements (Fig. 1.2c). Both claddings have some energy dissipation capability; however, their studies do not reveal how to assess the alleviation of blast action transmitted to the supporting frame.
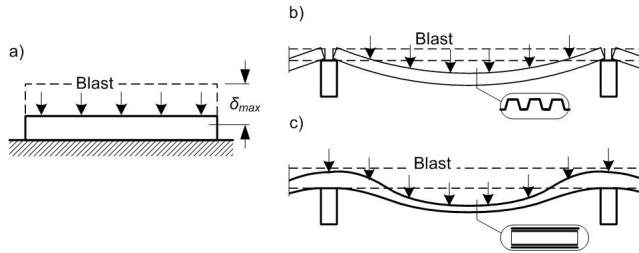
Fig. 1.2. Types of sacrificial cladding: a) sandwich cladding attached to a continuous base; b) profiled section wall supported by posts; c) sandwich cladding

All analytical SC models known to us attempt to predict deformations of individual cladding layers. An interaction between SC and supporting frame is not considered, and so criteria for cladding failure to accomplish the protective function are not expressed formally. However, some authors state that such a criterion should be based on a difference between the energy SC is capable to absorb, E_{absorb}, and the total energy imparted by the blast impulse, E_{blast}. Correspondingly, the failure criterion expressed through a safety margin m (a concept widely used in SRA) may have the form

$$m = E_{absorb} - E_{blast} \leq 0 \qquad (1.1)$$

Attempts to compute E_{absorb} and E_{blast} were made by Hansen *et al.* (2002) and Ma and Ye (2007).

A failure criterion derived from a dynamic modelling of the sandwich cladding shown in Fig. 1.2a is presented by Theobald and Nurrick (2010). They relate the failure criterion to a maximum crush distance of the sandwich core, δ_{max} (Fig. 1.2a). This distance is used to obtain the time at which compaction of the core occurs, t_c, and compare it to the total cladding response duration t_m. If $t_c \geq t_m$, the cladding will be able to absorb a prescribed blast load. The failure criterion can be expressed through a safety margin m as follows:

$$m = \ t_c - t_m \leq 0 \qquad (1.2)$$

Louca *et al.* (2004) proposed two safety margins based on a maximum dynamic response of the profiled section cladding shown in Fig. 1.2b:

$$m_1 = \ p_R - y_1 \leq 0 \qquad (1.3a)$$

$$m_2 = \ u_{pl,max} - u_{pl,dyn} \leq 0 \qquad (1.3b)$$

where p_R is the resistance (dynamic pressure capacity) of the profiled section; y_1 is the reflected peak overpressure of uniformly distributed blast loading; and $u_{pl,max}$ and $u_{pl,dyn}$ are the maximum dynamic plastic deflection and the dynamic plastic deflection due to the blast load, respectively. The above safety margins m_i ($i = 1, 2$) were derived by considering plastic deflection limit, that is, a limit point where all the reserve strength of the profiled section have been utilised. Consequently, the negative values of m_i mean that the profiled section is "sacrificed" and this involves large plastic deformation, possible tearing of welds at supports and potential formation of a projectile.

Analytical and numerical models of SC behaviour cited above are purely deterministic on both loading and structural side. The problem of model accuracy (uncertainty) is not considered formally in the aforementioned studies. From an SRA viewpoint, the deterministic analytical and numerical models of SC behaviour, m_i, may serve as a basis for a probabilistic analysis of this protective structure. The need for such an analysis will arise in the case where blast loading can vary to a large degree and is difficult to predict it with fair degree accuracy. Uncertainties can be inherent not only in the loading but also the response of SC to it. A consistent quantification of these uncertainties will generally require to apply methods developed in the field of QRA. By the way, an assessment of potential consequences caused by an accidental explosion is in essence a problem of QRA.

The standard QRA approach to uncertainty modelling is a separate treatment of stochastic and epistemic uncertainties, usually by applying a nested-loop stochastic simulation (e.g., Vaidogas 2009). This simulation will require to eval-

uate the SC models m_i a large number of times and so the complexity of m_i will be an important factor influencing the computational time.

Attempts to "marry" deterministic FE analysis and uncertainty quantification are well-known in SRA (e.g., Lemaire, M. 2009). Even though blast wall cladding is a relatively simple mechanical object, FE models expressing the safety margins m_i can be too cumbersome to incorporate them into a nested loop simulation procedure used in QRA for uncertainty propagation. Therefore, the further probabilistic analysis of blast wall cladding will be based on analytical and not numerical FE models, however accurate the latter might be. The objective to be pursued by this analysis will be an estimation of an SC failure probability which can be used as a measure of explosive damage to SC.

1.3.3. Safety barriers and elements of vehicle restraint sytems

A safety barrier deployed to resist effects of BLEVE may be exposed to a severe impact by fragments of road or railway tanker vessel. Fragments projected into the roadside territory are the furthers reaching hazard from BLEVE (T. Abassi and S. A. Abassi 2007). The launch velocity of these fragments can reach 200–400 km/h (Birk 1996). A cylindrical vessel of road or railway tanker can generate several major fragments. The largest range will have end-caps and oblong end-caps of the vessel (e. g., Mebarki *et al.* 2009a). Masses of typical road tanker vessels used in Lithuania are in the region of 10-14 tons, whereas masses of typical 4-wheel railway tanker vessels can range between 20 and 30 tons. Consequently, maximal masses of oblong end-caps generated by a BLEVE of a road or railway tanker can range roughly between 8 and 28 tons.

An impact of a cylindrical vessel fragment on a safety barrier resembles to some degree a collision of a road vehicle with elements a vehicle restraint system (VRS). The main elements of VRS, which are similar to the safety barriers considered in the present work, are guardrails along the edge of the road and median barriers (e. g., Čygas *et al.* 2009; Jasiūnienė *et al.* 2009).

VRSs have the aim to prevent vehicles from leaving the road. The European standard EN 1317 classifies VRSs into different containment levels and requires carrying out standardized full-scale impact tests of any newly developed VRS (EN 1317 2010). However, the full-scale impact tests require substantial expenses (e.g., Atahan *et al.* 2014). Therefore EN 1317 explicitly allows replacing those full-scale impact tests by computational simulations under certain limitations, in particular if a VRS is only subject to modifications (see Part 5 of EN 1317). At the moment FE models are the preferred choice for such simulations. While the use of FE modelling systems has been established for the application in structural engineering not only for static but also dynamic analysis (with both elastic and large plastic deformations), it can be observed that in par-

ticular on the US American market there is a strong party to favour the FE code LS-DYNA to simulate vehicle impacts to VRSs (Neuenhaus *et al.* 2013). This trend is followed also on the European market (e.g., Ren and Vesenjak 2005; Borovinšek *et al.* 2007; Reid *et al.* 2009; Prentkovskis *et al.* 2010, 2012).

In principle, FE modelling implemented in such codes as LS-DYNA could be applied to a simulation of a safely barrier collision with a large chunk of a tanker vessel. It could be particularly suitable to predict behaviour of highly deformable steel barriers, especially, barriers equipped with SC. However, there the subtlety of FE modelling of guardrail and safety barriers can be different. Guardrails must meet contradicting goals: on the one hand to keep vehicles on track, and on the other hand to keep the impact severity on the passengers sitting inside a car hitting the barrier at a minimum. Safety barriers will have to meet simpler goal: to stop the vessel fragment or to cause it to rebound off its surface. The barrier can sustain, in principle, any degree of damage including large plastic deformations or complete collapse (sacrificing). Thus FE modelling of safety barriers can be less accurate than simulation of vehicular impact on a guardrail.

Both guardrail and safety barrier can be designed as linear sacrificial structures and both will have to resist the action of an oblique impact. A normal impact will be less likely. These are the main similarities between guardrails and safety barriers. Differences between these two structures are more numerous than similarities. Table 1.1 lists some of the differences. In certain respects guardrails and safety barriers differ substantially. Therefore the experience gained in the development of guardrails can be only of limited use for the design of safety barriers. However, a guardrail can be deployed to protect a safety barrier against a vehicle impact if this barrier will be positioned in the immediate vicinity of the road. Such a barrier position will be the most effective if it has to serve as a blast wall (Smith 2010).

Table 1.1. Differences between elements of a VRS (guardrails and median barriers) and safety barriers

Guardrail	Safety barrier
The function	
Prevents vehicles from leaving the road and protects passengers inside vehicles	Protects objects in the territory behind the barrier
Actions to be resisted	
Impact by vehicle at a low altitude	Impact by vessel fragment and/or blast loading from such events as BLEVE and VCE; the impact point can be at a relatively high altitude

Table 1.1. Continued

Structural nature and behaviour	
Usually a long, continuous, horizontally oriented structure of relatively small height	Fence-shaped structure, not necessarily continuous in the longitudinal direction; can be relatively tall if necessary; segments can be idealised as cantilevers projecting from the ground; soil embankment providing an obstacle for vessel fragments projected by BLEVE
Uncertainties related to the actions to be resisted	
Relatively small	Large
Kinetic energy of impact	
Moderate as compared to the energy of the vessel fragments to be stopped by the safety barrier	Large due to high velocity of fragments generated by a BLEVE and relatively large mass of these fragments
Sitting	
Along the edge of the road or in the median; the horizontal layout is determined by the road geometry	In the available territory between the road and roadside objects to be protected; can be not necessarily a linear structure and have the horizontal layout providing maximum protection
Further functions	
Usually are not provided	A safety barrier can provide protection against the spread of hazardous material released from a road tanker and thermal radiation from a fire on road; the barrier can also serve as a part of a perimeter fence and/or reduce traffic noise
Acceptance test	
The European standard EN 1317 requires carrying out standardized full-scale impact tests of newly developed systems; the tests can cause substantial expenses	An acceptance test was not required until now by any normative document

The main methodological difference between the computer-aided modelling of guardrails and safety barriers will consist, in our opinion, in the prediction of impact actions on these structures. Masses, velocities and impact angles of vehicles colliding with guardrails can be assessed on the basis of large amount of data on past traffic accidents. In addition, masses and velocities of typical vehicles involved in collisions with the elements of VRS will vary within a relatively narrow range. The variation of masses and velocities of fragments generated by a bursting of a road or railway tanker vessel will be much larger, to say nothing

about the angle of oblique impact. In addition, the impact will occur at much higher speed. Therefore, the simulation will face the problem of assessing the dynamic enhancement of mechanical properties of steel and concrete (Linkutė *et al.* 2013).

1.4. First chapter conclusions and formulation of the dissertation tasks

This chapter presented a review of the published work on TRA and design of safety barriers. The review allows to make several conclusions about the state of dealing with risks posed by transportation of hazardous materials from the position of civil engineering:

1. A transportation of hazardous materials by road and rail poses serious risk to roadside population and built roadside property. Events which can cause damage to population are releases of toxic materials, fires and explosions of trucks and trains. Build property can be damaged by fires and explosions, the effects of which will spread into the roadside territory.

2. TRA is a scientific methodology developed for dealing with potential accidents during the shipment of hazardous materials. It is closely related to the general methodology of QRA. Both QRA and TRA methods of probability calculus and statistics to obtaining risk estimates.

3. Most applications of TRA deal with individual and societal risk to exposed population. The accident scenario prevailing in the applications of TRA is release of toxic materials and subsequent intoxication of population. Risk to built roadside property (buildings, objects of traffic infrastructure, industrial installations) is mentioned in the literature, but is not considered in detail.

4. The risk posed by potential fires and explosions on road and rail can be controlled by providing adequate separation distances between road and fixed roadside objects. A compensation for less than desired separation distances includes a construction of safety barriers between road (railway tracks) and vulnerable roadside object(s). Such barriers can minimise effects of blast and thermal radiation and stop projectiles ejected towards the vulnerable objects.

5. Safety barriers designed and built until now were mainly blast walls. They were used by the military to separate vulnerable objects from potential explosion which produces a blast loading capable to damage the object. A combined action of blast and projectiles on blast walls was not considered in detail in the open literature.

6. Blast walls can be built as sacrificial and non-sacrificial structures. Sacrificial blast walls are the better solution, because a part of blast energy can be absorbed by the wall when it sustains permanent, damaging deformation.

7. Studies of sacrificial blast walls published in the recent two decades provide different deterministic mathematical models allowing to predict modelling of blast wall behaviour. These models can be applied in combination with QRA methods and techniques of SRA. The latter two scientific fields provide systematic tools for an uncertainty quantification. A proper modelling of uncertainties allow to design better safety barriers.

Results of the literature review and the just listed conclusions of the first chapter allow to formulate the following tasks for this dissertation:

1. To analyse hazmat transportation accidents which can cause the greatest damage to built roadside objects.

2. To collect and process data on road traffic accidents, which could allow to predict the potential positions of road tanker explosions.

3. To develop a procedure suitable to predicting thermal effects of road tanker explosions on roadside objects.

4. To develop a QRA-friendly procedure allowing to predict impacts of a road tanker vessel fragments on a potential safety barrier.

5. To give provisions for sitting and layout of safety barriers to be built alongside traffic routes.

6. To give provisions for the design of a safety barrier with sacrificial cladding used to resist blast loading generated by an explosion of a railway tanker vessel.

7. To give provisions for the design of a safety barrier aimed at protecting roadside property against an impact of a fragment of a road tanker vessel.

2

Predicting the effects from hazmat transportation accidents capable to damage roadside property

The second chapter includes an identification of most hazardous accidents which can occur on road and rail and proposes three computational procedures for identifying thermal and mechanical effects generated by such accidents. BLEVE is recognised as a relatively frequent and highly damaging accident on road and rail. The second chapter is focused on predicting the two main effects of BLEVE: thermal radiation and projectile impact. The first procedure was developed to predict the position of road tanker vessel sustaining a BLEVE with respect to a potential target. The second procedure deals with assessing the thermal radiation of a BLEVE fireball which can impinge on roadside objects. The third procedure was developed for forecasting the impact of road tanker vessel fragments on roadside object or possible safety barrier. All three procedures are based on probabilistic modelling and can be incorporated into a transportation risk analysis. The present chapter summarises results of investigation published by Vaidogas *et al.* (2012ab), Vaidogas and Kisežauskienė (2012), Kisežauskienė and Vaidogas (2013).

2.1. Identification of the main hazards to roadside property posed by road and rail transportation

Safe transportation of hazardous materials is an important national issue in each country. The great majority of these materials move by either rail or truck. With an ever increasing number of trucks moving on highways, there is cause for concern not only over safety issues, but the impact on highway gridlock, environmental implications, and infrastructure deterioration.

The transportation of hazmats is an important problem due to their pervasiveness. Hazardous materials, or dangerous goods, include explosives, gases, flammable liquids and solids, oxidizing substances, poisonous and infectious substances, radioactive materials, corrosive substances, and hazardous wastes. Due to the nature of most chemicals, they can pose hazards of toxic release, fire and explosion.

Releases of toxic liquids and atmospheric dispersions of toxic clouds can cause damaging effects to environment and population located working in the vicinity of roads and rails. Fires and explosions pose the hazard of thermal and mechanical actions which can severely damage built property in the roadside territory. The frequency of fires and explosions and so the likelihood of these events in the future can be assessed by applying such databases as the Hazardous Materials Incident Reporting System (HMIRS) run by the US Department of Transportation (PHMSA 2014; Ronza *et al.* 2007). The HMIRS database is public and available online.

Tables 2.1 and 2.2 contain counts of hazmat transportation accidents and incidents in the 10-year period 2003–2012 on US roads and rails, respectively. The numbers of fires and explosions among these events are presented in separate columns. These numbers are relatively small as compared to the total number of events reported to HMIRS. However, HMIRS contains a very large number of incidents which caused little of no damage. Such incidents are mainly small spills and evaporations. Another obvious conclusion which follows from Tables 2.1 and 2.2 is that hazmat transportation by rail causes a substantially smaller number of accidents and incidents than shipping of such materials by trucks. This conclusion is confirmed also by other authors (e.g., Spraggings 2010).

The HMIRS database was searched for hazardous materials which most often are involved in transportation accidents. These materials are commercial energetic hydrocarbons (LNG; LPG; light fractions including petrol and naphtha, crude oil; kerosene and jet fuel; diesel fuel; gas oil and No. 1 and 2 fuel oil; No. 4, 5, 6 fuel oils) (Ronza *et al.* 2007).

Table 2.1. Numbers of fires and explosions in hazmat transportation accidents on US roads in the 11-year period 2003 to 2013 (extracted from the HMIRS database, PHMSA (2014))

Year	Total number of reported accidents	Number of fires	Number of explosions
2003	13 594	40	26
2004	13 068	49	24
2005	13 460	29	56
2006	17 159	30	49
2007	16 932	43	60
2008	14 802	48	46
2009	12 730	46	24
2010	12 652	49	47
2011	13 237	32	16
2012	13 249	63	13
2013	13 728	49	14
Total:	154 611	478	375

Table 2.2. Numbers of fires and explosions in hazmat transportation accidents on US railways in the 11-year period 2003 to 2013 (extracted from the HMIRS database, PHMSA (2014))

Year	Total number of reported accidents	Number of fires	Number of explosions
2003	802	4	1
2004	765	3	0
2005	745	2	1
2006	703	2	0
2007	753	6	2
2008	748	4	0
2009	642	2	0
2010	749	3	0
2011	745	2	2
2012	662	6	1
2013	665	2	2
Total:	7979	36	9

Every day large amounts of commercial hydrocarbons are shipped by road and rail to ensure a distribution to end-consumers in Lithuania. These materials are the main type of hazmats in the network Lithuanian land transportation (Batarlienė 2008). The increasing consumption of hydrocarbons in Europe and construction of new gas terminals along the eastern shores of Baltic sea may

drive up transportation of gases by road and rail in the Baltic states (Kavalov *et al*. 2009).

Traffic accidents of trucks and trains shipping commercial hydrocarbons pose serious risk to built infrastructure located in the vicinity of roads and railways (e. g., Oggero *et al.* 2006). These accidents can escalate into fires and explosions which are able to cause thermal and/or mechanical damage to roadside objects. The main types of fires and explosions on road and rail are common to similar transportation, fuelling, loading and unloading activities worldwide (e.g., Casal 2008; Quest Consultants 2009):

1. Pool fire (fire of a pool of combustible liquid resulting from a leak from a tank vessel);
2. Jet fire (combustion of flammable gas or vapour released at a certain velocity through a hole in a pressurised tank vessel);
3. Flash fire (a quick combustion of a cloud formed by a flash vaporisation of a flammable liquid or by evaporation of a pool of such liquid);
4. VCE (release of a flammable vapour from a tank vessel followed by formation, ignition and high-speed combustion of a flammable cloud; such combustion can produce a significant blast overpressure);
5. BLEVE (a blast of a tank vessel with flammable or non-flammable material caused by external heating).

Thermal effects of pool fire, jet fires and flash fires will be limited by a relatively small amount of flammable liquids and gases which are typically carried by road and railway tankers. The well-documented flash fire due to release of LNG from a railway tanker in Viareggio (Italy, in 2009) caused substantially smaller damage than the VCE triggered off by a release of caprolactanum in a fixed installation of Flixborough factory (UK, 1974). However, the fires mentioned above can cause secondary, "knock-on" accidents, such as a BLEVE (T. Abassi and S. A. Abassi 2007).

VCEs have a large potential of widespread mechanical damage to roadside property. However, most VCEs occurred in fixed industrial facilities. Lenoir and Davenport (1993) listed 103 suspected VCE accidents that produced observable overpressures during the period 1921–1991. Of these events, only 10 % were rail car and road tanker accidents and 7 % waterway vessel accidents. Consequently, one can state that land transportation of commercial hydrocarbons is not too much prone to VCE accidents. However, some VCE accidents in transportation caused major damage to built property. An often cited example was a VCE in East St. Louis (USE) on January 22, 1972 (Eichler and Napadentsky 1977). A railcar full of LPG rolled into another railcar during rail yard switching operations and was punctured. Approximately 54 tons LPG were released into the rail yard. The vapour cloud covered an area of more than $20\,000$ m^2 and

reportedly ignited in two different locations. The explosion was enhanced by the tightly congested arrangement of railcars throughout the large rail yard. An estimated 1000 buildings were damaged to various degrees. The property damage was estimated at US$45 million (FM Global 2013).

Another accidental phenomenon which can be extremely hazardous to roadside territory is BLEVE. The immediate effects of BLEVE are blast and projectiles. If the commodity in a tank vessel sustaining BLEVE is flammable and is ignited immediately then a fireball is possible with the associated hazards of fire engulfment and thermal radiation. If the flammable commodity is not ignited immediately, then delayed ignition may lead to widespread fires or, in some cases, explosions (Birk 1996).

Short reviews of accidents involving BLEVEs in transportation are presented by T. Abassi and S. A. Abassi (2007) and Tauseef *et al.* (2010). Planas-Cuchi *et al.* (2004) and Bonilla Marinez *et al.* (2012) described in detail two BLEVEs of road tankers which occurred in Spain in 2002 and 2011. However, neither of these publications attempted to systematise information on a greater or lesser number of BLEVEs in transportation in terms of, say, types commodities involved in accidents or damage to roadside property.

A relatively informative source of world-wide data on BLEVEs in transportation is the "hazardous materials knowledge base" known also as "failure and accidents technical information system" or, in brief, FACTS (FACTS 2014). It allows to identify hazmats involved in BLEVE accidents on road and rail. Tables A2 and A3 present information extracted from FACTS on 43 BLEVE accidents, which occurred on road, and 38 BLEVEs, in which railway cars were involved. Although these accidents present only a relatively small fraction of reported and unreported BLEVEs in transportation, information given in Tables A2 and A3 allows to make three obvious conclusions:

1. The hazmat, which was most frequently involved in BLEVEs on road and rail, is LPG (Figs. 2.1 and 2.2).
2. Most BLEVEs of road tankers occurred on roads and not inside or in the vicinity of build-up and industrialised areas. One can expect that the exposure of roadside objects to BLEVE effects and so the likelihood of domino accidents is lower on roads than in the aforementioned areas.
3. The prevailing locations of BLEVE in the railway transportation network were railways (21 case) and low-speed motion areas (rail yards and railway stations, 7 cases). The exposure of built objects to BLEVE effects is higher in the latter areas and in sparsely built areas along railways.
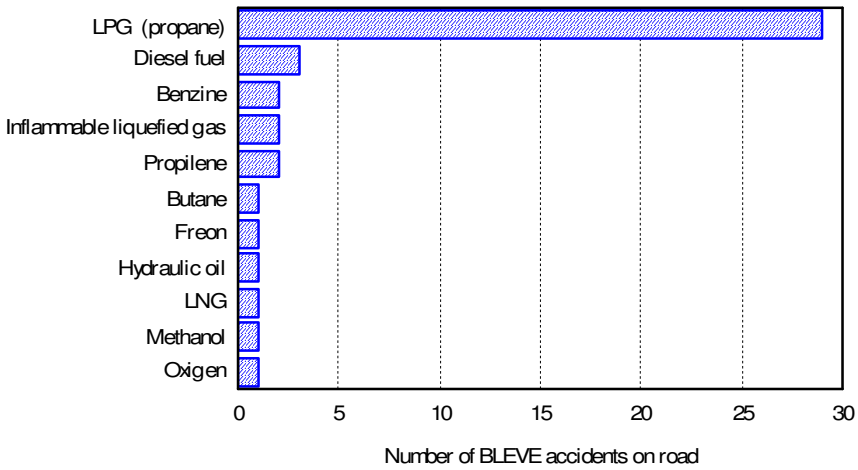
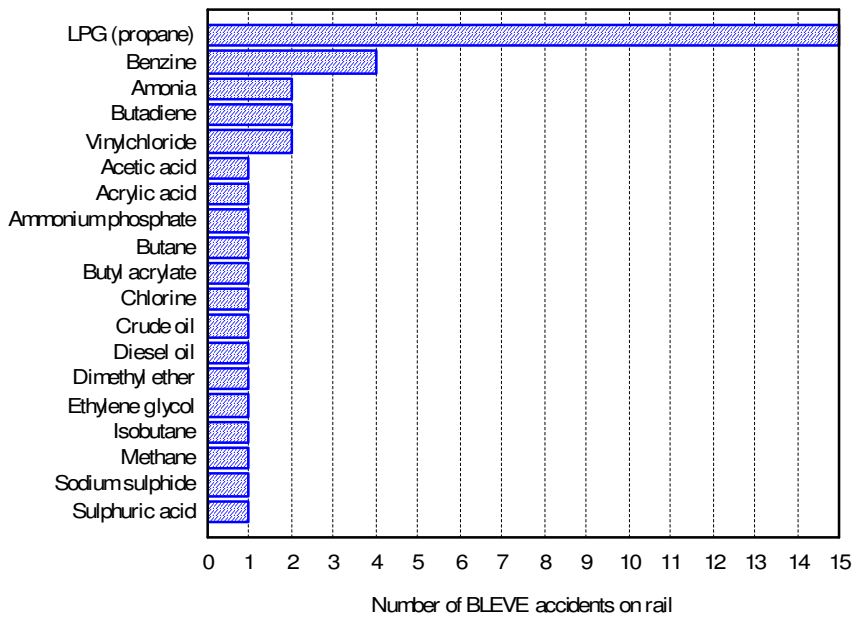**Fig. 2.1.** Hazardous materials shipped by road tankers and involved in 43 BLEVE accidents

Fig. 2.2. Hazardous materials involved in 38 BLEVE accidents on rail

Occurrence of devastating VCEs in transportation is less probable than occurrence of BLEVEs. A formation of a vapour cloud with flammable concentration and movement of this cloud towards a potential target in the roadside territory requires an existence of specific meteorological conditions (e.g., CCPS 1994). In addition, the cloud must meet an ignition source. Such source will not necessarily be present and the cloud can simply disperse in the air. A supersonic propagation of the flame in the cloud (a detonation) will be possible if the concentration of the cloud will be fairly uniform throughout its volume. Otherwise, the flame will propagate at subsonic speed (VCE will occur as a deflagration) and overpressure will be modest as compared to devastating overpressures generated by detonation. Finally, the combustion of the cloud can occur as a flash fire with negligible overpressure. Consequently, the chance that a flammable spill from a road or railway tanker will escalate into a VCE, which occurs as a detonation, is relatively small (Ronza *et al.* 2007).

A BLEVE of a road or railway tanker can be induced by external heating of the tank vessel followed by catastrophic failure of the tank and explosive release of boiling liquid and expanding vapour. Such an event is called a "hot" BLEVE. However, a BLEVE of a road or railway tanker can occur without external fire, namely, due to an instantaneous rupture of the tank with immediate release of its contents. BLEVEs of this type are caused by impact in a collision or derailment or material defects. They are called "cold" BLEVEs. The situation, leading to a "cold" BLEVE can be aggravated by cold temperature, corrosion, brittleness of tank vessel material. In road transport, 50 % of the cases are "cold" BLEVEs and 50 % of the cases are "hot" BLEVEs. As regards the rail transport, roughly 70–80 % of BLEVEs are "hot" ones (TNO 2005). Thus the number of possibilities for BLEVE to occur on road or rail is larger than the number of possibilities of a detonation of a vapour cloud formed by a flammable release from a road or railway tanker.

The question, which of the two phenomena, VCE or BLEVE, "outperforms" the other in terms of fire engulfment, has not a clear answer. The fireball generated by a BLEVE will emit a thermal radiation which may cover the area comparable to the area of burning vapour cloud.

Any study which compares in detail the risks posed by VCEs and BLEVEs on road and rail is not known to us. We were able to find only a relatively small number of transportation-related publications which consider occurrences of VCEs and BLEVEs independently of one another. However, we feel intuitively that the land transportation network is more prone to BLEVEs than to VCEs occurring as detonations. In addition, the effects of BLEVEs are ternary (a relatively moderate blast, thermal radiation and projectile impact), whereas VCEs will generate only blast which is more likely to occur as a deflagration than as a detonation. In order to limit the amount of our study, we decided to deal with the

BLEVEs only. This phenomenon can be considered to be the main hazard in the areas where roads and railway tracks used to ship commercial hydrocarbons and other flammable or explosive materials come into the vicinity of vulnerable roadside property. An example of such property is tank farms of oil transhipment facilities in the Lithuanian port of Klaipėda (Fig. 2.3). Currently, the tank farms stay unprotected against effects of a potential BLEVE. Such an event can trigger off a domino sequence in the transhipment facilities which could lead to a major disaster in the port area.

Fig. 2.3. An example of exposure of an industrial facility to the hazard of a railway tanker BLEVE: railway tracks coming along tank farms in the port of Klaipėda (obtained with maps.lt software)

2.2. Risk related to road tanker explosions

In terms of QRA, a BLEVE accident of a road tanker is a low-probability initiating event. It can be internal or external event with respect to exposed installation (e.g., Kumamoto 2007; Garrick 2008). QRA can be focused on a specific random damage event D, for instance, loss of containment of a tank or rupture of a pipeline due to mechanical and thermal actions of BLEVE. In this case the frequency of D can be expressed as a product of frequency of transportation (mission frequency) $Fr(M)$ and three conditional probabilities which relate M to D:

$$F_r(D) = F_r(M)\, P(A \mid M)\, P(B \mid A)\, P(D \mid B) \tag{2.1}$$

where A is the random event of a road accident, in which the road tanker will be involved, and B is the random event of BLEVE.

The estimation of the conditional damage probability $P(D \mid B)$ requires to assess mechanical and thermal effects of BLEVE. If these effects are grouped into a vector $\mathbf{y}$, the damage probability can be expressed as follows (Vaidogas and Juocevičius 2009):

$$P(D \mid B) = \int_{\text{all } \mathbf{y}} P(D \mid \mathbf{y}) f(\mathbf{y}) \mathrm{d}\mathbf{y} = \int_{\text{all } \mathbf{x}} P(D \mid \boldsymbol{\psi}(\mathbf{x})) f(\mathbf{x}) \mathrm{d}\mathbf{x} \tag{2.2}$$

where $P(D \mid \mathbf{y})$ is the fragility function relating the probability of D to $\mathbf{y}$; $\mathbf{x}$ is the vector of characteristics of BLEVE accident; $\boldsymbol{\psi}(\mathbf{x})$ is the vector-function which relates $\mathbf{x}$ to $\mathbf{y}$ (i.e., $\mathbf{y} = \boldsymbol{\psi}(\mathbf{x})$); and $f(\mathbf{x})$ and $f(\mathbf{y})$ are the joint probability density functions of $\mathbf{x}$ and $\mathbf{y}$, respectively.

The development of the fragility function $P(D \mid \mathbf{y})$ is a highly case-specific task of reliability-based structural analysis. It must be solved for individual components of installation subjected to the hazard of BLEVE (e.g., Vaidogas 2003, 2007ab). The development of $P(D \mid \mathbf{y})$ will not be considered here. We can only say that a BLEVE accident may require to develop $P(D \mid \mathbf{y})$ for a combined action of three effects (components of $\mathbf{y}$): blast wave, thermal radiation and missile impact. Any attempts to do this are not known to us. The closest result was obtained by Lee Fig 2.1 and Rosowski (2006) who developed a fragility function for a combined action of earthquake and snow.

Fitting the density $f(\mathbf{y})$ to the direct data on BLEVE effects is impracticable. BLEVE accidents on road are unique, short-lasting and unexpected events and the post mortem data on them is too sparse for fitting $f(\mathbf{y})$. However, the density $f(\mathbf{y})$ and so the probability $P(D \mid B)$ can be estimated by propagating uncertainties expressed by the lower-level density $f(\mathbf{x})$ through the model $\boldsymbol{\psi}(\mathbf{x})$ (Vaidogas 2007ab, 2009; Vaidogas and Juocevičius 2008ab, 2009; Juocevičius and Vaidogas 2010). The function $\boldsymbol{\psi}(\mathbf{x})$ can be composed of a relatively large number of models available currently for the prediction of individual effects of

BLEVE. Most of these models are deterministic, some are in competition in modelling individual effects. Table 2.3 contains a selection of literature on modelling the effects of BLEVE.

Table 2.3. A selection of literature on models used to predict BLEVE effects (components of the vector-function $\psi(x)$)

BLEVE effect	References
Blast	Prugh (1991); CCPS (1994); Planas-Chuci *et al.* (2004); CPD (2005); T. Abbasi and S. A. Abbasi (2007); Casal and Salla (2006); Casal (2008); Genova *et al.* (2008)
Fireball	CCPS (1994); Prugh (1994); Robets *et al.* (2000); CPD (2005); T. Abbasi and S. A. Abbasi (2007); Casal (2008)
Projectiles	Hauptmanns (2001); Gubinelli *et al.* (2004); CPD (2005); Vaidogas (2006a); T. Abbasi and S. A. Abbasi (2007) ; Casal (2008); Genova *et al.* (2008); Gubinelli and Cozzani (2009); Mébarki *et al.* (2009); Nguyen *et al.* (2009)

The density $f(x)$ expresses uncertainties in those characteristics of BLEVE accident which serve as input in the model $\psi(x)$. This density can be specified by means of two basic approaches to QRA known as classical Bayesian approach and predictive Bayesian approach (e.g., Aven 2003). We think that the latter approach is better suited to the assessment of risk posed by BLEVEs on road. However, an extensive discussion on the choice among the classical and predictive approaches will not be presented here. Such a discussion can be found in publications dedicated to methodological issues of QRA (e.g., Aven 2009; Aven and Zio 2011). All probabilistic models presented in the subsequent text will be interpreted in line with the predictive Bayesian approach.

The vector x must contain physical characteristics of the tank sustaining BLEVE. The effects of BLEVE will also depend on the position and orientation of the tank in relation to the target. A scattering of projectiles from a cylindrical vessel BLEVE is significantly directional; some studies indicate that the blast from BLEVEs can also be directional (Birk 1996; Casal 2008). The position and orientation are key input information for the models described in the references cited in Table 2.3. In what follows, the position and orientation of the tank will be expressed by the first three components of x:

1. The coordinates of explosion (tank) centre, x_1 and x_2, specified in a coordinate system which includes the target and the section of the road in which the explosion can happen (Fig. 2.4); and
2. The angle of the tank axis in relation to the road axis, x_3 (Fig. 2.4).
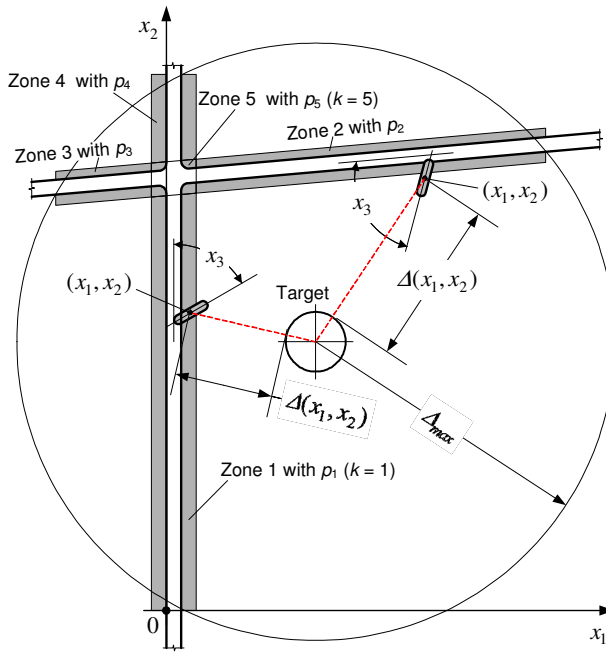
Fig. 2.4. Exposure of a roadside object (target) to the BLEVE hazard in the earth-fixed
coordinate system $\{0; x_1, x_2, x_3\}$

The further consideration is about the prediction of x_1, x_2, and x_3 for a specific situation of exposure to BLEVE hazard, and thus the prediction of the distance from the explosion to a target under analysis. This distance will be denoted by Δ (Fig. 2.4). Despite the fact that the dimensions x_1, x_2 and x_3 are not among physical characteristics of exploding tank, the proper choice of range and probability distribution of x_1, x_2 and x_3 can substantially influence results of further risk assessment.

2.2.1. Geometric information on road tanker accidents

The position and orientation of the tank after a road accident which escalates into BLEVE is growing in importance when the distance between tank and target decreases. Two coordinate systems can be used for the prediction of tank position and orientation (Franck and Franck 2010). The assessment of the risk to a fixed target requires to consider the position and orientation in the earth-fixed coordinate system $\{0; x_1, x_2, x_3\}$ (Fig. 2.4). However, the data on road tanker accidents can be collected and processed using a coordinate system based on

vehicle and travel lane, $\{0; y_1, y_2, y_3\}$ (Fig. 2.5). The data recorded in the latter system can be transformed into data related to the former one with relative ease.
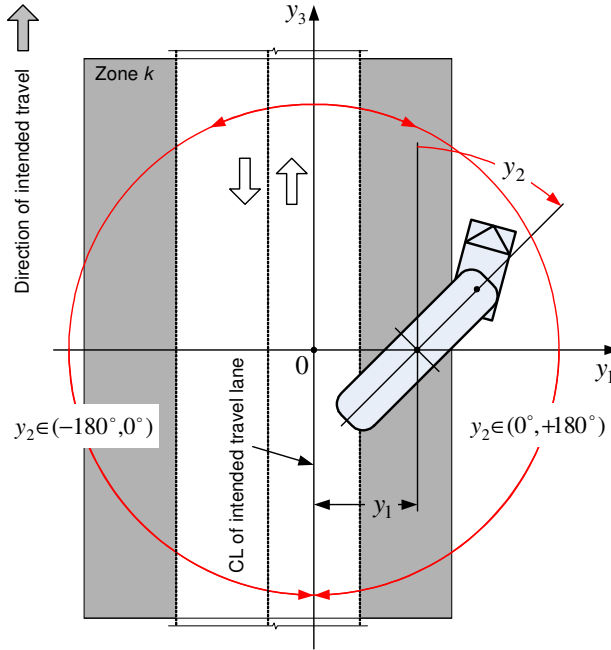
Fig. 2.5. Vehicle-based coordinate system $\{0; y_1, y_2, y_3\}$ used for collecting and processing data on road tanker accidents

2.2.1.1. Transverse rest position and departure angle

The prediction of the tank position and orientation after it comes to a complete stop and can explode consists in the choice of either joint probability density function $f(y_1, y_2)$ or marginal densities $f(y_1)$ and $f(y_2)$ for the transverse rest position of the tank centre, y_1, and the angle of rest departure of the tank relative to the travel lane centreline, y_2 (Fig. 2.5). For brevity, we will call y_1 and y_2 the transverse rest position and departure angle, respectively. In line with the aforementioned approaches to QRA, the densities $f(y_1, y_2)$ or $f(y_1)$ and $f(y_2)$ can be chosen using data on past accidents or expert opinion or both. The data can provide answer to the question of a stochastic dependence of y_1 and y_2.

We think that the statistical variability of transverse rest position y_1 and departure angle y_2 can be assessed from data on road tanker accidents. The potential data on y_1 and y_2 are of three sorts:

1. Data on road tanker accidents which escalated into BLEVEs (A-data, for brevity).
2. Data on accidents which did not escalated into BLEVEs but were capable to do so in consequence of spill of flammable liquid or fire impinging the tank ("near misses" in terms of QRA) (B-data).
3. Data on accidents of road tankers which transported liquids, but not necessarily liquefied gases, and had dynamic characteristics similar to road tankers capable to cause BLEVE (C-data).

The A- and B-data are likely to be more relevant to future BLEVE accidents on road than C-data. However, the amount of C-data exceeds considerably the amount of A- and B-data because the number of road accidents which developed into BLEVEs or occurred as "near misses" is relatively small (see, e.g., Oggero *et al.* 2006). In addition, information on y_1 and y_2 available in the reports on BLEVE accidents can be vague because tanks are displaced and destroyed during these explosions (see, e.g., Planas-Cuchi *et al.* 2004).

The potential sources of A-, B- and C-data are: hazmat transportation accident databases; accident databases of general nature; road accident databases collected and maintained usually by the police; and databases of occupational accidents including road transportation events in which workers were injured and killed on duty. These databases are maintained and updated by various official and professional bodies and organisations in many countries. However, several researchers have noticed the lack of statistical reliability of such databases due to the systematic underreporting of the circumstances of road accidents (see Trépanier *et al.* 2009 and the references cited therein). We think that a special study is necessary to determine whether these data sources contain such circumstantial data as rest position y_1 and departure angle y_2 of the tank. To our knowledge, none of Lithuanian organisations maintains a database which includes circumstantial information on y_1 and y_2. We also did not find any freely accessible database maintained outside Lithuania which would contain data on y_1 and y_2.

Information on y_1 and y_2 can be elicited from the reports on road tanker accidents presented by the mass-media and in the internet. These reports should not be neglected because they often contain pictures of the accident site and description accident circumstances. Consequently, such reports can serve as a source of C-data. We found a series of the reports and collected a small road tanker accident database containing 151 event mainly for 2007–2011 period. Our database includes records of 65 accidents of the tank trucks and 86 accidents of tank semi-trucks. In 120 cases the accidents took place in the area with flat or almost flat roadside territory and zero vertical grade (gradient). In 17 and 5 cases accidents occurred on downhill and uphill road segments, respectively. The vertical grade was difficult to assess in 9 cases. Most accidents occurred in

the US and were reported by US media. An extraction from the database is presented in Table 2.4.

Table 2.4. An extraction from a database containing information on 151 road tanker accident

Date	Location	Material	Quantity, m^3	y_1, m	y_2, degs
2007/12/06	Everett	gasoline	35.58	0.0	0
2009/07/25	Oak Park, Michigan	diesel	49.21	2.0	0
2009/10/22	Indianapolis	propane	20	8.5	85
2009/10/23	Fayetteville	fuel	not reported	2.0	0
2009/11/30	Kansas City	hydrochloride acid	20.41	2.0	340
2010/01/23	Melville, New York	fuel	45.42	6.5	340
2010/01/25	Monperlier, France	fuel	not reported	-6.5	270
2010/04/01	Chicago, Illinois	fuel	not reported	2.0	0
2010/04/02	Burverde, Texas	fuel	not reported	-3.0	260
2010/04/07	Wamsutter, Wyoming	crude oil	not reported	0.0	0
2010/04/14	Roy, Utah	diesel	28.39	9.0	270
2010/05/16	Miami Gardens, Florida	fuel oil	not reported	2.0	0
2010/05/28	Carona, Los Angeles	gasoline	33.31	3	0
2010/05/29	Tynsborough, Massach.	aerosol paint	not reported	3	0
2010/06/22	Foxboro, Mass.	jet fuel	41.64	5.0	45
2010/08/20	Coloma, Michigan	fuel	not reported	8	340
2010/08/20	Armold, Maryland	fuel	not reported	0	-5
2010/08/21	Arizona	diesel	18.9	15.0	50
2010/08/28	Utah	diesel	28.39	8.5	90
2010/08/29	Hamshire, Texas	isobutene	32.76	10.0	90
2010/09/03	Dearborn County, Indiana	ph. anhydride molten	15.14	13.0	40
2010/10/23	Fayetteville	fuel	not reported	2	0
2010/10/29	Albuquerque, New Mexico	fuel	not reported	-5.0	280
2010/11/09	California	tar	not reported	5.0	15
2010/12/20	Utah	crude oil	40.33	-5.0	310

Table 2.5. Descriptive measures of the samples consisting of observations of transverse rest position y_{1i} and departure angle y_{2i}

Measure	Positions y_{1i}	Angles y_{2i}
Sample size	129	122
Mean	2.02 m	2.83°
Std. deviation	5.62 m	56.8°
Minimum	-12.25 m	-170°
Maximum	18 m	180°
Skewness	0.0551	0.119
Kurtosis	-0.1059	1.679
Standardised skewness	0.256	0.536
Standardised kurtosis	-0.246	3.79

The values of the transverse rest position, y_{1i}, were determined visually for 129 events and the departure angle y_{2i} was obtained also visually for 122 events. The data allowed to form 119 observation pairs (y_{1i}, y_{2i}) for the assessment of the stochastic dependence of y_1 and y_2. Table 2.5 contains descriptive measures of the samples $\{y_{1i}, i = 1, 2, \ldots, 129\}$ and $\{y_{2i}, i = 1, 2, \ldots, 122\}$. Fig. 2.6 shows the histograms of these two samples. The scatter diagram of the pairs (y_{1i}, y_{2i}) is given in Fig. 2.7. The correlation coefficient computed for the pairs (y_{1i}, y_{2i}) was equal to 0.29. The *p*-value in Fig. 2.7 indicates a statistically significant relationship between y_1 and y_2.

Table 2.6. Goodness-of-fit tests for the sample of y_{1i} values

Measure	Normal	Logistic
Kolmogorov-Smirnov D_n	0.05755	0.05320
Kolmogorov-Smirnov p	0.7863	0.8586
Shapiro-Wilk W	0.9851	—
Shapiro-Wilk p	0.7542	—

It was possible to fit two well-known probability distributions, normal and logistic, to the values y_{1i}. Although neither of the distributions was rejected by standard goodness-of-fit tests, the logistic distribution Logistic(2.02 m, 3.10 m) fits the data better than the normal distribution N(2.02 m, 31.6 m^2) (see Table 2.6 and Fig. 2.6a). Thus the logistic distribution will be used for the purposes of the simulation described in Sec. 2.2.2.

The values y_{2i} do not seem to obey any standard probability distribution. An empirical distribution function of the sample of y_{2i} can be used as a tentative model for the purposes of simulation (e.g., Evans *et al.* 2001). This function is represented by the histogram of the cumulative frequencies shown in Fig. 2.6b.

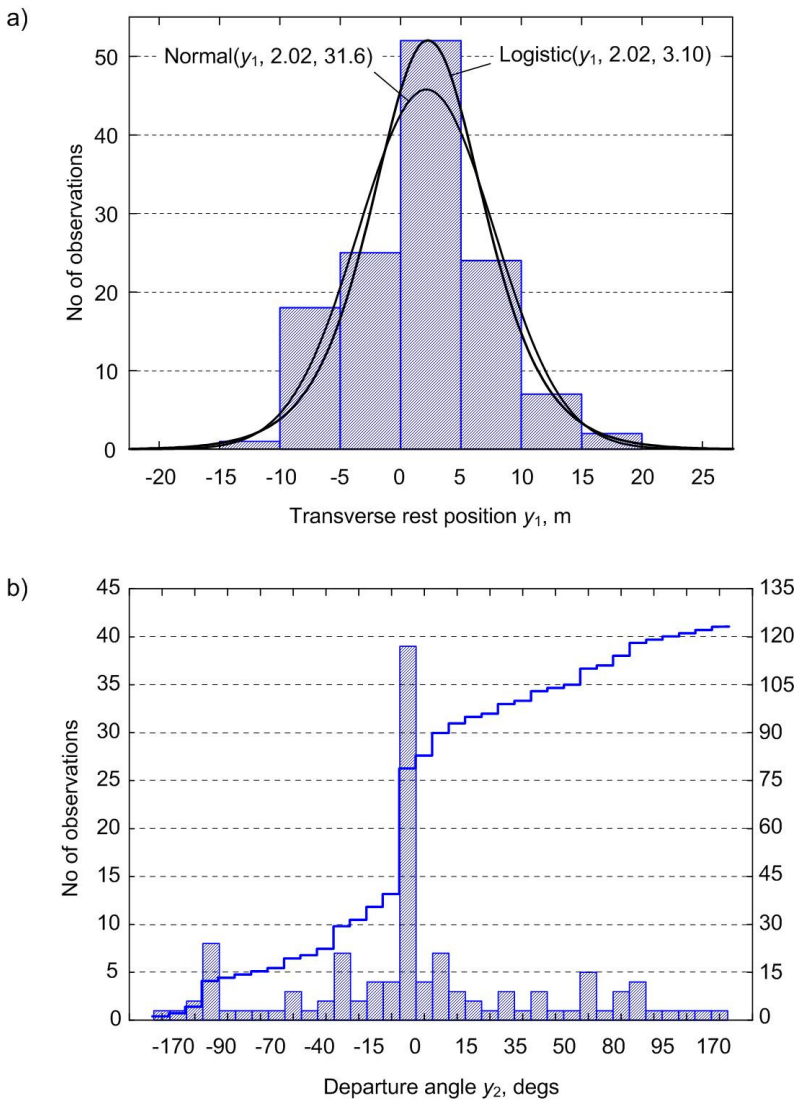**Fig. 2.6.** Visualisation of data on road tanker accidents: a) histogram of the transverse rest position values y_{1i} with superimposed normal and logistic densities; b) standard and cumulative histograms of the rest departure angle values y_{2i}
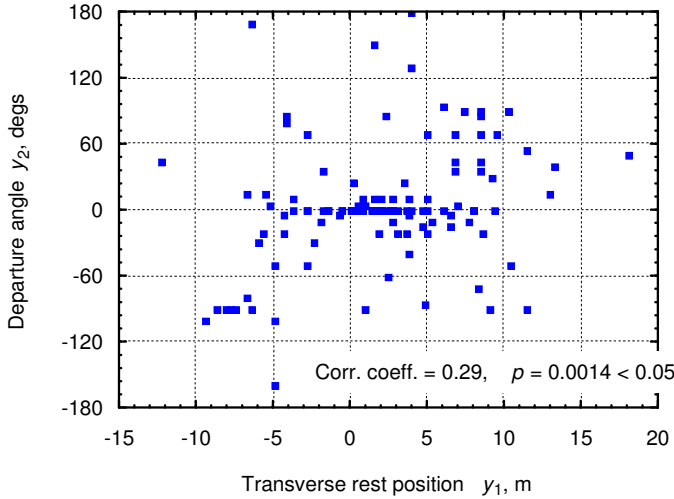
Fig. 2.7. Scatter diagram of the 119 observation pairs (y_{1i}, y_{2i})

The reports of the 151 accident underlying our database provide at least minimum statistical information on the probability distribution of the transverse rest position y_1 and the departure angle y_2. However, these reports tell little about the influence of accident situation and configuration of accident site on the rest position of the tank along its intended route. We will call this position the longitudinal rest position and denote it by y_3 (Fig. 2.5). Unfortunately, the data from the 151 accident do not allow to draw any specific conclusions about a stochastic relation between position y_3 and other two circumstantial characteristics y_1 and y_2.

2.2.1.2. Longitudinal rest position

A road tanker BLEVE will affect a relatively small territory within the transportation network. The road network fragment in this territory can be determined by introducing an unsafe distance around a vulnerable roadside object, for instance, the radius Δ_{max} around the "target" shown in Fig. 2.4. The most general and consistent criterion for the unsafe distance Δ_{max} can be a not exceedance of a tolerable value P_{max} of the damage probability $P(D \mid B)$ expressed as function of the explosion stand-off Δ:

$$\Delta_{max} = \operatorname*{argmax}_{\Delta} \{P(D \mid B, \Delta) \mid P(D \mid B, \Delta) \leq P_{max}\} \tag{2.3}$$

A solution of the above maximisation problem requires to predict uncertain BLEVE effects and to utilise methods of SRA for a repeated estimation of the

damage probability $P(D \mid B, \Delta)$ for different values of Δ (see, e.g., Vaidogas and Juocevičius 2007). The determination of Δ_{max} is beyond the scope of the present work.

As the road network fragment defined by Δ_{max} will be relatively small, any history of road tanker accidents in this area will almost certainly not be available. Consequently, a prediction of the longitudinal rest position y_3 will have to rely on either the knowledge about road tanker accidents in comparable situations or an educated guess. We think that the best way to deal with such a data situation is the predictive Bayesian approach to QRA (e.g., Aven 2003, 2009). Quantitative measures of uncertainty related to y_3 expressed in line with this approach can be integrated into a simulation-based prediction of accident locations.

2.2.2. Monte Carlo simulation of accident positions

2.2.2.1. Disaggregation of road segment

The prediction of the longitudinal rest position y_3 can be simplified by dividing the road network fragment within Δ_{max} into simpler shapes for which the density $f(y_3)$ can be assigned subjectively or on the basis of some prior knowledge. The roadway can be disaggregated into zones consisting of fixed length segments or homogenous segments in terms of roadway geometry, roadside features, traffic characteristics, etc. These zones should begin and end when their characteristics change. A disaggregation of road and rail network is basic to many applications of TRA, although the road network fragments considered in these applications are much larger than the area determined by the BLEVE-specific distance Δ_{max} (e.g., CCPS 1995; Gheorghe *et al.* 2005; Samuel *et al.* 2009). The disaggretation of roadways is also used for an assessment of road accident likelihoods (e.g., Chang 2005).

Fig. 2.4 shows a simple example of a disaggregation of the road segments within Δ_{max} into five zones with simple shapes. The width of these zones exceeds the road width to indicate that the transverse rest position of the tank can leave the road surface. In the absence of any historic data on road accidents in such zones, a uniform probability distribution of y_3 along the zone axes can be assumed for the purpose of simulation. Then the uniform density $f_k(y_3)$ will express maximum uncertainty related to the values of y_3 in the zone k.

The zones can be specified with relative ease for straight road segments and long horizontal curves. However, the specification can be conjectural and arbitrary to a degree in the road portions that have more complicated layout and/or indicate a higher proneness to road accidents. Such road portions are intersections and crossings, sharp curves, changes in the road width, wide variations in

traffic volume. Roadside features (e.g., numerous roadside objects) can also have influence on the specification of the zones.

The simulation requires to introduce a discrete probability distribution with the weights p_k ($k = 1, 2, \ldots, n_k$) assigned to individual zones, where n_k is the number of zones within Δ_{max} (e.g., $n_k = 5$ in Fig. 2.4). The weight p_k expresses the proneness of the zone k to a road accident involving tank vehicle. In line with the predictive Bayesian approach to QRA, the weights p_k quantify the analyst's degree of belief and can be a result of an educated guess or, alternatively, judgement based on some prior knowledge. In our opinion, there are at least four sources of such knowledge:

1. Statistical data allowing to obtain the distribution of relative frequencies of vehicle accidents by location (intersections, non-intersections, circles, etc.) (e.g., Al-Ghamdi 2003).
2. Mathematical models used to estimate the probabilities of vehicle accidents in specific locations (Spek *et al.* 2006; Ye *et al.* 2009; Haleen *et al.* 2010).
3. Models relating vehicle accidents to geometric design of roadway, roadside features, traffic characteristics and environmental conditions (Abdel-Aty and Radwan 2000; Lee and Mannering 2002; Chang 2005; Elvik *et al.* 2009).
4. Methods developed for an identification of crash hotspots (e.g., Cheng and Washington 2005; Huang and Abdel-Aty 2010; Montella 2010).

The data and models just listed have potential to be used for the specification of the weights p_k. However, we think that this body of knowledge is too loose and a special study is necessary to develop more or less formal procedures which utilise the knowledge for the choice of p_k. Practical procedures for ranking and weighting the zones can be borrowed in the field of multiple criteria decision making (MCDM). For instance, the weights p_k can be specified by organising an expert panel and utilising expert opinions by means of a well-known MCDM method called AHP (e.g., Luria and Aspinall 2003; Turskis and Zavadskas 2010; Vaidogas and Šakėnaitė 2010, 2011).

2.2.2.2. Modelling the transverse rest position

A further discrete probability distribution is necessary to choose a travel lane of the road tank. For brevity, we will consider a two-lane road only. Consequently, the distribution will have only two weights, say, π_1 and π_2. In the case where travelling frequencies of road tankers in both directions are equal, one can assume that $\pi_1 = \pi_2 = 0.5$. If the tank vehicles travel only in one direction, $\pi_1 = 0$ or $\pi_2 = 0$. With the weights π_1 and π_2 and the probability distribution of the

transverse rest position y_1 obtained in Sec. 2.2.1, the rest position of the tank centre with respect to the road centreline, y_4, can be modelled by the mixed density

$$\varphi(y_4|\,\pi_1,\,\pi_2) = \pi_1\,f(y_4|\,\theta_1) + \pi_2\,f(y_4|\,\theta_2) \tag{2.4}$$

where $f(\cdot)$ is the logistic density of the transverse rest position y_1 with the parameter vectors θ_1 and θ_2 adjusted to the cross-sectional dimensions of the road. If, for instance, the lane width is equal to 3 m and $y_1 \sim$ Logistic(2.02 m, 3.10 m), the densities $f(y_4|\,\theta_1)$ and $f(y_4|\,\theta_2)$ will be logistic ones with the parameter vectors

$$\theta_1 = (-3.52 \text{ m}, 3.10 \text{ m}) \text{ and } \theta_2 = (3.52 \text{ m}, 3.10 \text{ m}) \tag{2.5}$$

The logistic densities $f(y_4|\,\theta_1)$ and $f(y_4|\,\theta_2)$ with the above parameters are shown in Fig. 2.8a. This figure illustrates also the density $\varphi(y_4|\,\pi_1,\,\pi_2)$ with $\pi_1 = 0.7$ and $\pi_2 = 0.3$.

The densities $f(y_4|\,\theta_l)$ ($l = 1$ or 2) and $\varphi(y_4|\,\pi_1,\,\pi_2)$ in Eq. (4) are suited to the modelling of the transverse rest position y_4 in the case where y_4 is unbounded on both sides. However, the roadway and roadside territory can include natural and man-made obstacles which restrict the motion of vehicles after they leave the road surface or cross into opposite lanes of traffic. Examples of such obstacles are roadside barriers, medium barriers, backslopes, roadside structures.

A collision of a tank vehicle with a roadside obstacle (medium barrier) and its post-collision travel until a complete stop is a fairly uncertain process. A prediction of the transverse rest position y_4 resulting from this process is far from being trivial. However, one can say with fair degree of certainty that the obstacles, which are able to withstand an impact of a tank vehicle, determine the outermost values of y_4. Let these values be y_{4L} and y_{4R}. Then for the purposes of simulation one can assume that $y_4 \in [y_{4L}, y_{4R}]$ when obstacles are on both sides of the travel lane and $y_4 \in [y_{4L}, \infty[$ or $y_4 \in\,]-\infty, y_{4R}]$ when the obstacles are on the left or the right side, respectively. An illustration of y_{4L} and y_{4R} for a two lane road is shown in Fig. 2.8b, where $y_{4L} = 9$ m and $y_{4R} = -12$ m for the lane 1 and $y_{4L} = -12$ m and $y_{4R} = 9$ m for the lane 2.

Fitting a probability distribution of y_4 over the two-sided or one-sided intervals introduced above can be problematic. A relatively large amount of data required by standard fitting procedures will hardly be available for the reasons mentioned in Sec. 2.2.1. In addition, accident situations involving roadside obstacles are unique and this raises the question, whether the data collected in one roadside situation is representative to another situations.
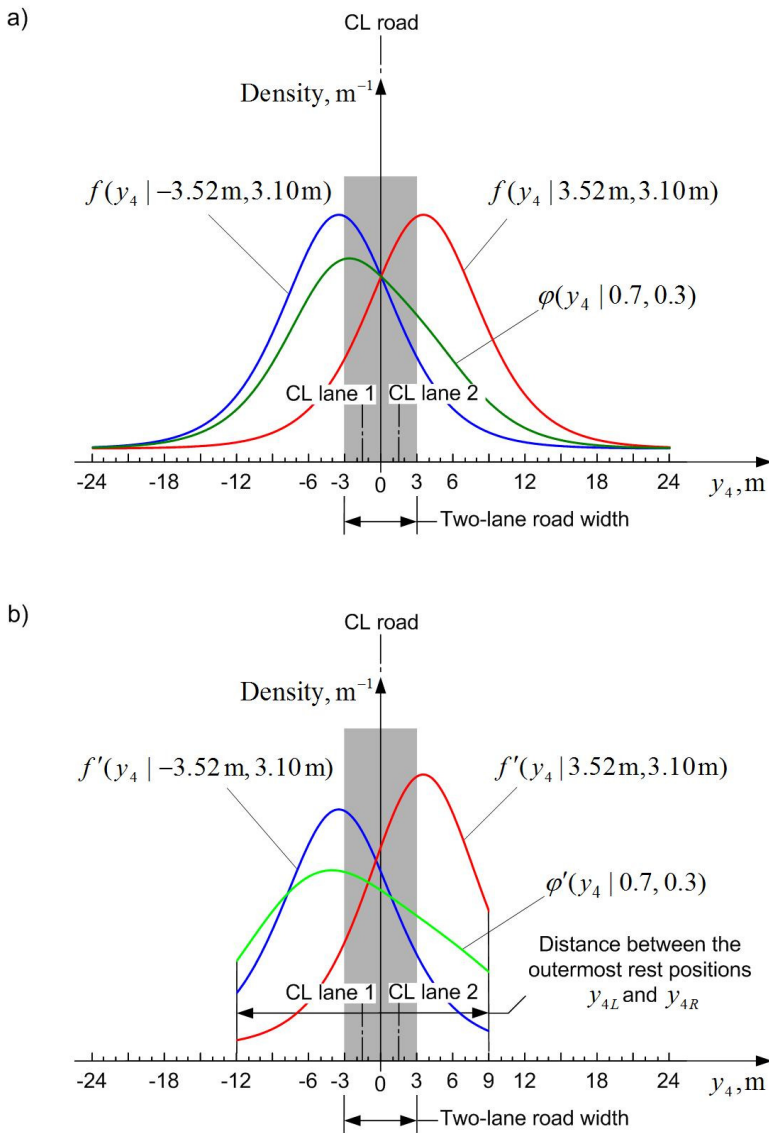
a)

CL road

Density, m^{-1}

$f(y_4 \mid -3.52\,\mathrm{m}, 3.10\,\mathrm{m})$

$f(y_4 \mid 3.52\,\mathrm{m}, 3.10\,\mathrm{m})$

$\varphi(y_4 \mid 0.7, 0.3)$

CL lane 1   CL lane 2

-24   -18   -12   -6 -3   0   3   6   12   18   24 y_4, m

Two-lane road width

b)

CL road

Density, m^{-1}

$f'(y_4 \mid -3.52\,\mathrm{m}, 3.10\,\mathrm{m})$

$f'(y_4 \mid 3.52\,\mathrm{m}, 3.10\,\mathrm{m})$

$\varphi'(y_4 \mid 0.7, 0.3)$

Distance between the
outermost rest positions
y_{4L} and y_{4R}

CL lane 1   CL lane 2

-24   -18   -12   -6 -3   0   3   6   9   12   18   24 y_4, m

Two-lane road width

Fig. 2.8. An illustration of the densities expressing uncertainties in the transverse rest position y_4 with respect to the centreline of a two-lane road: a) standard densities; b) truncated densities

However, the fact that values of y_4 are bounded by the values y_{4L} and y_{4R} suggests that the probability distribution of y_4 can be obtained by truncating the densities $f(y_4|\,\theta_l)$. The truncated density $f'(\,y_4|\,\boldsymbol{\theta}_l\,)$ is obtained from $f(\,y_4|\,\boldsymbol{\theta}_l\,)$ by means of the standard relations

$$f'(y_4) = \begin{cases} \dfrac{f(y_4)}{F(y_{4R}) - F(y_{4L})} & \text{if } y_4 \in]y_{4L}, y_{4R}[\\[2mm] \dfrac{f(y_4)}{1 - F(y_{4L})} & \text{if } y_4 \in]y_{4L}, \infty[\\[2mm] \dfrac{f(y_4)}{F(y_{4R})} & \text{if } y_4 \in]-\infty, y_{4R}[\end{cases} \qquad (2.6)$$

In the above relations, $F(y_4)$ is the cumulative distribution function of y_4 and the parameter vector θ_l is skipped for brevity. With the truncated densities related to opposite lanes, the truncated density related to the whole width of a two-lane road is obtained by

$$\varphi'(y_4|\,\pi_1, \pi_2) = \pi_1 f'(y_4|\,\boldsymbol{\theta}_1) + \pi_2 f'(y_4|\,\boldsymbol{\theta}_2) \qquad (2.7)$$

The density $\varphi'(\,y_4|\,\pi_1, \pi_2\,)$ is defined on the same interval as the constituent densities $f'(y_4|\,\boldsymbol{\theta}_l)$ (see Eq. (2.6)).

Fig. 2.8b presents an illustration of the densities $f'(y_4|\,\boldsymbol{\theta}_1)$ and $f'(y_4|\,\boldsymbol{\theta}_2)$ obtained by a truncation of a standard logistic density. The densities $f'(y_4|\,\boldsymbol{\theta}_1)$ and $f'(y_4|\,\boldsymbol{\theta}_2)$ are defined on the intervals $(y_{4L}, y_{4R}) = (9\ \text{m}, -12\ \text{m})$ and $(y_{4L}, y_{4R}) = (-12\ \text{m}, 9\ \text{m})$, respectively. Fig. 2.8b shows also the density $\varphi'(y_4|\,0.7, 0.3)$ calculated by means of Eq.(2.7).

The outermost rest positions y_{4L} and y_{4R} may not necessarily be fixed values. Such obstacles as trees and bushes planted in the roadside territory with moderate density may stop the motion of a tank vehicle after its departure from the road. Obstacles of this type may have randomly distributed distances from the road edge. In addition, the depth of a vehicle encroachment into the area of such obstacles may be highly random. Consequently, the outermost rest positions y_{4L} and y_{4R} may be uncertain quantities. They can be modelled as random variables with respective densities $f(y_{4L})$ and $f(y_{4R})$. Fig. 2.9 shows an illustration of the density $f(y_{4R})$ and the truncation point y_{4Rj} sampled from a probability distribution represented by $f(y_{4R})$.
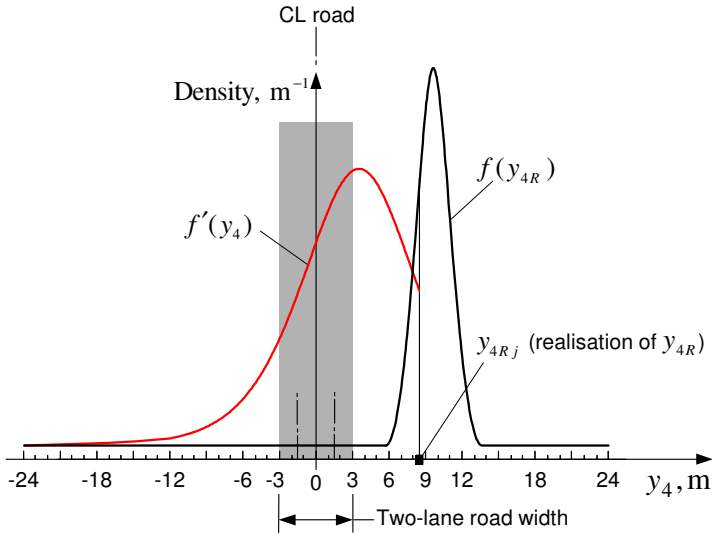
Fig. 2.9. The case of the density of the transverse rest position y_4 truncated at a random point

2.2.2.3. Algorithm of the simulation

With the models described in this section, the stochastic simulation of the tank rest position will consist in sampling values of the tank rest position and departure angle from underlying probability distributions. Each loop of the stochastic simulation of accident position, say, loop j should start from sampling of the zone number k from the discrete probability distribution defined by the weights p_k (Fig. 2.10). Then the values of the longitudinal and transverse position, y_{3j} and y_{4j}, must be sampled from corresponding probability distributions. This operation will be straightforward in case where y_3 and y_4 are considered to be independent. Finally the value of the departure angle y_{2j} can be sampled.

An application of the proposed simulation procedure with the flowchart shown in Fig. 2.10 is presented in the second part of this study (Vaidogas *et al.* 2012).The case study described in Sec. 2.2.4 applies the procedure to an existing site of potential BLEVE accident located in the coastal region of Lithuania.
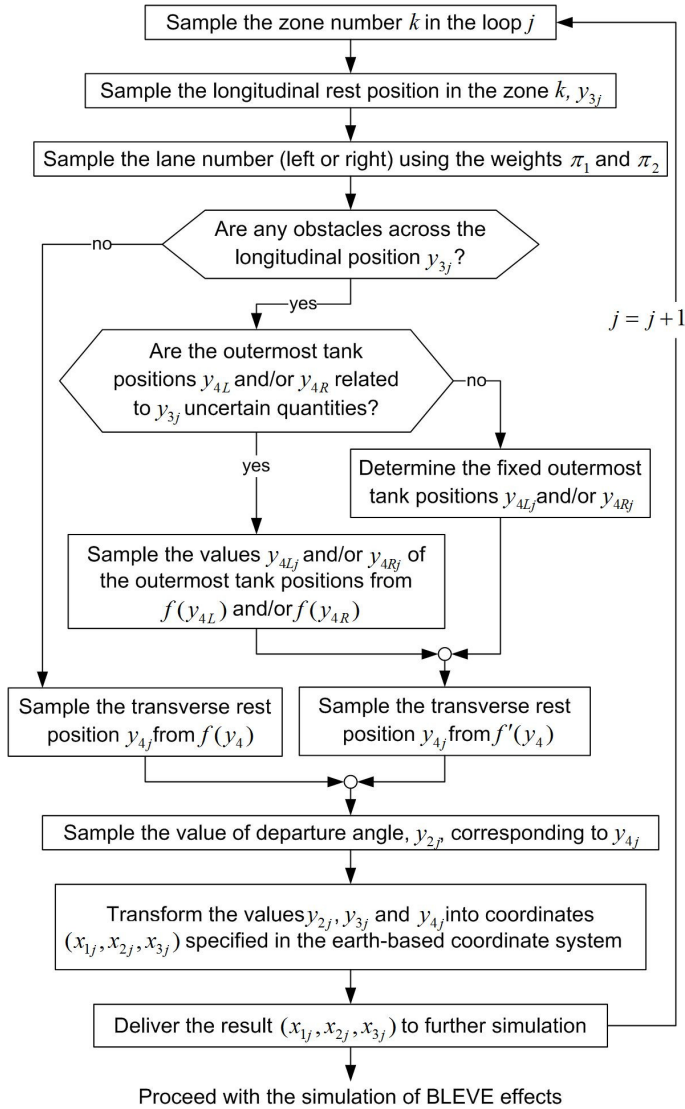
Fig. 2.10. A flowchart of the simulation step j

2.2.3. Prediction of fragment impact

2.2.3.1. Potential number of fragments

The potential number of fragments can be predicted by applying statistical data on previous BLEVEs of cylindrical vessels. Such data was presented by several authors and is systemized by Sun *et. al* (2012). The data covers BLEVEs which generated from one to nine fragments of cylindrical vessels. Such data is presented in the first two columns of Table 2.7.

Table 2.7. Data on fragmentation of cylindrical vessels in the course of BLEVEs (partially from Sun *et. al* 2012)

Number of fragments	Number of BLEVEs	Relative frequency	Number of BLEVEs with at least two fragments	Relative frequency
1	2	3	4	5
1	50	0.1931	—	—
2	98	0.3784	98	0.4689
3	78	0.3012	78	0.3732
4	24	0.0927	24	0.1148
5	3	0.0116	3	0.0144
6	2	0.0077	2	0.0096
7	3	0.0116	3	0.0144
8	0	0.0000	0	0.0000
9	1	0.0039	1	0.0048
Total:	259	1.0	209	1.0

One fragment was generated in 50 of 259 accidents. The case of only one fragment is characteristic for constrained vessels which are rigidly connected to a supporting structure. Vessels of tank cars can be considered to be unconstrained. The proof for that are the accidents with road tankers reported by Planas-Cuchi *et al.* (2004) and Bonilla Marinez *et al.* (2012). A fragmentation of such vessels in the case of a BLEVE will generate at least two projectiles which will fly in approximately opposite directions. Therefore, an estimation of the probabilities of specific numbers of fragments should be based on 209 accidents in which at least two fragments were generated (Column 4 in Table 2.7). Relative frequencies of BLEVE accidents with two to nine fragments are presented in Column 5 of Table 2.7. The latter frequencies are visualized in Fig. 2.11. This figure indicates clearly than the dominant numbers of fragments were two and three (84.2 % of cases). Four fragments were generated only in 11,5 % of cases. Five to nine fragments were encountered only in 4.3 % of cases.

A generation of two oblong end-caps must be considered the most hazard-ous in terms of a potential damage to roadside objects. The accidents of Spanish road tankers near San Carlos de la Rapita in 1978 and Tivissa in 2002 as well as in Murcia in 2011 clearly show that such fragments can be projected to long distances (Planas-Cuchi *et al.* 2004; Mannan 2005; Bonilla Marinez *et al.* 2012). Consequently, they may have large kinetic energy and damaging potential.
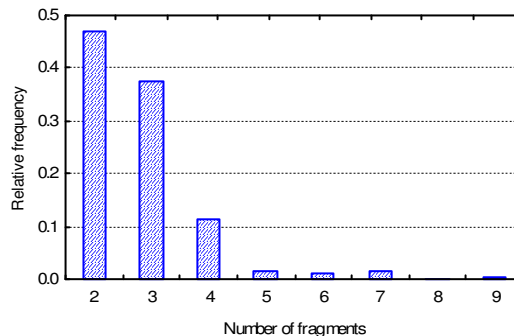

Fig. 2.11. Relative frequencies of generating two to nine fragments in BLEVEs of cylindrical vessels

The formation of two oblong end-caps can take place with and without a generation of further fragments (Gubinelli, Cozzani 2009; Mebarki *et al.* 2009). The tank vessel can burst simply into two fragments (Fig. 2.12ab). If the oblong end-caps will not involve the whole cylindrical part of the vessel, three or more fragments will be generated. The fragments other than end-caps will be parts of the cylindrical remainder (ring) (Fig. 2.12cd). These fragments are called "plates" (e.g., Nguyen *et al.* 2009).

The formation of two oblong end-caps can take place with and without a generation of further fragments (Gubinelli, Cozzani 2009; Mebarki *et al.* 2009). The tank vessel can burst simply into two fragments (Fig. 2.12ab). If the oblong end-caps will not involve the whole cylindrical part of the vessel, three or more fragments will be generated. The fragments other than end-caps will be parts of the cylindrical remainder (ring) (Fig. 2.12cd). These fragments are called "plates" (e.g., Nguyen *et al.* 2009).

The end-caps and oblong end-caps have a prevailing horizontal departure angles. Mebarki *et al.* (2009) notice that during the previous accidents:

1. A large number of end-caps and oblong end-caps were projected along the principal (longitudinal) axis of the vessel, whereas the plates were ejected in the perpendicularly to the principal axis.

2. A small number of end-caps and oblong end-caps were directed in the perpendicular direction, whereas a small number of plates were thrown along the longitudinal direction. The latter distribution of projectiles may result from possible rotation of end-caps, oblong end-caps and plates when they are unfolded and cut.
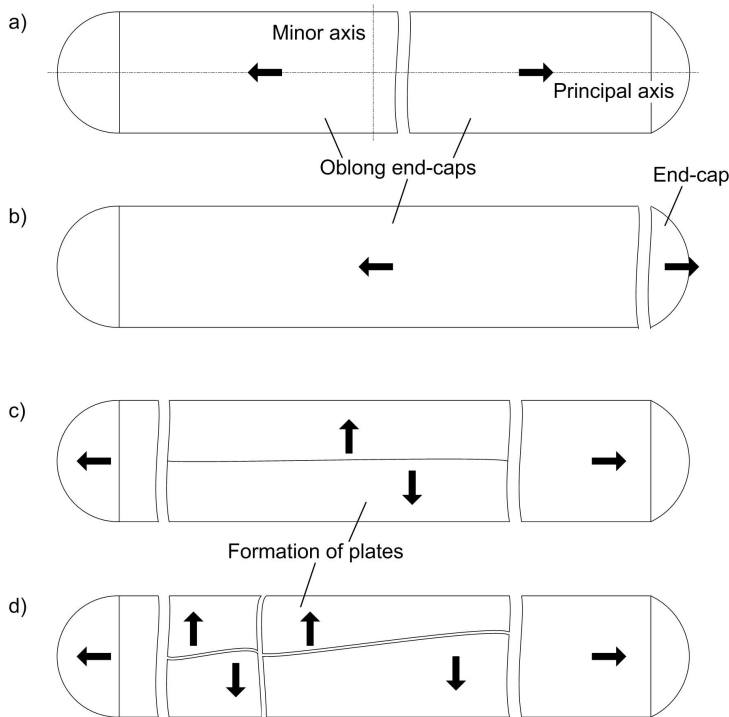

Fig. 2.12. Types of the tank car vessel fragmentation considered in the problem of projectile impact: a) and b) two fragments ejected in opposite directions; c) two oblong end-caps and unfolding cylindrical ring; d) the case of more than three fragments due to rupture of the cylindrical ring into several flattened fragments (plates)

In general, the fragmentation process can be more uncertain and complex. Some BLEVEs do not generate any projectiles (Holden 1988). Some of the generated fragments may not be projected far away. These fragments remain around the explosion centre and so do not endanger roadside objects. Furthermore, the oblong end-caps can disintegrate into two or three pieces, the flight of which is heavy to predict (Gubinelli and Cozzani 2009; Tugnoli *et al.* 2014). A BLEVE of a road tanker can also generate relatively light projectiles, which are internal elements of a tank vessel (baffles) and secondary fragments (tanker fittings and truck parts) (Planas-Cuchi *et al.* 2004).

Mathematical models, which allow an accurate prediction of number, shape and departure characteristics of all fragments generated by a BLEVE of a cylindrical vessel are not known to us. To facilitate the assessment of a potential impact of such fragments on safety barriers built in the roadside territory, the following simplifying assumptions were made:

1. The barrier must provide protection mainly against simple end-caps and oblong end-caps projected along the principal axis of the vessel. A possible, but not very probable projection of such fragments perpendicularly to the principal axis is ignored.
2. A safety barrier capable to protect against end-caps will provide protection against all other fragments of tanker vessel (mainly, flattened pieces of the cylindrical ring). Thus other fragmentations are less dangerous.
3. The probability of a generation of only two fragments (end-caps shown in Fig. 2.12a,b) is taken to be equal to the historical relative frequency 0.4689 given in Column 5 of Table 2.7.
4. Fragmentation of the tanker vessel into more than two pieces will occur as generation of two end-caps and cylindrical ring, which can form one fragment or disintegrate into two to three plates (Fig. 2.12c,d).
5. The probability of a generation of more than two fragments is equal to the relative frequency 0.5024. This number is a sum of the historical relatives frequencies given in Column 5 of Table 2.7 and related to the case of 3 to 5 fragments.

Consequently, the safety barriers were analysed not for all scenarios of BLEVE-induced vessel fragmentations. Only two fragmentations were considered. They are represented by the random events

B_2 = "Generation of only two end-caps (simple or oblong)"

B_{3-5} = "Generation of two end-caps and up to three additional fragments"

The conditional probabilities of these events given a BLEVE (random event B) are $P(B_2 \mid B) = 0.4689$ and $P(B_{3-5} \mid B) = 0.5024$. As other possibilities of vessel fragmentation were considered to be less dangerous and were ignored, the probabilities $P(B_2 \mid B)$ and $P(B_{3-5} \mid B)$ were adjusted to obtain their values which sum to unity. These probabilities were multiplied by the value $1/(0.4689 + 0.5024)$. Consequently, the values of $P(B_2 \mid B)$ and $P(B_{3-5} \mid B)$ used for the purposes of simulation are 0.4828 and 0.5172, respectively.

2.2.3.2. Masses and shapes of fragments

The masses of the fragments generated by a BLEVE of a tanker vessel can be modelled using two nominal masses: the mass of the end-cap, which will be

projected towards the target, $m_{e-c,\,front}$, and the linear mass of the cylinder, $m_{cyl,\,1}$ (Fig. 2.13a,b). The latter quantity can be obtained by dividing the total mass of the cylindrical part of the vessel by its length. Both masses, $m_{e-c,\,front}$ and $m_{cyl,\,1}$, can be calculated with sufficient accuracy from vessel specifications and may be treated as deterministic quantities. Geometry of opposite end-caps of some vessels can be not identical. Therefore, the simulation of the vessel position described in Secs. 2.2.1 and 2.2.2 must by used to determine which of the two non-identical ends of the tank will be directed towards a potential target or safety barrier.

a) disintegration into two fragments with the probability $P(B_2 \mid B) = 0.4828$
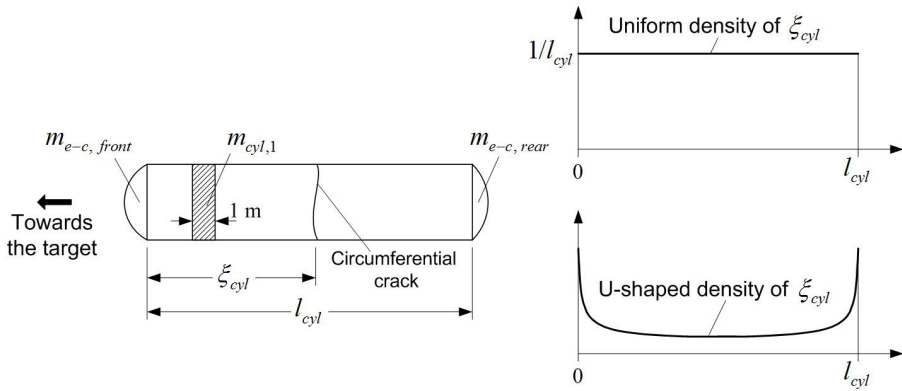
b) disintegration into more than two fragments with the probability $P(B_{3-5} \mid B) = 0.5172$

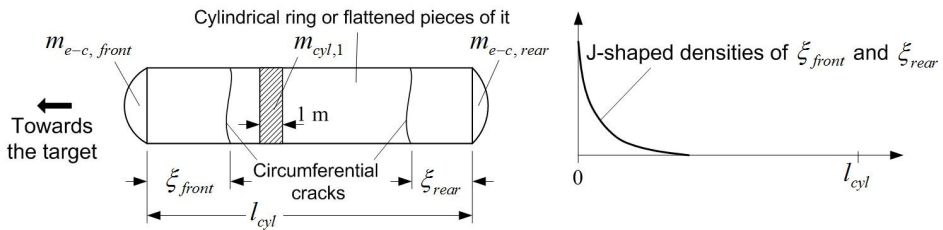**Fig. 2.13.** Deterministic and random quantities used to simulate masses of fragments: a) the case of two oblong end-caps; b) the case of two end-caps and one or several fragments generated by a disintegration of the cylindrical ring

In case of a formation of two fragments (simple or oblong end-caps), the random mass of fragment, ξ_{frg}, which is potentially directed towards the target, can be expressed by the simple formula

$$\xi_{frg} = m_{e-c,\,front} + m_{cyl,1}\,\xi_{cyl} \qquad\qquad (2.8)$$

where ξ_{cyl} is the length of the cylindrical part between the end-cap and circumferential crack, which will split the vessel into two fragments (Fig. 2.13a). Statistical data allowing to fit reliably a probability distribution of ξ_{cyl} seems not to be available. The main suggestion concerning the probability distribution of ξ_{cyl} is that this length may be assumed to be distributed uniformly over the interval $[0, l_{cyl}]$, where l_{cyl} is the length of the undamaged cylindrical part of the vessel (Mébarki *et al.* 2009; Nguyen *et al.* 2009). The uniform distribution will express maximum uncertainty in the position of the circumferential crack. In addition, an application of such distribution implies that the probability of a generation of simple, not oblong end-cups will be equal to zero, because $P(\xi_{cyl} = 0) = 0$ and $P(\xi_{cyl} = 1) = 0$.

If the annalist will feel that the formation of the circumferential crack in some parts of the cylinder is more likely than in other, he/she can apply a non-uniform distribution of the crack position ξ_{cyl}. For instance, the tendency of the circumferential crack to form closer to the cylinder ends can be expressed by a symmetrical or non-symmetrical U-shaped density. Fig. 2.13a shows an U-shaped beta density of ξ_{cyl} with the either of its shape parameters equal to 0.5. This distribution implies that the length of the ring attached to an end-cap will tend to be small. This means that a generation of fragments with the masses close to the mass of simple, not oblong end-cap will be likely.

Variety of simple and mixed univariate probability distributions potentially suitable to be fit to the interval $[0, l_{cyl}]$ is wide. Mixed univariate distributions can be applied to express subtleties of the crack position ξ_{cyl}. For instance, the cylindrical part may have two circumferential welds and the crack may tend to form in the vicinity of them. Then the position ξ_{cyl} can be expressed as a mixed random variable $\pi_1\xi_u + \pi_2\xi_{norm,1} + \pi_3\xi_{norm,2}$, where π_i ($i = 1, 2, 3$) are the weights, which sum to unity; ξ_{uni} is the uniformly distributed random crack position; $\xi_{norm,1}$ and $\xi_{norm,2}$ are two unimodal random variables (normal ones, say) with the mean values equal to positions of the welds.

Unfortunately, the crack position will depend on random factors, such as the place of maximal external heating as well as the position of mechanical defects and corrosive damage. Data and mathematical models, which allow to account for such factors, are not known to us. Therefore, our simulation was based on an application of the uniform distribution of the length ξ_{cyl}. This distribution expresses maximum uncertainty related to the circumferential crack position. At the same time, it implies a conservatively large probability of "heavy" oblong end-caps, that is, fragments with long portions of the cylindrical part.

Another case considered in our simulation was a formation of two simple or oblong end-caps and a cylindrical ring or several plates which can result from its disintegration (Figs 2.12c,d and 2.13b). The random mass of fragment, ξ_{frg}, which is potentially directed towards the target, can be expressed by the simple formula

$$\xi_{frg} = m_{e-c,\,front} + m_{cyl,1}\,\xi_{front} \tag{2.9}$$

where ξ_{front} is the length of the cylindrical part of the oblong end-cap which will be ejected towards the potential target (Fig. 2.13b).

The formation of two end-caps means that the simulation of fragment impact will have to take into account a formation of two circumferential cracks in the cylindrical part of the vessel. Positions of these cracks are random and can be expressed by two random variables ξ_{front} and ξ_{rear}. In case that only one end-cap will endanger a potential target, a specification of the probability distribution of only the front length ξ_{front} will be necessary. However, to determine what are the largest possible values of ξ_{front} and ξ_{rear} is very problematic. Therefore, the probability distributions of ξ_{front} and ξ_{rear} must be specified in such a way that the values of ξ_{front} and ξ_{rear} will not "overlap" and the length of the cylindrical fragment, $l_{cyl} - \xi_{front} - \xi_{rear}$, will be realistic.

As in the case of two fragments, we must state that statistical data allowing to fit reliably a probability distribution of ξ_{front} seems not to be available. As the first approximation, the crack positions ξ_{front} and ξ_{rear} will be modelled by applying a beta distribution adjusted to the intervals [0, l_{cyl}/2] and [l_{cyl}/2, l_{cyl}], respectively (Fig. 2.14). A beta distribution of this type with the shape parameters 0.41213 and 1.3926 is used to model fractional mass of a cylindrical tank vessel fragment (Mebarki *et al.* 2009; Nguyen *et al.* 2009). This distribution has a J-shaped density function. We modelled the random lengths ξ_{front} and ξ_{rear} by the product 0.5×ζ×l_{cyl}, where ζ is the random variable with a unimodal beta distribution Be(2.0, 4.0). The mode of this distribution is equal to 0.25. This means that the highest likelihood of formation of the circumferential cracks is at the distances 0.125 l_{cyl} and 0.875 l_{cyl} from the end of cylindrical part (Fig. 2.14). An application of a beta distributions to model ξ_{front} and ξ_{rear} has two advantages:

1. The values of ξ_{front} and ξ_{rear} will not exceed the half-length l_{cyl}/2 and so will not "overlap".
2. The beta distribution is very flexible and can be updated in the Bayesian sense when experimental or post-mortem data on fragmentation of cylindrical tanker vessels will become available.

To a first approximation, the crack positions ξ_{front} and ξ_{rear} may be modelled as two independent random variables.

With the random mass of the fragment directed towards a potential target and/or safety barrier, ξ_{frg}, as well as the geometry this fragment, a further simulation of fragment departure, flight and collision with the target (barrier) becomes possible.
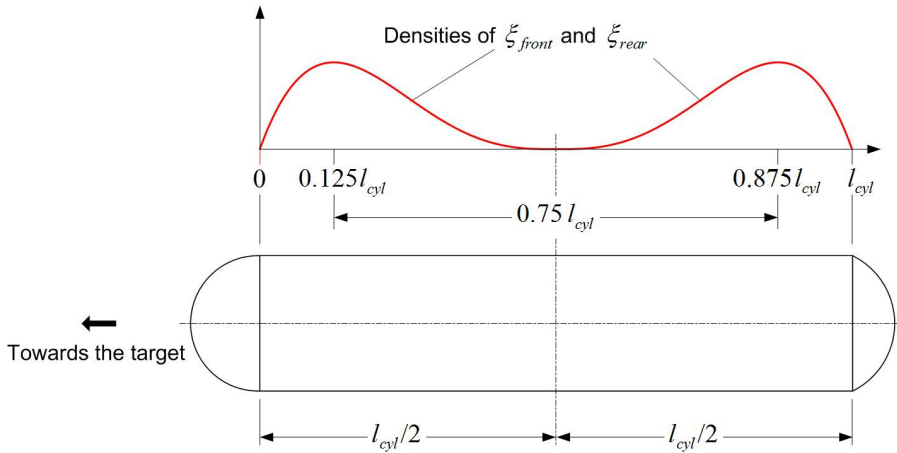

Fig. 2.14. A simulation of the random positions of two circumferential cracks, ξ_{front} and ξ_{rear}, in the case of the vessel fragmentation into two end-caps and a the cylindrical ring. The density functions shown in the figure are beta densities Be(2.0, 4.0) and Be(4.0, 2.0) adjusted to the half-length of the cylindrical part, $l_{cyl}/2$

2.2.3.3. Departure of characteristics and kinematics of fragments

There is a number of departure characteristics of simple and oblong end-caps which can be generated by a vessel fragmentation. Apart from masses and shapes of such fragments, the departure characteristics include:

1. The centre position of a vessel at the instant of a BLEVE.
2. The direction of the principal axis of the vessel in the coordinate systems which include vessel, road, target and/or a safety barrier (see an example in Fig. 2.15).
3. Horizontal and vertical departure angles (ς_1 and ς_2, say), within the aforementioned coordinate systems (see Figs. 2.15 and 2.16 as an example).
4. Departure velocity, say, v_{dep}.

The position and orientation of the vessel at the instance of fragmentation was considered in detail in Secs. 2.2.1 and 2.2.2. The departure velocity v_{dep} can be expressed as a random variable using models summarised by Mébarki *et al.*

(2009) and Nguyen *et al.* (2009). These models are explained in Annex B of the present work. The horizontal departure angle ς_1 can be assumed to be uniformly distributed over an angular sector of 60° around the principal axis shown in Fig. 2.15 (Holden 1988). Consequently, values of ς_1 will belong to the interval [–30°, 30°] and the density of ς_1 will be equal to 1/60 over this interval.

The vertical departure angle ς_2 is more difficult to predict than the horizontal one. Mébarki *et al.* (2009) stated that, from the existing literature, there is no reliable information about the vertical angle. They suggested to assume a uniform distribution of this angle over the interval [–90°, 90°].
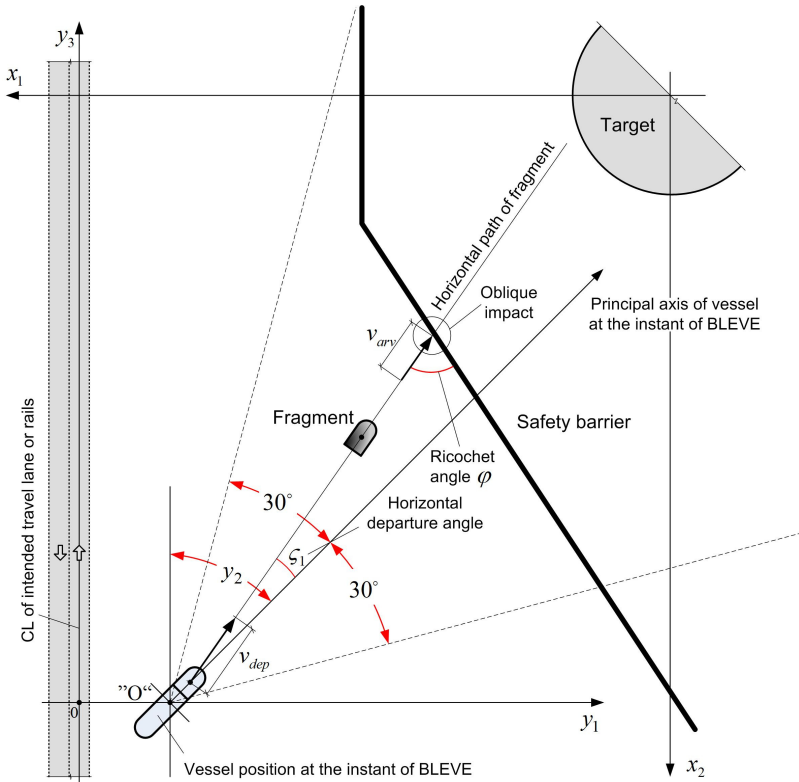

Fig. 2.15. Coordinate systems used to predict the impact of a fragment on target or safety barrier: earth-fixed coordinate system {0; x_1, x_2} and road- and vehicle-fixed coordinate system {0; y_1, y_2, y_3}
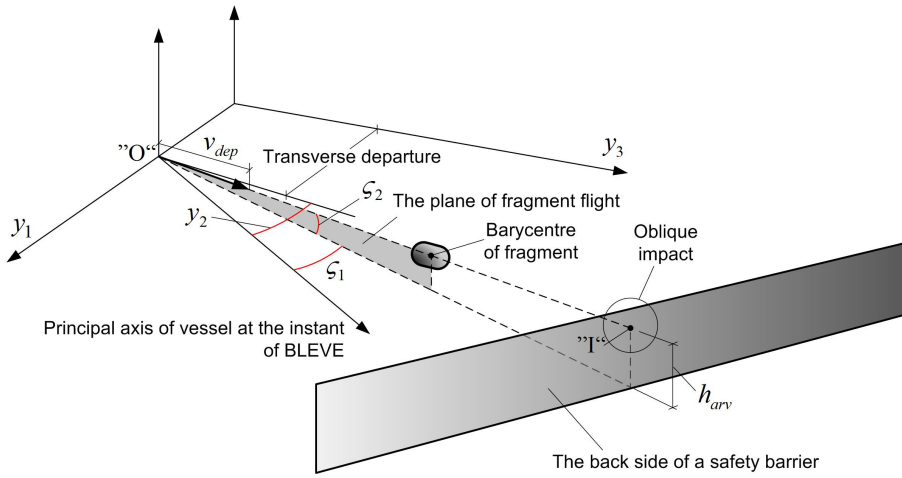
Fig. 2.16. Horizontal and vertical departure angles ς_1 and ς_2 in the road and vehicle-fixed coordinate system $\{0; y_1, y_2, y_3\}$

In our study of 151 road tanker accidents mentioned in Sec. 2.2.1, we detected one specific feature of three dominant rest position of tanker vessels:

1. In 70 cases, vessels were lying horizontally on carriageway or road shoulders (Fig. 2.17a).
2. In 15 cases, the vessels tumbled into the drainage channels outside the shoulders (Fig. 2.17b). The principal axis of the vessels was approximately parallel to the longitudinal road axis. Vessels were lying more or less horizontally. Pictures of a road tanker accident with such a vessel position before BLEVE are provided by Bonilla Marinez *et al.* (2012).
3. In 59 cases, the vessel came to the rest on side slopes. They were lying on the slopes and angles of inclination corresponded to those of the slopes (Fig. 2.17c).

The range of the vertical departure angle ς_2 can be assumed to vary within the range of 90° with respect to the principal and minor axes of the vessel (Fig. 2.17ac). However, the extreme values of ς_2 must take into account the inclination of surface, on which the vessel will rest before the explosion. This inclination may be measured with respect to the horizontal plane crossing the intersection of principal and minor axis of the vessel (Fig. 2.18). Let the inclination angle be ς_{ground}. Then the ranges of the vertical departure angle ς_2 with respect to this plane will be $[\varsigma_{ground}, 90°+ \varsigma_{ground}]$ and $[- \varsigma_{ground}, 90°- \varsigma_{ground}]$, as shown in Cases "a" and "b" of the Fig. 2.I, respectively.
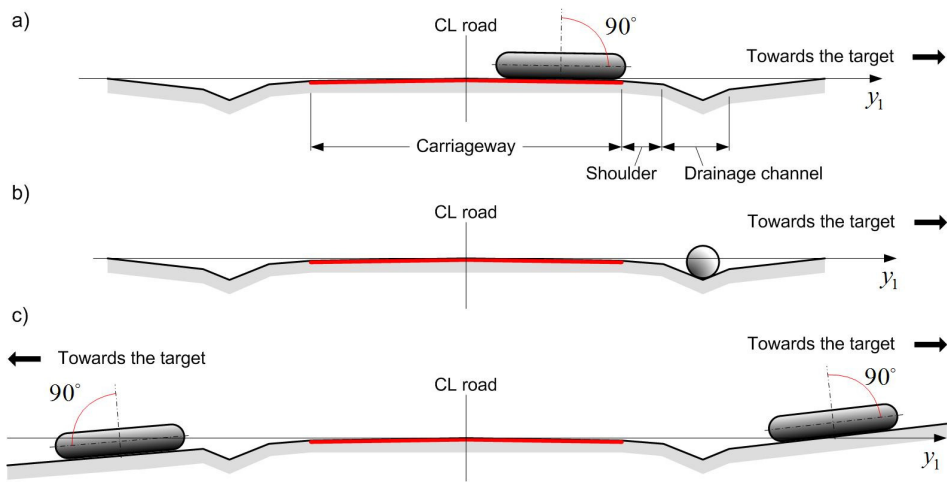
Fig. 2.17. The prevailing rest positions of road tanker vessels with respect to a horizontal orientation of the principal vessel axis: a) resting on carriageway with slight inclination; b) resting in the drainage channel; c) resting on roadside slopes with a non-negligible inclination
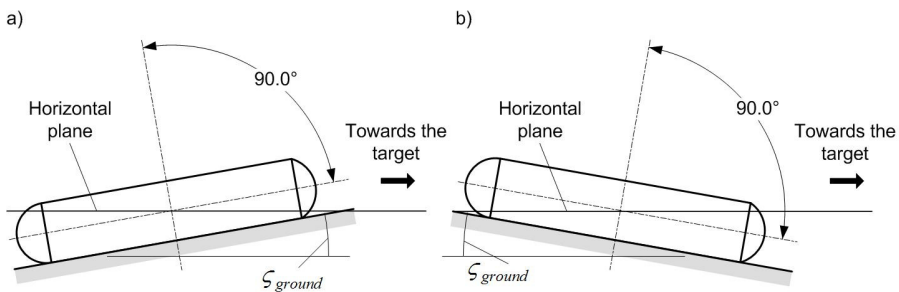
Fig. 2.18. The ranges of values of the vertical departure angle ς_2 prevailing rest positions of road tanker vessels with respect to with respect to a horizontal orientation of the principal vessel axis

The range of the vertical departure angle, $[\varsigma_{2,min}, \varsigma_{2,max}]$, is highly case-specific. In principle, it can be controlled and made less hazardous by changing the roadside relief in front of a target. For instance, Fig. 2.19b shows an upwards oriented slope which provokes a hazardous parabolic trajectory of a fragment. The roadside territory could be made less hazardous by flattering the area behind the drainage channel of the road.

The probability distribution of the vertical departure angle ς_2 must be ad-justed to the interval $[\varsigma_{2,min}, \varsigma_{2,max}]$. A sufficient amount of data allowing to relia-bly fit the distribution of ς_2 is not available, to the best or our knowledge. A uni-

form distribution of ς_2 over $[\varsigma_{2,min}, \varsigma_{2,max}]$ can be chosen, as suggested by Mébarki *et al.* (2009). However, this distribution seems to be too conservative in terms of the uncertainty related to the angle ς_2. We know the fact that the vertical departure angle ς_1 tends to be around the principal axis of the vessel. This allows to argue that vertical departure angle ς_2 will also be relatively small with respect to this axis. Therefore the probability density of ς_2 should be J-shaped and so exclude large values of ς_2. As a first approximation, we have chosen a beta distribution Be(0.7, 7) adjusted to the interval $[\varsigma_{2,min}, \varsigma_{2,max}]$ to model uncertainty related to values of ς_2. The beta densities of ς_2 are shown in Fig. 2.18. These densities imply that the probability of exceedance of the value $\varsigma_{2,min} + 30°$ are approximately equal to 3 %.

2.2.3.4. Kinematics of projected fragments

The trajectory of fragments projected from the exploding vessel results from the combined effects of inertia, gravitation and aerodynamics (drag and lift). A complete, three-dimensional (3D) model of fragment movement consists of three coupled differential equations presented in Annex B of this work. However, this model is often simplified making two assumptions (Nguyen *et al.* 2009):

1. The movement of the fragment can be described by the trajectory of its barycentre (Fig. 2.16).
2. The movement of the fragment can be analysed by using a bi-dimensional (2D) approach. The barycentre of the fragment will move in a plane which is perpendicular to a horizontal plane crossing the origin point "O". In Fig. 2.16 the latter plane is represented by the coordinate system $\{0; y_1, y_3\}$ and the vertical plane of the barycentre movement is determined by the horizontal departure angle ς_1.

In their classical book, Baker *et al.* (1983) suggest one further simplifying assumption. They state that the fragment will tumble during the flight and so the lift effect can be neglected (the lift coefficient can be taken equal to zero).

With the three simplifying assumptions listed above, the movement of fragment can be described by two coupled differential equations presented in Annex B. They can be solved numerically with the initial conditions given by vertical departure angle ς_2 and departure velocity v_{dep}. The solution of these equations will yield discrete points of trajectory. They can be used for estimating arrival (impact) velocity v_{arv} and the altitude of the impact point "I" on the surface of safety barrier or target (Figs. 2.16 and 2.18). The impact on barrier or target will be oblique. The ricochet angle of such an impact, φ, is shown in Fig. 2.15. This symbol and term is often used in the literature on the phenomenon of the oblique impact (e.g., Johnson *et al.* 1982). The angle φ can be deter-

mined by means of simple geometric calculations and will depend on the position of the origin point "O".
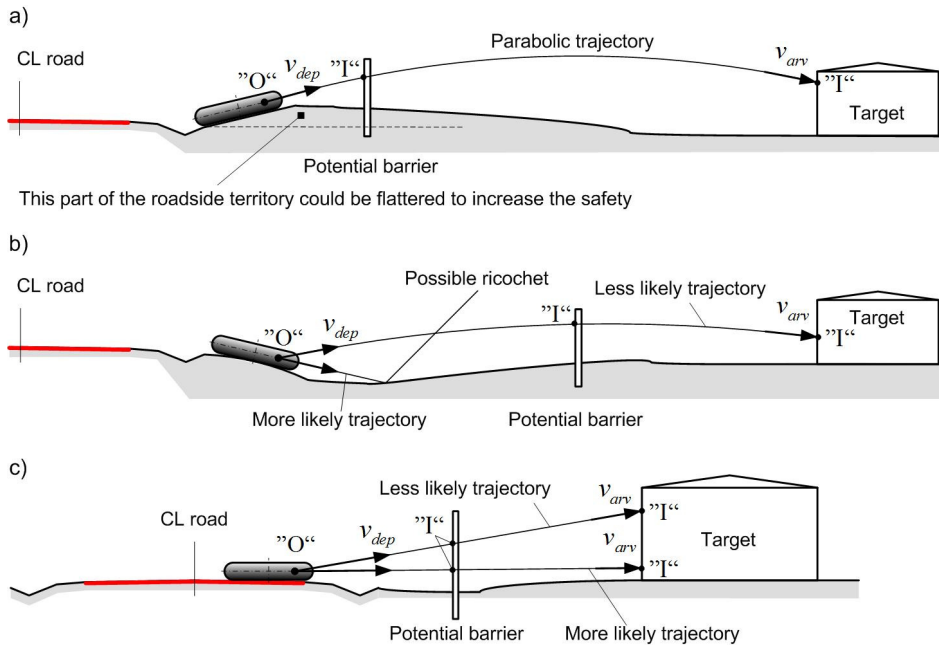
Fig. 2.19. The potential trajectories of projected fragments: a) parabolic trajectory; b) the possibility of a trajectory leading to a collision with ground; c) an approximately linear trajectory between vessel and target (barrier) located in close proximity

The departure velocity v_{dep} can be calculated by the formula suggested by many authors (e.g., Sun *et. al.* 2012):

$$v_{dep} = \sqrt{2E_k / \xi_{frg}} \qquad (2.10)$$

where E_k is the kinetic energy of generated fragment and ξ_{frg} is the mass of fragment given by Eqs. (2.8) or (2.9). The calculation of E_k is explained in Annex B.

The vertical departure angle ς_2, fragment trajectory will depend on the roadside relief. Long parabolic trajectories can be caused by an upwards inclination of vessel with respect to a target which is located relatively far from the road (Fig. 2.19a). In the case of a less hazardous downward inclination, trajectories may cause a collision of fragment with the ground (Fig. 2.19b). If the exploding vessel and target (barrier) will be located in close proximity, the curvilinearity of trajectory will be small and can be ignored. The trajectory can be assumed to be

linear (Fig. 2.19c). If the distance of fragment flight will be small, it will not loose much of energy. Then the departure velocity v_{dep} can be conservatively considered equal to the arrival velocity v_{arv}.

2.2.3.5. The case of railway tankers

The modelling of vessel fragmentation and projection of fragments outlined above is well-suited to the case of a road tanker BLEVE. In the past, accidents of this type involved only one tanker vessel. Although the number of well-documented BLEVE accidents on road is not large, the available information allows at least a rough prediction of vessel position and fragmentation at the instant of BLEVE. Data on BLEVEs of constrained vessels in fixed installations and general data on traffic accidents, in which road tankers were involved, can reinforce this prediction.

A prediction of position and spatial orientation of railway tanker vessels at the instance of a BLEVE is a more challenging problem. BLEVEs on railway occur in consequence of serious railroad accidents. They are caused by train derailments and impacts (Vaidogas *et. al.* 2012c). The cars are often chaotically scattered across tracks and the territory on either side of the tracks (e.g., TSB 1999). The derailed cars sustain considerable damage, are punctured and catch fires. They provokes " hot " BLEVES (Sec. 2.1).

The prediction of position and orientation of exploding vessel is complicated by the fact that the trains are often composed of several tank cars capable to sustain a BLEVE (BLEVE-prone cars). These cars are connected one after the other, that is, without intermediate cars which are BLEVE-proof (OTIF 2010). Therefore, a railroad accident can escalate into BLEVEs of two or more vessels. A classical example of such a scenario is the train accident in Crescent City (1970, US) (CCPS 1994). Fig. 2.20 shows derailment configuration and trajectories of fragments generated in this accident. The accident caused BLEVE explosions of two car vessels.

It is difficult to say in advance which of the BLEVE-prone cars will sustain the explosions as well as how many of these cars will explode. The considerable uncertainties related to railway tanker car explosions render a more or less accurate prediction of fragment projection a highly complicated task. Therefore, a safety barrier can be designed conservatively, namely, by applying two worst-case assumptions:

1. The exploding vessel will be at the closest possible distance from a potential safety barrier.
2. The safety barrier will have to resist a normal (not oblique) impact of a most hazardous fragment (heavy oblong end-cap).

The worst-case position of the exploding railway tanker vessel is illustrated in Fig. 2.20. The most conservative value of the vertical departure angle ς_2 can be assumed in addition to the assumptions just listed.
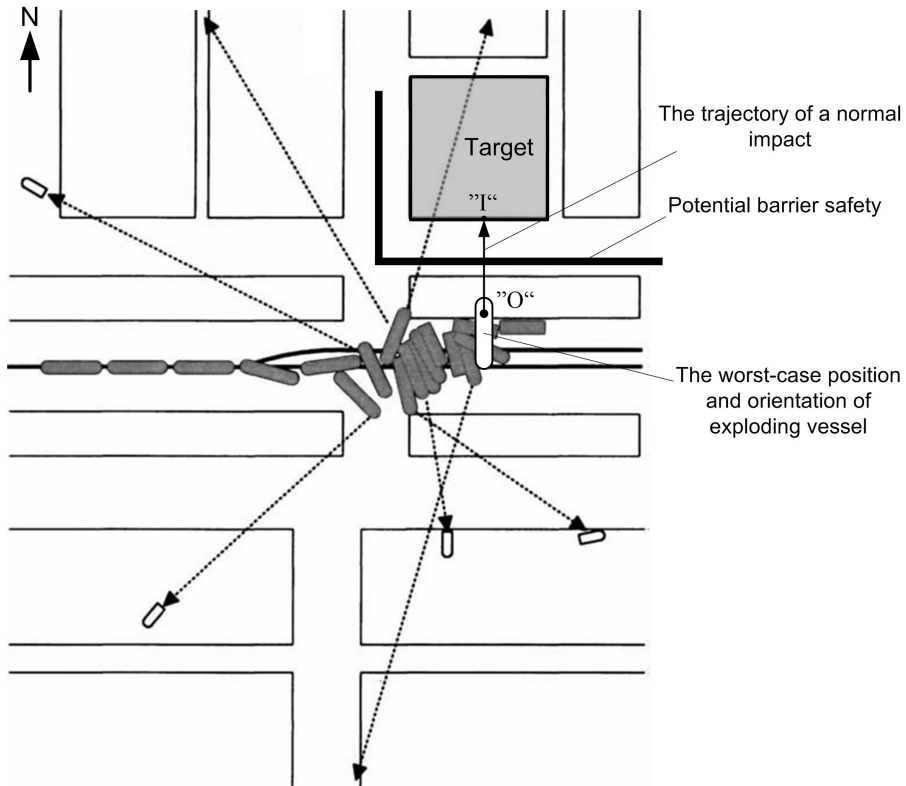
Fig. 2.20. The derailment configuration of Crescent City accident and the trajectories of major fragments shown by dotted lines. The figure shows also a worst-case position of a tanker car vessel with respect to a potential target (modified from CCPS 1994)

2.2.4. A practical application

2.2.4.1. The site of accident involving an explosion on road

The proposed approach to the simulation of the position of a road tanker accident will be illustrated by considering an oil transhipment facility built in Klaidpėda, the main seaport of Lithuania. The "target" in this example is three cylindrical reservoirs which can be damaged by a tank explosion on a road with two 3 m lanes going along the perimeter of the facility (Fig. 2.21). The road has

no gradient and the roadside territory is flat. Road tankers travel along the road in opposite directions with the approximate relative frequencies 70% and 30% (Fig. 2.22). Consequently, it is assumed that the probabilistic weights related to opposite lanes are $\pi_1 = 0.7$ and $\pi_2 = 0.3$.

Fig. 2.21. The three reservoirs exposed to the hazard of a road tanker BLEVE: a) view from the East side; b) view from the Northwest side (obtained by using the Google Earth software)

A schematic plan of the site under consideration is shown in Fig. 2.23. The unsafe segment of the road is determined by the distance Δ_{max} going from the centre of the 1st and 3rd reservoirs to the respective roadway edge. The distance Δ_{max} was assumed to be equal to 125 m. This is a tentative value serving as an illustration. The distance Δ_{max} was not specified by solving the optimisation problem given by Eq. (2.4) or by means of some other reasoning.

The road segment defined by Δ_{max} was disaggregated into five zones with different roadside features. The 13 m and 2 m land strips bounding the edge of the travel lanes in the zones indicate that tank rest position may lie outside the

road surface. The distance of 13 m is approximately equal to the typical length of a tank semi-trailer. Information on Zones 1 to 5 is summarised in Tables 2.3 and 2.4.

Fig. 2.22. The site of potential accident of a road tanker in vicinity of reservoirs
(obtained by using the Google Earth software)

The roadside territory of Zones 2 to 5 is bounded by densely growing trees on one roadside and the fence marking the perimeter of the facility on the opposite roadside. It is assumed that the fence constitutes an unmovable obstacle to the tank vehicle and so the outermost rest positions y_{4L} and y_{4R} will be transverse distances from the road centreline to the fence minus half-width of the tank semi-trailer (1.25 m, say). It is also assumed that the tank vehicle can encroach into the forest territory on the opposite roadside and therefore the outermost rest positions y_{4L} and y_{4R} related to this side will be considered random quantities and modelled by the normal distribution N(5 m, 0.25 m^2). Zone 1 is considered to have no obstacles on both sides of the road.

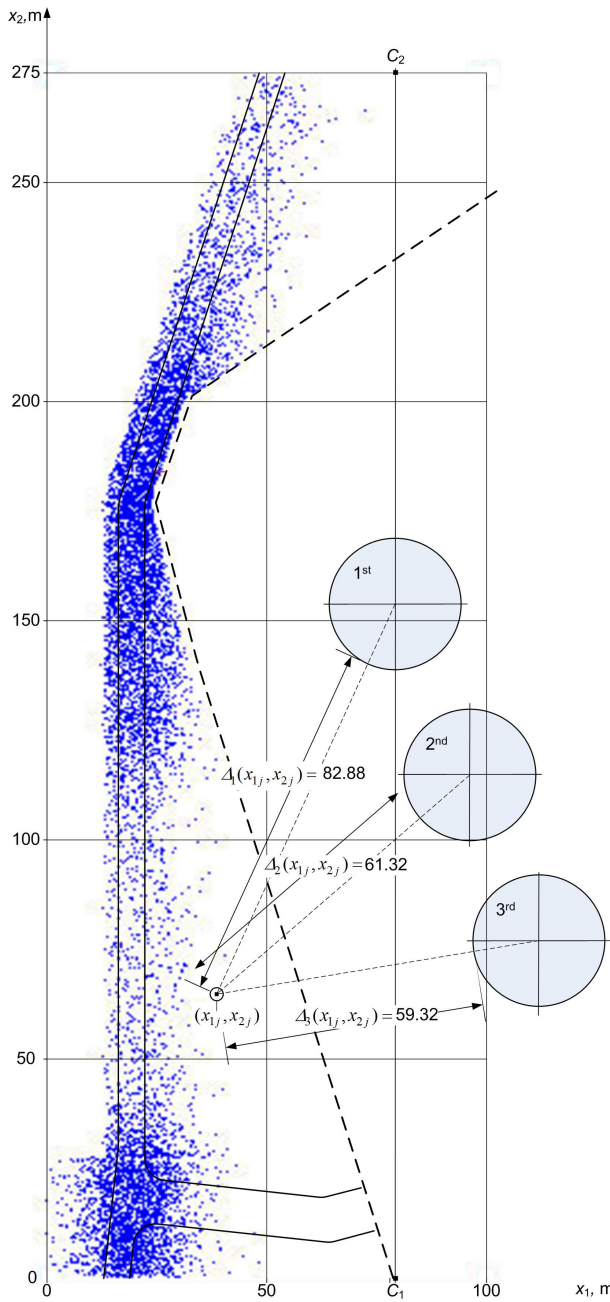**Fig. 2.23.** The scheme of the accident site

Fig. 2.24. Scatter diagram of the simulated accident coordinates (x_{1j}, x_{2j}) $(j = 1, 2, \ldots, N;$ $N = 10\ 000)$

Table 2.8. Information on the zones of the road segment introduced in Figs. 2.22 and 2.23

Zone number k	Length of zone, l_k, m	Road surface area A_k/A_{tot}^*, m^2/m^2	Probabilistic weight p_k
1	27	162/1650 = 0.0982	0.25
2	100	600/1650 = 0.3636	0.155
3	50	300/1650 = 0.1818	0.287
4	39	222/1650 = 0.1345	0.213
5	61	366/1650 = 0.2218	0.095

*A_{tot} = 1650 m^2;

** $f_{PF}(\cdot)$ and $f_T(\cdot)$ denote the power function density and triangular density, respectively (e.g., Evans *et al.* 2001)

Table 2.9. Probabilistic models of the longitudinal rest position of the tank in the zones 1 to 5

Zone number k	Probability density of the longitudinal rest position y_3
1	Uniform density: $f_{U1}(y_3) = 1/l_1$ ($y_3 \in [0, l_1]$)
2	Mixed power function** and uniform densities: $f_2(y_3) = 0.5\omega f_{PF}(y_3 \mid \boldsymbol{\theta}_1) + 0.5\omega f_{PF}(l_2 - y_3 \mid \boldsymbol{\theta}_2) + (1-\omega) f_{U2}(y_3)$ ($y_3 \in [0, l_2]$), where $\omega = 0.5$; $\boldsymbol{\theta}_1 = (12, l_2)$; $\boldsymbol{\theta}_2 = (19, l_2)$; $f_{U2}(y_3) = 1/l_2$
3	Mixed triangular** and uniform densities: $f_3(y_3) = \omega f_T(y_3 \mid \boldsymbol{\theta}) + (1-\omega)f_{U3}(y_3)$ ($y_3 \in [0, l_3]$), where $\omega = 0.2$; $\boldsymbol{\theta} = (0, l_3, l_3)$; $f_{U3}(y_3) = 1/l_3$
4	Mixed triangular and uniform densities: $f_4(y_3) = \omega f_T(y_3 \mid \boldsymbol{\theta}) + (1-\omega)f_{U4}(y_3)$ ($y_3 \in [0, l_4]$), where $\omega = 0.2$; $\boldsymbol{\theta} = (0, 0, l_4)$; $f_{U4}(y_3) = 1/l_4$
5	Mixed power function and uniform densities: $f_5(y_3) = \omega f_{PF}(l_5 - y_3 \mid \boldsymbol{\theta}) + (1-\omega)f_{U5}(y_3)$ ($y_3 \in [0, l_4]$), where $\boldsymbol{\theta} = (4, l_5)$; $f_{U5}(y_3) = 1/l_5$

2.2.4.2. Simulation of the longitudinal rest position

The probabilistic weights p_k ($k = 1, 2, \ldots, 5$) can be assigned to the zones in different ways. They include judgmental weighting often used for QRA (e.g., Aven 2003; Garrick 2008). However, as mentioned in Sec. 4.1, the weights p_k can also be specified by applying methods developed outside QRA, for instance, MCDM methods. A number of formal methods are suggested in the literature related to MCDM literature for specifying such weights as p_k in both crisp and fuzzy form (Hwang and Yoon 1981; Triantaphyllou 2000; Vaidogas and Šakėnaitė 2010 2011). These methods are used to elicit imprecise expert judg-

ments and convert the judgments into the weighs. However, these methods do not fully eliminate the specifying of p_k from subjectivity.

In the absence of any prior information, the weights p_k can be specified as the relative road surface areas of corresponding zones, A_k/A_{tot} (Table 2.8). However, one can argue that Zones 1, 3 and 4 are more prone to a vehicle accident that Zones 2 and 5. Therefore the weights p_k should reflect this increased proneness and not only the size of the zones.

Zone 1 includes a road intersection. Generally road intersections exhibit higher frequency of accidents as compared to other elements of roadway. For instance, Al-Ghamdi (2003) has found that the proportion of vehicle accidents at road intersections and non-intersections is approximately equal to 29% and 71%, respectively. As the stem of T-junction in Zone 1 is an access road to the facility and not a regular traffic artery, the proportion of 29% is too high for this intersection. We will use a somewhat reduced proportion expressed as the weight p_1 equal to 0.25 (Table 2.8). Consequently, the sum of the remaining four weights must be equal to 0.75.

Zones 4 and 5 have unfavourable roadside features. It is well-known that characteristics of roadside features have a significant effect on frequency and severity of traffic accidents (e.g., Lee and Mannering 2002). The fence and trees standing close to the roadway edge in Zones 4 and 5 impair visibility and restrict avoidance manoeuvre, especially at the turn between the zones. The weights p_3 and p_4 can be assigned to Zones 3 and 4 by comparing these zones to Zones 2 and 5. The latter pair is less prone to vehicle accidents because there are no turns on the ends of Zones 2 and 5 and these zones have roadside obstacles only on one side. Consequently, the sum $p_3 + p_4$ should exceed the sum $p_2 + p_5$. The absence of the obstacles on one side of Zones 2 and 5 can be the reason for the choice $(p_3 + p_4)/(p_2 + p_5) \geq 2$. A possible distribution of the pairs of weights can be $p_3 + p_4 = 0.5$ and $p_2 + p_5 = 0.25$. These aggregate weights can be distributed within the pairs p_3 and p_4 and p_2 and p_5 according to the relative road surface area A_k/A_{tot} given in Table 2.8:

$$p_{k(l)} = 0.25 \, A_{k(l)}/(A_k + A_l) \quad (k = 2, l = 5) \tag{2.11a}$$

$$p_{k(l)} = 0.5 \, A_{k(l)}/(A_k + A_l) \quad (k = 3, l = 4) \tag{2.11b}$$

where the subscript $k(l)$ indicates the weight p_k or p_l and the area A_k or A_l depending on which zone number is considered. The calculation with Eqs. (2.11) yielded the weights p_2 to p_5 given in Table 2.4. The distribution of the weights p_k along the 280 m road segment is shown in Fig. 2.25a.

The longitudinal rest position y_3 related to Zones 1, 2 and 5 was modelled by the uniform densities $f_k(y_3)$ defined in Table 1 and illustrated in Fig. 2.25b. The piece-wise uniform density shown in Fig. 2.25c is related to the entire

280 m road segment. This density was constructed from the products $p_k \times f_k(y_3)$. It is the simplest model of the longitudinal rest position with respect to the 280 m road segment. Unfortunately, the density shown in Fig. 2.25c has unnatural jumps. Therefore, mixed densities were applied to Zones 2 to 5 to smooth out these jumps. The general expression of the mixed densities is given by

$$f_k(y_3) = \omega\, f_{NU}(y_3) + (1-\omega)\, f_{Uk}(y_3) \qquad (2.12)$$

where $f_{NU}(\cdot)$ and $f_{Uk}(\cdot)$ are a non-uniform and uniform density, respectively. The non-uniform densities adapted to Zones 2 to 5 are explained in Table 2.5.

A power function distribution was used for smoothing out. This distribution is defined on a limited interval adaptable to the zone lengths l_k and allows a simple generation of random values by means of the inverse distribution function method (e.g., Evans *et al.* 2001). The triangular densities were applied to Zones 3 and 4. They are used to express a potentially increased concentration of y_3 values at the turn between the zones. The use of the mixed distributions of y_3 allowed to simulate the values of y_{3j} having a relatively smooth histogram (Fig. 2.25d).

2.2.4.3. Simulation of the transverse rest position

The sampling of the longitudinal rest position y_{3j} was followed by sampling of the transverse rest position y_{4j}. The values y_{4j} were generated from the logistic probability distributions fitted to the circumstantial data on road tanker accidents (Sec. 2.2.1). Each generation was preceded by a random choice among the lanes 1 and 2 with the respective weights $\pi_1 = 0.7$ and $\pi_2 = 0.3$ (Fig. 2.23).

In Zone 1, the position y_{4j} was sampled from standard (non-truncated) logistic distributions Logistic(–3.52 m, 3.10 m) and Logistic(3.52 m, 3.10 m) related to the lanes 1 and 2, respectively. In Zones 2 to 5, the position y_{4j} was sampled from logistic distributions with the same parameters; however, these distributions were truncated on both sides (Fig. 2.26). The unmovable truncation points y_{4Rj} or y_{4Lj} determined by the position of the fence and related to the respective lanes 1 or 2 were computed for each simulated value of the longitudinal rest position y_{3j}. The truncation points y_{4Rj} or y_{4Lj} related to the wood territory on the opposite road side were sampled from the normal distribution N(–5 m, 0.25 m^2) individually for each y_{3j}.

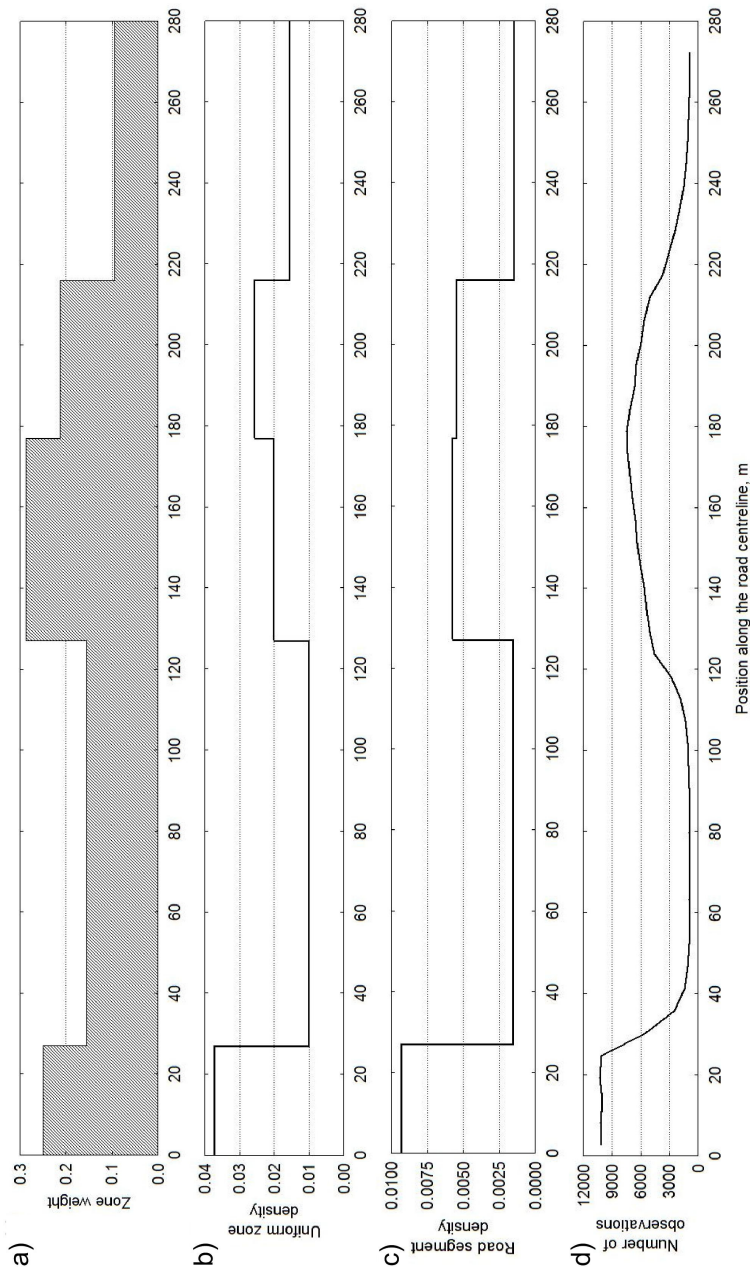**Fig. 2.25.** Modelling the longitudinal rest position y_3: a) the distribution of weights p_k assigned to Zones 1 to 5; b) the uniform densities $f_k(y_3)$ of y_3 related to individual zones; c) road segment density composed of the products $p_k \times f_k(y_3)$; d) the histogram of simulated values of y_{3j} obtained by smoothing the uniform densities as shown in Table 1 ($j = 1, 2, \ldots, N$; $N = 2\times10^{-5}$)
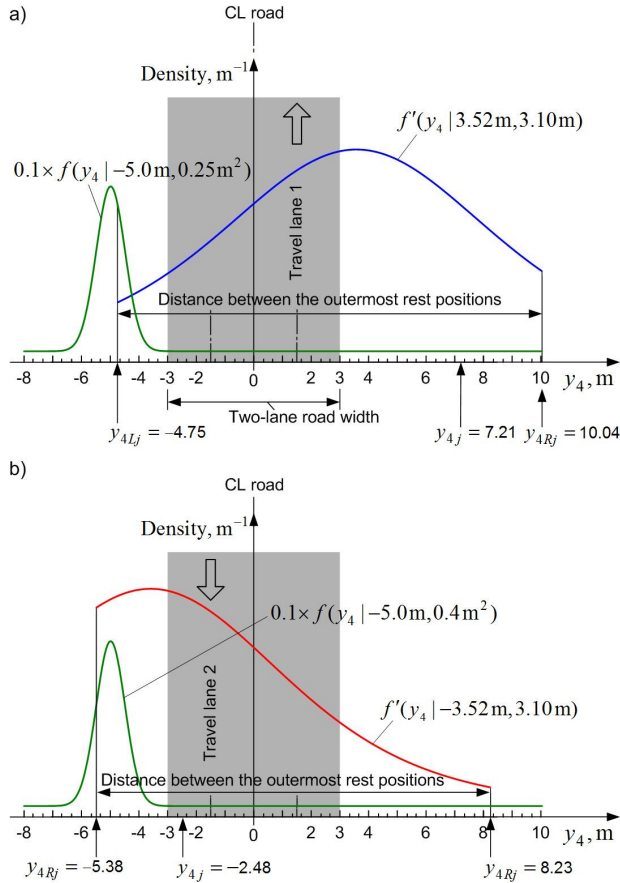
Fig. 2.26. Truncated logistic densities with the outermost rest positions [y_{4Lj}, y_{4Rj}] assigned to two values of the longitudinal rest position in Zone 3, y_{3j}: a) y_{3j} = 38.7 m; b) y_{3j} = –2.48 m

Fig. 2.26a shows the truncation interval [y_{4Lj}, y_{4Rj}] = [–4.75 m, 10.04 m] assigned to the longitudinal rest position y_{3j} = 38.7 m simulated for Zone 3 and travel lane 1. The transverse rest position y_{4j} = 7.21 m was sampled from the truncated Logistic(3.52 m, 3.10 m) with the density presented in Fig. 2.26a. The right truncation point y_{4Rj} = 10.04 m is the distance between road centreline and fence minus 1.25 m (half-width of tank semi-trailer). The left truncation point y_{4Lj} = –4.75 m was sampled from N(–5 m, 0.25 m^2) with the density shown in Fig. 2.26a. The truncation interval [y_{4Lj}, y_{4Rj}] = [8.23 m, –5.38 m] shown in Fig. 2.26b is related to the travel lane 2 in Zone 3. The value y_{4j} = –2.48 was sampled from the truncated density defined on this interval and shown in Fig. 2.26b.

Sampling from the truncated logistic distributions was carried out by applying the inverse distribution function method (e.g., Gentle 2003). The following formula was used for the generation:

$$y_{4j} = F^{-1}(u_j(F(y_{4Rj}) - F(y_{4Lj})) + F(y_{4Lj}) \mid \boldsymbol{\theta}_l) \tag{2.13}$$

where $l = 1$ or 2 depending on which lane is considered; $F(\cdot)$ and $F^{-1}(\cdot)$ are the direct and inverse distribution function of the logistic distribution, respectively.

The simulated pairs (y_{3j}, y_{4j}) related to the coordinate systems of individual zones were transformed into the rest position (x_{1j}, x_{2j}) in the coordinate system $\{0; x_1, x_2\}$ shown in Fig. 2.23. A scatter diagram drawn for 10 000 pairs (x_{1j}, x_{2j}) and in Fig. 2.24 reveals the concentration of potential BLEVE accidents in the territory under study. However, the tank centre coordinates (x_{1j}, x_{2j}) alone do not say anything about the orientation of the tank with respect to the road centreline and so the potential targets of BLEVE effects (reservoirs).

2.2.4.4. Simulation of the departure angles

The simulation of the departure angles y_2 was the most problematic part of this study. Values of the departure angle, y_{2j}, were sampled after sampling the pairs of the longitudinal and transverse rest position, (y_{3j}, y_{4j}). The sampling of y_{2j} was divided into two tasks:

1. Task 1: sampling of y_{2j} in the case where the road tanker is far from roadside obstacles and its rotation can not be restricted by them.
2. Task 2: sampling of y_{2j} when the obstacles can or will restrict the tank rotation.

In the current simulation step j, the tasks were distinguished by considering the difference between transverse rest position y_{4j} and distance to a potential obstacle, y_{oj}. Task 1 was solved when difference $|y_{oj} - y_{4j}|$ exceeded the half-length of tank semi-trailer (6.5 m in our case), whereas Task 2 took place when $|y_{oj} - y_{4j}| \leq 6.5$ m (Fig. 2.27).

Task 1 was performed by a data-based sampling of the values y_{2j} from the empirical distribution of y_2 introduced in the first part of this study (Vaidogas and Linkutė 2012). The weak stochastic dependence between transverse rest position y_4 and departure angle y_2 was expressed by a coefficient of correlation between y_4 and y_2 equal to 0.29. The values y_{2j} were sampled by means of the inverse transform method applied to a frequency polygon (e.g., Rubinstein and Melamed 1998). The stochastic dependence between the transverse rest position y_4 and the departure angle y_2 was regarded by applying the Thomson-Taylor data-based simulation (Gentle 2003).

Task 2 was much more difficult to solve due to lack (inaccessibility) of probabilistic models and circumstantial accident data allowing to simulate the departure angles in vicinity of roadside obstacles. Attempts to model in detail an interaction of vehicles with roadside objects are few and not directly applicable to a prediction of vehicle rotation angles (e.g., Ray 1999). Therefore the simulation of y_2 was underpinned by preliminary models which can be refined or replaced after new circumstantial information will be available.

The data-based sampling from the empirical distribution of y_2 was extended by an approach similar to the acceptance-rejection method widely used in the field of stochastic simulation (e.g., Korn *et al.* 2010). The initially simulated angle y_{2j} was rejected and replaced by a maximum possible rotation angle $y_{2j,max}$ in those simulation steps where $|y_{oj} - y_{4j}| \leq 6.5$ m (Fig. 2.27). The initial value y_{2j} was accepted or replaced by a new one using the simple rule

$$y_{2j} = \begin{cases} y_{2j,max} & \text{if } y_{2j} \geq y_{2j,max} \\ y_{2j} & \text{otherwise} \end{cases} \tag{2.14}$$

where $y_{2j,max}$ is the maximum possible rotation angle. The value of $y_{2j,max}$ was determined by the position of the fence on one roadside or trees on the opposite roadside.

The computation of $y_{2j,max}$ determined by the fence was straightforward. However, the restriction of the tank rotation by the wood on the opposite side of the road and so the simulation of $y_{2j,max}$ was nontrivial. It was assumed that values of maximum outmost point of the tank, y_o, are strongly and negatively correlated with the maximum outmost position of the tank centre represented by the truncation points on the roadside planted with trees, y_{4R} or y_{4L}. The pairs (y_{4Lj}, y_{oj}) and (y_{4Rj}, y_{oj}) related to the respective travel lanes 1 and 2 were sampled from a bivariate normal distribution with the correlation coefficient equal to – 0.9. Further parameters of this distribution are indicated in Fig. 6. The bivariate model assumes that the deeper is encroachment of the car into the wood the stronger is restriction of its rotation Fig. 2.28 illustrates the marginal densities of y_{4R} and y_o for the travel lane 2.

The simulation of the departure angles y_{2j} yielded the triples (y_{2j}, y_{3j}, y_{4j}) which were transformed into the coordinates (x_{1j}, x_{2j}, x_{3j}). The latter triples are visualized in Fig. 2.29 by means of arrows with the centre coordinates expressed by (x_{1j}, x_{2j}) and the rotation angle given by x_{3j} ($x_{3j} \in [0°, 360°]$).
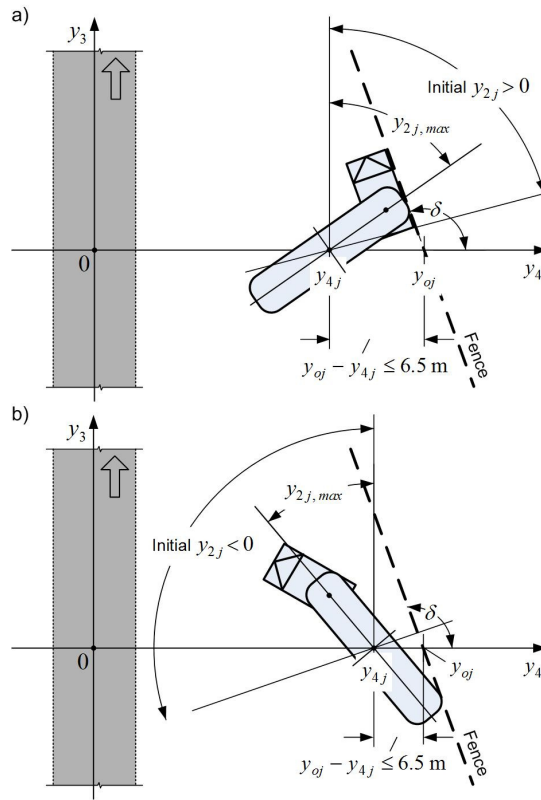
Fig. 2.27. Simulation of the departure angle y_2 in vicinity of the fence represented by the dimensions y_{oj} and δ: a) clock-wise rotation of the tank; b) counter clockwise rotation of the tank

2.2.4.5. Simulation of fragment impact on a potential barrier

The simulated coordinates (x_{1j}, x_{2j}, x_{3j}) can be used for assessing effects of fragments generated by a road tanker BLEVE. These fragments can be projected towards the reservoirs or a future safety barrier. The coordinates (x_{1j}, x_{2j}, x_{3j}) will express the position of tanker vessel at the instance of BLEVE.

A safety barrier can be built to protect the reservoirs depicted in Figs. 2.21 to 2.23. The barrier can run along the fenced perimeter of the facility. A possible barrier line (axis) is shown in Fig. 2.30 by the polygonal line $B_1 - B_5$. This figure also shows an illustration of four subsequent positions of a vessel sustaining a BLEVE, namely, (x_{1k}, x_{2k}, x_{3k}), $k = j, j + 1, j + 2$ and $j + 3$. The positions $j, j + 1$ and $j + 2$ are capable to generate a fragment with a trajectory which can intersect

the line $B_1 - B_5$. The position $j + 3$ means that such an intersection is impossible, as long as it is assumed that the horizontal departure angle ς_1 can vary within the 60 ° segment introduced in Sec. 2.2.3. Even if this segment will overlap the line $B_1 - B_5$, the fragment trajectory determined by the angle ς_1 will not necessarily intersect this line.
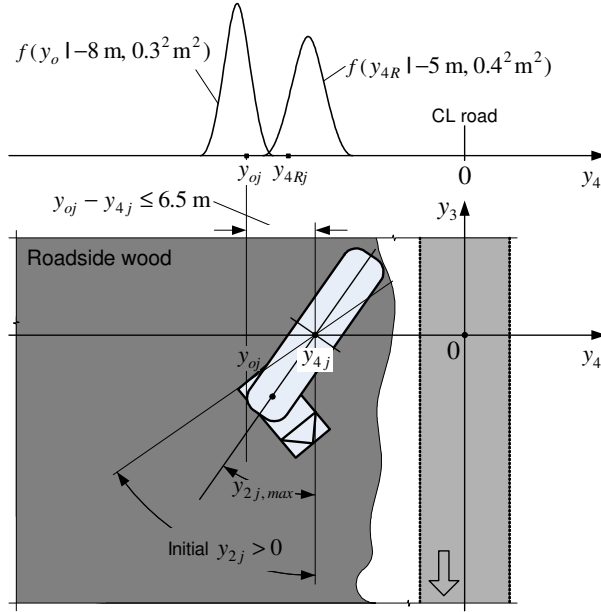
Fig. 2.28. Simulation of the departure angle y_2 in the case of a road tanker encroachment in the roadside wood with a clock-wise rotation with respect to travel direction

For each triplet (x_{1j}, x_{2j}, x_{3j}), values of the vertical and horizontal departure angles, ς_{1j} and ς_{2j}, can be sampled from the probability distributions suggested in Sec. 2.2.3. If the horizontal path of fragment shown in Fig. 2.30 will intersect the line $B_1 - B_5$, the simulation can be continued for the current triplet (x_{1j}, x_{2j}, x_{3j}). This simulation should start from sampling a value of the mass of fragment, $\xi_{frg,j}$, using the assumptions and probability distributions introduced in Sec. 2.2.3. The value $\xi_{frg,j}$ can be sampled by applying Eqs. (2.8) and (2.9) incorporated into the following formula:

$$\xi_{frg,j} = \begin{cases} m_{e-c,front} + m_{cyl,1}\, \xi_{cyl,j} & \text{if } u_j \in]0, 0.4828] \\ m_{e-c,front} + m_{cyl,1}\, \xi_{front,j} & \text{if } u_j \in]0.4828, 1[\end{cases} \qquad (2.15)$$

Fig. 2.29. A visualization of the simulated departure angle values x_{3j} shown by the arrows directed towards the front part of the tank vehicle ($j = 1, 2, \ldots, N$; $N = 1000$)

where u_j is a value random variable uniformly distributed over the interval]0, 1[; $\xi_{cyl,j}$ is a value of the cylindrical part between the end-cap and circumferential crack sampled form a uniform distribution over the interval]0, ξ_{cyl}[(Fig. 2.13a); $\xi_{front,j}$ is a value of the length of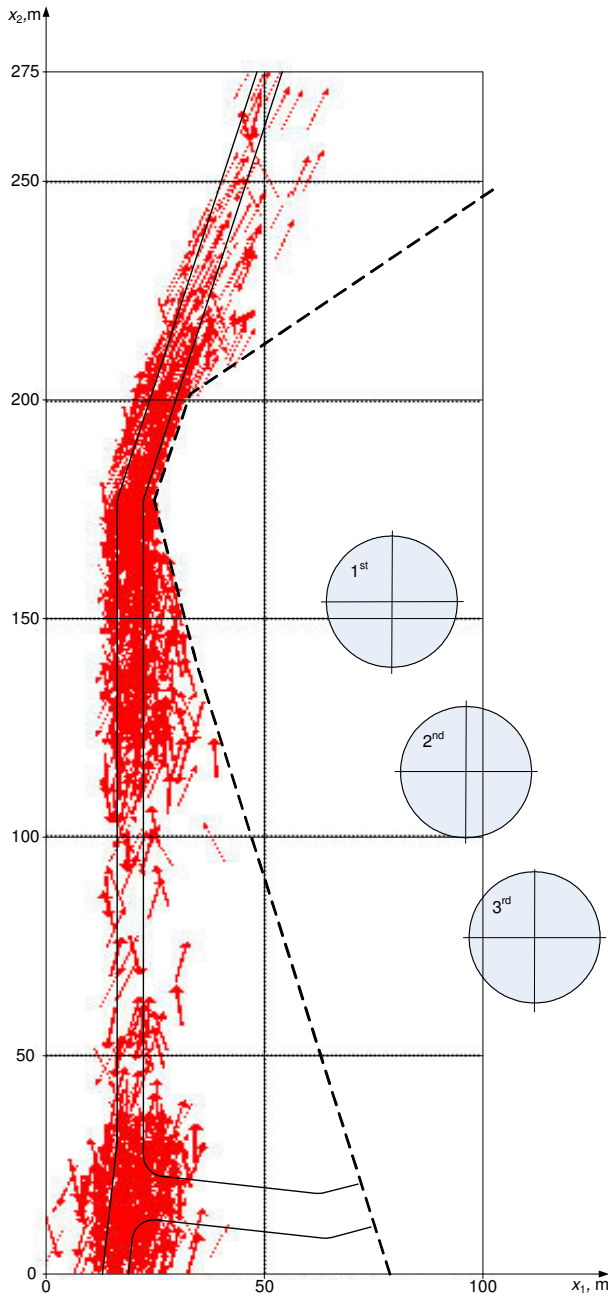 the oblong end-cap which will be ejected towards the line $B_1 - B_5$ (Fig. 2.13b). The value $\xi_{front,j}$ was sampled from the beta distribution Be(2.0, 4.0) adjusted to the interval [0, l_{cyl}/2]. The number 0.4828 given in Eq. (2.15) is the probability that the explosion will generate only two end-caps (Sec. 2.2.3). The masses $m_{e-c, \, front}$ and $m_{cyl,1}$ were calculated for a specific road tanker model (Annex C).

With the value of fragment mass, $\xi_{frg,j}$, a value of the departure velocity, $v_{dep,j}$ can be sampled using the formula

$$v_{dep,j} = \sqrt{2E_{k,j} / \xi_{frg,j}} \qquad (2.16)$$

where $E_{k,j}$ is a value of the kinetic energy of the fragment. This value can be simulated by applying the model described in Annex B.

The simulated values ς_{1j}, ς_{2j}, $\xi_{frg,j}$ and $v_{dep,j}$ yield initial conditions for a computation of fragment trajectory. Generally, this trajectory should be computed by solving the differential equations presented Annex B. However, the distances between the road segment $D_1 - D_3$ shown in Fig. 2.30 and the line $B_1 - B_5$ are relatively small. The largest distance is between the points D_3 and B_5. It is approximately equal to 65 m. In addition, the relief between road and reservoirs is flat and nears a horizontal plane (Fig. 2.21). Therefore we assumed that the fragment trajectories will be approximately linear and can be modelled as shown in Fig. 2.19c. In addition, it was assumed that the arrival (impact) velocities $v_{arv,j}$ and will be equal to the departure velocities $v_{dep,j}$. This assumption is also justified by the small distances between the road and the line $B_1 - B_5$.

To assess the impact of fragments on a barrier, which will run along the line $B_1 - B_5$, the following numbers of the triplets (x_{1j}, x_{2j}, x_{3j}) were generated:

1. A total of 1×10^6 triplets for estimating the frequencies of an impact of fragments on the individual barrier segments $B_1 - B_2$, $B_2 - B_3$, $B_3 - B_4$ and $B_4 - B_5$ (see Fig. 2.30).
2. 100 000 triplets for calculating descriptive measures of simulated samples of fragment impact characteristics.
3. 10 000 triplets for visualising characteristics of the samples just mentioned.

x_2, m

275

250

18°

$x_{3,j+1}^{-i}$

(x_{1j+1}, x_{2j+1})

D_1

B_1

$v_{dep,j+1}$

$\varsigma_{1,j+1}$

$\varsigma_{inc,j+1}$

(x_{1j+2}, x_{2j+2})

$\varsigma_{inc,j+2}$

$v_{arv,j+1}$

$v_{dep,j+2}$

B_2

200

$\varsigma_{1,j+2}$

$v_{arv,j+2}$

177

D_2 B_3

Fenced perimeter of the facility = Potential barrier line

1st reservoir

150

B_4

127

←16.2→ ←6

2nd reservoir

100

(x_{1j+3}, x_{2j+3})

$v_{arv,j}$

ς_{1j}

30° 30°

x_{3j}

$\varsigma_{inc,j}$

3rd reservoir

50

$v_{dep,j}$

(x_{1j}, x_{2j})

27

Access road

0

0   D_3 50   78   100   130 x_1, m

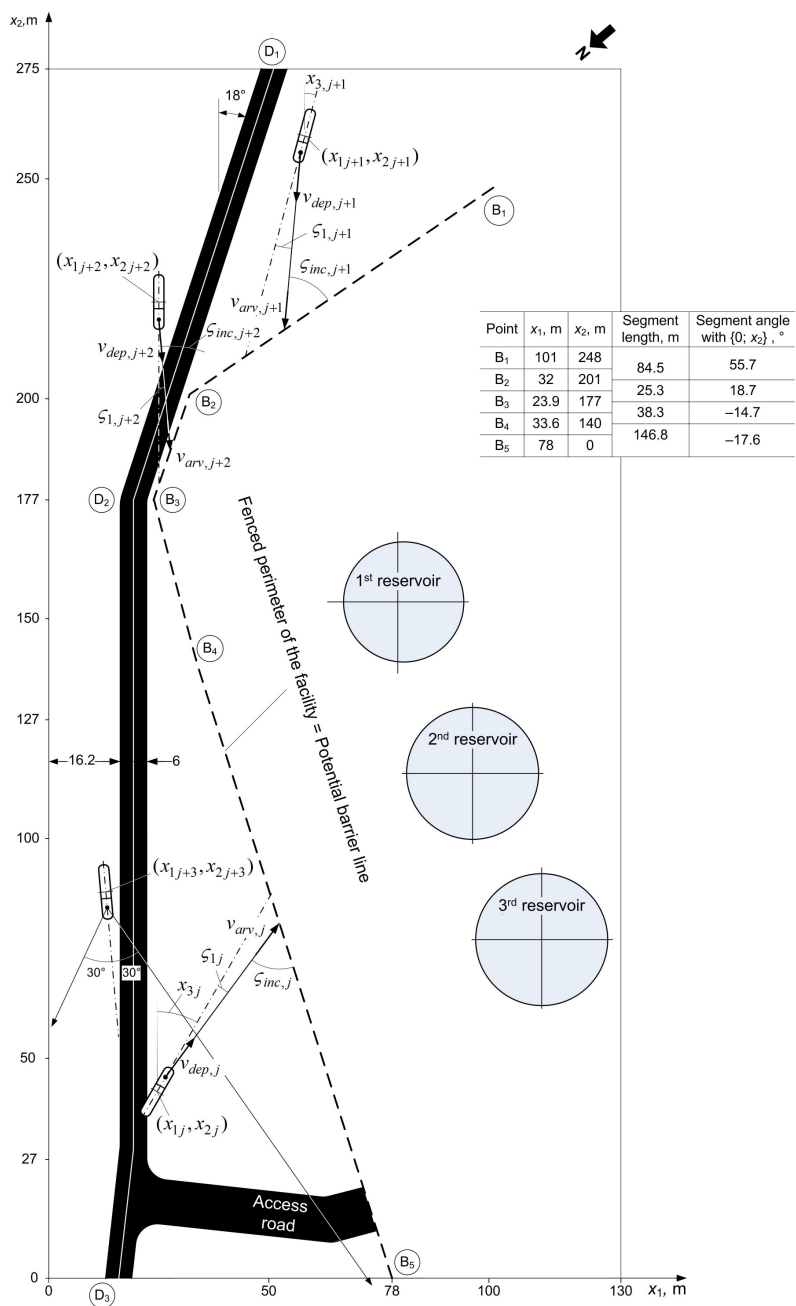| Point	x_1, m	x_2, m	Segment length, m	Segment angle with {0; x_2}, °
B_1	101	248	84.5	55.7
B_2	32	201	25.3	18.7
B_3	23.9	177	38.3	−14.7
B_4	33.6	140	146.8	−17.6
B_5	78	0		

Fig. 2.30. An illustration of simulated trajectories of the fragments generated by a road tanker BLEVE

For each triplet (x_{1j}, x_{2j}, x_{3j}), the values of the horizontal and vertical departure angles, ς_{1j} and ς_{2j} were sampled from the corresponding probability distributions and it was checked, whether the horizontal path of fragment trajectory will cross the line $B_1 - B_5$. In 483 216 cases from 1×10^6 simulations, the fragment trajectories crossed this line. Thus, a rough estimate of the probability that the fragment will hit the barrier given a BLEVE is equal to 0.483. The numbers of crossings of individual barrier segments $B_1 - B_2$, $B_2 - B_3$, $B_3 - B_4$ and $B_4 - B_5$ along with relative frequencies and mean values of the samples of simulated impact characteristics are given in Table 2.10.

Fig. 2.31 shows a three-dimensional scatter diagram of 4774 points, where the fragment trajectories crossed the vertical plane running along the points B_1 to B_5. These points were obtained with 10 000 simulations of vessel fragmentation and fragment flights. Fig. 2.37 shows the scatter diagram of the points where fragment trajectories crossed the vertical plane running along the barrier segment $B_4 - B_5$. Figs. 2.31 contain histograms of the simulated samples of impact characteristics: masses of impacting fragments, $\xi_{frg,j}$, impact velocities $v_{arv,j}$, ricochet angles φ_j and altitudes of impact points $h_{arv,j}$ (see Figs. 2.15 and 2.16 for a visualisation of φ_j and $h_{arv,j}$; $j = 1, 2, ... , 4774$).
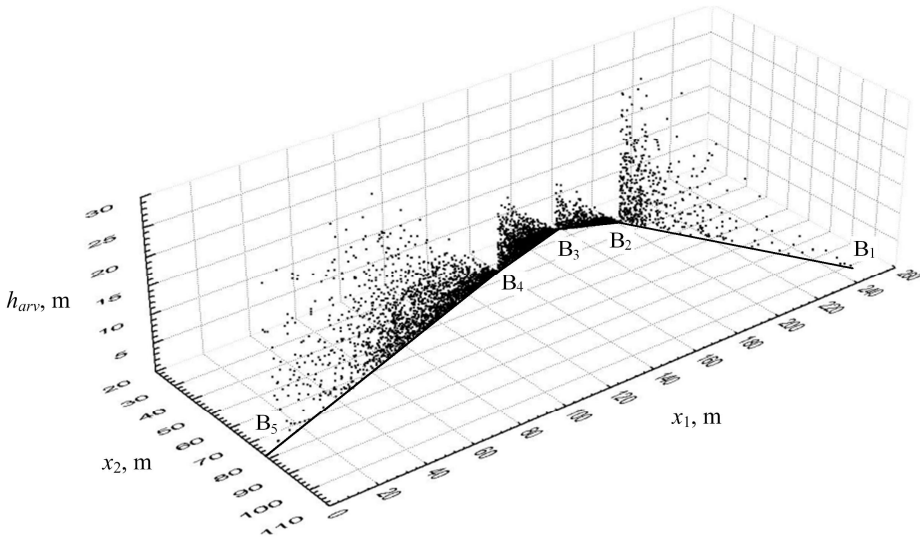

Fig. 2.31. The scatter diagram of 4774 triplets $(x_{1,j}, x_{2,j}, h_{arv,j})$ showing the points, where the fragments crossed the vertical plane running along the barrier line $B_1 - B_5$ ($x_{1,j}$ and $x_{2,j}$ are the horizontal coordinates of intersection point j and $h_{arv,j}$ is the altitude of this point)

The 483 216 intersections counted in 100 000 simulations produced four samples consisting of values of $\xi_{frg,j}$, $v_{arv,j}$, φ_j and $h_{arv,j}$. Mean values of these samples are given in Table 2.10, whereas comprehensive information about them can be found in Annex D. This information consists of descriptive measures of the samples as well as coefficients of correlation between sample components.

Table 2.10. Results of the simulation of fragment flights across the barrier segments B_1–B_2, B_2–B_3, B_3–B_4 and B_4–B_5

Simulation result	Barrier segment			
	B_1–B_2	B_2–B_3	B_3–B_4	B_4–B_5
Number of crossings[1]	50 768	55 315	167 342	209 791
Relative frequency of crossings[1]	0.50768	0.55315	0.167342	0.209791
Mean of $\xi_{frg,j}$ values, kg[2]	3931	4073	4137	4117
Mean of $v_{arv,j}$ values, km/h[2]	208	202	200	199
Mean of φ_j values,° [2]	49.3	24.1	30.4	38.0
Mean of $h_{arv,j}$ values, m[2]	13.1	2.2	3.17	9.0
Mean of $d_{hor,j}$ values[2]	23.4	16.3	46.7	75.0

[1] Obtained with 1×10^6 simulations of fragment flights
[2] Obtained with 1×10^5 simulations of fragment flights
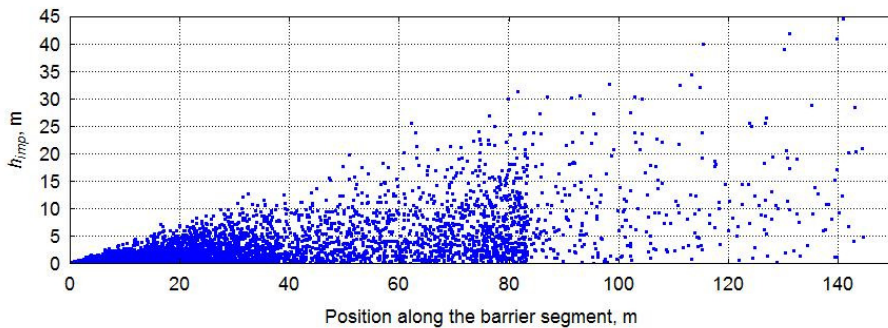
Fig. 2.32. The scatter diagram of the points where fragment trajectories crossed the vertical plane running along the barrier segment $B_4 - B_5$ (2074 points obtained in 10 000 simulations)
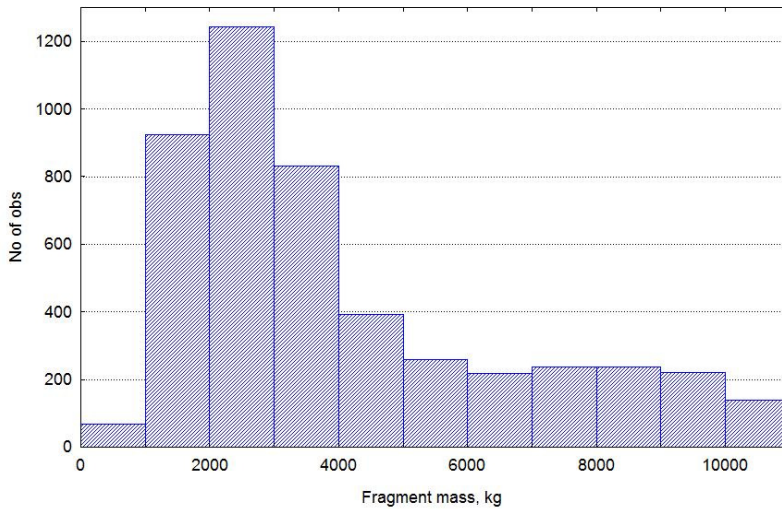
Fig. 2.33. The histogram of the simulated fragment mass values $\xi_{frg,j}$ related to the barrier segment $B_4 - B_5$ ($j = 1, 2, \ldots, 2074$)
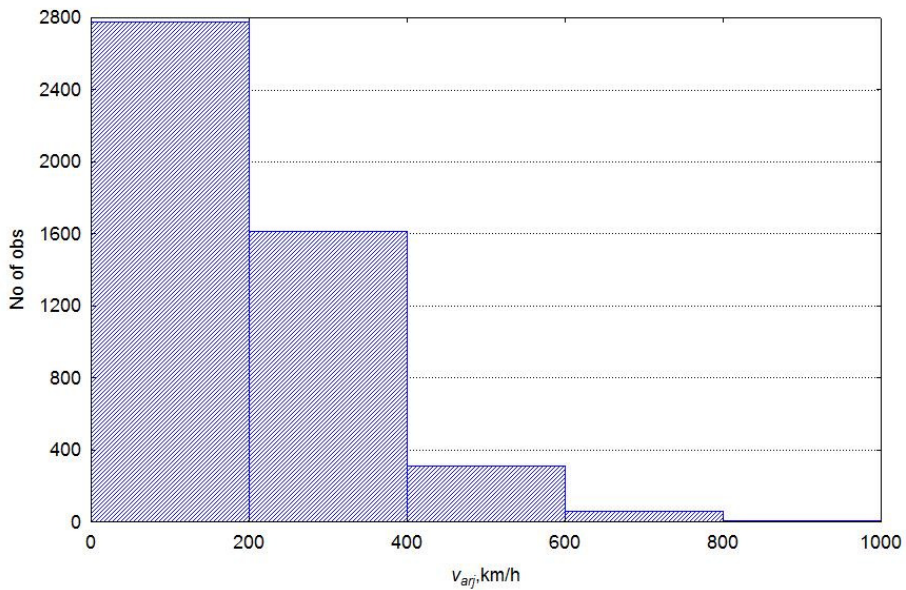
Fig. 2.34. The histogram of the simulated fragment impact velocities $v_{arv,j}$ related to the barrier segment $B_4 - B_5$ ($j = 1, 2, \ldots, 2074$)

Fig. 2.35. The histogram of the simulated ricochet angles φ_j related to the barrier segment $B_4 - B_5$ ($j = 1, 2, ... , 2074$)

Fig. 2.36. The histogram of the simulated impact altitudes $h_{arv,j}$ related to the barrier segment $B_4 - B_5$ ($j = 1, 2, ... , 2074$)

Samples of the values $\xi_{frg,j}$, $v_{arv,j}$, φ_j and $h_{arv,j}$ can be applied to a reliability-based design of safety barriers. The most natural way to utilis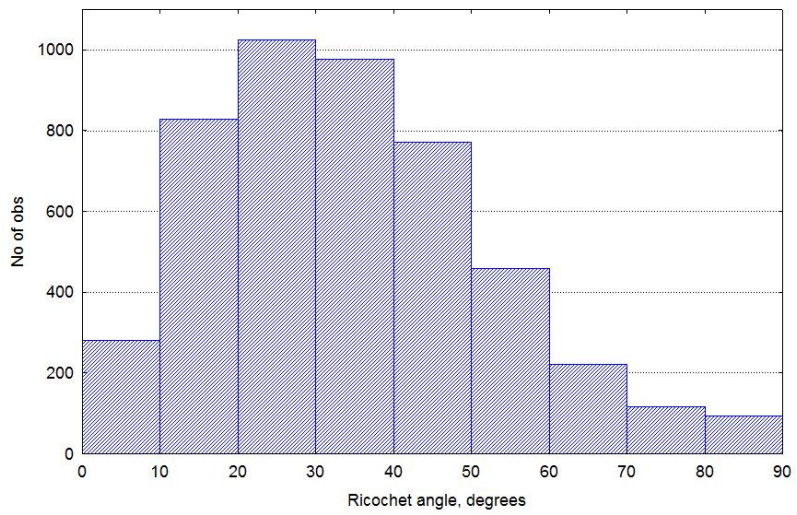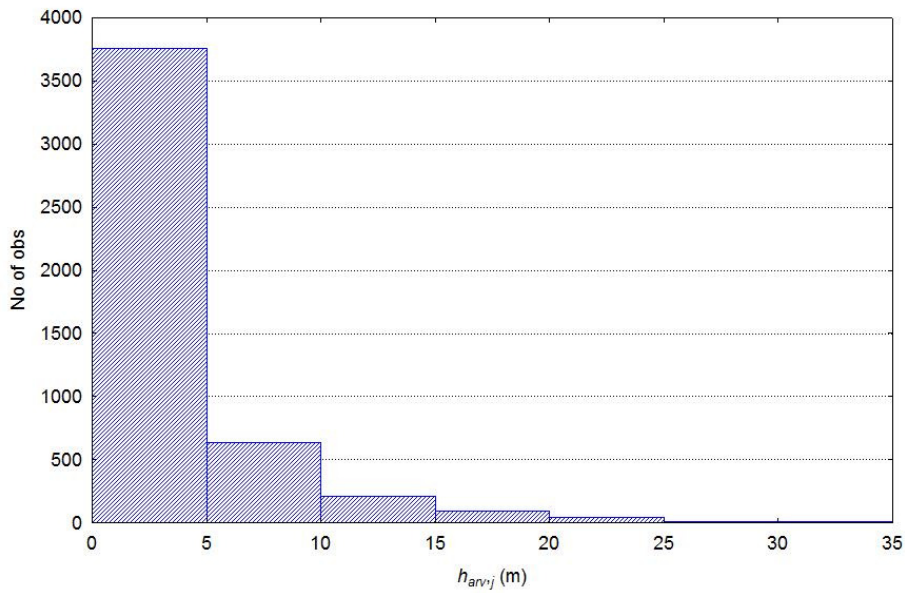e these samples for such a design is to incorporate them into the Monte Carlo simulation of barrier behaviour under fragment impact (see, e. g., Marek *et. al.* 2003). This simulation will yield an estimate of the probability of barrier damage (failure), P_{fe}. The estimate P_{fe} will correspond to the definition of the damage event and mechanical model expressing damage criteria, say, a limit state function $g(z, \xi_{frg}, v_{arv}, \varphi, h_{arv})$. In this function, the vector z is includes basic input variables on the side of barrier resistance and may include some basic variables representing the process of impact loading (e.g., impulse). The set of simulated values $\xi_{frg,j}$, $v_{arv,j}$, φ_j and $h_{arv,j}$ can be used to calculate values of the binary (zero-one) function $\mathbf{1}(z, \xi_{frg}, v_{arv}, \varphi, h_{arv})$ which will represent failure or survival conditions of the barrier, namely,

$$\mathbf{1}(z_j, \zeta_{frg,j}, v_{arv,j}, \varphi_j, h_{arv,j}) = \begin{cases} 1 & g(z_j, \zeta_{frg,j}, v_{arv,j}, \varphi_j, h_{arv,j}) \leq 0 \\ 0 & \text{otherwise} \end{cases} \quad (2.17)$$

where z_j is the value of the vector of random basic variables $\mathbf{Z}$ generated in addition to the values $\xi_{frg,j}$, $v_{arv,j}$, φ_j and $h_{arv,j}$. With the values $\mathbf{1}(z_j, \xi_{frg,j}, v_{arv,j}, \varphi_j, h_{arv,j})$ the estimate of the failure probability can be computed by means of the standard formula

$$P_{fe} = \frac{1}{N} \sum_{j=1}^{N} \mathbf{1}(z_j, \zeta_{frg,j}, v_{arv,j}, \varphi_j, h_{arv,j}) \quad (2.18)$$

where N is the number of Monte Carlo simulations. If the event of barrier damage by a fragment (failure due to fragment impact) is for instance, a complete collapse of the barrier, it can be designed for a fairly low value of the failure probability P_f.

In theory, a multivariate probability distribution can be fitted to the samples of $\xi_{frg,j}$, $v_{arv,j}$, φ_j and $h_{arv,j}$. This distribution could be applied to the estimation of the damage probability P_f in such methodological formats as FORM and SORM methods (e.g., Melchers 2002). However, fitting a four-dimensional probability distribution to the samples of $\xi_{frg,j}$, $v_{arv,j}$, φ_j and $h_{arv,j}$ can be highly complicated due to a stochastic dependency between the impact characteristics ξ, v_{arv}, φ and h_{arv}.

Alternatively, the samples of $\xi_{frg,j}$, $v_{arv,j}$, φ_j and $h_{arv,j}$ can be used to specify a combination of conservative, unfavourable values of the impact characteristics ξ_{frg}, v_{arv}, φ and h_{arv}. These values can be used as characteristic or design values for a conventional, deterministic design of barriers. However, the simulated values of the four impact characteristics ξ_{frg}, v_{arv}, φ and h_{arv} will generally be interdependent. Therefore, a specification of only one and "reliable" set of

design values can be problematic. The barrier should be analysed for several sets of design values representing different combinations of values of ξ_{frg}, v_{arv}, φ and h_{arv}. For instance, one can use the following two-step procedure:

1. A set of percentiles of the samples consisting of the simulated values $\xi_{frg,j}$, $v_{arv,j}$, φ_j and $h_{arv,j}$ is specified. The 10th, 25th, 50th, 75th and 90th percentiles of each sample can be used. This will yield 20 values of the impact characteristics ξ_{frg}, v_{arv}, φ and h_{arv}. An example of 50th and 90th percentiles of the impact characteristics related to the barrier segment $B_4 - B_5$ is presented in Table 2.10.

2. The barrier is analysed for each combination of the aforementioned percentiles. The most hazardous combination of impact characteristics is determined by the maximum response of the barrer to the impact loading.

Some percentiles can be excluded from the aforementioned combinations. For instance, percentiles the ricochet angle φ which are smaller than a critical value must be considered in a separate analysis, because such angles of entry will lead to a reflection of a fragment by the target (Johnson *et al.* 1982). Some percentiles can be too conservative and require unrealistic design decisions. For example, the 90th percentile of the impact altitude h_{arv} requires to design a barrier which is almost 12 m tall. Such a barrier will intercept the fragment crossing the line B_4–B_5 with 90 % probability. However, if the height of the barrier segment B_4–B_5 will be reduced to the more realistic 7 m, the probability of interception will be still high and approximately equal to 80 %.

Table 2.11. Median values and 90th percentiles of the samples of the simulated impact characteristics $\xi_{frg,j}$, $v_{arv,j}$, φ_j and $h_{arv,j}$ related to the barrier segment B_4–B_5 ($j = 1, 2, ... , 20\ 899$)

Median values	90th percentiles
$\hat{\zeta}_{frg,0.5} = 3157$ kg	$\hat{\zeta}_{frg,0.9} = 8593$ kg
$\hat{v}_{arv,0.5} = 171.2$ km/h	$\hat{v}_{arv,0.9} = 374$ km/h
$\hat{\varphi}_{0.5} = 36.5$ °	$\hat{\varphi}_{0.9} = 60.5$ °
$\hat{h}_{arv,0.5} = 2.48$ m*	$\hat{h}_{arv,0.9} = 11.5$ m*

* The value of the impact altitude h_{arv} equal to 7 m is the approximately the 80th percentile of the sample $h_{arv,\ 1}$, $h_{arv,\ 2}$, ... , $h_{arv,\ 20\ 899}$

2.3. Thermal effects from road tanker explosions

Thermal effects of BLEVE on roadside objects can be predicted by mathematical models, most of which are strictly deterministic. These models cover blast,

fireballs, and projection of fragments (projectiles) generated by BLEVEs (CCPS 1994; CCPS 2005a; CPR 2005; Vaidogas 2006b; Casal 2008). The models of BLEVE effects can be applied to predicting damage to roadside objects. A methodological framework for such predicting is available in the field of transportation risk assessment (CCPS 1995). An example of an application of TRA to an assessment of individual and societal risk due to LG transportation was reported by Paltrinieri *et al.* (2009). TRA is a widely developed methodology. However, our impression is that applications of TRA lack "attention to detail", where a potential damage to built roadside objects is of concern (Vaidogas *et al.* 2012ab). An assessment of such damage will require to consider two aspects of a BLEVE accident: transportation aspect (potential position of the explosion within the road segment from which it can endanger a roadside object in question) and structural aspect (response of the roadside object to potential BLEVE effects).

The present section attempts to give guidance on assessing the damage to built roadside objects from thermal radiation emitted by BLEVE fireballs. Such a radiation is not the furthest reaching BLEVE effect. However, it can be very intense in the roadside territory and, unlike blast and projectiles from an LG tank vessel fragmentation, it will impinge on objects build relatively close to the road from high elevation. The thermal radiation can be very problematic in terms of fire safety. The study focuses on a stochastic (Monte Carlo) simulation of position of road tankers before they sustain a BLEVE and thermal radiation from a BLEVE which can cause the thermal damage. The simulation results can be useful for a design of future objects and protection of existing objects located in the vicinity of the roads used for LG transportation.

2.3.1. Risk related to thermal damage

An accident occurring as a BLEVE of a road tanker will be initiated by a traffic accident, in which the tank vehicle is involved (Block 1, Fig. 2.37). Then the initiator can be followed by two typical sequences of events leading to an engulfment of a tank by a fire and BLEVE of the tank (Blocks 2 to 7, Fig. 2.37). The fire can be fed by LG leaking from the tank or by other source, most probably, fuel of a tank truck. A fire of both LG and fuel is also possible (Planas-Cuchi *et al.* 2004).

A BLEVE can be external or internal event with respect to exposed roadside infrastructure. An external exposure to BLEVE hazard can result from a transportation of LGs over adjacent public (off-site) roads or access roads. An example of an external exposure to a BLEVE is given in Fig. 2.38. The internal expose will take place during the transportation of LGs over on-site roads. In congested vulnerable industrial areas adjoined by on-site roads, the on-site

transportation of LGs can be more hazardous than the transportation over off-site, public roads.
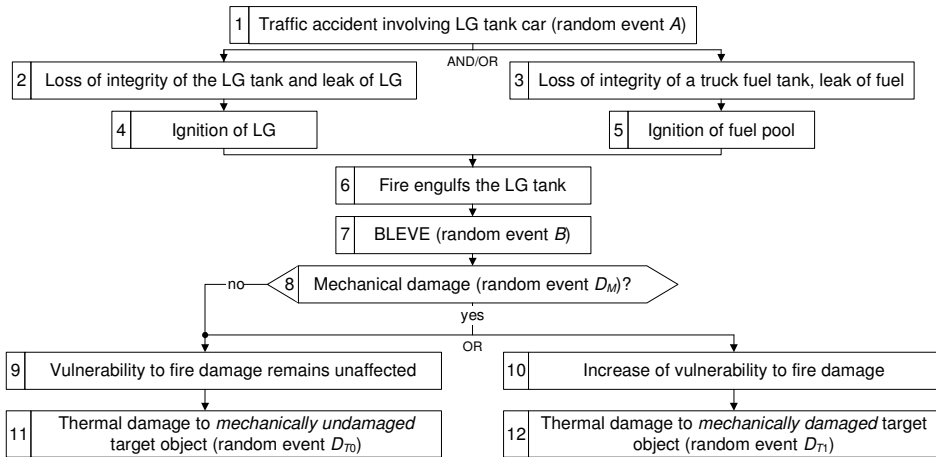

Fig. 2.37. Sequences of the events leading to a road tanker BLEVE and subsequent damage to a roadside object

BLEVE damage to a roadside object can be caused by three effects generated by explosion: blast, projectile impact and thermal radiation from a fireball. Blasts from BLEVEs are localised and not as far reaching as fireball and projectile effects. If safe distances between the road and roadside objects can be established for fireballs then they will be safe for the blast. Such distances are also known as separation distances (CCPS 2005b). A separation distance equal to four times the potential fireball radius R is suggested as reasonable for thermal radiation effects and blast effects Birk (1996). An illustration of the distance $4R$ is given in Figs. 2.33 and 2.34. However, at this distance the hazard from projectiles is still very significant. At a distance of $4R$ from the side of a tank, approximately 80-90% of fragments should fall. A compensation for less than desired separation distances can be safety barriers built alongside the road. If designed properly, the safety barriers will provide protection against blast and projectiles. For effective protection, the potential BLEVE epicentre should be at relatively short range from the front of the barrier (Smith 2010).

Unfortunately, barriers can provide no protection against fireball radiation because dimensions of fireballs from BLEVEs of road tankers exceed any reasonable dimensions of barriers. An illustration of these dimensions is given in Fig. 2.39. The geometry of the fireball shown in Fig. 2.39 was calculated for a typical tank semi-trailer carrying 24.7 tons of propane by applying the so-called

TNO fireball model CPD (2005). The model and the data used for the calculation are presented in Tables 2.7 and 2.8.

A protection of roadside objects against thermal radiation from BLEVE fireballs should be based on either providing adequate separation distances or compensating less than desired safety distances by adequate resistance of target objects to thermal radiation. The latter option can be achieved by shielding the target objects from thermal radiation or making them inherently more resistant to such radiation. Both options require to predict intensity of thermal radiation from a road tanker BLEVE and to assess the risk of thermal damage to exposed roadside object. An assessment of this risk will require to deal with transportation and structural aspect of the problem.
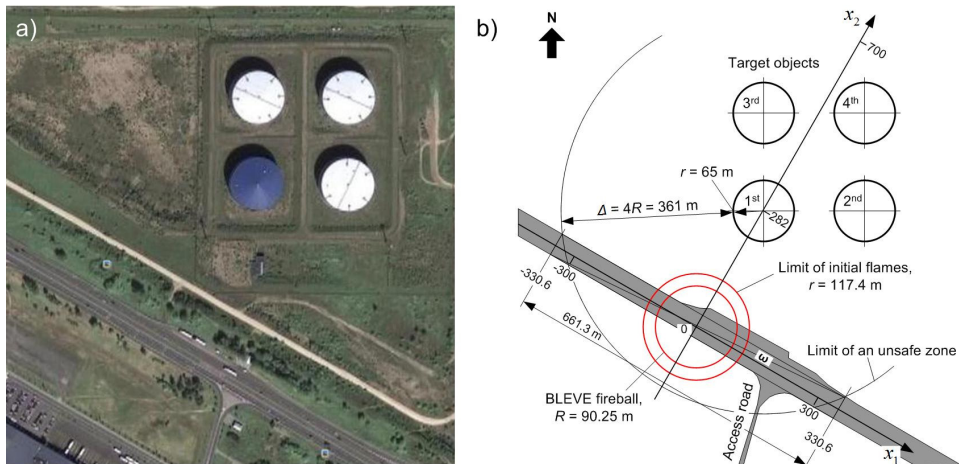
Fig. 2.38. An example of external exposure of a potential target to a BLEVE on road: a) an aerial view of four reservoirs of flammable materials in the vicinity of a road with a frequent transportation of LGs; b) schematic view with a coordinate system {0; x_1, x_2} based on road centreline and one of the reservoirs

2.3.2. Geometric information on road tanker accidents

Blast and projectiles generated by a road tanker BLEVE can cause mechanical damage, whereas the thermal radiation can ignite combustible parts of the exposed object and so the damage will be caused by a subsequent, secondary fire. Many combustible materials ignite at ten-second exposure to 50 kW/m^2 radiation (Prugh 1994). The duration of a fireball generated by a BLEVE of a typical road tanker is up to 20 seconds. Blast and projectiles will reach the target object within first two or three seconds after the explosion and act a very short time.

Thermal radiation from a fireball will act on the object a longer time and will increase from zero to a maximum value during the first third of fireball duration (Casal 2008). If the events of mechanical and thermal damage are modelled by the respective random events D_M and D_T, the event D_M will occur first and D_T will follow D_M (Blocks 8 to 11, Fig. 2.37).
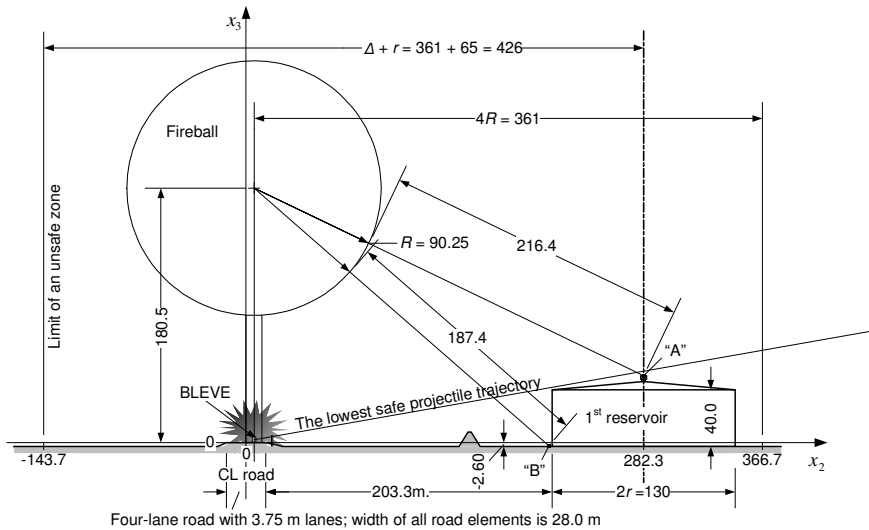
Fig. 2.39. Exposure of a roadside object (target) to the fireball generated by a BLEVE of a road tanker carrying 24.7 tons of propane (the dimensions of the fireball were estimated by means of the TNO model (CPD 2005)

An occurrence of the mechanical damage event D_M can lead to two conditions of the target object with respect to the vulnerability of this object to thermal radiation:

1. An occurrence of D_M does not change the vulnerability to fire damage (Block 9, Fig. 2.37) (e.g., a local damage to a masonry wall of an industrial building hit by a projectile from a tank vessel fragmentation will not affect the vulnerability of its roof to thermal radiation, Fig. 2.40a). The events D_M and D_T can be considered independent and so the probability $P(D_T | B)$ estimated independently from $P(D_M | B)$, where B denotes the random event of BLEVE (Block 7, Fig. 2.37).

2. An occurrence of D_M increases abruptly the vulnerability to fire damage (Block 10, Fig. 1) (e.g., loss of containment by a reservoir used to store flammable liquid due to a projectile impact and so spill and exposure of this liquid to the direct action of thermal radiation will increase the

chance of fire, Fig. 4b). The events D_M and D_T can not be considered to be independent and so $P(D_T \mid D_M \cap B) > P(D_T \mid B)$.

The probabilities $P(D_T \mid B)$ and $P(D_T \mid D_M \cap B)$ represent two different accident scenarios. They can be related to the frequency of thermal damage, $F_r(D_T)$, by a simple expression

$$F_r(D_T) = F_r(T) \times P(A \mid T) \times P(B \mid A) \times P(D_T \mid B) \text{ (or} \times P(D_T \mid D_M \cap B)) \qquad (2.19)$$

where $F_r(T)$ is the usually annual frequency of LG transportation through the road segment under analysis (event T); $P(A \mid T)$ is the conditional probability of a traffic accident (event A) given T (the random event A is shown in Block 1, Fig. 2.37) and $P(B \mid A)$ is the probability of a BLEVE given A.
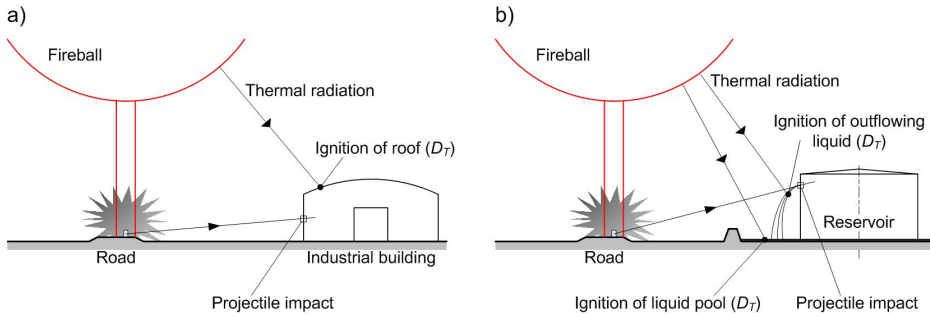
Fig. 2.40. An illustration of the thermal damage event D_T: a) the case of an independent occurrence of D_T with respect to the mechanical damage by a projectile; b) the case where D_T (ignition of flammable liquid) is dependent on an occurrence of mechanical damage (perforation of a reservoir wall by a projectile and subsequent leak of liquid)

If D_T is a stand-alone event, a vector of consequence severities, S, can be assigned to $F_r(D_T)$ and the pair $\{F_r(D_T), S\}$ considered a simple expression of risk. In the case of an escalation of D_T into a larger, domino accident, the estimation of the frequency $F_r(D_T)$ can be treated as an estimation of frequency of an initiating event which triggers out a domino sequence. In both cases, the estimation of $F_r(D_T)$ will involve an estimation of the thermal damage probabilities $P(D_T \mid B)$ and $P(D_T \mid D_M \cap B)$.

2.3.3. Estimating the probability of thermal damage to roadside structures

The estimation of the conditional thermal damage probability $P(D_T \mid B)$ is similar to that of $P(D_T \mid D_M \cap B)$, with the difference that the first probability must be estimated for a mechanically undamaged target object and the second one for an

object in a damaged state and so more vulnerable to a thermal impact. Due to this similarity and for the sake of brevity, the symbol $P(D_T|B)$ will represent both probabilities. The thermal damage probability $P(D_T|B)$ can be expressed b the formula (2.2). In this formula, the general symbol D must be replaced D_T and the remaining symbols must be interpreted as follows: $\boldsymbol{y} = (y_1, y_2)$ is a two-component vector, the first component of which, y_1, expresses a thermal radiation intensity (heat flux) and the second, y_2, the duration of exposure to this radiation (fireball duration); $P(D_T|\boldsymbol{y})$ is the fragility function relating the probability of D_T to $\boldsymbol{y}$; $\boldsymbol{x}$ is the vector of characteristics of BLEVE accident resulting in the impact expressed by $\boldsymbol{y}$; $\psi(\boldsymbol{x})$ is the vector-function which relates $\boldsymbol{x}$ to $\boldsymbol{y}$ (i.e., $\boldsymbol{y} = \psi(\boldsymbol{x})$); and $f(\boldsymbol{x})$ and $f(\boldsymbol{y})$ are the joint probability density functions (p.d.f.s) of $\boldsymbol{x}$ and $\boldsymbol{y}$, respectively.

The development of the fragility function $P(D_T|\boldsymbol{y})$ is a highly case-specific task of probabilistic structural analysis. Fragility functions are widely applied to seismic risk assessment and extreme-wind risk assessment. However, any attempts to develop a fragility function for thermal actions of external fires are not known to us. What is more, recipes allowing to relate the thermal radiation y_1 and duration y_2 to a specific thermal damage are very sparse and deterministic in nature. It is stated in the books CCPS (1994) and CCPS (2005a) that the radiation of 37.5 kW/m^2 is sufficient to cause damage to process equipment and 12.5 kW/m^2 is the minimum energy required for ignition of wood and melting of plastic tubing. Most sources interpret the thermal damage simply as an ignition of materials exposed to thermal radiation and distinguish between ignition and non-ignition by specifying a pair of fixed threshold values $(y_{1,min}, y_{2,min})$ (Casal 2008; Prugh 1994, Tewarson 2002, Babrauskas 2003). Unfortunately, such values are insufficient to easily develop a fragility function $P(D_T|y_1, y_2)$, especially for short-term exposures (values of y_2 ranging roughly between 5 and 20 seconds). It is highly probable that at present the analyst will have to rely on a simplified fragility function expressed as

$$P(D_T|y_1, y_2) = \begin{cases} 1 & \text{if } y_1 \geq y_{1,min} \text{ and } y_2 \geq y_{2,min} \\ 0 & \text{otherwise} \end{cases} \qquad (2.20)$$

Fitting a well-known bivariate density $f(\boldsymbol{y})$ to the direct data on BLEVE effects can be problematic. BLEVE accidents on road are unique, short-lasting and unexpected events. The post mortem data on them is too sparse for fitting $f(\boldsymbol{y})$. However, the density $f(\boldsymbol{y})$ and so the probability $P(D_T|B)$ can be estimated by propagating uncertainties expressed by the lower-level density $f(\boldsymbol{x})$ through the model $\psi(\boldsymbol{x})$ Prugh 1994. The function $\psi(\boldsymbol{x})$ can be composed of a relatively large number of models available currently for the prediction of individual effects of BLEVE. These models are strictly deterministic, some are in competition for modelling individual characteristics of BLEVE fireballs (T. Ab-

basi and S. A. Abbasi 2007). Tables 2.12 and 2.13 contain an example of $\psi(x)$ composed of two sub-models $\psi_1(x)$ and $\psi_2(x)$ developed for a prediction of fireball radiation y_1 and duration y_2, respectively.

Table 2.12. Input vector x of the model $\psi(x)$

Component of x	Description	Units	Value
x_1	Position of the BLEVE centre along the axis $\{0; x_1\}$* (Fig. 2.37b)	m	0
x_2	Position of the BLEVE centre along the axis $\{0; x_2\}$ (Figs. 2.32b and 2.33)	m	5.65
x_3	Position of the BLEVE centre along the axis $\{0; x_3\}$ (Fig. 2.38)	m	0
x_4	Capacity of the tank	m^3	56.14
x_5	Pressure in the vessel just before the explosion*	N/m^2	20×10^5
x_6	Degree of tank filling	%	85
x_7	Density of LG (propane)	kg/m^3	585
x_8	Combustion heat of LG at its boiling point	J/kg	46.0×10^6
x_9	Vaporisation heat of LG at its boiling point	J/kg	0.426×10^6
x_{10}	Specific heat capacity at constant pressure	J/(kg°K)	0.002582
x_{11}	Temperature of the fireball flame	°K	2000
x_{12}	Partial vapour pressure of carbon dioxide in the atmosphere	N/m^2	30.39
x_{13}	Ambient temperature	°C	10
x_{14}	Relative humidity	%	70

* Relief pressure of the safety valve can be assumed as the pressure at the instant of explosion (Casal 2008)

Table 2.13. Components (sub-models) of the model $\psi(x) = (\psi_1(x), \psi_2(x))$ developed in by the Dutch organisation TNO (2005)

Component of $\psi(x)$	Description	Expression of the submodel
$\psi_1(x)$	Intensity of thermal radiation	$\psi_1(x) = E(x) F_{view}(x) \tau_a(x)$*
$\psi_2(x)$	Fireball duration	$\psi_2(x) = 0.852(x_4 x_5 x_6)^{0.8}$

* $E(x) \equiv E(x_1, x_2, \dots, x_{12})$ is the emissive power of the fireball surface; $F_{view}(x) \equiv F_{view}(x_1, x_2, \dots, x_6)$ is the view factor; $\tau_a(x) \equiv \tau_a(x_1, x_2, \dots, x_6, x_{13}, x_{14},)$ is the atmospheric transitivity; see (CPD 2005) for a detailed description of the sub-models $E(\cdot)$, $F_{view}(\cdot)$ and $\tau_a(\cdot)$

The estimation of the thermal damage probability $P(D_T \mid B)$ has an apparent transportation aspect. The thermal effect from a BLEVE fireball depends on a number of transportation-specific characteristics which can be taken as components of the input vector x in the model $\psi(x)$. A list of these

characteristics depends on the type of the model used to predict the thermal radiation $\psi_1(x)$ and the fireball duration $\psi_2(x)$. For instance, the TNO model described in Tables 2.7 and 2.8 allows to classify transportation-specific components of x as follows:

1. The position of exploding tank in respect to a target object.
2. The segment of road from which a road tanker BLEVE can endanger the target object (unsafe road segment).
3. Characteristics of the tank vessel used to ship LG: capacity, degree of filling, relief pressure of the safety valve built into the vessel and, more generally, mechanical characteristics of the vessel metal heated by an external fire preceding BLEVE.
4. Characteristics of LG being shipped in the vessel: type and density of LG, combustion and vaporization heat, specific heat. Temperature of the fireball flame can also be attributed to the characteristics of LG.

The tank position can be defined by applying a coordinate system fixed to both road and target object. An example of such a coordinate system denoted by $\{0; x_1, x_2\}$ is shown in Fig. 2.38b. If the altitudes of BLEVE centre and target object differ much and/or the road has a non-negligible gradient, a three-dimensional coordinate system $\{0; x_1, x_2, x_3\}$ must be used (e.g., Fig. 2.39). Unlike scattering of projectiles from a cylindrical vessel BLEVE and blast generated by such an explosion, the propagation of the thermal radiation is not directional Birk (1996). Therefore there is no need to model the orientation of the exploding tank (the angle of tank axis in relation to the road axis) in the coordinate system $\{0; x_1, x_2\}$ Vaidogas *et al.* (2012a).

The unsafe road segment denoted by, say, ω can be determined by plotting a safety distance around the target object. If this object has a relatively simple geometry in plan, the safety distance can be determined a single variable, say, Δ. Figs. 2.33b and 2.34 illustrate such a distance for the cylindrical tank "1". It was assumed that Δ is equal to four fireball radii R estimated by applying the deterministic model and data given in Tables 2.7 and 2.8. The safety distance Δ plotted around the target object formed a road segment ω with the length of 661.3 m (Fig. 2.38b). The geometry and of a target object and road network in the vicinity of the object can be irregular. However, the unsafe road segment ω can be identified also in such a case (Vaidogas and Linkute 2012).

Generally, all component of the input vector x should be considered random and modelled by random variables. However, the variability of some components can be expected to be small one and so these components can be represented by fixed values. The position of the BLEVE centre in the road segment ω in undoubtedly uncertain and must be modelled by two random variables X_1 and X_2. For the model $\psi(x)$ described in Tables 2.7 and 2.8, they

will be the first two random input variables. The altitude of the explosion centre with respect to the target, x_3, can be expressed as a linear function of X_1 if the road within $\boldsymbol{\omega}$ has a longitudinal gradient. Consequently, X_3 will have the same probability distribution as X_1. The capacity of the tank, x_4, and the relief pressure of the safety valve, x_5, can be assumed to be fixed values if it is known what type of the tank vessel will sustain a BLEVE. However, the degree of tank filling, x_6, can vary more than x_4 and x_5 and so this degree should be modelled by a random variable X_6.

The characteristics of LG expressed by the components x_7 to x_{10} will depend on the type of LG and chemical composition of LG (Table 2.12). The variability of x_7 to x_{10} must be determined by tests of LGs shipped by road tankers. If a specific material shipped by a road tank, which may sustain a BLEVE, is known in advance, the LG characteristics x_7 to x_{10} can be assumed to be fixed. However, the temperature of fireball flame, x_{11}, should be modelled as a random variable X_{11}. This temperature is influenced by several random factors and, in addition, is difficult to measure it in experiments (Babrauskas 2003; Roberts *et al.* 2000).

The ambient conditions in the TNO model are expressed by the input variables x_{12} to x_{14} (Table 2.12). Partial vapour pressure of carbon dioxide in the atmosphere, x_{11}, do not vary much and can be considered non-random and equal to a fixed value given in Table 2.12 (CPD 2005). The ambient temperature at the instant of BLEVE, x_{13}, and the corresponding relative humidity x_{14} are clearly uncertain values and they must be modelled by the respective random variables X_{13} and X_{14}. These variables are not inherent characteristics of the LG transportation process. They can be attributed to the target object because depend on the location of a potential BLEVE accident. However, certain combinations of values of X_{13} and X_{14} can create dangerous traffic conditions, say, impaired visibility due to fog or icy road surface. They may increase the chance of traffic accident, in which the road tanker car will be involved, and so the chance of BLEVE. Consequently, the input variables X_{13} and X_{14} can not be completely detached from the transportation aspect of the damage prediction problem.

The uncertainties related to the components of the input vector $\boldsymbol{x}$ call for replacing this vector by a vector with some random components, namely,

$$X = (X_1, X_2, X_3, x_4, x_5, X_6, x_7, x_8, x_9, x_{10}, X_{11}, x_{12}, X_{13}, X_{14}) \qquad (2.21)$$

With the random input vector X, the output of the model $\boldsymbol{\psi}(X) = (\psi_1(X), \psi_2(X))$ will be random and can be modelled by two random variables: random thermal radiation $Y_1 = \psi_1(X)$ and random fireball duration $Y_2 = \psi_2(X)$. The probability distributions of Y_1 and Y_2 can be estimated by applying a simulation-based propagation of uncertainties through the model $\boldsymbol{\psi}(\cdot)$. Values of the random input vector, $\boldsymbol{x}_j$, can be sampled from probability distributions of the

random components of X and the corresponding output values y_{1j} and y_{2j} calculated by means of $\psi(\cdot)$. A repetition of this process a large number of times, say, N will yield an estimate of the damage probability $P(D_T | B)$, namely,

$$P_e(D_T | B) = N^{-1} \sum_{j=1}^{N} P(D_T | y_{1j}, y_{2j}) \tag{2.22}$$

where $P(D_T | y_{1j}, y_{2j})$ is a value of the fragility function $P(D_T | y)$ computed for the pair (y_{1j}, y_{2j}).

2.3.4. Case study

The potential thermal damage from a road tanker BLEVE fireball to the 1st of the four reservoirs shown in Fig. 2.38 will be analysed. The thermal radiation will be estimated at the centre of reservoir roof, where system components sensitive to thermal radiation are installed (point "A"), and at the bottom of the diked area around the reservoirs, were piping and other system components are attached to the reservoir (point "B") (Fig. 2.39). Characteristics of the points "A" and "B" are given in Table 3. A BLEVE of a road tanker semi-truck carrying 24.7 tons of propane will be considered. The BLEVE can occur on an unsafe road segment ω with the length of 661.3 m (Fig. 2.38b). The area between the road and the reservoirs is flat; the road segment ω has no gradient. The road has four lanes, each 3.75 m wide and a 5,5 m wide median which separates opposing lanes of traffic (Fig. 2.41). The LG is transported along the road segment ω with relative frequencies $\pi_1 = 0.35$, $\pi_2 = 0.04$, $\pi_3 = 0.07$ and $\pi_4 = 0.54$ shown in Fig. 2.36a. These frequencies were obtained from an observation of traffic in the road segment ω.

Table 2.14. Probability distributions of the random components of the vector X used to describe a road tanker BLEVE accident

Random variable	Mean	Coefficient of variation (standard deviation)	Probability distribution
X_1	335.1* m	0.577 (193.4 m)	Uniform over the length of ω
X_2	2.174 m	5.20 (11.31 m)	Mixed distribution
X_6	0.85	0.05 (0.0425)	Normal
X_{11}	2000 °K	0.11 (220 °K)	Lognormal
X_{13}	15 °C	0.20 (3 °C)	Normal
X_{14}	70%	0.1 (7%)	Normal

* In the accident simulation the mean value of X_1 was shifted to the zero value of the axis $\{0; x_1\}$

Table 2.15. Characteristics of two vulnerable points in the reservoir system that can be ignited by a BLEVE fireball

Point	Position in the coordinate system $\{0; x_1, x_2, x_3\}$	Condition of thermal damage		Estimate of damage probability, $P_e(D_T|B)$* (see Eq.(2.35))
		$y_{1,min}$ (kW/m^2)	$y_{2,min}$ (s)	
A	(0 m, 282.3 m, 47.5 m), Fig. 2.38	25	10	1.021×10^{-3}
B	(0 m, 215 m, –2.17 m) , Fig. 2.38	30	10	0.1814
* Computed with $N = 1 \times 10^5$				

The BLEVE accident is described by the vector X defined by Eq. (2.21). Values of the deterministic components of this vector, x_4, x_5, x_7, x_8, x_9, x_{10} and x_{12}, are given in Table 2.12. The probability distribution of the longitudinal rest position of the road tanker and so the position of a potential BLEVE centre, X_1, was assumed to be uniformly distributed over the length of $\boldsymbol{\omega}$ (Fig. 2.38b, Table 2.14). This distribution expresses maximum uncertainty related to a potential BLEVE centre along the axis $\{0; x_1\}$. The road segment did not experienced tank car accidents in previous years. The probability distribution of the transverse tank position after it comes to a complete stop and can explode, X_2, depends on the lane of intended travel. Our previous analysis of tank car accident data led to the result that the transverse rest position of the tank centre with respect to the centreline of intended travel lane can be modelled by a logistic distribution Logistic(2.02 m, 3.10 m) Vaidogas *et al.* (2012a). The positive location parameter of this distribution, 2.02 m, means that the transverse rest position lies in average 2.02 m outwards the travel lane centreline. The distribution Logistic(2.02 m, 3.10 m) can be associated with each of the four lanes of the road under consideration by adding (subtracting) its location parameter to (from) the coordinate of the lane centreline along the axis $\{0; x_2\}$ (Fig. 2.42a). This will allow to construct a mixed p.d.f. of X_2, in which the frequencies π_1 to π_4 will play the role of probabilistic weights:

$$\varphi(x_2) = \pi_1 f_1(x_2|-10.4, 3.10) + \pi_2 f_2(x_2|-6.65, 3.10) +$$

$$+ \pi_3 f_3(x_2|6.65, 3.10) + \pi_4 f_4(x_2|10.4, 3.10) \qquad (2.23)$$

where $\varphi(x_2)$ denotes the mixed p.d.f. of X_2 and $f_l(x_2 | \cdot, \cdot)$ (l = 1, 2, 3, 4) are the logistic p.d.f.s related to the respective travel lanes. Parameters of the densities $f_l(x_2 | \cdot, \cdot)$ in Eq. (2.23) are in meters. The graph of the bimodal density $\varphi(x_2)$ is shown in Fig. 2.42a.

The probability distributions of the remaining random variables considered in the present example, X_6, X_{11}, X_{13} and X_{14}, were assumed by following the

recommendations given by Papazoglou and Aneziris (1999) who considered the quantification of uncertainties related to the BLEVE thermal radiation.
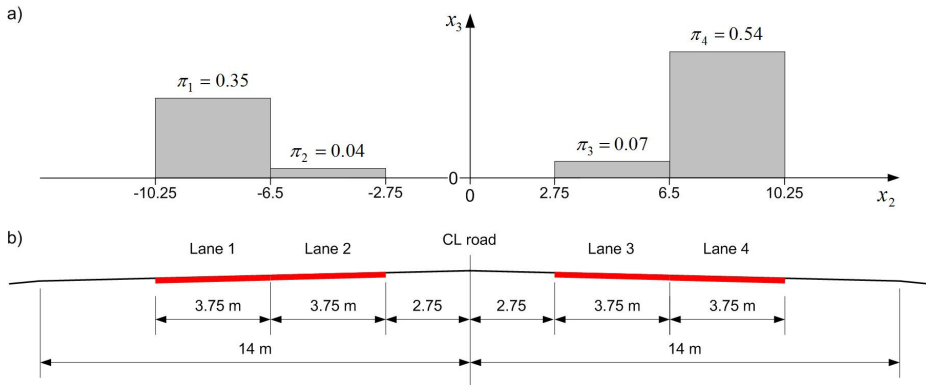
Fig. 2.41. Simulation of the transverse rest position of road tanker which can sustain a potential BLEVE: a) relative frequencies of LG transportation through individual lanes; b) transverse profile of the road
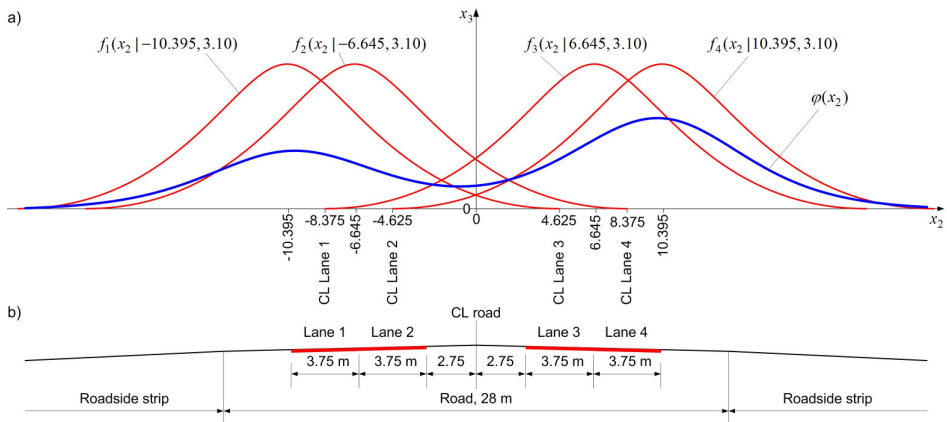
Fig. 2.42. Probabilistic model of the transverse rest position of the tank: a) densities of the transverse departure from the centrelines of individual lanes and a mixture of these densities, $\varphi(x_2)$; b) road profile and adjacent roadside territory
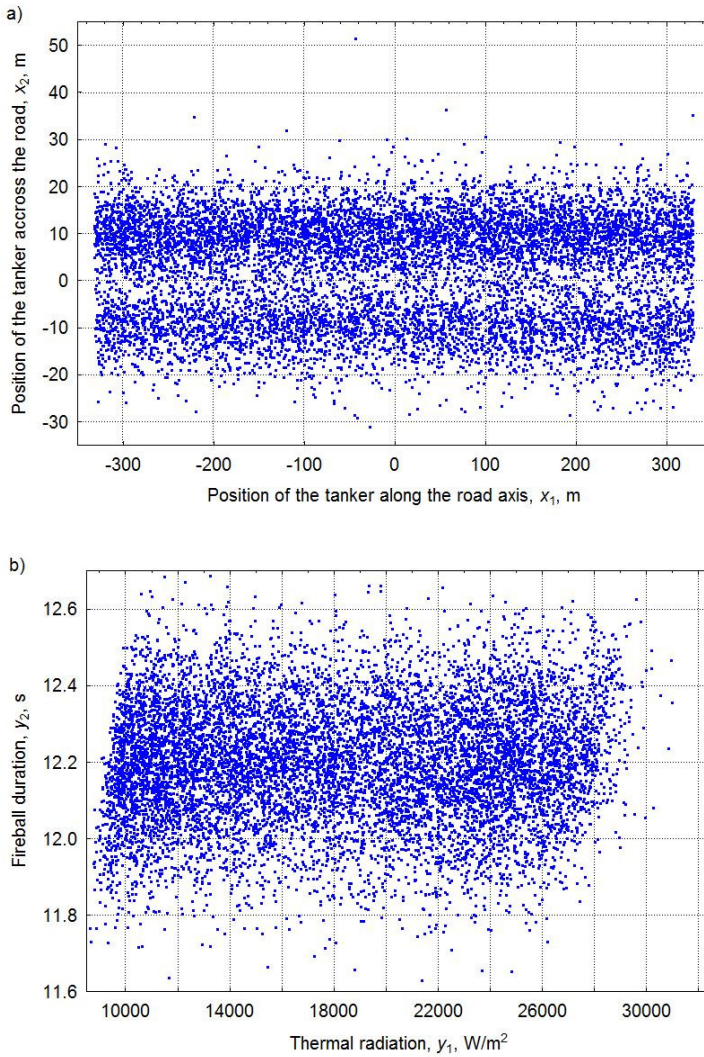
Fig. 2.43. Results of the simulation of a BLEVE thermal radiation at point "B" a) simulated positions of the road tank, (x_{1j}, x_{2j}); b) simulated pairs of the thermal radiation and fireball duration, (y_{1j}, y_{2j})

The values x_j of the random input vector X were sampled by means of a stochastic simulation from the probability distributions given in Table 2.14. Then the simulated values x_j and the model $\psi(\cdot)$ described in Table 2.13 were used to compute values of the thermal radiation and fireball duration, y_{1j} and y_{2j}. The simulation was repeated 1×10^5 times ($N = 10\,000$). Fig. 2.43 shows the

scatter diagram of the pairs (x_{1j}, x_{2j}) and (y_{1j}, y_{2j}). With the pairs (y_{1j}, y_{2j}), estimates of the probability of thermal damage, $P_e(D_T|B)$, were computed for points "A" and "B" (see Table 2.15). These estimates indicate that the point "B" is much more vulnerable to thermal radiation than "A" and so thermal insulation (shielding) should be provided in order to protect this part of the reservoir system against BLEVE.

2.4. Second chapter conclusions

This chapter presented results of investigation of hazmat transportation accidents as well as thermal and mechanical effects induced during these accidents on built roadside property. Two methods suitable for a probabilistic prediction of these effects were proposed. The following conclusions summarise findings presented in the second chapter and results of application of the proposed methods:

1. Two hazmat transportation accidents with the greatest potential of damage to the built roadside property are BLEVE and VCE. The prevailing materials involved in BLEVE and VCE accidents on road and rail are commercial energetic hydrocarbons, especially, propane.

2. Thermal and mechanical effects of BLEVE will substantially depend on the position and orientation of road or railway tanker vessel sustaining the explosion with respect to a potential target (vulnerable structure or future safety barrier). The position of vessel centre will substantially influence the thermal radiation incident on a roadside target. The orientation will determine the most probable movement trajectories of vessel fragments.

3. The prediction of the position can be subdivided into the prediction of three circumstantial characteristics: longitudinal and transverse rest positions of the vessel with respect to road centreline or other longitudinal reference line as well as departure angle of the tank. These three characteristics are uncertain quantities and uncertainty related to them must be modelled by means probability distributions. Some of these distributions can be fitted to statistical data; others will have to be specified subjectively in line with the principles of QRA.

4. Any systematic set of data on the position of tanker vessels which sustained BLEVEs is not available or, at least, accessible. BLEVEs on road and rail are relatively rare, unexpected and short-lasting events. However, data on transverse rest position and departure angles can be gained from accidents which were precursors of BLEVEs or accidents of non-explosive tanks which were similar to tanks capable to cause BLEVEs.

5. It was possible to extract such data from reports on past road tanker accidents presented in the mass-media and the internet. Data on 151 road tanker accident collected from these sources allowed us to fit a logistic probability distribution for the transverse rest position and to establish empirical probability distribution for the departure angle. The stochastic dependence between these two circumstantial characteristics is weak, albeit statistically significant.

6. A probabilistic modelling of the tanker vessel rest position along a road segment, from which BLEVE can affect a vulnerable roadside object, is problematic in terms of data. Such a road segment will be relatively short and data on tank accidents in this or similar segments will hardly be available. Consequently, the probability distribution of the longitudinal rest position will have to be chosen subjectively. Methods of the specification of subjective probabilities and probability distributions developed and widely applied in the field of QRA can be used for the modelling of the longitudinal rest position.

7. The design of a safety barrier aimed at protection against effects from a BLEVE will require to assess the impact of fragments of a cylindrical tanker vessel on the barrier. The fragment impact can be assessed by means of the deterministic models developed in the field of industrial safety. These models are suitable to extend the probabilistic modelling of the tanker vessel position and orientation. An application of the fragment impact models must include a quantification of uncertainties related to their input variables and, if necessary, parameters. This will allow to incorporate them into the framework of QRA.

8. An assessment of thermal effects induced by a BLEVE fireball on a roadside target will require to simulate the position of tanker vessel with respect to the target. This simulation can be supplemented by a computation of the heat flux (thermal radiation) generated by the fireball. The heat flux can be estimated in given points on the surface of the roadside object and for a given position of the vessel sustaining a BLEVE.

9. The dimensions of the fireballs, which will be generated by BLEVEs of typical road and railway tanker vessels, will be large. They can be up to 300 m tall. Therefore, an effective protection of roadside objects by wall-shaped barriers and soil embankments will be impossible. The protection can be achieved by providing sufficiently large separation distances between the road (railway tracks) and the vulnerable roadside object. A thermal shielding of the roadside object can also be applied, because duration of BLEVE fireballs is short and typically does not exceed 20 seconds.

3

Proposals for the design of safety barriers aimed at protection of roadside property

The third chapter formulates a series of proposals to the design of safety barriers aimed at protection of roadside objects against thermal and mechanical effects of BLEVEs on road and rail. The first proposal considers the sitting of barriers in the area of potential construction and choosing the horizontal configuration for them. The second proposal deals with a design of a steel barrier intended for a protection of blast loading and fragment impact from a railway tanker BLEVE. It is demonstrated how to design the barrier using methods of SRA and QRA. The design is based on a utilisation of a small-size sample of blast loading characteristics. The third proposal consists in recommendations of how to design a reinforced concrete barrier capable to sustain impact by fragments from a tanker vessel. All three proposals are expressed in the form of technical design solutions. A detailed dimensioning of the barriers is not considered. The third chapter presents the results of investigation published by Vaidogas and Linkutė (2012), Linkutė *et al.* (2013) and Vaidogas *et al.* (2013).

3.1. The scope of barrier design

A safety barrier must separate a vulnerable object from a potential explosion or fire which produce effects capable to damage the object. Safety barriers can be deployed to provide structural protection against blast loading and projectile

97

impact. To a certain degree, safety barriers are suitable to mitigate the level of thermal radiation generated by fires occurring during a hazmat transportation. Blast loading, fragment impact and thermal radiation may occur in combination during BLEVE accidents. A barrier deployed to protect roadside property must be designed to provide a maximum mitigation of these three effects.

The cost of rigid, non-destructible barriers is often prohibitive and a significant mitigation of blast and impact loading can be achieved using relatively lightweight frangible or sacrificial barriers (Bogosian and Piepenburg 2002). The energy of blast loading can be absorbed by lightweight systems used as sacrificial cladding. They can be mounted on the front of a non-sacrificial structure which will be a component of a blast wall (Guruprasad and Mukherjee 2000ab; Hanssen *et al.* 2002; Juocevičius 2011).

The process of barrier design can be subdivided into three subsequent tasks:

1. Sitting the barrier within available area between roadside object(s) to be protected and potential centre of fire and/or explosion on road or rail.
2. Choice of barrier material (usually steel or reinforced concrete). Soil embankment and large separation distance can also be considered as options of barrier design.
3. Design of individual barrier elements (e.g., sacrificial cladding, supporting structure, barrier segments made of reinforced concrete).

The remainder of this chapter describes considerations on how these three tasks could be solved.

3.2. Sitting the barrier

3.2.1. Determination of an unsafe road segment

3.2.1.1. Geometry of an unsafe area

There are two obvious geometric factors which can influence the degree of damage to a roadside object from an accidental explosion on road, namely, distance from road to target object and relief of the terrain where the explosion can occur. The role of a large distance in minimising effects of a violent release of energy during an explosion is obvious. However, these effects can be enhanced or reduced if the explosion will take place on a road built on embankment or in cutting, respectively (e.g., Elvik *et al.* 2009).

Road segments located at large distances from the target object are naturally safe. When the road comes closer to the object, the distance alone may be insufficient to ensure safety and a safety barrier may be required to protect the target object. The configuration of the barrier in the roadside terrain will directly

depend on the layout of the road segment where the explosion can occur and a safety distance around the target object.

In the safety engineering, the terms "safety distance" and "separation distance" are used to denote a distance at which a hazard source can be placed and after an accident causes no destruction or risk of any kind to living beings and their facilities (EIGA 2007; Marangon *et al.* 2007; Bangash 2009; Cozzani *et al.* 2009). In what follows the term "safety distance" will be applied to a minimum separation between an explosion on road (near the road) and a roadside object which will mitigate explosion effects and prevent damage to the object. Such effects can be air blast, fireball, primary and secondary projectiles (e.g., Casal 2008). The above definition of the safety distance expresses only a general idea. A mathematical definition of this term will require to characterise it in a more precise way (see the subsequent subsection "Dealing with uncertainties ...").

Safety distances plotted in all directions around the target object will form a perimeter of an unsafe zone (zone **Ω**, say) (Fig. 3.1). Safety distances can be significantly directional and so the layout of the unsafe zone **Ω** can be fairly complex. Relief around the target object and incursions of the road into environment (embankments and cuttings) may contribute to this complexity.
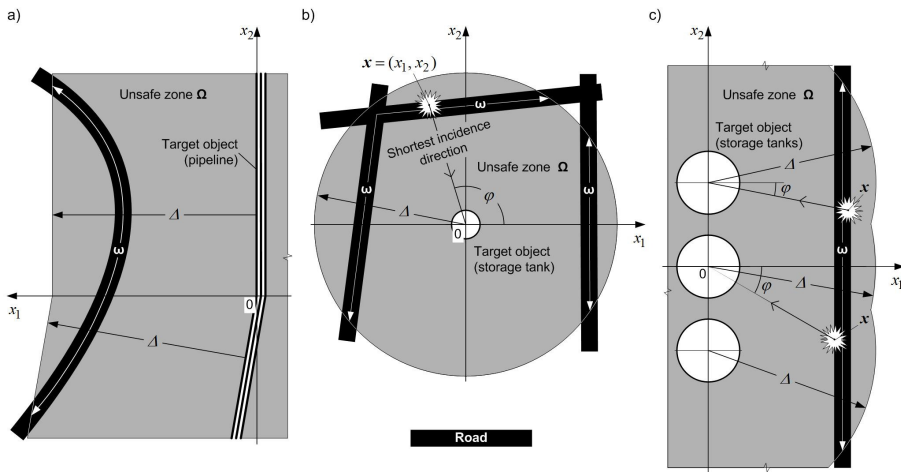
Fig. 3.1. Safety distance *Δ*, unsafe zone **Ω** and unsafe road segment *ω* at different configurations of the target object: a) above-ground pipeline or other energy supply line; b) circular storage tank; c) storage tanks arranged in a row

In a somewhat idealised case of one or several structures having relatively simple geometry in plan, the safety distance can be expressed by a single variable *Δ*. In such a case the unsafe zone **Ω** will be either a land strip along a linear structure (e.g., pipeline or power transmission line, Fig. 3.1a) or a circle around

a cylindrical structure (e.g., a storage tank, Fig. 3.1b) or an area with a relatively simple shape along several similar structures built in a row (Fig. 3.1c).

An intersection of the unsafe zone Ω by road network will form a road segment from which an accidental explosion can damage the target object. This segment will be denoted by the symbol ω and called the unsafe road segment (Fig. 3.1). The area ω can be interpreted as a set of explosion centre positions $x = (x_1, x_2)$ defined in a coordinate system $\{0; x_1, x_2\}$ which is fixed, for instance, to the target object. Clearly, an explosion can occur also outside the road surface denoted by ω. For example, a road tanker BLEVE may happen after a tank vehicle is involved in a traffic accident, departs from the road surface and encroaches on the roadside territory inside the zone Ω. Generally the position of a potential accidental explosion on road, x, is uncertain. A bivariate probability density function $f(x)$ is a natural means for quantifying this uncertainty (Vaidogas *et al.* 2012ab). It is evident that the density $f(x)$ must be defined on the zone Ω and not only on the segment ω.

With the coordinate system introduced above, the direction of incidence of explosion effects can be expressed through the position of explosion centre x (Fig. 3.1b). Then the safety distance can be formulated, where appropriate, as a function of an incidence angle φ, in brief, Δ_φ. The angle φ is determined by the explosion position x and can be related to the coordinate system $\{0; x_1, x_2\}$ or principal axes of an individual target structure (Fig. 3.1bc). The safety distance can be a directional quantity even in the case of the cylindrical tank structures shown in Fig. 3.1b. Piping and other system components are attached to the tanks only in one or several points and so cylindrical structures can in some directions be more vulnerable than in others.

An individual structure or a set of structures built close together can be very irregular in plan. Safety distances Δ_φ estimated for such structures can be highly directional and a corresponding unsafe zone Ω indicate an irregular layout. However, a road segment ω within such an area will in many cases have a regular layout (Fig. 3.2a).

3.2.1.2. Dealing with uncertainties in specifying the unsafe road segment

Factors determining safety distances around hazardous *stationary* equipment are more or less obvious and well-documented (e.g., EIGA 2007; Marangon *et al.* 2007). A determination of safety distances in the case where the hazard source (vehicle with an explosion potential) is moving in a relative vicinity of a target object involves several aggravating factors:
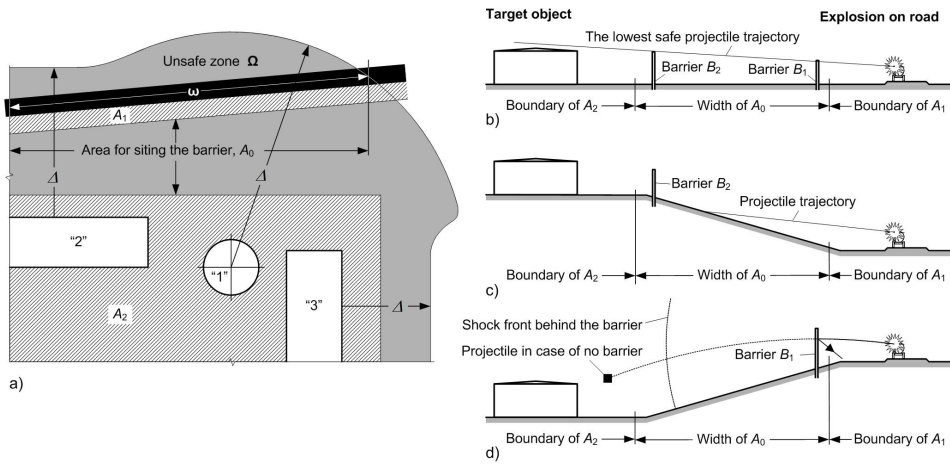
Fig. 3.2. The area A_0 available for sitting the barrier between road and target object(s): a) A_0 formed by the unsafe zone with irregular shape around the target objects "1" to "3" and the areas A_1 and A_2 in which a barrier construction is prohibited; b) the choice between two barriers in a flat horizontal area A_0; c) and d) sitting the barrier by taking into account the influence of the relief on attenuation or strengthening of explosion effects

1. The possibility of several explosions of different nature within the same road segment $\boldsymbol{\omega}$ (e.g., road tanker BLEVE and detonation of the load of explosive material).
2. Uncertainty related to characteristics of specific explosion (e.g., orientation and tonnage of a liquefied gas tank at the instant of BLEVE).
3. Uncertain position of explosion centre x within or near $\boldsymbol{\omega}$ and variability in features of the territory between the position x and target object.
4. The possibility of different degree of damage to the target object which can be caused by explosion of a specific type.

An estimation of the safety distance for all possible combinations of the aforementioned factors is a challenging task. It will become simpler by estimating the distance for a discrete set of values of the incidence angle φ. The task can also be simplified by taking into account the fact that variety of accidental explosions on road is not wide. The safety distance can be estimated for each type of probable explosion and the most conservative value assumed as Δ_φ.

Generally, an explosion related to the direction φ and represented by the random event E_φ can lead to some number of outcomes $O_{\varphi r}$ with the outcome likelihoods $P(O_{\varphi r} \mid E_\varphi) \times L(E_\varphi)$, where $P(O_{\varphi r} \mid E_\varphi)$ is the conditional probability of $O_{\varphi r}$ given E_φ and $L(E_\varphi)$ is the likelihood of E_φ. Alternative accident scenarios leading to different outcomes $O_{\varphi r}$ are related to different degrees of damage to

the target object. Outcome severity can be expressed by the vector $s_{\varphi r} = (s_{1\varphi r}, s_{2\varphi r}, \ldots, s_{s\varphi r}, \ldots)$ including lost money, lost time, number of fatalities, etc. and related to specific direction φ and accident scenario r (Kumamoto 2007; Zavadskas and Vaidogas 2009). With the above accident characteristics, the direction φ can be associated with the risk profile

$$\text{Risk}_\varphi \equiv \{(P(\text{O}_{\varphi r} \mid E_\varphi) \times L(E_\varphi), s_{\varphi r}) \; r = 1, 2, \ldots, n_\varphi\} \tag{3.1}$$

where n_φ is the number of accident scenarios associated with φ. The above expression of risk posed a potential explosion is well-known in the field of QRA applied to technologies involving fire and explosion hazards (e.g., Aven and Vinnem 2007; Vinnem 2007). The risk expressed by Eq. (3.1) presents diverse and comprehensive information, especially if the vector $s_{\varphi r}$ has more than one component. It is difficult to specify the safety distance Δ_φ on the basis of such information. In the case where the list of components n_s of $s_{\varphi r}$ is identical for all r, the risk can be expressed in a more concise form, namely, through the vector of expected severities:

$$(\bar{s}_{s\varphi}, s = 1,2,...,n_s) = \left(L(E_{\varphi r}) \sum_{r=1}^{n_s} P(\text{O}_{\varphi r} \mid E_\varphi) s_{s\varphi r}, s = 1,2,...,n_s \right) \tag{3.2}$$

Decisions concerning Δ_φ can be made on the basis of this vector. The simple decision rule is to choose such Δ_φ which corresponds to expected severities $\bar{s}_{s\varphi}$ satisfying the inequalities $\bar{s}_{s\varphi} \leq s_{s,tol}$ for all s, where $s_{s,tol}$ is a tolerable value of $\bar{s}_{s\varphi}$. In brief, one can write

$$\Delta_\varphi = \min\{\Delta \mid \bar{s}_{s\varphi}(\Delta) \leq s_{s,tol}, \forall s\} \tag{3.3}$$

where Δ is used as an optimisation (design) variable. Estimation of the expected severities $\bar{s}_{s\varphi}$ and specification of the corresponding tolerable values $s_{s,tol}$ for a given incidence direction φ can be a non-trivial task. In addition, this estimation must be carried out repeatedly until a satisfactory value of Δ_φ is found.

The task of estimating the expected severities can be sidestepped in the case where all accident scenarios include the same random damage event D which can escalate into the outcomes $O_{\varphi r}$. Examples of D are relatively simple events:

1. Toxic release due to loss of containment by a storage tank or rupture of a pipeline in consequence of an explosion.
2. Ignition of flammable material released due to mechanical and thermal effects of an explosion.
3. Interruption to service of a critical infrastructure (e.g., energy transportation system) due to explosive damage.

If D can be specified for a given target object, the conditional probability $P(D \mid E_{\varphi})$ can be estimated and $\varDelta_{\varphi}$ chosen as a distance for which $P(D \mid E_{\varphi})$ does not exceed some tolerable value P_{tol}:

$$\varDelta_{\varphi} = \min\{\varDelta \mid P(D \mid E_{\varphi}, \varDelta) \leq P_{tol}\} \qquad (3.4)$$

where $P(D \mid E_{\varphi}, \varDelta)$ denotes the damage probability expressed as a function of the optimisation variable $\varDelta$.

The decision rules given by Eqs. (3.3) and (3.4) are analogous to the problem of a reliability-based structural optimisation, in which a tolerable failure probability must be specified or, in other words, the problem "how safe is safe enough" solved (e.g., Lemaire 2009). Eqs. (3.3) and (3.4) yield a fixed value of $\varDelta_{\varphi}$ although this value is obtained by carrying out a probabilistic analysis, that is, an estimation of the damage probability $P(D \mid E_{\varphi}, \varDelta)$ (Fig. 3.3a).
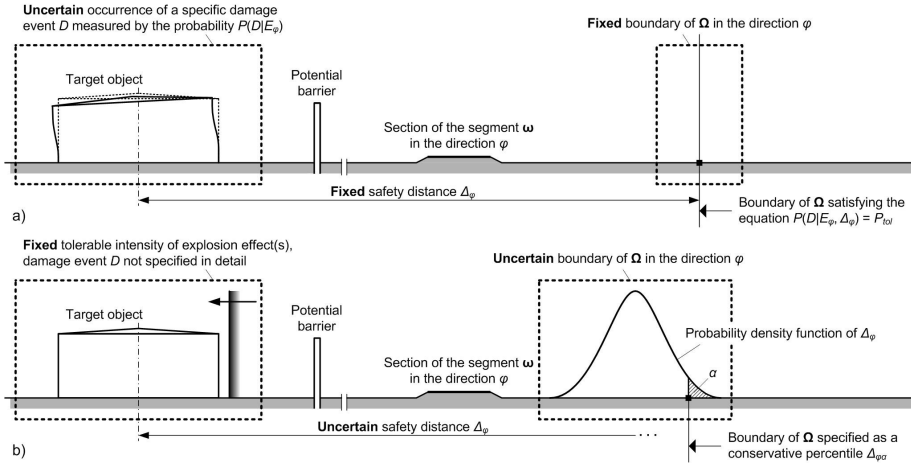
Fig. 3.3. Two approaches to a specification of the safety distance $\varDelta_{\varphi}$: a) specification of a fixed value of $\varDelta_{\varphi}$ based on a tolerable value P_{tol} of the damage probability $P(D \mid E_{\varphi})$; b) specification of $\varDelta_{\varphi}$ based on a fixed tolerable value of explosion effect and yielding a boundary of the unsafe zone $\mathbf{\Omega}$ defined by a percentile $\varDelta_{\varphi\alpha}$ of $\varDelta_{\varphi}$

An estimation of $P(D \mid E_{\varphi}, \varDelta)$ is a problem of a reliability-based structural analysis (RBSA). There is vast literature on a deterministic analysis and design of structures for explosive actions, to say nothing of the literature devoted to the design for fire actions (e.g., CPR 2005; Bangash and Bangash 2006; Bangash 2009). However, RBSA applications to assessing specific explosive damage to large, real-world structures (not individual structural elements) are limited and not systematized in widely known documents. The estimation of $P(D \mid E_{\varphi}, \varDelta)$ is

possible in theory by applying sophisticated methodology of RBSA. In practice, such estimation will require highly specific statistical data used to feed models developed for predicting explosion effects and describing interaction of complex structures with these effects. This data can be inaccessible to the designer (land use planner). Our impression is that in some highly specific cases the aforementioned data and models may not be available at all.

In the case where the damage event D can be caused by air blast only and D expressed by broad categories of explosive damage to buildings or industrial installations (minor damage, major damage, collapse), the probability $P(D \mid E_\varphi, \Delta)$ can be approximately estimated with relative ease using simple empirical models (probit functions) given in such documents as the Green book published by a Dutch organisation TNO (CPD 1992; CPR 2005). The event D can be associated with damage levels represented by either overpressure levels of incident shock wave, $\hat{p}_0$, or iso-damage diagrams (incident pressure-impulse diagrams or, in brief, p_0-i_0 diagrams). Overpressure levels $\hat{p}_0$ were chosen empirically and p_0-i_0 iso-curves were developed both empirically and analytically for typical structural elements. The safety distance Δ_φ corresponding to given values of $\hat{p}_0$ and regions of p_0-i_0 plots can be traced back from the models which relate values $\hat{p}_0$ and pairs (p_0, i_0) to explosion characteristics (e.g., Krauthammer 2008). Schematically these models can be represented by the functions

$$\hat{p}_0 = \psi(\Delta(\varphi) \mid e, \pi) \tag{3.5a}$$

and

$$\begin{pmatrix} p_0 \\ i_0 \end{pmatrix} = \boldsymbol{\psi}(\Delta_\varphi \mid e, \boldsymbol{\pi}) = \begin{pmatrix} \psi_p(\Delta_\varphi \mid e, \boldsymbol{\pi}) \\ \psi_i(\Delta_\varphi \mid e, \boldsymbol{\pi}) \end{pmatrix} \tag{3.5b}$$

where e is the explosion energy (mass of explosives) and π and $\boldsymbol{\pi}$ are the scalar variable and vector used to express uncertainty in (inaccuracy of) the models $\psi(\cdot)$ and $\boldsymbol{\psi}(\cdot)$, respectively.

A solution of Eqs. (3.5) for given values of $\hat{p}_0$, (p_0, i_0), π and $\boldsymbol{\pi}$ will yield a fixed value of the safety distance Δ_φ. However, the deterministic application of $\psi(\cdot)$ and $\boldsymbol{\psi}(\cdot)$ is questionable due to at least two reasons:

1. The energy (mass) e and inaccuracy measures π and $\boldsymbol{\pi}$ will be uncertain in many practical applications; the uncertainty in e, π and $\boldsymbol{\pi}$ is quantified by means of random variables, say, random variables $\tilde{e}$ and $\tilde{\pi}$ and vector of random variables, $\tilde{\boldsymbol{\pi}}$ (e.g., Aven and Zio 2011).

2. The damage levels D are represented by intervals of $\hat{p}_0$ and areas of pairs (p_0, i_0) in the incident pressure-impulse diagrams; the distance Δ_φ can be determined with most conservative values of $\hat{p}_0$ and (p_0, i_0) related to specific damage level; however, this conservative approach is not automatically justified and so $\hat{p}_0$ and (p_0, i_0) related to specific damage level should be considered uncertain.

Even though the quantities on the left-hand side of Eqs. (3.5) are fixed, the safety distance Δ_φ will be a function of random variables and so a random variable itself:

$$\Delta_\varphi = \psi^{-1}(\hat{p}_0 \mid \tilde{e}, \tilde{\pi}) \tag{3.6a}$$

$$\Delta_\varphi = \boldsymbol{\psi}^{-1}(p_0, i_0 \mid \tilde{e}, \tilde{\boldsymbol{\pi}}) \tag{3.6b}$$

where $\psi^{-1}(\cdot)$ and $\boldsymbol{\psi}^{-1}(\cdot)$ denote the inverse functions of $\psi(\cdot)$ and $\boldsymbol{\psi}(\cdot)$, respectively. A probability density function of Δ_φ can be estimated by means of Monte Carlo simulation. With the random safety distances Δ_φ, the unsafe zone $\boldsymbol{\Omega}$ will be fuzzy (uncertain) and its boundary can be specified by means of conservative percentiles $\Delta_{\varphi\alpha}$ of Δ_φ as shown in Fig. 3.3b.

The two approaches to the specification of the safety distances Δ_φ illustrated in Fig. 3.3 present two alternative ways of defining the unsafe zone Ω. The specification of Δ_φ by estimating the damage probabilities $P(D \mid E_\varphi, \Delta)$ is applicable to all types of explosion accidents and consistent in terms of uncertainty quantification and propagation. However, such specification can be difficult to implement. The specification of Δ_φ on the basis of the overpressure levels $\hat{p}_0$ and iso-damage $(p_0\text{-}i_0)$ diagrams is significantly simpler; however, it is applicable only to specific accidents and broad damage categories caused by these accidents.

An estimation of the safety distance Δ_φ for fires will be somewhat simpler than for explosions. The distance Δ_φ can be determined by using criteria of thermal damage given in such documents as the guidelines CCPS (2005a). Methods developed for modelling thermal radiation of pool fires and BLEVE fireballs can be applied to relate Δ_φ to a radiation intensity which can be tolerated by a roadside object subjected to a fire on road (e.g., Casal 2008).

3.2.2. Barrier configuration within an available area

The terrain physically available for barrier construction can be restricted by factors of very different nature:

1. Land ownership.
2. Legal requirements and regulations (e.g., prohibition of construction in the immediate vicinity of the road, say, in the area A_1 shown in Fig. 3.2a).
3. Configuration of facility involving the target object.
4. Irregular relief of the terrain and problematic geological conditions.
5. Architectural and aesthetical considerations.

In some cases restrictions posed by land ownership or construction regulations may force the owner of the facility at risk to built a barrier along the perimeter of the facility or even inside its territory. In such cases little space may be left for a barrier configuration in plan. In other cases, some area for barrier sitting, say, A_0, will be available. The area A_0 will form a part of the unsafe zone Ω and lie between two areas A_1 and A_2 in which the construction is either prohibited or impossible (Fig. 3.2a). The area along the road, A_1, can be required or recommended by regulations of road construction. For instance, a Lithuanian road regulation recommends 3-15 m wide clear strips alongside the roads with 70-130 km/h speed limits (KTR 2008). The opposite restricting area A_2 can be formed by installations surrounding the target object, for instance, diked area around storage tanks.

If the area A_0 is sufficiently wide to attenuate explosion effects (air blast, projectiles, thermal radiation), positioning the barrier may face at least three different situations:

1. If A_0 is flat and horizontal, the barrier can be deployed in any position within available space (Fig. 3.2b). The barrier built in the vicinity of the road (barrier B_1) will have to be strong enough to resist the so-called local explosion (e.g., Bulson 1997). The barrier sited in front of the area A_2 (barrier B_2) will have sustain a generally weaker distant "free field" explosion. The barrier B_1 can be lower than B_2 to provide protection against an impact by projectiles generated, for instance, by a road tanker BLEVE.
2. If A_0 is a sufficiently steep slope or even a banquette going upwards in relation to the road, the inclined A_0 will attenuate air-blast and catch some of projectiles as shown in Fig. 3.2c (Gebbeken and Döge 2010). In such a case it makes sense to build the barrier in front of the area A_2 (i.e., barrier B_2 in Fig. 2c).

3. In case where A_0 is a relatively steep downward slope, explosion effects will have favourable conditions to propagate towards the target object (Fig. 3.2d). Such surface will create the conditions for an explosion which can be considered intermediate between near-surface and open air explosion (e.g., Bulson 1997). In this case a sound decision is to build the barrier in front of the area A_1 (i.e., barrier B_1 in Fig. 3.2d).

A sufficiently wide space between the areas A_1 and A_2 opens up a possibility to give the barrier different forms in plan. The simplest and probably cheapest to build will be a straight barrier often called the blast wall (Fig. 3.4a). If the barrier will have to resist very intense explosion effects, it can be shaped as "an arrow headed bastion" (Fig. 3.4bc). Such a shape allows to increase the potential angle at which air-blast and projectiles will be reflected by the barrier.
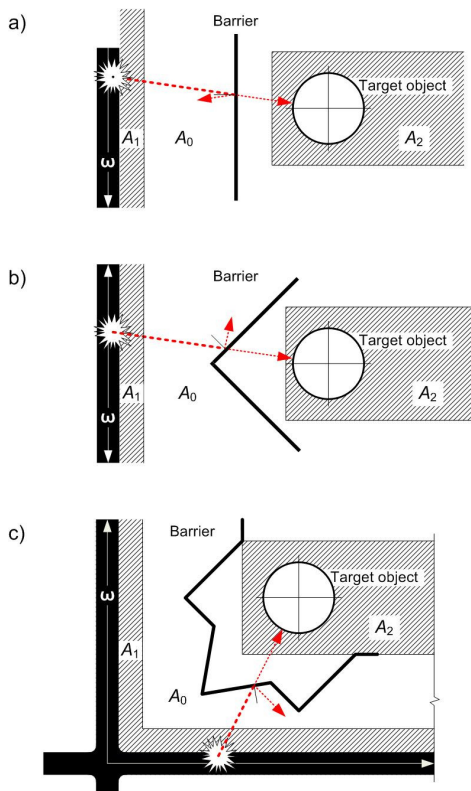

Fig. 3.4. Possibilities of a horizontal configuration of a barrier in the available area A_0: a) straight single-segment barrier ("blast wall"); b) two-segment ("arrow headed") barrier; c) multi-segment barrier ("arrow headed bastion")

The type of structural material, vertical section and protective capacity of a barrier do not need to be constant along its length. Individual barrier segments may differ substantially according to the demand for protective capacity. In the case where characteristics of explosion or fire do not depend on the position of vehicle within the unsafe road segment ω, this demand will be governed mainly by the distance between the target object and ω as well as the position of barrier within the area A_0.

Effectiveness of a safety barrier can be very limited when it comes to protecting against a BLEVE fireball. The height and diameter of a fireball generated during a road tanker BLEVE may exceed 100 m (Casal 2008). In the case where the horizontal distance between BLEVE and target object is small, a barrier protecting against blast and projectiles will not be able to stop thermal radiation. Consequently, shielding from thermal radiation should be provided in addition to the barrier. Such a case will be illustrated by an example presented in the next section.
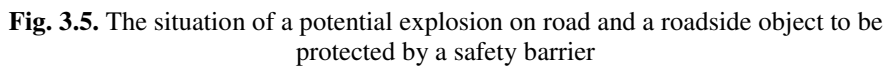
3.2.3. A practical application

The roadside object to be protected by a future safety barrier consists of three cylindrical reservoirs built in an oil transhipment facility located on the shore in the main sea port of Lithuania (Fig. 3.5, see also Figs. 2.12 and 2.13). The reservoirs can be damaged by fire or explosion of a tank vehicle on a two-lane public road going along the perimeter of the facility. The speed limit on this road is 70 km/h. The terrain schematically depicted in Fig. 3.5 is flat and horizontal.

No land acquisition is planned by facility owners and so the barrier is to be built inside the fenced perimeter of the facility. The area available for barrier construction, A_0, will be partially restricted by a 4 m clear strip alongside the road, A_1, recommended in a Lithuanian road regulation (KTR 2008). On the opposite side, A_0 will border the rectangular area A_2 where the barrier construction is prohibited due to technological reasons.

In order to keep the area occupied and obstructed by the barrier at a minimum, this structure should have the form of a wall and can either be built along the facility perimeter (points B_1 to B_6, Fig. 3.5) or correspond with the contour of the area A_2 (points C_1 to C_3, Fig. 3.5). Barriers sited in these two alternative positions will be called barrier "B" and barrier "C" and, for brevity, the word "barrier" will be skipped in some cases.

Barrier "C" lies farther away from the road than barrier "B". However, the distance between them is relatively small, especially between barrier segments protecting the 1st reservoir. Thus the position of "C" is not much better than the one of "B" in terms of a larger separation from a potential explosion or fire.

Fig. 3.5. The situation of a potential explosion on road and a roadside object to be protected by a safety barrier

Cross-sectional shape and distribution of protective capacity along the axes of "B" and "C" can be chosen by applying methods of structural optimisation. Different variants of "B" and "C" can be designed and the best one selected by means of formal methods of MCDM (Vaidogas 2007c; Zavadskas and Vaidogas 2009). However, pros and cons of "B" and "C" can be weighted before the optimisation. Tables 3.1 and 3.2 list advantages and disadvantages of "B" and "C", respectively, for the case where the barriers have to protect the facility not only against BLEVE but also against pool fire and formation of vapour cloud with subsequent flash fire or explosion. One can conclude at this stage of barrier design that, at least arithmetically, barrier "B" "overweights" barrier "C".

The position of endpoints of barriers "B" and "C" was chosen by introducing an unsafe road segment ω in the manner shown in Fig. 1c. The outermost points of ω, D_1 and D_3, correspond to a safety distance Δ which is approximately equal to 125 m (Fig. 3.5). Two lines connecting D_1 and D_3 to the point D_2 are tangents to the 3rd reservoir. These lines show two extreme trajectories of projectiles which can be ejected by an explosion on road and collide with the reservoirs. The barriers can be ended where they intersect the line segments D_1–D_2 and D_2–D_3.

The safety distance Δ used in this example is hypothetical and serves as an illustration. Generally, Δ should be estimated by solving the optimisation problem given by Eq. (3.4). The random damage event D in this problem is a loss of containment by at least one of the reservoirs. If the reservoirs are nominally identical, the distance Δ can be estimated only for one of them and the unsafe zone Ω plotted as shown in Fig. 3.1c.

An estimation of the damage probability $P(D \mid E_\varphi, \Delta)$ in Eq. (3.4) is a nontrivial task, especially for such a complex event as BLEVE. A solution of this task requires a great deal of space and is beyond the scope of this study. At present one can only say that the estimation of $P(D \mid E_\varphi, \Delta)$ may face two problems: scarcity of data on effects of fires and/or explosions recorded during/after past accidents and need to predict these effects and response of reservoirs to them by means of models which are not necessarily very accurate. The best way to deal with these problems is an application of methods based on the Bayesian statistical theory and widely used for QRA (Juocevičius and Vaidogas 2010; Vaidogas 2003, 2006a, 2007a, 2009; Vaidogas and Juocevičius 2007, 2008a, 2009).

If designed properly, barriers "B" and "C" will protect the reservoirs against effects of blast and projectiles. They can provide also protection against pool fire and flash fire, both preceded by accidental release of flammable liquid or gas from a road tank. However, such event as a road tanker BLEVE will generate a fireball, the height of which may considerably exceed the height of "B" and "C".

Table 3.1. List of advantages of the barriers "B" and "C"

Barrier "B" (points B1 to B6, Fig. 3.5)
▪ Protects larger area of the facility than barrier "C".
▪ Can serve as vehicle barrier (anti-ram wall) if so designed (barrier segment B_2 to B_5 should be capable to resist vehicular impact).
▪ Can prevent a vapour cloud accidentally released from a tank vehicle from encroaching on the facility area along the line B_1–B_6 in order to avoid a Viareggio-type accident (Pontigia *et al.* 2011).
▪ Can prevent a pool of flammable liquid accidentally discharged from a tank vehicle in the vicinity of the segment B_3–B_4 from encroaching on the facility area.
▪ Can be lower than "C", especially in the segment B_3–B_4 due to reasons explained in Fig. 3.2b.
▪ Can safely collapse onto the area A_0 and so can be designed as a sacrificial barrier (Krauthammer 2008).
▪ The space behind "B" is available to provide counterforts, if necessary.
▪ Does not restrict access to the technological area A_2.
▪ May serve as a part of perimeter fencing.
▪ Construction of "B" should not hinder technological activities in the area A_2.
Barrier "C" (points C1 to C3, Fig. 3.5)
▪ Can serve as an "arrow headed" barrier with a knee joint in point C_2 which is closest to the turn of the road.
▪ If designed taller than "B", provides larger area of shielding against thermal radiation.
▪ Will not reduce visibility at the turn of the road.

Table 3.2. List of disadvantages of the barriers "B" and "C"

Barrier "B" (points B1 to B6, Fig. 3.5)
▪ Must have higher resistance than "C", especially in the segment B_3–B_4.
▪ Can hinder visibility on the road along the segment B_3–B_4.
▪ Provides little of its surface for a reflection of blast and projectiles at large angles.
Barrier "C" (points C1 to C3, Fig. 3.5)
▪ Protects the technological area A_2 only.
▪ Can not be designed as a "sacrificial barrier" if a collapse onto the technological area is not allowed.
▪ The space behind "C" is limited to provide counterforts.
▪ Will not prevent vapour cloud or pool of flammable liquid accidentally released from a tank vehicle from an encroaching on the facility territory.
▪ Construction of "B" can hinder technological activities in the area A_2.

Characteristics of the fireball can be estimated by simple deterministic models (e.g., Casal 2008). For instance, if a typical LPG semi-trailer with a volume of 56 m^3, 85% of which are filled with propane, is heated by a fire to 55 °C

(approximately 19 bar) and bursts, the mass of fuel involved in the fireball will be 23 800 kg. Estimates of fireball diameter and height of its centre are 167 m and 125 m, respectively. The duration of the fireball will be around 11 seconds. If the centre of BLEVE will be in the point E_1, which is placed only 40 m apart from the 1st reservoir, the fireball will fully cover the 1st reservoir and partially the 2nd reservoir (Fig. 3.5). Thermal radiation of the fireball on the top edge of the 1st reservoir (point E_2) is 38.5 kW/m². Such a radiation can damage the reservoirs (CCPS 2005a). A thermal shielding of these structures must be provided because barriers "B" and "C" will not adequately protect against thermal radiation coming from the altitude far above the ground surface.

3.3. Design of barrier with sacrificial cladding

3.3.1. Failure probability of sacrificial cladding as a measure of damage degree

In the case where all individual components of SC are nominally identical or a continuous SC can be discretised notionally into nominally identical components, a different number of them will fail (will be "sacrificed") at different intensities of reflected blast wave. Characteristics of a pressure history of this wave can be represented by a n_y-dimensional vector y with the components y_1, y_2, y_3, ... , y_{n_y} expressing overpressure, positive duration, impulse, etc. ($n_y \geq 1$).

Then the relative number of the failed components and so the degree of damage to SC can be estimated by a conditional probability of failure of an individual component:

$$P_f(y) = P(\bigcup_i D_i \mid y) \tag{3.5}$$

where D_i is the random event of damage to an SC component related to the failure mode i (the ith damage event, in brief). The function $P_f(y)$ is known in SRA and QRA as a fragility function and its arguments y are called the demand variables (e.g., Bah *et al*. 2005; Langdom *et al*. 2010).

If the blast wave characteristics are uncertain and represented by a random vector Y, the unconditional probability of SC component failure, P_f, can be expressed as a mean value of the fragility function $P_f(\cdot)$ with a random arguments Y, namely,

$$P_f = \int_{\text{all } y} P_f(y)\, f_Y(y)\, \mathrm{d}\, y = E_Y(P_f(Y)) \tag{3.6}$$

where $f_Y(y)$ is the joint probability density function of Y. Eq. (3.6) is a standard definition of a failure probability widely used in SRA. The problem of estimat-

ing P_f for blast loading generated by an accidental explosion is that statistical data for fitting the model $f_Y(y)$ will typically be unavailable. However, P_f can be estimated with a small-size sample consisting of observations y_j of Y obtained by experiment (Vaidogas 2007a). Let this sample be

$$y = \{y_1, y_2, \ldots, y_j, \ldots, y_n\} \tag{3.7}$$

Elements of y can be transformed into fragility function values $P_f(y_j)$ and a new, artificial sample $\{P_f(y_1), P_f(y_2), \ldots, P_f(y_j), \ldots, P_f(y_n)\}$ formed. The latter sample can be used to compute a bootstrap confidence interval $]0, \overline{P}_f[$ for P_f. The closer is the upper limit $\overline{P}_f$ to unity, the larger number of SC components should be expected to be lost in case of an explosion. Consequently, $\overline{P}_f$ can be used as a conservative measure of the damage to a blast wall.

The interval estimate $]0, \overline{P}_f[$ comes from the classical, Fisherian statistics. If necessary, the sample y can be used to estimate P_f in a Bayesian format, namely, by a conservative percentile of a posterior distribution obtained by applying y (Vaidogas 2009; Vaidogas and Juocevičius 2009; Juocevičius 2011).

The form of the sample y assumes that there are no uncertainties in the data y_j. This assumption may not be correct in a number of cases. For example, if the blast wave characteristics are not directly recorded in experiment but are obtained by means of a mathematical modelling, the elements of y can be uncertain (fuzzy). Uncertainty in an individual element of y, say, the element j can be quantified by an epistemic probability distribution with the density $f_j(y)$ (Yang and Fallah 2011). A one-dimensional visualisation of a crisp and uncertain data points y_j and $f_j(y)$ is shown in Fig. 3.6. The interval estimation of P_f is possible also with the uncertain, as shown in the next section.

3.3.2. Dealing with uncertainties in the mechanical model of sacrificial cladding

In the case where the damage event(s) D_i are backed by the model(s) m_i, the fragility function $P_f(y)$ can be expressed as

$$P_f(y) = P(\bigcup_i (m_i(Z, y \mid \boldsymbol{\theta}) \leq 0)) \tag{3.8}$$

where Z is the vector of random input variables; $\boldsymbol{\theta}$ is the vector of parameters of the model of $m_i(\cdot)$. The random safety margin $m_i(Z, y \mid \boldsymbol{\theta})$ is a standard function of SRA, in which the vector Z and so the function m_i express the stochastic uncertainty. The uncertainty modelling prevailing in QRA requires to consider an epistemic uncertainty related to the parameter vector $\boldsymbol{\theta}$ (e.g., Li *et al.* 2009). This uncertainty can be expressed by a random vector $\boldsymbol{\Theta}$ with a joint density $\pi(\boldsymbol{\theta})$.

One or more components of $\boldsymbol{\Theta}$ can be used to express uncertainty in the accuracy of the model $m_i(\cdot)$. One can interpret the epistemic density $\pi(\boldsymbol{\theta})$ as a prior distribution which can be updated, at least in theory, given a new data. Then the posterior density will have the form $\pi(\boldsymbol{\theta}\,|\,\text{data})$.
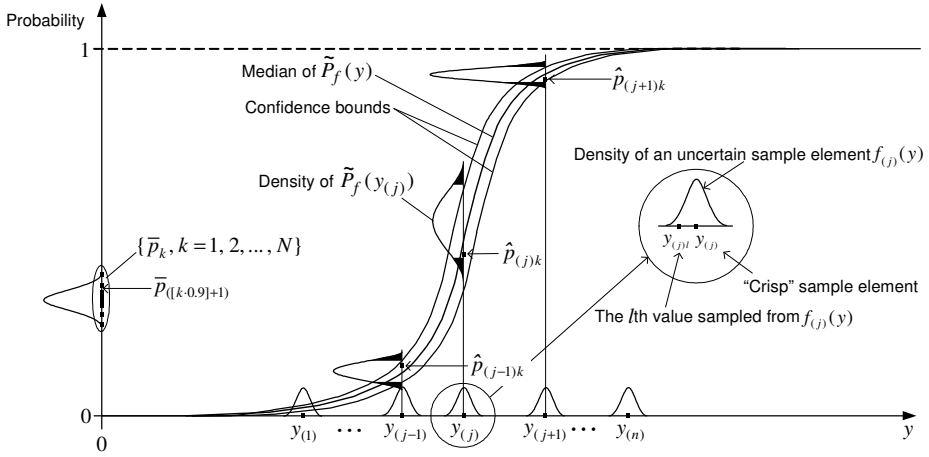

Fig. 3.6. A schematic illustration of the epistemic uncertainty in the value of the fragility function $\tilde{P}_{\mathrm{f}}(\boldsymbol{y})$

With the random parameter vector $\boldsymbol{\Theta}$, the fragility function $P(D_i\,|\,\boldsymbol{y})$ becomes an epistemic random variable defined as

$$\tilde{P}_{\mathrm{f}}(\boldsymbol{y}) = P_{\mathrm{f}}(\boldsymbol{y}\,|\,\boldsymbol{\Theta}) = P(\textstyle\bigcup_i (m_i(\boldsymbol{Z}, \boldsymbol{y}\,|\,\boldsymbol{\Theta}) \leq 0)) \qquad (3.9)$$

An illustration of the random fragility function $\tilde{P}_{\mathrm{f}}(\boldsymbol{y})$ is shown in Fig. 3.6. This illustration assumes that the vector $\boldsymbol{y}$ has only one component, for instance, the positive overpressure of the reflected blast wave.

The typical approach to dealing with epistemic uncertainties in fragility functions is establishing confidence bounds around the point estimates of fragility curve or median fragilities (e.g., Boh *et al.* 2005). Most authors consider the confidence bounds as the final result of analysis. However, a further propagation of the epistemic uncertainty quantified by $\boldsymbol{\Theta}$ is necessary to estimate the failure probability P_{f}. In case where the explosion demand $\boldsymbol{y}$ is represented by the small-size sample $\boldsymbol{y}$, the estimation of P_{f} can be expressed as an estimation of a mean of fragility function values with uncertain (fuzzy) data $\tilde{P}_{\mathrm{f}}(\boldsymbol{y}_j)$ ($j = 1, 2, \ldots, n$). Such data can be used for updating a Bayesian prior distribution expressing epistemic uncertainty in P_{f} (Vaidogas 2009). However, if

a development of a prior for P_f is problematic or there is no interest in the Bayesian estimation of P_f, the failure probability can be estimated by a Fisherian confidence interval computed by means of a simulation-based procedure explained in the remainder of the present section.
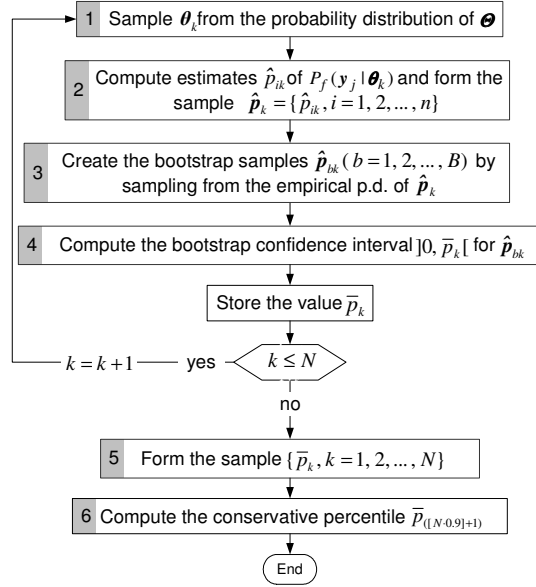

Fig. 3.7. The flowchart of estimating the failure probability of the sacrificial cladding, P_f

An estimate of P_f can be obtained by computing estimates of the fragility function values $P_\mathrm{f}(\boldsymbol{y}_j \mid \boldsymbol{\theta}_k)$ for all n elements $\boldsymbol{y}_j$ of the sample $\boldsymbol{y}$ and the values $\boldsymbol{\theta}_k$ of the parameter vector $\boldsymbol{\Theta}$ generated from $\pi(\boldsymbol{\theta})$ or $\pi(\boldsymbol{\theta} \mid \mathrm{data})$ ($k = 1, 2, \ldots, N$). This will require to estimate the fragility function $n \times N$ times. The kth loop of the estimation of P_f should start from sampling the value $\boldsymbol{\theta}_k$ (Fig. 3.7, Block 1). For each $\boldsymbol{\theta}_k$, the estimates $\hat{p}_{jk}$ of $P_\mathrm{f}(\boldsymbol{y}_j \mid \boldsymbol{\theta}_k)$ should be computed for all elements of $\boldsymbol{y}$ and grouped into the sample $\hat{\boldsymbol{p}}_k = \{\hat{p}_{jk}, j=1,2,\ldots,n\}$ (Fig. 3.7, Block 2). An illustration of three elements of $\hat{\boldsymbol{p}}_k$ is given in Fig. 2. The sample $\hat{\boldsymbol{p}}_k$ can be used to calculate a one-sided bootstrap confidence interval $]0, \overline{p}_k[$ for P_f (Fig. 3.7, Blocks 3 and 4). A repetition of this process N times will yield a sample consisting of N upper limits of the confidence interval, namely, $\{\overline{p}_k, k = 1, 2, \ldots, N\}$ (Fig. 3.7, Block 5). This sample will express the epistemic uncertainty related to the upper limit of this interval (see the abscissa axis in Fig. 2). A conservative percentile of this sample, say, $\overline{p}_{([N \cdot 0.9]+1)}$ can be used as

the final result of the conservative estimation of the failure probability P_f (Fig. 3.7, Block 6).

In the case of the uncertain data expressed by the densities $f_j(\mathbf{y})$, the procedure of the estimation of P_f can be applied in a similar way, with the difference that some number N_l of the samples $\mathbf{y}_l = \{\mathbf{y}_{1l}, \mathbf{y}_{2l}, \ldots, \mathbf{y}_{jl}, \ldots, \mathbf{y}_{nl}\}$ will have to be sampled from the distributions $f_j(\mathbf{y})$ ($j = 1, 2, \ldots, n$). A one-dimensional illustration of the sample element $\mathbf{y}_{jl}$ is given in Fig. 3.6. The procedure shown in Fig. 3.7 should be applied to each $\mathbf{y}_l$. A repetition of this process N_l times will yield a sample of confidence interval limits, $\{\bar{p}_k, k = 1, 2, \ldots, N \times N_l\}$. A percentile of this sample, say, $\bar{p}_{([N \cdot N_l \cdot 0.9]+1)}$ may serve as a conservative estimate of P_f. Clearly, the estimates $\bar{p}_{([N \cdot N_l \cdot 0.9]+1)}$ will tend to be more conservative than $\bar{p}_{([N \cdot 0.9]+1)}$, because the variability of the limits $\bar{p}_k$ will be larger in the former case than in the latter.

3.3.3. Practical application

The estimation of the SC failure probability P_f will be illustrated for a blast wall intended to protect against a railway tanker BLEVE. The tank car is used for a transportation of liquefied propane. Mechanical effects of BLEVE occur as blast and projectiles (Vaidogas and Juocevičius 2007). The present case study will consider the blast loading only whereas the protection against projectiles will be addressed in brief at the end of this section.

The object to be protected by the blast wall is a diesel fuel tank ("target") located 63 m from external railway tracks (Fig. 3.8). The worst case scenario will be considered, according to which the angle of incidence of the blast wave will be equal to 90 degrees (Fig. 3.9). The fuel tank is surrounded by a protective embankment used to stabilise the blast wall. The wall is to be built from non-sacrificial posts and SC consisting of profiled steel sections (Figs. 3.10 and 3.11).
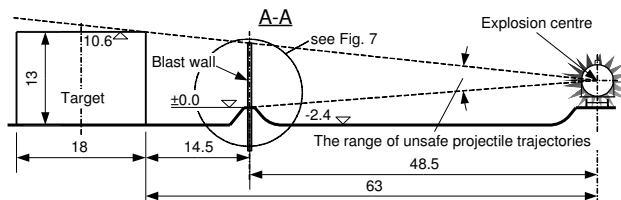
Fig. 3.8. The elevation of the accident situation

The elements $y_j = (y_{1j}, y_{2j})$ of the sample y will consist of overpressure y_{1j} and positive phase duration y_{2j} of the reflected blast wave, respectively. Experiments which could yield y are very expensive. Therefore, y was obtained by calculation and not by a direct recording y_j. The real-world statistical sample used in this case study was compiled from 30 data pairs (x_{1j}, x_{2j}), where x_{1j} and x_{2j} is weight and pressure of liquefied propane in the tank car j, respectively (Table 3.3, Cols. 2 and 3). The pairs (x_{1j}, x_{2j}) were used to calculate the mass of trinitrotoluene (TNT) which could cause an explosion with an energy equivalent to the energy of BLEVE (Table 3.3, Col. 4) (Vaidogas and Juocevičius 2007). The TNT mass and the explosion stand-off equal to 48.5 m were used to calculate y_{1j} and y_{2j} by applying a standard empirical model developed for TNT (Palanivelu *et al*. 2010) (Table 3.3, Cols. 5 and 6).

Fig. 3.9. The plan of the potential accident site

Fig. 3.10. Details of the blast wall: a) vertical section; b) profiled steel section; c) view from the back showing a safety net; d) plan

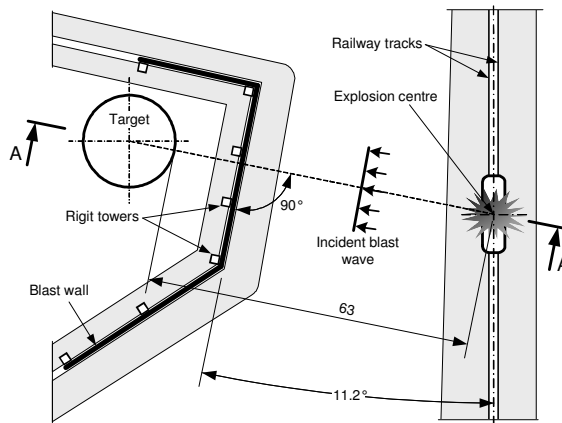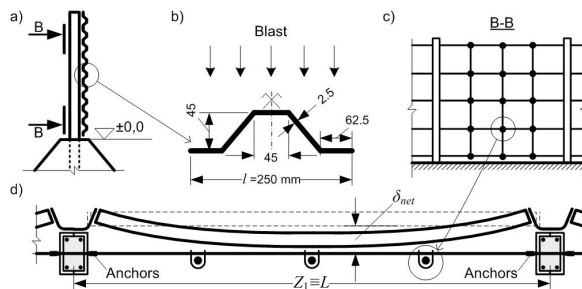**Table 3.3.** Characteristics of the reflected blast wave, y_{1j} and y_{2j}

j	x_{1j}, kg	x_{2j},kPa	TNT, kg	y_{1j}, kPa	y_{2j}, ms
1	2	3	4	5	6
1	60939	2575	83.29	13.51	24.74
2	57566	2462	90.30	14.04	25.08
3	57419	2395	77.14	13.04	24.43
4	59472	2602	99.41	14.69	25.48
5	54108	2453	73.21	12.72	24.21
6	56751	2312	66.63	12.18	23.84
7	61307	2615	71.69	12.60	24.13
8	59950	2264	89.97	14.01	25.06
9	55176	2572	74.78	12.85	24.30
10	58094	2531	73.30	12.73	24.22
11	57839	2446	83.50	13.53	24.75
12	58116	2270	52.10	13.42	24.68
13	57777	2424	83.45	13.52	24.75
14	60724	2457	79.33	13.21	24.54
15	56333	2411	77.83	13.09	24.46
16	55878	2193	71.71	12.60	24.13
17	59339	1922	64.05	11.96	23.68

   Two random damage events D_1 and D_2 related to the maximum dynamic response of profiled sections and backed by the respective safety margins m_1 and m_2 expressed by Eq. (1.3) will be considered. The fragility function $P_f(\boldsymbol{y})$ will have the form $P(D_1 \cup D_2 \mid \boldsymbol{y})$. The safety margins expressed as functions of random variables present in the mechanical model of profiled sections have the form

$$m_1(\boldsymbol{Z}, \boldsymbol{y} \mid \boldsymbol{\Theta}) = p_R(\boldsymbol{Z} \mid \boldsymbol{\Theta}) - y_1 \qquad (3.10a)$$

$$m_2(\boldsymbol{Z}, \boldsymbol{y} \mid \boldsymbol{\Theta}) = u_{pl,\boldsymbol{max}}(\boldsymbol{Z}, \boldsymbol{y} \mid \boldsymbol{\Theta}) - u_{pl,dyn}(\boldsymbol{Z}, \boldsymbol{y} \mid \boldsymbol{\Theta}) \qquad (3.10b)$$

where $\boldsymbol{Z} = (Z_1, Z_2, Z_3, Z_4)$ and $\boldsymbol{\Theta} = (\Theta_1, \Theta_2, ..., \Theta_5)$ are the vectors used to model aleatory and epistemic uncertainties, respectively (Table 3.4); $p_R(\cdot)$, $u_{pl,max}(\cdot)$ and $u_{pl,dyn}(\cdot)$ are deterministic functions used to compute quantities given in Eqs. (1.3).

Table 3.4. Aleatory and epistemic random variables used in the analysis of the blast wall under design

Description and notation (notation used this study ≡ notation from the original text by Louca *et al.* (2004))	Mean/coeff. of variation	Probability distribution
Aleatory random quantities (components of Z)		
Span (spacing of posts) $Z_1 \equiv L$ (m) (see Fig. 3.10d)	2.0/0.005[*]	Lognormal
Static yield strength of profiled section steel, $Z_2 \equiv p_y$ (MPa)	554/0.11[*]	Lognormal
Modulus of elasticity of profiled section steel, $Z_3 \equiv E$ (GPa)	200/0.06[*]	Normal
Natural period of elastic vibration of profiled sections, $Z_4 \equiv T$ (ms)	3.4/0.05	Normal
Epistemic random quantities (components of Θ)		
Enhancement factor for steel strength, $\Theta_1 \equiv \gamma$, the uncertainty in Θ_1 was modelled by the expression $1 + \Delta \times \xi$[**] ($\Delta = 0.12$)	1.012/0.011	Beta, $\xi \sim Be(1, 9)$
The factor of uncertainty related to the model of ductility ratio μ, Θ_2	1/0.04	Normal $N(1, 0.04)$
Reduction factor for stiffness of profiled sheet, $\Theta_3 \equiv f_K$; the uncertainty in Θ_3 was modelled by the expression $1 - \Delta \times \xi$[***] ($\Delta = 0.3$); the mode of Θ_3 is equal to 0.85	0.85/0.05	Beta, $\xi \sim Be(6, 6)$
Reduction factor for transverse stress effect, $\Theta_4 \equiv f_C$	0.99/0.085	Beta $Be(70, 1)$
Reduction factor for flattering of cross-section, $\Theta_5 \equiv f_F$; the uncertainty in Θ_5 was modelled by the expression $1 - \Delta \times \xi$[***] ($\Delta = 0.2$); the mode of Θ_5 is equal to 0.952	0.933/0.0382	Beta, $\xi \sim Be(2, 4)$

[*] Spaethe (1987)

[**] This linear transformation is used to obtain a Beta distribution defined on the interval]1, 1.12 [which covers potential values of the strength enhancement factor (Juocevičius and Vaidogas 2010)

[***] This linear transformation is used to obtain a Beta distribution defined on the interval [Δ, 1]

Probability distributions of the components of Z and Θ were chosen partly on the basis of information on natural variability of the quantities used in the analysis and partly on the basis of subjective reasoning. Cross-sectional dimensions of profiled sections are considered to be fixed (deterministic) quantities (Fig. 3.10b).

The probability distributions of the random variables Z_1 to Z_3 can be easily specified from information on random properties of steel structures (e.g., Spaethe 1987). The natural period of elastic vibration, Z_4, is considered to be an

aleatory quantity because it can be measured experimentally. We assumed the nominal value of this period, 3.4 ms, given by Louca *et al.* (2004) to be a mean value of a normal distribution of Z_4. The probability distributions of the epistemic variables grouped into the vector $\boldsymbol{\Theta}$ were used to express uncertainty related to parameters of the models $p_R(\cdot)$, $u_{pl,max}(\cdot)$ and $u_{pl,dyn}(\cdot)$. These distributions quantify the doubts expressed by Louca *et al.* (2004) and Juocevičius and Vaidogas (2010) about quantities represented by $\boldsymbol{\Theta}$.

The functions on the right-hand side of Eqs. (9) are based on a mechanical model of profiled sections proposed by Louca *et al.* (2004). The dynamic pressure capacity is given by

$$p_R(\boldsymbol{Z} \mid \boldsymbol{\Theta}) = \frac{8Z_2\Theta_1 w_{el}}{l_E^2(Z_1,\Theta_3)l}\Theta_4\Theta_5 \tag{3.11}$$

where $l_E(\cdot)$ is the effective span; w_{el} is the deterministic elastic section modulus depending on the cross-sectional dimensions; l is the cross-sectional width (Fig. 3.10b).

The maximum plastic dynamic deflection capacity is given by

$$u_{pl,\boldsymbol{max}}(\boldsymbol{Z},\boldsymbol{y} \mid \boldsymbol{\Theta}) = \frac{5}{48} \cdot \frac{Z_2\Theta_1 l_E^2(Z_1,\Theta_3)}{0.5Z_3 h} \times$$

$$\times \frac{\Theta_4\Theta_5}{\Theta_3}\mu(Z_1,Z_2,Z_4,y_1,y_2 \mid \Theta_1,\Theta_3,\Theta_4,\Theta_5) \tag{3.12}$$

where $\mu(\cdot)$ is the function used to compute the ductility ratio and given by

$$\mu(\boldsymbol{Z},\boldsymbol{Y} \mid \boldsymbol{\Theta}) = \Theta_2\varphi\left(\frac{y_2}{Z_4}, \frac{p_R(Z_1,Z_2 \mid \Theta_1,\Theta_3,\Theta_4,\Theta_5)}{p_r(y_1)}\right) \tag{3.13}$$

where $\varphi(\cdot,\cdot)$ is the function fitted to the graphs developed by Biggs (1964) and used for retrieving values of $\mu(\cdot)$.

The dynamic plastic deflection due to the blast load is computed using the following expression

$$u_{pl,dyn}(\boldsymbol{Z},\boldsymbol{y} \mid \boldsymbol{\Theta}) = \frac{p_r(y_1)l_E^4(Z_1,\Theta_1)}{384Z_3} \cdot \delta(y_2) \tag{3.14}$$

where $\delta(y_2)$ is the dynamic loading factor computed by

$$\delta(y_2) = \max_t \left(\begin{array}{c} 1 - \cos(2\pi t / Z_4) + \\ + \dfrac{\sin(2\pi t / Z_4)}{2\pi y_2 / Z_4} - \dfrac{t}{y_2} \end{array} \middle| \; 0 \le t \le y_2 \right) \qquad (3.15)$$

In the present case study, these ranges of the sample components y_{1j} and y_{2j} are [11.6 kPa, 14.4 kPa] and [23.0 ms, 25.8 ms], respectively. An illustration of the fragility function $P_f(y \mid \boldsymbol{\theta}_k)$ estimated for one realisation $\boldsymbol{\theta}_k$ of $\boldsymbol{\Theta}$ is shown in Fig. 3.11.

Fig. 3.12 shows a histogram of the sample $\{\bar{p}_k, k = 1, 2, ..., 500\}$ obtained by generating 500 values $\boldsymbol{\theta}_k$ and applying the procedure shown in Fig. 3.7 ($N = 500$). Exceeding the maximum dynamic plastic deflection (the event D_2) was dominating failure mode and this failure determined the confidence limits $\bar{p}_k$. The 90th percentile of the above sample, $\bar{p}_{([N \cdot 0.9]+1)}$, is equal to 0.263. This value is a conservative estimate of the SC failure probability P_f. It means that less than 26.3% of profiled sections will be destroyed ("sacrificed") in case of an explosion. This percentage can be changed as needed by redesigning SC, say, choosing a different profiled section.

A BLEVE produces high-energy projectiles generated by a rupture of tank car vessel (Vaidogas and Juocevičius 2007). It is highly probable that the blast wall under study will have to sustain an impact by some of them. Therefore, the height of the wall will be governed by unsafe trajectories of potential projectiles (Fig. 3.9). The profiled sections will not be able to stop larger projectiles and, in our opinion, a safety net should be added behind the cladding (Fig. 3.10c and d). The net can be designed to sustain not only primary projectiles from vessel rupture but also profiled sections which will fail under blast loading and/or projectile impact. The space between cladding and safety net, δ_{net}, should allow to reach the maximum dynamic plastic deflection of the profiled sections, $u_{pl,max}$ (Fig. 3.10d). As this deflection is a random quantity, the value of δ_{net} can be chosen by reducing the probability $P(u_{pl,max}(\mathbf{Z}, y \mid \boldsymbol{\Theta}) \ge \delta_{max})$ to some small and tolerable value.
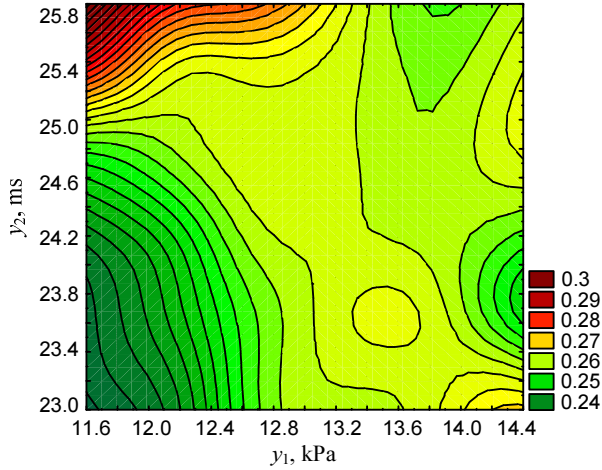
Fig. 3.11. The surface of the fragility function $\tilde{P}_{\mathrm{f}}(\boldsymbol{y})$ with the demand variables y_1 (peak overpressure) and y_2 (positive phase duration)
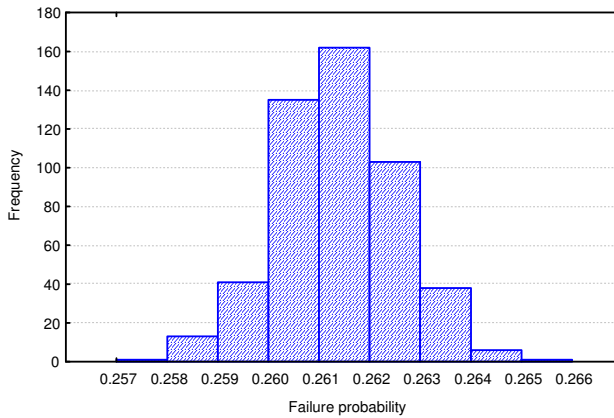
Fig. 3.12. Histogram of the sample $\{\bar{p}_k, k = 1, 2, \ldots, 500\}$

The horizontal cables of the net can span over several posts. Cable ends can be anchored in rigid towers distributed along the barrier (Fig. 3.9). Additional anchors can be added where the cables cross the posts (Fig. 3.10d). This will add extra stability to the posts and so the cladding. However, a detailed design of safety net, posts, and towers was beyond the scope of this case study.

3.4. Proposals to design of a reinforced concrete barrier capable to resist fragment impact

3.4.1. The choice of barrier material

A safety barrier to be built in an industrial area must be relatively cheep and not necessarily attractive in the architectural sense. The barrier intended to protect roadside property against fragments resulting from a BLEVE on road or rail can be built from three obvious materials: reinforced concrete (RC), steel and soil. A combination of these materials in one barrier is also possible. An example of such a combination is shown in Fig. 3.10.

An RC barrier can be from in-situ concrete. However, a better choice is to apply precast concrete segments similar to those used in the Berlin wall and known also as *Stützwandelement UL 12.11* (Fig. 3.13). A barrier built of precast RC segments can be massive, tall, require minimum maintenance and occupy a relatively little space. One can expect that it will be substantially cheaper than a structural steel barrier with similar dimensions and protective capacity. A proper provision of reinforcement may assure a "sacrificial" behaviour of an RC barrier during the impact. In addition, the RC barrier will provide protection not only against fragment impact but also a blast resulting from a BLEVE. Finally, RC segments, which are relatively narrow in front, will allow to easily adjust the barrier to the relief where the area of barrier construction is not flat.

A barrier made of structural steel will require constant maintenance. Moreover, barrier elements capable to withstand an impact of large high-energy fragments of road and railway tanker vessels will have to be massive and so expensive. It is highly probable that a steel barrier will include RC components, such as foundations and posts or similar cantilever elements. In addition, a steel barrier built in the vicinity of road or tracks can be insufficiently resistant to open-air fires.

A soil embankment can assure a good protection against fragment impact provided that it is adequately dimensioned and will cross the most of probable fragment trajectories. An embankment can be relatively cheap and build in a short time. However, a sufficiently tall embankment will be very wide at original ground surface. Thus, it will occupy large area between roadside target and centre of a potential explosion. In some cases such area will be unavailable. In addition, slopes of an embankment can be insufficiently steep to provide an adequate protection against blast loading.
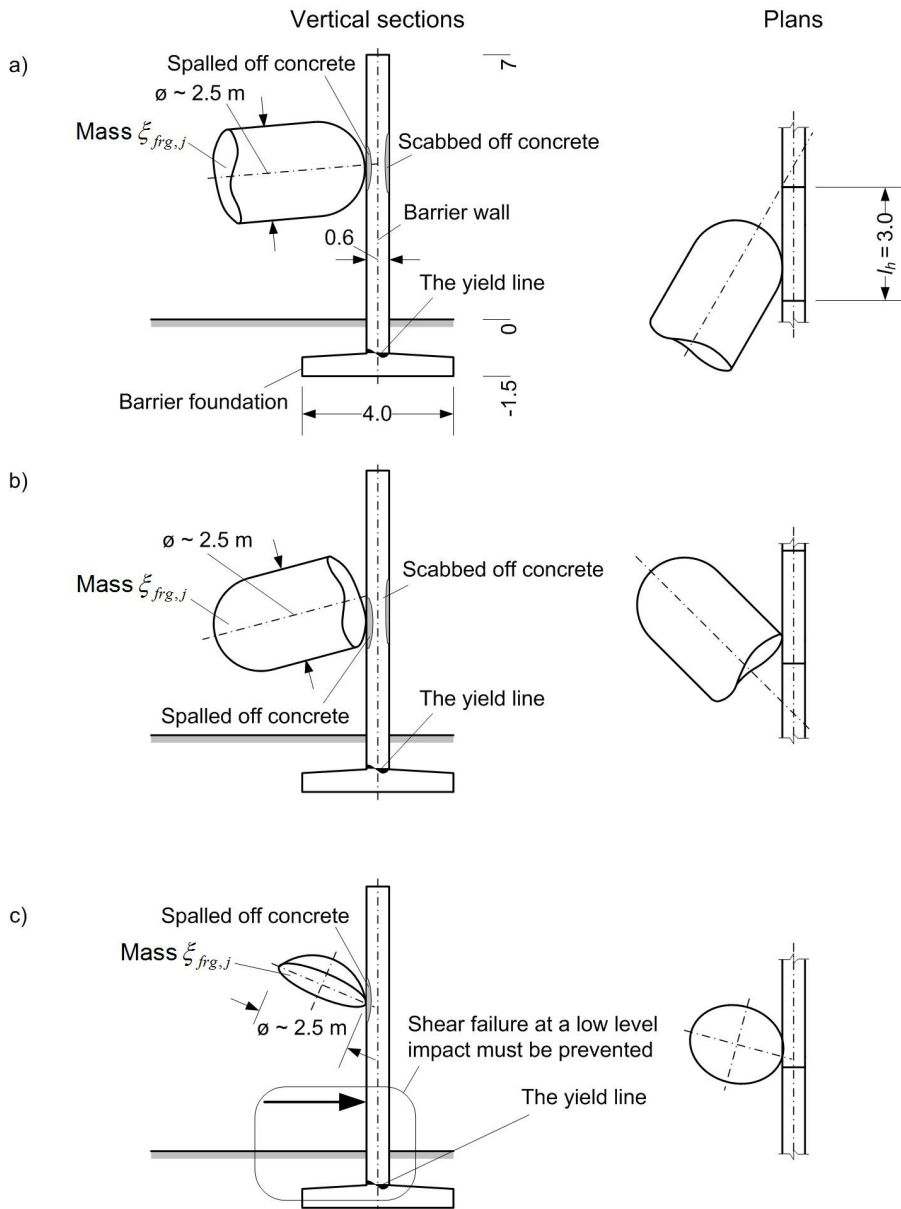
Fig. 3.13. Impact of fragments on a Berlin-wall-type barrier a) impact by the blunt end of an oblong end-cap at large obliquity; b) impact by the sharp edge of the oblong end-cap; c) impact by the sharp edge of a simple end-cap and impact at a low altitude
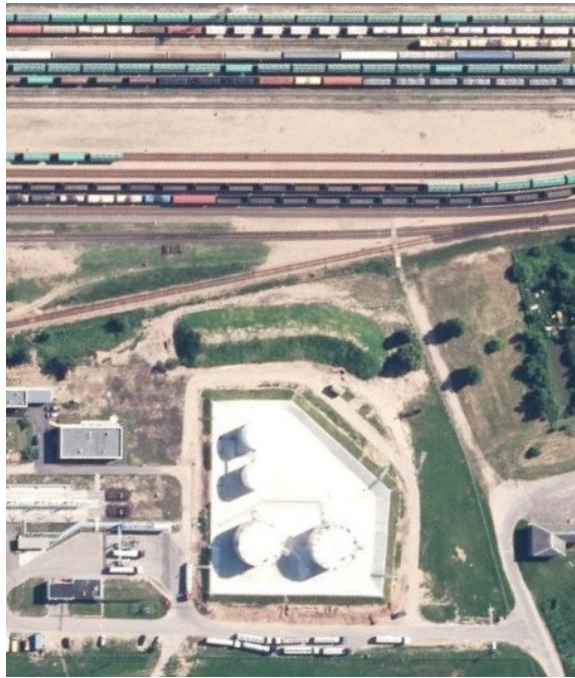
Fig. 3.14. Two views of the soil embankment built in the Lithuanian railway infrastructure to protect fuel tanks against a potential BLEVE on tracks (the top photo was obtained from maps.lt website, the bottom photo was made by the author)

An example of a really existing embankment build to protect fuel tanks against fragment impacts is shown in Fig. 3.14. A construction of such a barrier was encouraged by a safety study carried out for Lithuanian railways (Vaidogas *et al.* 2012c).

The pros and cons of an application of the three aforementioned building materials allow to conclude that a barrier made of precast RC segments can be a fairly good solution in many practical situations. A more formal choice of the

material for a construction of a safety barrier is suggested by Zavadskas and Vaidogas (2009). They suggested to apply MCDM methods for such a choice.

3.4.2. Good barrier design practice

Fragment impact on the safety barrier will result in both local wall damage and in overall dynamic response of the barrier. Local damage will consist of spalling of concrete from the front (impacted) face and possible scabbing of concrete from the rear face of the wall with fragment penetration into the wall (Fig. 3.13). End-caps of road and railway tanker vessels will be large as compared to, say, most military missiles and their velocities will be relatively low (in most cases less than 400 km/h, see Fig. 2.31). Therefore, a perforation of the barrier wall by an end-cap with subsequent passing through the wall is not likely unless the wall is inadequately thin. It is natural to expect that the local damage will be deeper if the barrier is hit by a sharp edge of an end-cap. If the obliquity of the impact will be large and, in addition, the barrier will be hit by a ”blunt“ end of the end-cap, the fragment may bounce off (ricochet) without creating any considerable damage (Fig. 3.13a).

Good barrier design practice should be based on the following attitudes:

1. Local damage to the barrier can be of any magnitude and include even a perforation, as long as the barrier will stop the fragment, bounce it off or decrease its kinetic energy to a safe level.
2. Collapse of the barrier resulting from its inability to withstand the energy absorbed from the projectile should be prevented.
3. A specific barrier segment or set of adjacent segments will be hit by a vessel end-cap only once per accident involving one or several BLEVEs. BLEVEs of road tankers reported in the literature involved only one vessel. Some railway accidents caused several BLEVEs of railroad tankers. However, fragments of tanker vessels were projected in different directions without the hazard of hitting the same target more than one time. The Crescent City railway accident is an illustration of such a situation (CCPS 1994).
4. The dimensions of potential end-caps of tanker vessels suggest that an impact will damage up to three adjacent wall segments with the width in front of 2 to 3 meters (Fig. 3.13a). These segments can be ”sacrified“ and replaced by new ones at relatively low cost.

A reinforced concrete barrier should be designed so that it will fail in ductile manner and absorb the inputted energy without collapse. To ensure ductility, the barrier should be designed to have grater lateral load carrying capacity in shear than in bending and should be under-reinforced so that the bending capaci-

ty is governed by yielding of tensile reinforcement rather than crushing of the concrete in compression.

3.4.3. The problems of design of a concrete barrier

A great deal of work has been done on the penetrative power of cased explosives but information pertaining to vessel burst fragments is less extensive. Fragments generated from road and railway tanker vessels are of irregular shape and relatively low energy density. Their penetrative or destructive power depends on their orientation at the moment of impact with a target. Due to their irregular shape, fragments usually produced by the bursting of a vessel have much lower penetrating power, often only half, than compact blunt fragments, while pointed projectiles have appreciably more (Mannan 2005). As the size of the fragment increases, the response of the target (safety barrier) becomes increasingly significant. Kennedy (1976) has proposed that the target response may be modelled by assuming it to be subject to a rectangular pulse forcing function. With this assumption it is then possible to apply conventional structural response techniques to estimate the susceptibility of a structure to a missile hit.

Collapse of a ductile barrier will occur when the kinematic energy absorbed by the barrier from the impacting fragment will exceed the strain energy capacity of the barrier. Thus, to evaluate the capacity of a barrier wall to withstand the overall effect of a fragment impact, it is necessary to determine both the strain energy capacity of the barrier, and the kinetic energy of the barrier and the kinetic energy absorbed by the barrier from the impacting fragment.

A number of analysis techniques can be used to ensure that a ductile barrier wall has sufficient energy absorbing capacity to prevent collapse when subjected to a fragment impact. These techniques were suggested several decades ago, among others, by Willamson and Alvy (1973), Kennedy (1976) and Baker *et. al.* (1978), and Johnson *et. al.* (1982).

3.4.3.1. Impact obliquity and ricochet of fragments

A fragment from a tanker vessel will impinge the barrier at some obliquity. Fig. 3.15 shows the configuration of an oblique impact characterised by the angle of obliquity, θ. The ricochet of the fragment refers to the impact phenomenon, whereby a fragment, which strikes the barrier at high velocity and small angle of inclination (ricochet angle) φ, changes its direction of flight without being stopped by the barrier and without passing through it. The ricochet of the fragment happens by the lateral component of the target reaction or contact forces and is opposed to bouncing in which the elastic recovery forces within the

fragment or other projectile and the barrier (target) are responsible for the rever-
sal of fragment (projectile) trajectory.

At sufficiently high speed v_{arr}, there can exist a critical angle of entry (criti-
cal ricochet) angle φ_c, below which the ricochet occurs. The critical ricochet
angle φ_c was assessed for series of small and hard bodies which resemble mili-
tary projectiles (Johnson *et. al.* 1982). However, any systematic investigation of
the ricochet and the angle φ_c of such projectiles as large chunks of tanker vessels
generated by BLEVE does not seem to exist. And so the existence of φ_c for ves-
sel fragments can be assumed only hypothetically. The determination of φ_c for
vessel fragments can be fact that unbalanced forces at the nose of the impacting
fragment can produce a moment which could turn the fragment away from an
initial ricochet angle φ.
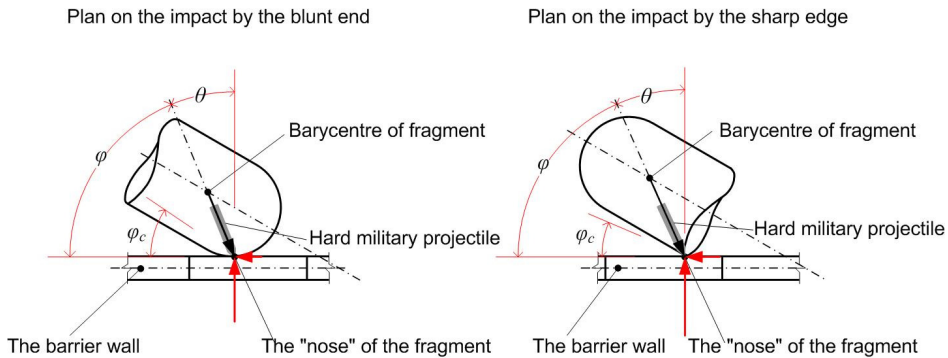
Fig. 3.15. The configuration of an oblique impact by a vessel fragment into a safety
barrier

The conditions $\varphi < \varphi_c$ and $\varphi > \varphi_c$ represent two different cases of impact
loading on a barrier. In the case $\varphi < \varphi_c$, the fragment will be diverted from a po-
tentially hazardous trajectory and minor local damage to the barrier can be ex-
pected. The impact will cause an overall dynamic response of the barrier. In the
opposite case $\varphi < \varphi_c$, the ricochet will not occur and the impact will cause certain
local damage and the overall response. The local damage will consist of spalling
of concrete from the impacted face and scrabbing of concrete from the rear face
of the barrier together with fragment penetration into the barrier wall (Fig. 3.13).

The impact by a fragment will be a "plastic impact" if the fragment will
stick to the barrier after impact or else will fall from the barrier with effectively
no rebound energy (Kennedy 1976). In the case of the plastic impact, portions of
the total kinetic energy of the impacting fragment, KE_F, will be converted to
strain energy associated with deformability of the fragment and energy losses

associated with barrier penetration. The remainder of the energy KE_F will be absorbed by the barrier.

3.4.3.2. Conservation of energy for fragment impact

In the case of the plastic impact, the conservation of energy requires that the following relation is satisfied:

$$KE_F = SE_F + E_L + KE_B \qquad (3.16)$$

where KE_F is the total kinetic energy of the fragment just prior to impact; SE_F is the strain energy absorbed in the fragment as a result of non-recoverable fragment deformation; E_L is the energy loss associated with local fragment penetration of barrier; and KE_B is the kinetic energy absorbed by the barrier during impact.

The kinetic energy of the fragment prior to impact, KE_F, is defined by the standard expression $0.5\,\xi_{frg}\,v_{avr}^2$. By conservation of momentum it can be shown that for the plastic impact the kinetic energy absorbed by the barrier, KE_B, is related to the fragment kinetic energy by the following equation (Kennedy 1976):

$$KE_B = \left(\frac{R_M}{1 + R_M} \right) KE_F \qquad (3.17)$$

where the variable R_M represent the mass ratio given by

$$R_M = \frac{W_F}{W_B} \qquad (3.18)$$

where W_F is the fragment weight (N) and W_B is the effective inertial weight of the barrier at the end of impact (N). The value W_B is a function of the deformed shape of the barrier immediately following impact and is generally less than the total barrier weight.

When one assumes both non-deformable fragment and a massive barrier, then both R_M and SE_F go to zero (Fig. 3.16). Then all of the fragment kinetic energy is available to penetrate the target. With a deformable fragment of a non-massive barrier, a portion of the fragment kinetic energy is used to deform the fragment and the barrier. This reduces the energy available to penetrate the barrier.

3.4.3.3. Fragment deformability and impact loading time history

Using the fragment impact pressure or impact force time history and input loading, the overall barrier response time history can be determined by performing a dynamic analysis of the barrier. The barrier's response in many cases will go beyond elastic response and so such an analysis would have to generally be a non-linear analysis.
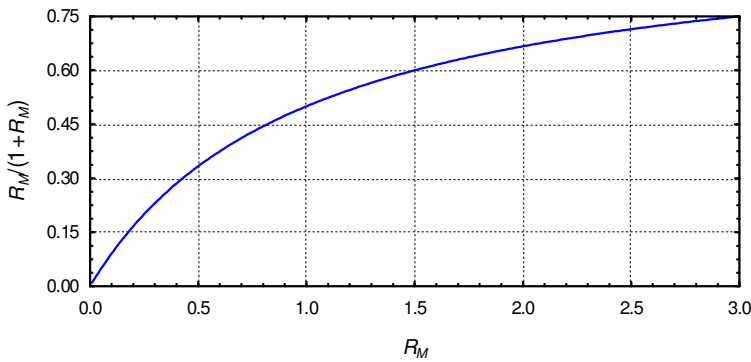
Fig. 3.16. The relation between the mass ratio R_M and the ratio of the barrier and fragment kinetic energies, KE_B/KE_F, expressed as the ratio $R_M/(1 + R_M)$

The impact pressure time history of a non-deformable fragment will have the peak value of pressure or force (Fig. 3.17). For such a fragment, the real impact pressure time history can be replaced by an approximate time history which has a constant time history throughout the duration of impact. The approximate time history should the proper total impulse applied to the barrier.

Fig. 3.17 shows the influence of fragment deformability on the impact pressure (force) time history. If a fragment undergoes a significant crash upon impact this crush significantly lengthens the duration of impact and reduces the depth of possible penetration.

3.4.3.4. Ensuring ductility of the barrier

An analysis of the barrier has not necessarily to ensure that the barrier will not collapse as a result of a fragment impact. However, such an analysis should ensure that the barrier will fail in ductile manner. To ensure ductility, the barrier should be designed to have greater lateral load carrying capacity in shear than in bending and should be under-reinforced so that the bending capacity is governed

by yielding of the tensile reinforcement rather than crushing of the concrete in compression.
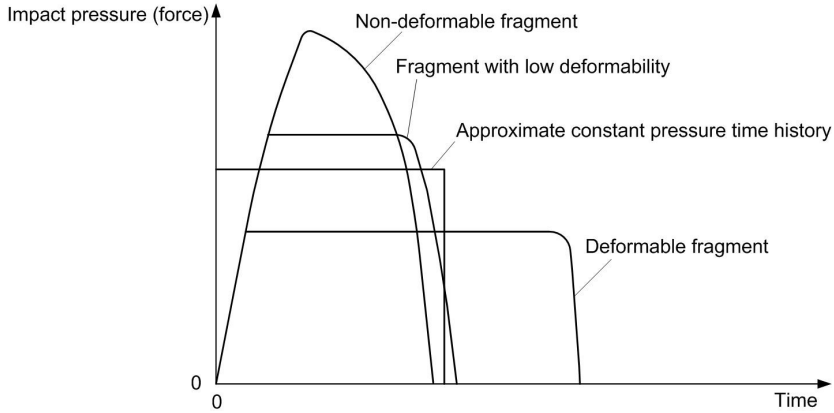
Fig. 3.17. A schematic representation of impact pressure (force) time histories of deformable and non-deformable fragments (in line with Kennedy (1976))

Collapse of the barrier will occur when the kinetic energy absorbed by the barrier from the impacting fragment will exceed the strain energy capacity of the barrier, SE_B. Therefore, to evaluate the capacity of the barrier to overall effect it is necessary t determine both the strain energy capacity of the barrier, SE_B, and the kinetic energy absorbed from the impacting missile, KE_B.

For the plastic impact, the kinetic energy absorbed by the barrier, KE_B, is defined by Eq. (3.17). For a barrier failing in flexure, the strain energy capacity SE_B can be conservatively determined by yield line analysis. One can assume that

1. Yield hinges occur whenever the moment reaches the ultimate moment capacity.
2. Sufficient hinges form to develop a collapse mechanism prior to collapse.

Assuming that all of the strain energy occurs along these yield hinges and ignoring any elastic strain energy in zones outside of the zone of yielding, a conservative estimate of the total strain energy capacity of the barrier is obtained from the following equation:

$$SE_B = \sum_{h=1}^{N_h} m_{uh} r_{uh} l_h \qquad (3.19)$$

where N_h is the number of yield hinges; m_{uh} is the moment capacity per unit length of the hinge h; r_{uh} is the total rotation of the hinge h at the time of collapse; and l_h is the length of the hinge h. The yield line of the concrete barrier shown in Fig. 3.13 will form at the bottom of the barrier wall ($N_h = 1$). The length of this line, l_h, will be equal to the length of the barrier segment. The barrier will collapse when the rotational capacity is exceeded along the yield line.

The ultimate moment capacity m_{uh} can be determined in accordance with the principles of ultimate strength design. The rotational capacity of under-reinforced concrete beams with laced tensile and compressive reinforcement, the rotational capacity should be limited to 5° (0.0873 rad) (Kennedy 1976). For rotations beyond this limit, the concrete cover over compressive steel begins to crush and the moment capacity of the beam is reduced.

To ensure that a barrier can develop the strain energy capacity defined by Eq. (3.19), it is necessary to prevent a premature shear failure at a low level impact (Fig. 3.13c). This can be prevented by ensuring that the concentrated load capacity of the slab in shear either significantly exceeds the load capacity in flexure or else exceeds the peak impact force applied at a low altitude, whichever is less.

3.4.3.5. The problems to be investigated prior to a barrier design

The phenomena of impact dynamics, impact damage and response of barrier to impact loading described in this section must be taken into account in order to design a barrier capable to resist the impact of large chunks of road or railway tanker vessels. However, the practical design should be preceded by an investigation or clarification of some aspects of the aforementioned phenomena:

1. An existence of the ricochet phenomenon must be proved and the critical ricochet angle φ_c determined for typical impact orientations and shapes of impacting fragments (Fig. 3.15).
2. The deformability of the fragments, which could impact the barrier, must be estimated. This will allow to classify the fragment as "hard" or "soft" projectiles depending on whether the fragment deformability is small or large relative to the target deformability. The deformability of the fragment will determine the character of impact pressure (force) time history (Fig. 3.17). This investigation should allow to estimate the strain energy absorbed in the fragment as a result of non-recoverable fragment deformation, SE_F (see Eq. (3.16)).
3. The penetration of the barrier by fragment at blunt and sharp orientations must be investigated in order to assess the energy loss associated with local penetration, E_L (see Eq. (3.16)).

4. An algorithm of the assessment of the effective inertial weight of the barrier, W_B, must be developed (see Eq. (3.18)).

5. Mathematical models allowing to determine components of the strain energy capacity of the barrier SE_B should be made available (see Eq. (3.19)). This especially pertains to the rotational capacity of barrier hinges, r_{uh}.

A development of practical procedures of the safety barrier design might require to solve further problems on the side of predicting the impact loading and the side of barrier response to this loading. One of these problems is an investigation of a combined effect of blast and fragment impact caused by a tanker vessel BLEVE. The design of a safety barrier which will be deployed in the immediate vicinity of a potential BLEVE epicentre will be another problem to be solved in the future. A formal, mathematical optimisation of the barrier cross-sectional geometry and positioning with the available sitting area might also belong to the future problems. Safety barriers are not a panacea for all hazards posed by hazmat transportation. But, in case of a severe accident, most property owners will wellcome a barrier deployed between accident epicentre and vulnerable objects belonging to them.

3.5. Third chapter conclusions

An exploration of the possibilities to design safety barriers aimed at protection of roadside objects against mechanical and thermal effects of BLEVEs on road and rail has led to the following conclutions:

1. The main problems of sitting a safety barrier include: a) determination of a road segment from which roadside property can be damaged; b) specification of an area for a barrier construction between the unsafe road segment and property to be protected; and c) positioning the barrier in the available area. A solution of these three problems will yield input information for a detailed design of the barrier.

2. The determination of the unsafe road segment will be a non-trivial problem. A comprehensive solution of this problem requires assessing a potential explosion and/or fire damage to an unprotected roadside object by applying methods of SRA and QRA. A layout of the unsafe road segment will determine the area where the barrier is required. This area should fully overlap the area available for barrier construction. A configuration of the latter area will be influenced by factors of very different nature. The size, layout and obliquity of the construction area will influence decisions concerting a configuration of the barrier in plan and posi-

tioning it between road (railway tracks) and roadside objects subjected to the hazard of fire or explosion on road.

3. Methods applied to solving problems of sitting a safety barrier will range from rigorous mathematical techniques of probabilistic structural analysis to a judgemental choice of barrier configuration and position in plan. Results produced by these methods can positively contribute to improving the final design of the barrier and so increasing safety of hazmat transportation.

4. The barrier aim at a protection from the blast loading generated by BLEVE can be designed with a sacrificial cladding. Such a design may face considerable uncertainties related to potential blast loading. The behaviour of SC components subjected to blast loading may also be uncertain to a large degree. A consistent quantification and propagation of these uncertainties is possible by combining methods of SRA and QRA.

5. An application of SRA and QRA methods to an analysis of SC components can yield an estimate of probability of their failure under blast loading. This probability can be used as a measure of explosive damage to SC provided that the SC consists of nominally identical components. A component failure probability will be proportional to the relative number of the components which may fail (be "sacrificed") in case of an explosion.

6. An estimation of the SC failure probability will require to specify a probabilistic model of blast wave characteristics. Such model can be difficult to obtain as post-mortem data on transportation-related BLEVES are rarely available in the amount allowing to compile a statistical sample for fitting the model. However, the SC failure probability can be estimated without such model.

7. A small-size sample of blast loading characteristics recorded in experiment or estimated by explosion simulation can be directly applied to the probability estimation. Such estimation can be carried out by a simulation-based propagation of stochastic and epistemic uncertainties through a fragility function developed for an SC component. The estimate will have the form of a one-sided confidence interval of the failure probability. The upper limit of this interval can be used for making decisions concerning the degree of the damage to SC which may be caused by an explosion.

8. Massive reinforced concrete barriers can be deployed where they will have to resist an impact by tanker vessel fragments. These barriers can be constructed from segments which may be similar to widely-known Berlin-wall segments. The segments can be connected to each other, to achieve a redistribution of impact effects among several segments. The

high of the segments can be determined by a simulation of fragment trajectories described in the second chapter of this dissertation. The reinforcement of the barriers can be provided in such a way which allows large plastic deformations of the barrier wall and so an absorption of certain part of kinetic energy of impacting fragment.

9. In the case where the horizontal distance between BLEVE and target object is small, a barrier protecting against blast and projectiles will not be able to stop thermal radiation. Consequently, shielding from thermal radiation should be provided in addition to the barrier. Alternatively, the target object can be protected by providing a large separation distance between target object and potential epicentre of BLEVE.

General conclusions

The results presented in the dissertation were obtained by an investigation of the risk posed to build roadside property by transportation of hazardous materials (in brief, hazmat transportation). Such risk can be controlled by deploying safety barriers between road (railway tracks) used for hazmat transportation and vulnerable roadside object(s). Design of such barrier is a complex multidisciplinary problem. Exploring the possibilities to solve this problem led to the following conclusions:

1. An review of applications of the transportation risk assessment developed to manage hazmat transportation accidents and often abbreviated to TRA, led to the conclusion that most TRA applications deal with individual and societal risk to exposed population. The accident scenario prevailing in these applications is release of toxic materials and subsequent intoxication of population. Risk to built roadside property (buildings, objects of traffic infrastructure, industrial installations) is mentioned in the literature but is not considered in detail.

2. An analysis of hazmat transportation accident data led to the result that the greatest potential of damage to the built roadside property possesses boiling liquid vapour explosion known by the abbreviation BLEVE and vapour cloud explosion often abbreviated to VCE. The prevailing materials involved in BLEVEs and VCEs on road and rail are commercial energetic hydrocarbons, especially, propane. This material was involved in 65 % of BLEVE accidents on road and 40 % of accidents on rail. BLEVEs are more frequent, as compared to VCEs. Therefore BLEVEs pose the largest risk to the roadside property.

3. A consideration of how to reduce the risk to roadside property posed by BLEVEs on road and rail led to the conclusion that this can be done by means of safety barriers. They can be deployed between the road (railway trucks) used for hazmat transportation and vulnerable roadside objects. Safety barriers can be designed as fence-shaped structures or soil embankments. Adequate separation distances between traffic routes and vulnerable nearby objects can also serve, where possible, as safety barriers.

4. An analysis of possibilities to assess thermal and mechanical effects of a BLEVE on a roadside object led to the result that a solution of this problem should be based on predicting the position and orientation of a road or railway tanker vessel sustaining the BLEVE. Such predicting will face considerable uncertainties and these must be quantified by means of probability distributions. Some of these distributions can be fitted to statistical data on traffic accidents; others will have to be specified subjectively in line with the principles of the quantitative risk assessment usually abbreviated to QRA. Data on traffic accidents of road tankers indicate that the transverse rest position of the tank can be modelled by a logistic probability distribution with the mean of 2.02 m and the standard deviation of 5.62 m. The departure angle of the tank can be characterised by an empirical distribution with the mean of 2.83° and the standard deviation of 56.8°.

5. An analysis of deterministic models developed to predict thermal and mechanical effects of BLEVEs revealed that these models can supplement the modelling of tanker vessel position and orientation. Probabilistic elements can be incorporated into the models of the thermal and mechanical effects. They will allow to quantify uncertainties in the effects according to the principles of QRA. Technically, these uncertainties can be expressed by means of probability distributions and propagated by applying a stochastic (Monte Carlo) simulation.

6. An examination of the possibilities to design safety barriers in line with the principles of QRA led to the conclusion that this structure can be developed using two types of statistical samples of BLEVE effects: a large-size sample obtained by the stochastic simulation and a small size-sample gained by experiment, post-mortem investigation of accidents or in other similar way. Information delivered by these samples can be used to estimate the probability of barrier failure. This figure can serve as the main measure of barrier behaviour under the actions of BLEVE.

7. A consideration of potential materials for constructing safety barriers allows to conclude that steel barriers can be effective as sacrificial blast walls. Massive reinforced concrete barriers and soil embankments will

be effective against fragments generated by BLEVEs of road and railway tanker vessels. Mass of these fragments can reach 10 tons and the impact velocity can be up to 400 km/h. Given the characteristics of blast loading and fragment impact, conventional structural response techniques can be applied to estimate the susceptibility of steel and reinforced concrete barriers to these effects.

8. A study of the thermal effects of BLEVEs reveals that the dimensions of the fireballs, which can be generated by explosions of typical road and railway tanker vessels, will be large. They can be up to 300 m tall and the fireball diameter can reach 200 m. Therefore, an effective protection of roadside objects by wall-shaped barriers and soil embankments will be ineffective. The protection can be achieved by providing sufficiently large separation distances between the road (railway tracks) and the vulnerable roadside object. A thermal shielding of the roadside object can also be applied, because duration of BLEVE fireballs is short and typically does not exceed 20 seconds.

9. A consideration of the methodological procedures proposed in this work led to the conclusion that the success of their a practical application will depend on designer's skills in solving two tasks: predicting thermal and mechanical effects of fires and explosions on road and rail (or, in brief, Task "A") and, secondly, utilising results of this predicting to a design of a safety barrier (briefly, Task "B"). The design of a safety barrier conceptualised as a fence or a soil embankment or an adequate separation distance will be a manageable problem as long as the potential effects of fires and explosions were predicted appropriately.

10. A solution of the tasks "A" and "B" is a multi-disciplinary problem. The task "A" lies, in essence, beyond the scope of the traditional civil engineering. Typically, it is solved by chemical, mechanical and fire safety engineers capable to deal with such phenomena as BLEVE and VCE. Ideally, these specialists should be skilled at modelling uncertainties related to effects of BLEVE or VCE or, alternatively, their team should include a person capable to do this.

11. The aforementioned task "B" is within the competence of the structural engineer who will design a safety barrier. If effects of BLEVE or VCE were predicted in line with probabilistic principles of QRA, the design of the barrier by means of structural reliability analysis will make the best of this prediction. The barrier can also be designed by means of traditional, deterministic methods. However, the deterministic design will require to represent highly uncertain and interdependent effects of BLEVE or VCE by fixed design values. Such values can be inaccurate or insufficiently conservative.

References

Abbasi, T.; Abbasi, S.A. 2007. The boiling liquid expanding vapour explosion (BLEVE): Mechanism, consequence assessment, management, *Journal of Hazardous Materials* 141(3): 489–519.

Abdel-Aty, M. A. and Radwan, A. E. 2000. Modelling traffic accident occurrence and involvement, *Accident Analysis and Prevention* 32(5): 633–642.

Abdolhamidzadeh, B.; Abbasi, T.; Rashtchian, D.; Abbasi, S.A. 2010a. Domono effect in process-industry accidents – An inventory of past events and identification of some patterns, *Journal of Loss Prevention in Pocess* 24(5): 575–593.

Abdolhamidzadeh, B.; Abbasi, T.; Rashtchian, D.; Abbasi, S.A. 2011. A new method for assessment domino effects in chemical process industry. *Journal of Hazardous Materials* 182(1–3): 416–426.

Al-Ghamdi, A. S. 2003. Analysis of traffic accidents at urban intersections in Riyadh. *Accident Analysis and Prevention* 35(5): 717–724.

Atahan, A. O.; Yücel, A. Ö.; Erdem, M. M. 2014. Crach testing and evaluation of a new generation L1 containment level guardrail, *Engineering Failure Analysis* 38: 25–37.

Aven, T. 2003. *Foundations of Risk Analysis. A Knowledge and Decision Related Perspective*. Chichester: Wiley.

Aven, T.2009. Perspectives on risk in a decision-making context – Review and discussion, *Safety Science* 47(6): 798–806.

Aven, T.; Vinnem, J. E. 2007. *Risk Management: with Applications from Offshore Petroleum Industry*. 1st edition. London: Springer. 212 p.

Aven, T.; Zio, E. 2011. Some considerations on thetreatment of uncertainties in risk assessment for practical decision making. *Reliability Engineering and System Safety* 96(1): 64–74.

Babrauskas, V. 2003. *Ignition Handbook*. Issaquah: Fire Science Publishers.

Bahei-El-Din, Y. A.; Dvorak, G. J.; Fredricksen, O. J. 2006. A blast-tolerant sandwich plate design with a polyurea interlayer, *International Journal of Solids and Structures* 43(25-26): 7644–7658

Baker, W. E.; Kulesz, J. J.; Ricker, R. L; Bessey, R. L.; Westine, V. B.; Parr, V.B.; Oldham, G. A. 1997. *Workbook for preciting pressure wave and fragment effects of exploding propellant tanks and gas storage vessels. Nasa contractor report 134906*. Springfield: NASA. 561 p.

Bakke, J. R.; van Wingender, K.; Hoorelbeke, P.; Brewerton, B. 2010. A Study on the Effect of Trees on Gas Explosions, *Journal of Loss Prevention in the Process Industries* 23(6): 878–884.

Bangash, M. Y. H. 2009. *Shock, Impact and Explosion: Structural Analysis and Design*. 1st edition. Berlin: Springer. 1410 p.

Bangash, M. Y. H.; Bangash, T. 2006. *Explosion-Resistant Buildings: Design, Analysis and Case Studies*. 1st edition. Berlin: Springer. 805 p.

Batarlienė, N. 2008. *Pavojingų krovinių vežimo pagrindai: mokomoji knyga*. Vilnius: Technika 152 p.

Baum, M. R. 1988. Disruptive failure of pressure vessels: Preliminary design guidelines for fragment velocity and extent of hazardous zone, *Journal of Pressure Vessel Technology* 110(2): 168–176.

Baum, M. R. 1995. Rupture of a gas-pressurised cylindrical vessel: the velocity of a detached end-cap, *Journal of Los Prevention in the Process Industies* 8(3): 149–161.

Baum, M. R. 2001. The velocity of large missiles resulting from axial rupture of gas pressurised cylindrical vessels, *Journal of Loss Prevention in the Process Industries* 14(3): 199–203.

Biggs, J. M. 1964. *Introduction to structural dynamics*. New York etc.: McGraw-Hill. 178 p.

Birk, A.M. 1996. Hazards from propane BLEVESs: An update and proposal for emergency responders, *Journal of Loss Prevention in the Process Industries* 9(2): 173–181.

Bogosian, D.; Piepenburg, D. 2002. Effectiveness of frangible barriers for blast shielding. Proceedings of the 17th International Symposium on the Military Aspects of Blast and Shock. June 2002, Las Vegas. USA, 1–11.

Boh, J.W.; Louca, L.A.; Choo, Y.S. 2005. Energy absorbing passive impact barrier for profiled blastwalls, *International Journal of Impact Engineering* 31(8): 976–995.

Bonilla Martinez, J. M.; Belmonte Perez, J.; Marin Ayala, J. A. 2012. Analysis of the explosion of a liquefied-natural-gas road tanker, *Securidad y Medio Ambiente* 32(127): 1–20.

Borovinšek, M.; Vesenjak, M.; Ulbin, M.; Re, Z. 2007. Simulation of crach test for high containment levels of road safety barriers, *Engineering Failure Analysis* 14(8): 1711–1718.

Boudet, H. Sc.; Jayasundera, D. Ch.; Davis, J. 2011. Drivers of Conflict in Developing Country Infrastructure Projects: Experience from the Water and Pipeline Sectors, *Journal of Construction Engineering and Management* 137(7): 498–511.

Bubbico, R.; Di Cave, S.; Mazzarotta, B. 2004a. Risk analysis for road and rail transport of hazardous materials: a simplified approach, *Journal of Loss Prevention in Pocess Industries* 17(6): 477–482.

Bubbico, R.; Di Cave, S.; Mazzarotta, B. 2004b. Risk analysis for road and rail transport of hazardous materials: a GIS approach, *Journal of Loss Prevention in Pocess Industries* 17(6): 483–488.

Bulson, P. S. 1997. *Explosive Loading on Engineering Structures*. London: E & FN Spon. 272 p.

Cahen, B. 2006. Implementation of New Legislative Measures on Industrial Risks Prevention and Control in Urban Areas, *Journal of Hazardous Materials* 130(3): 293–299.

Casal, J. 2008. *Evaluation of the Effects and Consequences of Major Accidents in Industrial Plants*. Amsterdam etc.: Elsevier. 378 p.

Casal, J.; Salla, J. M. 2006. Using liquid superheat energy for a quick estimation of overpressure in BLEVEs and similar explosions, *Journal of Hazardous Materials* A137(3): 1321–1327.

Chang, L. Y. 2005. Analysis of freeway accident frequencies: Negative binomial regression versus artificial neural network, *Safety Science* 43(8): 541–557.

Changlong, Z.; Juncheng, J.; Xiongjun, Y. 2012. Study on ignition probability of flammable materials after leakage accidents, *Procedia Engineering* 45: 435–441.

CCPS 1994. *Guidelines for Evaluating the Characteristics of Vapor Cloud Explosions, Flash Fires, and BLEVEs*. New York: Center for Chemical Process Safety of AIChE.

CCPS 1995. *Guidelines for Chemical Transportation Risk Analysis*. New York: Center for Chemical Process Safety of AIChE.

CCPS 2005a. *Guidelines for Chemical Process Quantitative Risk Analysis. 2ʰᵉ*ed. New York: Center for Chemical Process Safety of AIChE.

CCPS 2005b. *Guidelines for Facility Siting and Layout*. New York: Center for Chemical Process Safety of AIChE.

Cheng, W.; Washington, S. P. 2005. Experimental evaluation of hotspot evaluation methods, *Accident Analysis and Prevention* 37(5): 870–881.

Chi, Y.; Langdon, G. S.; Nurick, G. N. 2010. The influence of core height and face plate thickness on the response of honeycomb sandwich panels subjected to blast loading, *Materials and Design* 31(4): 1887–1899.

Cozzani, V.; Bandini, R.; Basta, C.; Christou, M. D. 2006. Application of Land-Use Planning Criteria for the Control of Major Accident Hazards: A case-study, *Journal of Hazardous Materials A*136(2): 170–180.

Cozzani, V.; Tugnoli, A.; Saalzano, E. 2009. The Development of an Inherent Safety Approach to the Prevention of Domino Accidents, *Accident Analysis and Prevention* 41(6): 1216–1227.

CPD 1992. *Methods for the Determination of Possible Damage to People and Objects from Releases of Hazardous Materials – 'Green Book'*. The Hague: Committee for the Prevention of Disasters.

CPD 1999. *Guidelines for Quantitative Risk Assessment – 'Purple Book'. Publication Series on Dangerous Substances (PGS3)*. The Hague: Committee for the Prevention of Disasters.

CPD 2005. *Methods for the Calculation of Physical Effects due to Releases of Hazardous Materials (Liquids and Gases) – 'Yellow Book'. Publication Series on Dangerous Substances (PGS2)*. The Hague: Committee for the Prevention of Disasters.

CPR 2005. Methoden voor het Bepalen van Mogelijke Schade aan Mensen en Goederen door Het Vrijkomen van Gevaarlijke Stiffen – 'Green Book'. Den Haag: Commissive van preventive van rampen door gevaarlijke stiffen.

Čygas, D; Jasiūnienė, V.; Bartkevičius, M. 2009. Assessment of special plans and technical design with regard to traffic safety, *Journal of civil engineering and management* 15(4): 411–418.

Darbra, R. M.; Palacios, A.; Casal, J. 2010. Domino Effect in Chemical Accidents: Main Features and Accident Sequences, *Journal of Hazardous Materials* 183(1–3): 565–573.

Eichler, T. V.; Napadentsky, H. S. 1977. Accidental Vapour Phase Explosions on Transportation Routes Near Nuclear Power Plants. Final Report Prepated to US Nuclear Regulatory Commission. Washington: NUREG.

EIGA 2007. *Determination of Safety Distances. IGC Doc 75/07/E*. Brussuels: European Industrial Gases Association.

Elvik, R.; Høve, A., Vaa, T. Sørensen, M. 2009. *The Handbook of Road Safety Measures*. 2nd ed. Bingley: Emerald. 1009 p.

EN 1317 2010. *Road restraint systems. European standard EN 1317 Parts 1–8. English version*. Brussels CEN.

Evans, M.; Hastings, N. Peacock, B. 2001. *Statistical Distributions*. 3rd ed. New York etc.: Wiley.

Fabiano, B.; Curro, F. Palazzi, E.; Pastorino, R. 2002. A fremawork for risk assessment and decision-making strategies in dangerous good transportation, *Journal of Hazardous Materials* 93(1): 1–15.

FACTS 2014. Hazardous materials accidents knowledge base. Retrieved April 18, 2014, From FACTS Link: http://factsonline.nl/browse-chemical-accidents-in-database.

FM Global 2013. *Evaluationg vapour cloud explosions using a flame acceleration method. Property Loss Prevention Data Sheets*. Johnston: Factory Mutual Insurance Company.

Forster, H.; Gunther, W. 2009. Explosion Protection for Vehicles Intended for the Transport of Flammable Gases and Liquids – an Investigation into Technical and Operational Basics, *Journal of Hazardous Materials* 164 (2–3): 1064–1073.

Franck, H., Franck, D. 2010. Mathematical methods for ccident reconstruction. A forensic engineering perspective. Boca Raton: Taylor & Francis Group.

Garrick, B. J. 2008. Quantifying and Controlling Catastrophic Risks. Amsterdam: Elsevier.

Gebbeken, N.; Doge, T. 2010. Explosion Protection – Architectural Design, Urban Planning and Landscape Planning, *International Journal of Protective Structures* 1(1): 1–22.

Genova, B.; Silvestrini, M.; Leon Trujillo, F.J. 2008. Evaluation of the blast-wave overpressure and fragments initial velocity for a BLEVE event via empirical correlations derived by a simplified model of released energy, *Journal of Loss Prevention in the Process Industries* 21(1): 110–117.

Gentle, J. E. 2003. *Random Number Generation and Monte Carlo Methods*. 2th ed. New York etc.: Springer.

Gheorghe, A. V.; Birchmeier, J.; Vamanu, D.; Papazoglou, I., Kröger, W. 2005. Comprehensive risk assessment for rail transportation of dangerous goods: a validated platform for decision making, *Reliability Engineering and System Safety* 88(3): 247–272.

Grislis, A. 2010. Longer combination vehicles and road safety, *Transport* 25(3): 336–343.

Gubinelli, G.; Zanelli, S.; Cozzani, V. 2004. A simplified model for the assessment of the impact probability of fragments, *Journal of Hazardous Materials* 116(3): 175–187.

Gubinelli, G.; Cozzani, V. 2009. Assessment of missile hazards: evaluation of the fragment number and drag factors, *Journal of Hazardous Materials* 161(1): 439–449.

Guruprasad, S.; Mukherjee, A. 2000a. Layered sacrificial claddings under blast loading. Part I–analytical studies, International Journal of Impact Engineering 24(9): 957–973.

Guruprasad, S.; Mukherjee, A. 2000b. Layered sacrificial claddings under blast loading. Part II–experimental studies, *International Journal of Impact Engineering* 24(9): 975–984.

Haleem, K.; Abdel-Aty, M.; Mackie, K. 2010. Using a reliability process to reduce uncertainty in predicting crashes at unsignalised intersections, *Accident Analysis and Prevention* 42(2): 654–666.

Hanssen, A. G.; Enstock, L.; Langseth, M. 2002. Close-range loading of aluminium foam panels, *International Journal of Impact Engineering* 27(6): 593–618.

Hauptmanns, U. 2001a. A procedure for analyzing the flight of missiles from explosions of cylindrical vessels, *Journal of Loss Prevention in Pocess Industries* 14(5): 395–402.

Hauptmans, U. 2001b. A Monte-Carlo based procedure for treating the flight of missiles from tank explosions, *Probabilistic Engineering Mechanics* 16(4): 307–312.

Holden, P. L. 1988. *Assessment of Missile Hazards: Review of Incident Experience Relevant to Major Hazard Plant*. Warrington, Cheshire: Safety and Reliability Directorate.

Huang, H.; Abdel-Aty, M. 2010. Multilevel data and Bayesian analysis in traffic safety, *Accident Analysis and Prevention* 42(6): 1556–1565.

Hwang, C. L.; Yoon K. S. 1981. Multiple Decision Making Methods and Applications, *Lecture Notes in Economics and Mathematical Systems*. Berlin: Springer 186 p.

Jasiūnienė, V.; Čygas, D. 2013. Raod accident prediction model for the roads of national significance of Lithuania, *The Baltic Journal of Road and Brigde Engineering* 8(1): 66–73.

Johnson, D. M. 2010. The Potential for Vapour Cloud Explosions – Lessons from the Buncefield Accident, *Journal of Loss Prevention in the Process Industries* 23(6): 921–927.

Johnson, W.; Sengupta, A. K.; Ghosh, S. K. 1982. High velocity oblique impact and ricochet mainly of long rod projectiles: an overview, *International Journal of Mechanical Sciences* 24(7): 425–436.

Juocevičius, V. 2011. A method for assessing risk to engineering structures exposed to accidental actions, Doctoral dissertation. Vilnius, Technika. 144 p.

Juocevičius, V.; Vaidogas, E. R. 2010. Effect of explosive loading on mechanical properties of concrete and reinforcing steel: towards developing a predictive model, *Mechanika*, 81(1): 5–12.

Karagiozova, D., Langdon, G. S.; Nurick, G. N. 2010. Blast attenuation in Cymat foam core sacrificial claddings, *International Journal of Mechanical Sciences* 52(5): 758–776.

Kavalov, B., Petric, H., Georgakaki, A. 2007. Liquefied Natural Gas for Europe – Some Important Issues for Consideration. *JRC Reference Report*. Luxembourg: European Communities.

Kazanci, Z.; Mecitoglu, Z. 2008. Nonlinear dynamic behaviour of simply supported laminated composite plates subjected to blast load, *Journal of Sound and Vibration* 317(3–5): 883–897.

Kelly, D. L.; Smith, C. L. 2009. Bayesian inference in probabilistic risk assessment – the current state of the art, *Reliability Engineering and System Safety* 94(2): 628–643.

Kennedy, R. P. 1975. A review of procedures for the analysis and design of concrete structures to resist missile impact effects, *Nuclear Engineering and Design* 37(2): 183–203.

Korn, R.; Korn, E.; Kroisandt. 2010. *Monte Carlo Methods in Finance and Insurance*. Boca Raton etc.: CRC Press.

Krauthammer, T. 2008. *Modern Protective Structures*. Boca Raton etc: CRC Press. 528 p.

KTR 2008. *Kelių techninis reglamentas KTR 1.01:2008*. Vilnius: Lietuvos Respublikos Aplinkos Ministerija.

Kumamoto, H. 2007. *Satisfying Safety Goals by Probabilistic Risk Assessment*. London: Springer.

Langdon, G. S.; Karagiozova, D.; Theobald, M. D.; Nurick, G. N.; Lu, G.; Merrett, R. P. 2010. Fracture of aluminium foam core sacrificial cladding subjected to air-blast loading, *International Journal of Impact Engineering* 37(6): 638–651.

Lee, J.; Mannering, F. 2002. Impact of roadside features on the frequency and severity of run-off-roadway accidents: an empirical analysis, *Accident Analysis and Prevention* 34(2): 149–161.

Lee, K. H.; Rosowsky, D. V. 2006. Fragility analysis of woodframe buildings considering combined snow and earthquake loading, *Structural Safety* 28(3): 289–303.

Lees, F. P. 2001. *Loss Prevention in the Process Industries. Hazard Identificatin, Assessment and Control*. Oxford: Butterworth & Heinemann.

Lemaire, M. 2009. *Structural Reliability*. London: ISTE. 504 p.

Lenoir, E. M.; Davenport, J. A. 1993. A survey of vapor cloud explosions: Second update, *Process Safety Progress* 12(1): 12–33.

Li, R.; Kardomateas, G. J.; Simitses, G. J. 2009. Point-wise impulse (blast) response of a composite sandwich plate including core compressibility effects, *International Journal of Solids and Structures* 46(10): 2216–2223.

Louca, L. A.; Boh, J. W.; Choo, Y. S. 2004. Design and analysis of stainless steel profiled blast barriers, *Journal of Constructional Steel Research* 60(12): 1699–1723.

Lozano, A.; Munoz, A.; Antun, J. P.; Granados, F.; Guarneros, L. 2010. Analysis of Hazmat Transportation Accidents in Congested Urban Areas, Based on Actual Accidents in Mexico, *Procedia Social and Behavioral Sciences* 2(3): 6053–6064.

Luria, P.; Aspinall, P. A. 2003. Evaluating a multi-criteria model for hazard assessment in urban design, *Environmental Impact Assessment Review* 23(5): 625–653.

Ma, G. W.; Ye, Z. Q. 2007. Energy absorption of double-layer foam cladding for blast alleviation, *International Journal of Impact Engineering* 34(2): 329–347.

Mannan, S. (ed.) 2005. *Lees's Loss Prevention in the Process Industries*. Elsevier: Amsterdam etc.

Marangon, A.; Carcassi, M.; Engebo, A.; Nilsen, S. 2007. Safety Distances: Definition and Values, *International Journal of Hydrogen Energy* 32(13): 2192–2197.

Marek, P; Brozzetti, J.; Guštar, M; Tikalsky, P. 2003. *Probabolistic Asssessment of Structures using Monte Carlo Simulation: Background, Exercises and Software*. 2 nd edition. ITAM CAS CR: Praha. 471 p.

Melchers, R. E. 2002. *Structural Reliability Analysis and Prediction. 2 nd ed.* John Wiley & Sons Ltd: England.

Mébarki, A.; Mercier, F.; Nguyen, Q. B; Ami Saada, R.; Meftah, F.; Reimeringer, M. 2007. A probabilistic model for the vulnerablility of metal plates under the impact of cylindrical projectiles, *Journal of Loss Prevention in the Process Industries* 20(4): 128–134.

Mébarki, A.; Mercier, F.; Nguyen, Q. B; Ami Saada, R.; Reimeringer, M. 2008. Reliability analysis of metallic targets under metallic rods impact: towards a simplified probabilistic approach, *Journal of Loss Prevention in the Process Industries* 21(4): 518–527.

Mébarki, A.; Mercier, F.; Nguyen, Q. B; Ami Saada, R. 2009a. Structural fragments and explosions in industrial facilities. Part I: Probabilistic description of the source terms, *Journal of Loss Prevention in the Process Industries* 22(4): 408–416.

Mébarki, A.; Nguyen, R; Mercier, F. 2009b. Structural fragments and explosions in industrial facilities. Part I: Projectile trajectory and probability of impact, *Journal of Loss Prevention in the Process Industries* 22(4): 417–425.

Montella, A. 2010. A comparative analysis of hotspot identification methods, *Accident Analysis and Prevention* 42(2): 571–581.

Nagashima, M.; Tsuchiya, M.; Asada, M. 2011. Reducing the Economic Risk of LNG Tank Construction under Conditions of Fluctuating Resource Prices, *Journal of Construction Engineering and Management* 137(5): 382–391.

Neuenhaus, D. H. J. F.; Geβler, U. J.; Feldman, M. 2013. Using multibody–system modeling to make accurate pradictions of vehicle impacts on road restraint systems, *International Journal of Non-Lineear Mechanics* 53: 24–31.

Nguyen, Q. B; Mébarki, A.; Ami Saada, R.; Mercier, F.; Remeringer, M. 2009. Integrated probabilistic framework for domino effect and risk analysis, *Advances in Engineering Software* 40(9): 892–901.

Oggero, A.; Darbra, R. M.; Darbra, R. M.; Munoz., M.; Planas, E.; Casal, J.; 2006. A survey of accidents occurring during the transport of hazardous substances by road and rail, *Journal of Hazardoud Materials* 133(1–3): 1–7.

OTIF 2010. *Composition of Dangerous Goods Trains to Prevent a BLEVE and its Effect on External Safety*. Berne: Intergovernmental Organisation for International Carriage by Rail.

Palanivelu, S.; Van Paepegem, W.; Degrieck, J.; Kakogiannis, D.; Van Ackeren, J.; Van Hemelrijck, D.; Wastiels, J.; Vantomme, J. 2010. Comparative study of the quasi-static energy absorption of small-scale composite tubes with different geometrical shapes for use in sacrificial cladding structures, *Polymer Testing* 29(3): 381–396.

Paltrinieri, N.; Landucci, G.; Molag, M.; Bonvicini, S.; Spadoni, G.; Cozzani, V. 2009. Risk reduciton in road and rail LPG transportation by passive fire protection, *Journal of Hazardous Materials* 167(1–3): 332–344.

Papazoglou, I. A., Aneziris, O. N. (1999). Uncertainty Quantification in the Health Consequences of the Boiling Liquid Expanding Vapour Explosion. *Journal of Havardous Materials* 67(3): 217–235.

Pellissetti, M.F.; Schueller, G. I. 2006. On general purpose software in structural reliability – An overview, *Structural Safety* 28(1-2): 3–16.

PHMSA 2014. Pipeline and Hazardous Materials Safety Administation. Retrieved April 18, 2014, From PHMSA Link: http://phmsa.dot.gov/hazmat/library/data-stats/incidents.

Planas-Cuchi, E; Gasulla, N.; Ventosa, A.; Casal, J. 2004. Explosion of a road tanker containing liquefied natural gas, *Journal of Loss Prevention in Process Industries* 17 (4): 315–321.

Pontiggia, M.; Landucci, G.; Busini, V.; Derudi, M.; Alba, M.; Scaioni, M.; Bonvicini, S.; Cossani, V.; Rota, R. 2011. CFD Model Simulation of LPG Dispersion in Urban Areas, *Atmospheric Environment* 45(24): 3913–3923.

Prentkovskis, O.; Beljatynskij, A.; Juodvalkienė, E.; Prentkovskienė, R. 2010. A study of the deflections of metal road guardrail post, *The Baltic Journal of Road and Bridge Engineering* 5(2): 104–109.

Prentkovskis, O.; Tretjakovas, J.; Švedas, A.; Bieliatynskyi, A.; Daniūnas, A.; Krayushkina, K. 2012. The analysis of the deformation state of the double-wave guardrail mounted on bridges and viaducts of the motor roads in Lithuania and Ukraine, *Journal of Civil Engineering and Management* 18(5): 761–771.

Prugh, R. W. 1991. Quantutative evaluation of "BLEVE" hazards, *Journal of Fire Protection Engineering* 3(1): 9–24.

Prugh, R. W. 1994. Quantitative evaluation of fireball hazards, *Process Safety Progress* 13(2): 83–91.

Quest Consultants 2009. *Comparative Quantitative Risk Analysis of Motor Gasoline, LPG, and Anhydrous Ammonia as an Automotive Fuel. Prepared for Iaowa State University*. Norman, Oklahoma: Quest Consultants Inc.

Ray, M. H. 1999. Impact conditions on side- impact collisions with fixed roadside ogjects. *Accident Analysis and Prevention* 3(1): 21–30.

Reid, J. D.; Kuipers, D.; Sicking D. L.; Faller, R. K. 2009. Impact performance of W–beam guardrail installed at variuos frlare rates, *International Journal of Impact Engineering* 36(3): 476–485.

Ren, Z.; Vesenjak, M. 2005. Computational and experimental crach analysis of the road safety barrier, *Engineering Failure Analysis* 12(6): 963–973.

Roberts, T.; Gosse, A.; Hawksworth, S. 2000. Thermal radiation from fireballs on failure of liquefied peotroleum gas storage, *Institution of Chemical Engineers* 78(3): 184–192.

Ronza, A.; Vilchez, J. A.; Casal, J. 2007. Using transportation accident databases to investigate ignition and explosion probabilities of flammable spills, *Journal of Hazardous Materials* 146 (1–2): 106–123.

Rubinstein, R. Y.; Melamed, B. 1998. *Modern Simulation and Modelling*. New York: Wiley.

Samuel, C.; Keren, N.; Shelly, M.C.; Freeman, S.A. 2009. Frequency analysis of hazardous material transportation incidents as a function of distance from origin to incident location, *Journal of Loss Prevention in Process Industries* 22(6): 783–790.

Smith, P. D. 2010. Blast Walls for Structural Protection against Hight Explosive Threats: A Review, *International Journal of Protective Structures* 1(1): 67–84.

Spaethe, G. 1987. *Die Sicherheit tragender Baukonstruktionen*. Berlin: VEB Verlag für Bauwesen. 124 p.

Spek, A. C. E.; Wieringa, P. A.; Janssen, W. H. 2006. Intersection approach speed and accident probability, *Transportation Research Part F: Traffic. Psychology and Behaviour* 9(2): 155–171.

Spraggings, B. H. 2010. The case for rail transportation of hazardous materials, *Journal of Management and Marketing Research*, 3(1): 88–95.

Straub, D., Der Kiureghian, A. 2008. Improved seismic fragility modelling from empirical data, *Structural Safety* 30(4): 320–336.

Su, Y.; Wu, C. Q.; Griffith, M. 2008. Mitigation of blast effects on aluminium foam protected masonry walls, *Transactions of Tianjin University* 14(1): 558–562.

Sun, D.; Jiang, J.; Zhang, M.; Wang, Z.; Huang, G.; Qiao, J. 2012. Parametric appraoch of the domino effect for structural fragments, *Journal of Loss Prevention in the Process Industries* 25(1): 114–126.

Tauseef, S. M., Abbasi, T., Abbasi, S. A. 2010a. Risks of Fire and Explosion Associated with the Increasing Use of Liquefied Petroleum Gas. *Journal of Failure Analysis and Prevention* 10(4): 322–333.

Taveau, J. 2010b. Risk assessment and land-use planning regulations in France following the AZF disaster, *Journal of Loss Prevention in the Process Industries* 23(6): 813–823.

Tewarson, A. 2002. Generation of Heat and Chemical Compounds in Fires. In *SFPE Handbook of Fire Protection Engineering*, 5th ed. Quincy, MA: NFPA & SFPE.

Theobald, M. D.; Nurick, G. N. 2010. Experimental and numerical analysis of tube-core claddings under blast loads, *International Journal of Impact Engineering* 37(3): 333–348.

TNO 2005. Tanks. Reduction of the risk of a BLEVE. TNO Report. The Hague: TNO.

Trépanier, M.; Leroux, M. H.; De Marcellis-Warin, N. 2009. Cross-analysis of hazmat road accidents using multiple databases, *Accident Analysis and Prevention* 41(6): 1192–1198.

Triantaphyllou, E. 2000. *Multi-Criteria Decision Making Methods: A Comparative Study*. Series Applied Optimization 44, Dordrecht: Kluwer Academic Publisher.

TSB 1999. *Railway Investigation Report. Derailment and Collision. Canadian National Train No. U-783-21-30 and Train No. M-306-31-30 Mile 50.84, Saint-Hyacinthe Subdivision Mont-Saint-Hilaire, Quebec, 30 December 1999. Report Number R99H0010*. Gatineau: Trasportation Safety Board of Canada.

Tugnoli, A.; Milazzo, M. F.; Landucci, G.; Cozzani, V.; Maschio, G. 2014. Assessment of the hazard due to fragment projection: A case study, *Journal of Loss Prevention in the Process Industries* 28(1): 36–46.

Turskis, Z.; Zavadskas, E. K. 2010. A new fuzzy additive ratio assessment method (ARAS-F). Case study: the analysis of fuzzy multiple criteria in order to select the logistic centerns location, *Transport* 25(4): 423–432.

Vaidogas, E. R. 2003. Accidental explosions: Bayesian uncertainty handling in assessing damage to structures. *Proceedings of the 9th International Conference on Applications of Statistics and Probability in Civil Engineering, July 6-9, 2003, San Francisco, CA, Eds. A Der Kiureghian, S. Madanat, J. M. Pestana.* Rotterdam: Milpress Science Publishers 1: 1191–198.

Vaidogas, E. R. 2006a. First step towards preventing losses due to mechanical damage from abnormal actions: Knowledge-based forecasting the actions, *Journal of Loss Prevention in the Process Industries* 19(5): 375–385.

Vaidogas, E. R. 2006b. Bayesian Approach to Forecasting Damage to Buildings from Accidental Explosions on Railway. *Transport and Telecommunication* 7(1): 34–43.

Vaidogas, E. R. 2007a. Handling uncertainties in structural fragility by means of the Bayesian bootstrap resampling. *Proceedings on CD of the 10th Int. Conf. on Applications of Statistics and Probability in Civil Engineering (ICASP10),* Tokyo, Japan, Jul 31-Aug 03, 2007, Eds. J. Kanda, T. Takada, H. Furuta. London: Taylor & Francis.

Vaidogas, E. R. 2007b. *Prediction of Accidental Actions Likely to Occur on Building Structures. An Approach Based on Stochastic Simulation*. Vilnius: Technika 247 p.

Vaidogas, E. R. 2007c. Risk Oriented Design of Protective Highway Structures, *The Baltic Journal of Road and Bridge Engineering* 2(4): 155–163.

Vaidogas, E. R. 2009. On applying sparse and uncertain information to estimating the probability of failure to to rare abnormal situations, *Information Technology and Control* 38(2): 135–146.

Vaidogas, E. R.; Juocevičius, V. 2007. Assessing external threats to structures using limited statistical data: an approach based on data resampling, *Technological and Economic Development of Economy* 13(2): 170–175.

Vaidogas, E. R.; Juocevičius, V. 2008a. Reliability of a timber structure exposed to fire: estimation using fragility function, *Mechanika* 73(5): 35–42.

Vaidogas, E. R.; Juocevičius, V. 2008b. Sustainable Development and Major Industrial Accidents: The Beneficial Role of Risk-Oriented Structural Engineering, *Technological and Economic Development of Economy* 14(4): 612–627.

Vaidogas, E. R.; Juocevičius, V. 2009. Assessment of Structures Subjected to Accidental Actions Using Crisp and Uncertain Fragility Functions, *Journal of Civil Engineering and Management* 15(1): 95–104.

Vaidogas, E. R., Juocevičius, V.; Kisežauskienė, L.; Stulgys, D. 2012c. *„BLEVE" sprogimo galimo poveikio darbuotojams, kuro bazei ir kitiems strateginiams objektams AB „Lietuvos geležinkeliai" Vaidotų geležinkelio stotyje. Tyrimų studija*. Vilnius: Lietuvos geležinkeliai.

Vaidogas, E. R.; Šakėnaitė, J. 2010. Protecting built property against fire disasters: multi-attribute decision making with respect to fire risk, *International Journal of Strategic Property Management* 14(4): 391–407.

Vaidogas, E. R.; Šakėnaitė, J. 2011. Multi-Attribute Decision-Making in Economics of Fire Protection, *Inzinerine Ekonomika– Engineering Economics* 22(3): 262–270.

Vinnem, J. E. 2007. *Offshore Risk Assessment. Principles, Modelling and Applications of QRA Studies.* 2nd edition. London: Springer. 577 p.

Yang, Y.; Fallah, A. S; Saunders M.; Louca A. 2011. On the dynamic response of sandwich panels with different core set-ups subjected to global and local blast loads, *Engineering Structures* 33(10): 2781–2793.

Yang, Y.; Fallah, A. S. 2011. On the dynamic response of sandwich panels with different core set-ups subject-ed to global and local blast loads, *Engineering Structures* 33(10): 2781–2793.

Ye, X.; Pendyala, R. M.; Washington, S. P.; Konduri, K.; Oh, J. 2009. A simultaneous equations model of crash frequency by collision type for rural intersections, *Safety Science* 47(3): 443–452.

Zavadskas, E. K.; Vaidogas, E. R. 2009. Multiattribute Selection from Alternative Designs of Infrastructure Components of Accidental Situations, *Computer-Aided Civil and Infrastructure Engineering* 24(5): 346–358.

The list of author's scientific publications on the subject

In reviewed scientific periodical publications

Linkutė (Kisežauskienė), L.; Juocevičius, V.; Vaidogas, E. R. 2013.A probabilistic design of sacrificial cladding for a blast wall using limited statistical information on blast loading, *Mechanika* 19(1): 58–66.

Vaidogas, E. R.; Linkutė (Kisežauskienė), L. 2012. Sitting the barrier aimed at protecting roadside property from accidental fires and explosions on road: a pre-optimisation stage, *The Baltic journal of road and bridge engineering* 7(4): 277–287.

Vaidogas, E. R.; Linkutė (Kisežauskienė), L.; Stulgys, D. 2012a. Simulation-based predicting the position of road tank explosions. Part I: data and models, *Transport* 27(1): 14–24.

Vaidogas, E. R.; Linkutė (Kisežauskienė), L.; Stulgys, D. 2012b. Simulation-based predicting the position of road tank explosions. Part II: a case study, *Transport* 27(2): 118–128.

In other editions

Linkutė (Kisežauskienė), L. 2011. Data on traffic accidents involving fires and explosions, *14-osios Lietuvos jaunųjų mokslininkų konferencijos „Mokslas – Lietuvos ateitis" 2011 metų teminės konferencijos „Statyba" (2011 m. kovo 23–25 d.) straipsnių rinkinys Vilnius: Technika*: 1–6.

Linkutė (Kisežauskienė), L.; Juocevičius, V.; Vaidogas, E. R. 2011. Numerical evaluation of concrete and steel strain rate in the RC section subjected to high rate loading, *Mechanika proceedings of the 16th international conference, 7, 8 April, 2011, Kaunas University of Technology, Lithuania*. 209–214.

Linkutė (Kisežauskienė), L.; Vaidogas, E. R. 2011. Design of roads and railways used for the transport of explosive materials. *8th International Conference "Environmental Engineering", May 19-20, 2011, Vilnius, Lithuania. Sustainable Urban development. Roads and Railways. Technologies of Geodesy and Cadastre. Vilnius: Technika* 3: 1121–1127.

Vaidogas, E. R.; Kisežauskienė, L. 2012. Transportation of liquefied gasses: assessing the risk of thermal damage to roadside infrastructure from a road tank "Bleve", *Transport and telecommunication* 13(4): 284–293.

Vaidogas, E. R.; Kisežauskienė, L. 2013. Risk to built property posed by transportation of liquefied gasses , *Journal of Polish Safety and Reliability Association (JPSRA 2013)* 4(1): 43–50.

Vaidogas, E. R.; Kisežauskienė, L. 2014. Technogeninės avarijos – rimtas iššūkis statinių projektuotojams, *Statyba ir architektūra* 8: 42–44.

Vaidogas, E. R.; Kisežauskienė, L.; Juocevičius, V. 2013. An assessment of reliability of a blast wall using limited statistical information on blast loading, *Journal of Polish Safety and Reliability Association (JPSRA 2013)* 4(2): 259–265.

Vaidogas, E. R.; Kisežauskienė, L.; Stulgys, D. 2013. Assessing risk to built roadside property posed by transportation of liquefied gasses, *TRANSBALTICA 2013: the 8th International Conference May 9–10, 2013, Vilnius, Lithuania: selected papers Vilnius: Technika*: 254–259.

Summary in Lithuanian

Problemos formulavimas

Darbe tiriamos avarijos transportuojant pavojingąsias medžiagas ir tų avarijų keliamos rizikos mažinimo galimybės. Tokios avarijos pasireiškia kaip pavojingųjų medžiagų nuotėkiai, sprogimai ir gaisrai. Jie įvyksta vežant pavojingąsias medžiagas automobiliais bei traukiniais. Šių avarijų pasekmės būna sunkios: jų metu net žūsta žmonės, pažeidžiami ir prie transporto linijų esantys pakelės objektai. Tokių objektų pažeidimus sukelia šiluminė spinduliuotė ir mechaniniai poveikiai.

Šiame darbe pagrindinis dėmesys skiriamas statybinių objektų, esančių ties keliais ir geležinkeliais, apsaugai nuo gaisrų ir sprogimų. Apsauga užtikrinama statant saugos barjerus tarp transporto linijų ir pažeidžiamų pakelės objektų. Pagrindinė problema, kylanti projektuojant tokius barjerus, yra neapibrėžtumai, susiję su šilumine spinduliuote ir mechaniniais poveikiais, sukeliamais gaisrų ir sprogimų automobilių kelių ir geležinkelių infrastruktūroje.

Darbo aktualumas

Šio darbo aktualumą lemia avarijos, kylančios vežant pavojingąsias medžiagas. Nepaisant to, kad transporto saugos srityje diegiama daug naujovių, gaisrus ir sprogimus sukeliančios sunkvežimių ir traukinių avarijos įvyksta dažnai. Kai kurios gerai žinomos avarijos įvyko tankiai užstatytose teritorijose ir buvo labai stambios. Verta paminėti tokias avarijas: traukinio cisternos sprogimus Viaredžo (Italija, 2009) ir Balstogės (Lenkija, 2010) miestuose, bei automobilinių cisternų sprogimus Ispanijoje 1978, 2002, 2011. Todėl žmonių, turto ir gamtos apsaugojimas nuo tokių avarijų vis dar lieka opia problema.

Tyrimų objektas

Disertacijos tyrimo objektas yra rizikos, kylančios greta kelių ir geležinkelių esantiems, sprogimams ir gaisrams jautriems statybiniams objektams, vertinimas ir mažinimas. Tiriama, kaip mažinti riziką, statant saugos barjerus tarp pavojingųjų medžiagų transportavimo arterijų ir pažeidžiamų pakelės statinių.

Darbo tikslas

Pagrindinis darbo tikslas – pasiūlyti, kaip projektuoti saugos barjerus, tinkamus apsaugoti pažeidžiamus pakelės objektus nuo gaisrų ir sprogimų, kylančių keliuose ir geležinkeliuose. Šie pasiūlymai apima rekomendacijas, kaip prognozuoti gaisrų ir sprogimų poveikį. Taip pat buvo siekta sukurti projektinius saugos barjerų pasiūlymus.

Darbo uždaviniai

1. Nustatyti pavojingųjų medžiagų vežimo avarijas, kurios gali sukelti didžiausias statybinių pakelės objektų pažaidas.

2. Ištirti kelių eismo įvykius, siekiant prognozuoti potencialias automobilinių cisternų sprogimų padėtis ir poveikius pakelės objektams.

3. Ištirti, kaip vertinti šiluminį sprogstančios automobilinės cisternos poveikį pakelės objektams, atsižvelgiant į galimą šio poveikio neapibrėžtumą.

4. Sukurti kiekybiniu rizikos vertinimu grindžiamą procedūrą, leidžiančią prognozuoti automobilinės cisternos skeveldrų poveikį saugos barjerui.

5. Ištirti, kaip išdėstyti saugos barjerus greta transporto arterijų.

6. Pasiūlyti saugos barjero su sunaikinamuoju apdaru projektą. Šis barjeras turi sumažinti sprogimo bangą, sukeliamą geležinkelio cisternos sprogimo.

7. Pasiūlyti projektinį gelžbetoninio saugos barjero sprendimą. Barjeras turi būti statomas iš surenkamų segmentų ir apsaugoti pažeidžiamus pakelės objektus, nuo sprogstančios cisternos skeveldrų smūgių.

Tyrimų metodika

Tyrimų metodika buvo sudaryta derinant kiekybinės rizikos vertinimo, matematinės statistikos, stochastinio modeliavimo ir konstrukcijų patikimumo analizės metodus. Metodologinė tyrimo ašis yra neapibrėžtumų, susijusių su gaisrų ir sprogimų poveikiais, vertinimas ir transformavimas. Kiekybinio neapibrėžtumų modeliavimo rezultatai taikomi projektuojant saugos barjerus. Transformuoti neapibrėžtumus taikomas stochastinis (Monte Karlo) modeliavimas. Neapibrėžtumų modeliavimo rezultatai buvo suderinti su derterministiniais saugos barjerų skaičiavimo modeliais.

Dabo mokslinis naujumas

Pagrindinis darbo naujumas glūdi idėjoje, kaip remiantis kiekybinės rizikos analizės principais projektuoti saugos barjerus, galinčius apsaugoti statybinius pakelės objektus nuo gaisrų ir sprogimų transporto arterijose. Iki šiol panašūs barjerai buvo įrengiami tik aplink karinius objektus, kuriems grėsė išorės pavojus. Kiti nauji elementai yra:

1. Tikimybių teorijos metodų taikymas modeliuojant neapibrėžtumus, susijusius su gaisrų ir sprogimų keliuose ir geležinkeliuose poveikiais.

2. Stochastinio modeliavimo taikymas projektuojant saugos barjerus.

3. Saugos barjerų projektavimas naudojant mažas statistines imtis, kurias sudaro duomenys apie poveikius barjerams.

4. Projektiniai plieninio ir gelžbetoninio saugos barjerų, galinčių apsaugoti pakelės objektus nuo cisternų sprogimų, pasiūlymai.

Darbo rezultatų praktinė reikšmė

Šis darbas suteikia galimybę mažinti pavojingųjų medžiagų vežimo riziką. Santykinai mažos investicijos į pakelėje statomus saugos barjerus leis išvengti didelių nuostolių, sukeliamų gaisrų ir sprogimų keliuose ir geležinkeliuose. Darbe siūlomas metodas padės apsaugoti pažeidžiamus pakelės objektus, saugos barjerus projektuojant kiekybinio rizikos vertinimo principais. Metodo šerdį sudaro tikimybinis gaisrų ir sprogimų poveikių pakelės objektams neapibrėžtumų modeliavimas. Šie neapibrėžtumai yra dideli ir tik metodiškai atsižvelgiant į juos bus galima projektuoti praktiškai naudingus, realiai saugą užtikrinančius barjerus. Darbe pateikti projektiniai dviejų saugos barjerų pasiūlymai padės praktiškai įgyvendinti tokių konstrukcijų projektavimą.

Ginamieji teiginiai

1. Pavojingiausi statybiniams pakelės objektams degių ir sprogių medžiagų vežimo avarijų scenarijai yra besiplečiančių verdančio skysčio garų sprogimas (toliau vadinamas anglišku trumpiniu BLEVE) ir garų debesies sprogimas (literatūroje dažnai žymimas trumpiniu VCE). BLEVE yra dažnesni už VCE ir jų poveikiai įvairesni. Taigi, BLEVE kelia didžiausią pavojų pakelės objektams.

2. BLEVE tipo avarijų mechaninio ir šiluminio poveikių prognozavimas susijęs su dideliais neapibrėžtumais. Šiuos neapibrėžtumus reikia kiekybiškai vertinti, kartu taikant tikimybinį ir stochastinį modeliavimą. Toks modeliavimas leidžia generuoti dideles statistines BLEVE poveikių reikšmių imtis, tinkančias saugos barjerų projektavimui.

3. Turint statistiniu požiūriu mažo dydžio sprogimo apkrovos reikšmių imtį, gautą eksperimentuojant arba tiriant praeities avarijas, saugos barjerą reikia projektuoti derinant kartotinį statistinį ėmimą su konstrukcijų patikimumo teorijos metodais. Tai leis įvertinti barjero pažaidų tikimybes ir jų pagrindu priimti projektinius sprendimus.

4. Saugos barjerų parinkimą įtakoja galimų konstrukcinių sprendimų įvairovė. Plienas, gelžbetonis ar net gruntas gali būti naudojami projektuojant ir statant saugos barjerus. Tačiau projektuoti reikia taikant kiekybinio rizikos vertinimo ir konstrukcijų patikimumo teorijos metodus. Jie leis tinkamai atsižvelgti į sprogimų ir gaisrų keliuose ir geležinkeliuose poveikių neapibrėžtumus.

Darbo rezultatų aprobavimas

Pagrindiniai šios disertacijos teiginiai buvo išspausdinti septyniuose moksliniuose straipsniuose: keturi iš jų – *ISI Web of Science* duomenų bazėje (Vaidogas *ir kt.* 2012ab,

Vaidogas ir Linkutė 2012, Linkutė *ir kt.* 2013), trys straipsniai kituose žurnaluose (Vaidogas ir Kisežauskienė 2012, Vaidogas *ir kt.* 2013ab).

Pagrindiniai darbo teiginiai pateikti trijose tarptautinėse konferencijose:

– 11-oje tarptautinėje konferencijoje „Mechanika 2011", Kaune, 2011;

– 8-oje tarptautinėje konferencijoje „Aplinkos inžinerija", Vilniuje, 2011;

– 8-oje tarptautinėje konferencijoje „Transbaltica 2013", Vilniuje, 2013.

Disertacijos struktūra

Darbas susideda iš įvado, 3 skyrių, išvadų, literatūros sąrašo, autoriaus publikacijų sąrašo ir šešių priedų.

Disertacijos apimtis yra 169 puslapiai be priedų. Darbe pateiktos 49 formulės, 62 paveikslai ir 20 lentelių. Literatūros sąrašą sudaro 171 cituotos publikacijos.

1. Pavojingųjų medžiagų vežimo keliama rizika: apžvalga statybos inžinerijos požiūriu

Pirmame skyriuje apžvelgiamos ir vertinamos publikacijos apie riziką, kylančią vežant pavojingąsias medžiagas. Taip pat nagrinėjami iki šiol sukurti metodai, skirti projektuoti saugos barjerus, statomus pažeidžiamiems pakelės objektams apsaugoti nuo gaisrų ir sprogimų keliuose bei geležinkeliuose. Publikacijų apžvalga apima bendruosius transporto rizikos analizės aspektus, pakelės objektus galinčius pažeisti reiškinius, statybinius šios analizės aspektus ir apsauginių barjerų projektavimo problemas. Dalis apžvalgos pateikta straipsniuose Vaidogas *ir kt.* (2012ab) bei Linkutė *ir kt.* (2013).

Pavojingųjų medžiagų vežimo avarijos dažniausiai pasireiškia gaisrais, rečiau sprogimais ir dar rečiau dujų nuotėkiais (Darbra *ir kt.* 2010). Apžvalginis skyrius pradedamas trumpu rizikos, kurią kelia pavojingųjų medžiagų vežimas, kiekybinio vertinimo aprašymu. Ši mokslo sritis yra vadinama transporto rizikos analize. Konstatuojama, kad iki šiol vertinant pavojingųjų medžiagų vežimo riziką, daugiausiai dėmesio buvo telkiama į nuodinguosius nuotėkius, darančius žalą pakelėje esantiems žmonėms (CCPS 1995; CPD 1999; Fabiano *ir kt.* 2002; Bubbico *ir kt.* 2004ab; Gheorghe *ir kt.* 2005; Grislis 2010). Daug mažiau dėmesio buvo skirta keliuose ir geležinkeliuose vykstantiems gaisrams ir sprogimams, galintiems pažeisti statybinius pakelės objektus.

Degiųjų ir sprogiųjų medžiagų vežimas keliais ir geležinkeliais nemažėja. Tokių medžiagų daugiau vežama geležinkeliais nei automobilių keliais. Todėl, vežant krovinius geležinkeliais, vyksta didesni gaisrai ir sprogimai, nei vežant keliais (pvz., Pontigia *ir kt.* 2011). Tačiau žala, padaryta užsidegus ar sprogus automobilinei cisternai arba kitos rūšies automobiliui, gali būti didesnė, nes keliai dažnai tiesiami tankiai apgyvendintose plotuose, arti pažeidžiamų statybinių pakelės objektų, pavojingųjų pramonės įmonių teritorijose (Lozano *ir kt.* 2010).

Pirmame skyriuje teigiama, kad didelį pavojų statybiniams pakelės objektams kelia dviejų rūšių sprogimai: gaisro kaitinamos geležinkelio arba automobilinės cisternos sprogimas ir iš tokios cisternos nutekėjusių dujų arba garų debesies sprogimas. Pirmasis

sprogimas yra vadinamas besiplečiančių verdančio skysčio garų sprogimu ir dažnai žymimas anglišku trumpiniu BLEVE. Antrasis sprogimas dar vadinamas garų debesies sprogimu ir neretai žymimas anglišku trumpiniu VCE. Sprogimas VCE būdu sukelia mechaninį sprogimo bangos poveikį. Debesies degimo plote pasireiškia ir šiluminis poveikis. Sprogimas BLEVE būdu sukelia mechaninius sprogimo bangos ir skeveldrų poveikius bei šiluminę ugnies kamuolio spinduliuotę (pvz., CCPS 1994; Casal 2008).

Pirmame skyriuje rašoma, kad apsaugoti statybinius pakelės objektus nuo tokių reiškinių, kaip BLEVE arba VCE, galima dviem būdais: įrengiant saugos barjerą tarp kelio (geležinkelio) ir pakelės objekto arba užtikrinant didelį, saugų atstumą tarp transporto arterijos ir objekto. Saugos barjerai yra panašūs į sprogimo sienas (angl. *blast walls*), skirtas apsaugoti nuo karinių ginklų poveikių arba improvizuotų sprogstamųjų užtaisų (pvz., Smith 2010). Abi konstrukcijos turi sumažinti sprogimo bangos energiją. Todėl patirtis projektuojant sprogimo sienas gali būti naudojama projektuojant saugos barjerus. Tačiau tarp sprogimo sienų ir saugos barjerų yra skirtumų. Sprogimo sienos užtikrina apsaugą nuo karinės amunicijos ir nėra skirtos apsaugoti nuo aukštų ugnies kamuolių bei sunkių ir santykinai lėtų skeveldrų, susidarančių sprogstant geležinkelio arba automobilinei cisternai. Sprogimo siena apriboja matomumą ir tuo pačiu mažina saugumą. Matomumo sumažėjimas, įrengus saugos barjerą, neturėtų būti problema, kol jis nekenkia eismo saugumui ir (arba) nevėlina darbuotojų įspėjimo apie gresiantį gaisrą ar sprogimą kelyje.

Šiame disertacijos skyriuje trumpai apžvelgiama sprogimo sienų skaičiavimo ir projektavimo patirtis, kuri gali būti naudinga įrengiant saugos barjerus. Standus, mažai besideformuojantis saugos barjeras atspindės dalį sprogimo bangos energijos atgal į sprogimo šaltinio pusę, todėl pažeidžiamas objektas bus saugesnis. Daugiau deformuotis galintis barjeras yra racionalesnis, nes sugers nemažą dalį šios energijos. Barjeras taip pat gali būti projektuojamas kaip lengva konstrukcija, kurią sunaikins sprogimo banga, arba turėti sunaikinamą dangą, įrengiamą ant standaus jo pagrindo. Tokios dangos pavyzdžiai yra parodyti S1 pav.
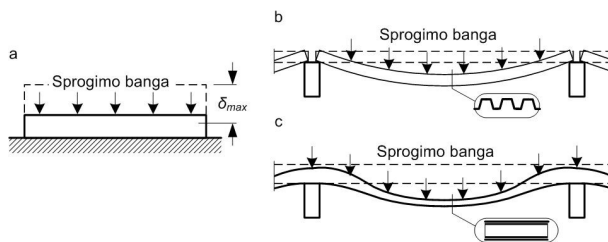
S1 pav. Sunaikinamos saugos barjero dangos rūšys: a) sluoksniuotoji danga, pritvirtinta prie ištisinio pagrindo; b) profiliuotųjų lakštų siena, paremta statramsčiais, c) sluoksniuotoji danga, pritvirtinta prie statramsčių (Linkutė *ir kt.* 2013)

Pirmo skyriaus pabaigoje saugos barjerai lyginami su apsauginiais atitvarais, užtikrinančiais saugų automobilių eismą. Nustatyta, kad tarp šių konstrukcijų yra panašumų. Dinaminiai baigtinių elementų metodai, taikomi skaičiuojant apsauginius atitvarus, gali būti pritaikyti ir projektuojant sunaikinamas saugos barjerų dangas. Tačiau kartu teigiama, kad tarp šių konstrukcijų yra daugiau skirtumų, nei panašumų. Jos

nemažai skiriasi pagal paskirtį, poveikius, laikyseną apkrovimo metu, galimą statybos vietą, norminį reguliavimą. Tačiau arti kelio esančius saugos barjerus galima statyti kartu su apsauginiais atitvarais, kad barjerai būtų apsaugoti nuo avarinių automobilių smūgių.

Pirmas disertacijos skyrius užbaigiamas išvadomis ir disertacijos uždavinių formulavimu.

2. Avarijų vežant pavojingąsias medžiagas poveikių prognozavimas

Antras skyrius pradedamas pavojingiausių avarijų, galinčių įvykti keliais ir geležinkeliais vežant degias ir sprogias medžiagas, nustatymu. Nustatyta, kad didžiausią pavojų kelia geležinkelio ir automobilinių cisternų sprogimai BLEVE būdu. Antrame disertacijos skyriuje pasiūlytos trys skaitinės procedūros, skirtos vertinti šiluminius ir mechaninius BLEVE sprogimų poveikius. Dėmesys sutelktas į du BLEVE poveikius: šiluminę sprogimo sukeliamo ugnies kamuolio spinduliuotę ir sprogimo metu susidarančių skeveldrų smūgius. Pirmoji procedūra sukurta prognozuoti sprogstančių automobilinių cisternų padėtį galimo taikinio atžvilgiu. Antroji procedūra skirta vertinti BLEVE sprogimo sukeliamo ugnies kamuolio poveikį pakelės objektui. Trečioji procedūra leidžia prognozuoti automobilinių cisternų skeveldrų poveikį pakelės objektui arba galimam saugos barjerui. Visos trys procedūros pagrįstos tikimybiniu modeliavimu. Jos gali būti panaudotos vertinant pavojingųjų krovinių transportavimo riziką. Antro skyriaus rezultatai yra paskelbti straipsniuose Vaidogas *ir kt.* (2012ab), Vaidogas ir Kisežauskienė (2012), Kisežauskienė ir Vaidogas (2013).

Gaisrai ir sprogimai keliuose ir geležinkeliuose kyla vežant, pakraunant ir iškraunant degias ir sprogias medžiagas. Dažniausiai tokias avarijas sukeliančios medžiagos yra komerciniai energetiniai angliavandeniliai. Duomenų apie avarijas vežant pavojingąsias medžiagas šaltiniai yra tokios duomenų bazės, kaip pavojingųjų medžiagų transportavimo incidentų sistema (HMIRS) (PHMSA 2014; Ronza *ir kt.* 2007). Ši duomenų bazė yra vieša ir prieinama internete. Kokybiškas informacijos apie BLEVE avarijas šaltinis yra FACTS duomenų bazė (FACTS 2014). Rengiant disertaciją, buvo išnagrinėtos FACTS duomenų bazėje aprašytos 43 BLEVE avarijos keliuose ir 38 avarijos geležinkeliuose. BLEVE avarijų dažniai, jas skirstant pagal vežamas medžiagas, pateikti S1 ir S2 lentelėse. Matyti, kad dažniausiai sprogimus BLEVE būdu sukeldavo komerciniai angliavandeniliai: propanas, benzinas, dyzelinas. Siekiant per daug neišplėsti tyrimų srities, disertacijoje buvo nagrinėjami tik geležinkelio ir automobilinių cisternų sprogimai BLEVE būdu. Saugos barjerų projektavimas buvo analizuotas vertinant du pagrindinius BLEVE poveikius: galimus skeveldrų smūgius ir šiluminę ugnies kamuolio spinduliuotę.

Sprogimo BLEVE būdu sukeliamas statybinio pakelės objekto (taikinio) pažeidimas gali būti laikomas atsitiktiniu įvykiu D, kurio dažnį galima suskaičiuoti pagal formulę

$$F_r(D) = F_r(M) \, P(A\,|\,M) \, P(B\,|\,A) \, P(D\,|\,B). \qquad (S1)$$

čia $F_r(\cdot)$ – dažnio simbolis; $P(\cdot|\cdot)$ – sąlyginės tikimybės simbolis; M – pavojingosios medžiagos vežimo įvykis; A – atsitiktinis eismo avarijos, galinčios eskaluotis į sprogimą BLEVE būdu, įvykis; B – atsitiktinis sprogimo BLEVE būdu įvykis.

Vertinant pakelės objekto pažeidimo tikimybę $P(D|B)$, reikės prognozuoti mechaninius ir šiluminius BLEVE poveikius. Nusakius šiuos poveikius vektoriumi $\boldsymbol{y}$, tikimybę $P(D|B)$ galima išreikšti:

$$P(D|B) = \int_{\text{visi } \boldsymbol{y}} P(D|\boldsymbol{y}) f(\boldsymbol{y}) \mathrm{d}\boldsymbol{y} = \int_{\text{visi } \boldsymbol{x}} P(D|\boldsymbol{\psi}(\boldsymbol{x})) f(\boldsymbol{x}) \mathrm{d}\boldsymbol{x} . \tag{S2}$$

čia $P(D|\boldsymbol{y})$ – pažeidžiamumo funkcija, siejantį įvykį D su sprogimų poveikių vektoriumi $\boldsymbol{y}$; $\boldsymbol{x}$ – BLEVE avarijos charakteristikų vektorius; $\boldsymbol{\psi}(\boldsymbol{x})$ – vektorinė funkcija, siejanti $\boldsymbol{y}$ su $\boldsymbol{x}$; $f(\boldsymbol{y})$ ir $f(\boldsymbol{x})$ – simultaninės vektorių $\boldsymbol{y}$ ir $\boldsymbol{x}$ tikimybinio tankio funkcijos.

Pažeidžiamumo funkcija $P(D|\boldsymbol{y})$ turi būti sudaroma pasitelkiant statybinių konstrukcijų patikimumo teorijos metodus. Parinkti tankio funkciją $f(\boldsymbol{y})$ yra sunku dėl duomenų stokos. Tačiau tikimybę $P(D|B)$ galima vertinti parenkant žemesnio lygio tankio funkciją $f(\boldsymbol{x})$ ir pasitelkiant deterministinius BLEVE poveikių modelius, kuriuos galima įtraukti į funkciją $\boldsymbol{\psi}(\boldsymbol{x})$.

S1 lentelė. Sprogimų BLEVE būdu, įvykusių vežant pavojingąsias medžiagas keliais, pasiskirstymas pagal medžiagą (duomenys gauti išnagrinėjus 43 sprogimus)

BLEVE sprogimą sukėlusi vežama medžiaga	Sprogimų BLEVE būdu skaičius
Propanas	28
Dyzelinas	3
Degios suskystintos dujos	2
Benzinas	2
Butanas, deguonis, freonas, hidraulinis tepalas, metanas, metanolis, propilenas	Po vieną sprogimą

S2 lentelė. Sprogimų BLEVE būdu, įvykusių geležinkeliais vežant pavojingąsias medžiagas, pasiskirstymas pagal medžiagą (duomenys gauti išnagrinėjus 38 sprogimus)

BLEVE sprogimą sukėlusi vežama medžiaga	Sprogimų BLEVE būdu skaičius
Propanas	15
Benzinas	4
Vinilchloridas	2
Butadienas	2
Amoniakas	2
Acto rūgštis, akrilo rūgštis, amonio fosfatas, butanas, chloras, dimetileteris, dyzelinas, etilenglikolis, isobutanas, metanas, naftos žaliava, natrio sulfidas, sieros rūgštis	Po vieną sprogimą

Vektorių $\boldsymbol{x}$ turi sudaryti BLEVE būdu sprogstančios cisternos charakteristikos. BLEVE poveikiai galimam taikiniui priklausys nuo cisternos padėties ir pasisukimo kampo sprogimo metu. Išanalizavus susidariusių skeveldrų pasiskirstymą sprogus cisternai, buvo nustatyta, kad jų trajektorijos stipriai priklauso nuo cisternos padėties

(yra kryptinės) (Birk 1996; Casal 2008). Todėl cisternos padėtį ir orientaciją galima išreikšti trimis x komponentais:
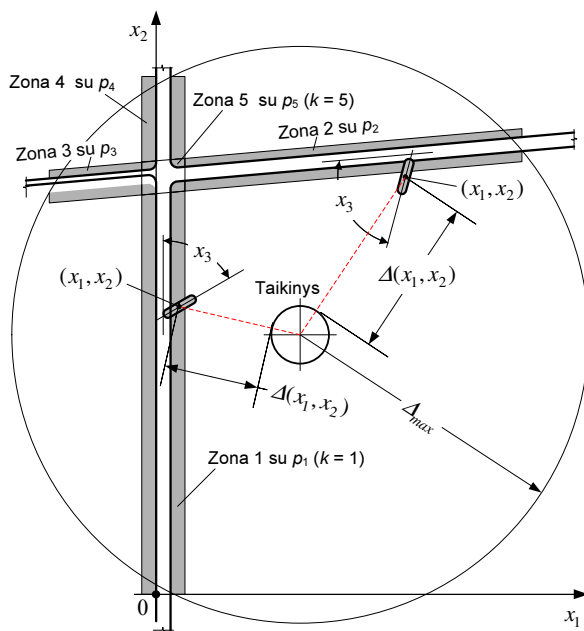
S2 pav. Pakelės objekto (taikinio) padėtis BLEVE pavojaus atžvilgiu su žemės paviršiumi susietoje koordinačių sistemoje {0; x1, x2, x3} (Vaidogas ir kt. 2012a)

1. Cisternos centro koordinatėmis x_1 ir x_2 koordinačių sistemoje, kuri apima kelią ir taikinį (S2 pav.).
2. Cisternos pasisukimo kampu x_3, matuojamu judėjimo krypties ir kelio ašies atžvilgiu (S2 pav.).

Žinant koordinates x_1, x_2 ir x_3, galima apskaičiuoti atstumą $\varDelta$, susidarantį tarp BLEVE sprogimo centro ir taikinio bei vertinti šio sprogimo poveikius (S2 pav.).

Siekiant parinkti koordinačių x_1, x_2 ir x_3 tikimybių skirstinius ir sukaupti informaciją apie kitas BLEVE charakteristikas, disertaciniame darbe buvo sudaryta automobilinių cisternų avarijų duomenų bazė (žr. priedą A). Ji talpina informaciją apie 151 transporto įvykį. Dauguma jų vyko 2007–2011 metais. 120 avarijų įvyko lygiose vietovėse arba vietovėse beveik su lygiais pakelės plotais. 17 avarijų atveju cisternos sustojo nuokalnėje ir 5 atvejais – įkalnėje. Vertikalų gradientą buvo sunku nustatyti tik 9 atvejais. Skersinė po avarijos sustojusios automobilinės cisternos padėtis (skersinis nuokrypis) x_2 buvo įvertinta 129 atvejams, o pasisukimo kampas x_3 – 122 atvejams. Reikšmių x_{2i} (i = 1, 2, ... , 129) ir x_{3i} (i = 1, 2, ... , 122) histogramos pavaizduotos S3 pav. Nuokrypį x_2 pasiūlyta aprašyti logistiniu tikimybių skirstiniu, o pasisukimo kampą x_3

apibūdinti empirine pasiskirstymo funkcija. Tikimybinį išilginės sustojimo koordinatės x_1 skirstinį buvo sunkiausia parinkti dėl duomenų stokos. Todėl, vertinant BLEVE sukeliamą riziką, koordinatę x_1 galima nusakyti tolygiuoju tikimybių skirstiniu. Jis išreikš maksimalų neapibrėžtumą x_1 atžvilgiu.

Parinkus koordinačių x_1, x_2 ir x_3 tikimybių skirstinius, buvo stochastiškai modeliuojamos (generuojamos) šių dydžių reikšmės, gaunami vektoriai $\boldsymbol{x}_j = (x_{1j}\ x_{2j},\ {}_{3j})$ ir skaičiuojamos poveikių vektoriaus $\boldsymbol{y}$ reikšmės $\boldsymbol{y}_j = \boldsymbol{\psi}(\boldsymbol{x}_j)$ (j = 1, 2, ... , N, o N – modeliavimo ciklų skaičius). Vektoraus $\boldsymbol{y}$ reikšmėmis buvo imami tokie dydžiai:

1. Vertinant cisternos skeveldrų smūgius į taikinį arba saugos barjerą, vektoriaus $\boldsymbol{y}$ komponentai buvo: skeveldros masė ($y_1 \equiv \xi$), skeveldros greitis smūgio metu ($y_2 \equiv v_{arr}$) ir rikošeto kampas ($y_3 \equiv \varphi_{arr}$) (S4 pav.).

2. Vertinant šiluminį BLEVE sprogimo metu susidarančio ugnies kamuolio poveikį, vektoriaus $\boldsymbol{y}$ komponentai buvo: šiluminė spinduliuotė pasirinktame taikinio taške (y_1) ir ugnies kamuolio egzistavimo trukmė (y_2) (S5 pav. vaizduoja du taikinio (talpyklos) taškus, kuriuose gali būti vertinama šiluminė spinduliuotė).
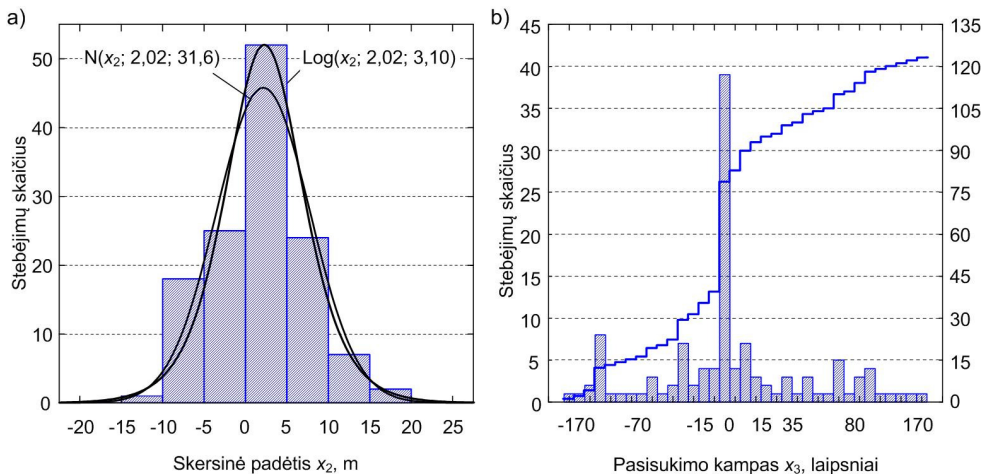
S3 pav. Duomenų apie automobilinių cisternų avarijas apdorojimo rezultatai: a) sustojimo padėtis skersai kelio; b) pasisukimo kampas sustojus (Vaidogas *ir kt.* 2012a)

Vertinant skeveldrų smūgius į projektuojamą saugos barjerą (taikinį), funkcija $\boldsymbol{\psi}(\boldsymbol{x})$ buvo sudaryta iš deterministinių modelių, nusakančių cisternos skilimą į skeveldras ir skeveldrų skriejimo trajektorijas. Vertinant šiluminę ugnies kamuolio spinduliuotę, funkcija $\boldsymbol{\psi}(\boldsymbol{x})$ buvo sukonstruota taikant deterministinį Olandijos mokslo tyrimo organizacijos TNO modelį (CPD 1992; CPR 2005). Abiem atvejais, įvesties vektorius $\boldsymbol{x}$ be koordinačių x_1, x_2 ir x_3 turėjo ir daugiau komponentų, būtinų poveikių $\boldsymbol{y}$ reikšmėms skaičiuoti. Atlikus stochastinį modeliavimą, buvo gautos BLEVE poveikių reikšmių $\boldsymbol{y}_j$ imtys, kurias galima taikyti vertinant galimas taikinio pažaidas arba projektuojant saugos barjerą. Jei nagrinėjamą taikinio arba barjero pažaidą laikyti atsitiktiniu įvykiu D, tai

reikšmės y_j gali būti taikomos vertinant sąlyginę pažaidos tikimybę $P(D|B)$ (žr. (S1) lygtį). Šios tikimybės įvertį galima skaičiuoti pagal formulę:
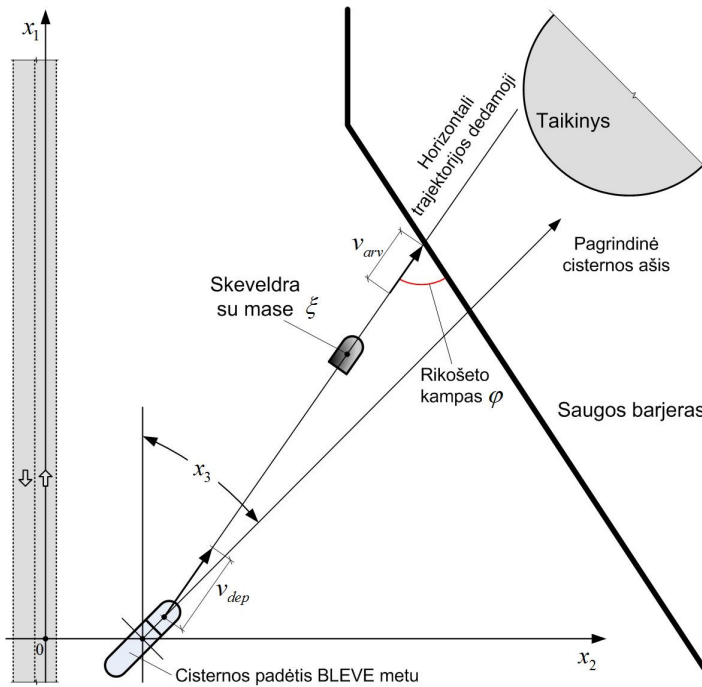
S4 pav. Skeveldros smūgio į saugos barjerą charakteristikos (vektoriaus **y** komponentai)
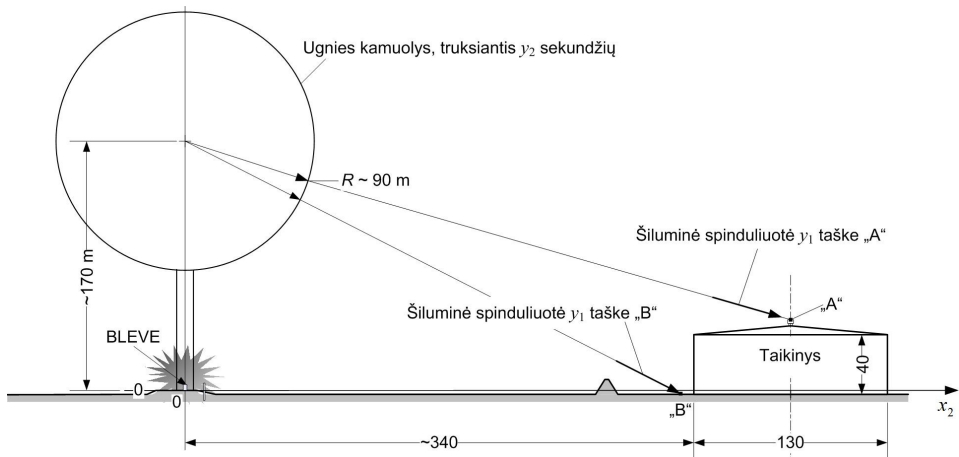
S5 pav. Ugnies kamuolys, susidarysiantis BLEVE būdu sprogus 24,7 tonų propano cisternai, bei du taikinio taškai, kuriuose vertinama šiluminė spinduliuotė (Vaidogas ir Kisežauskienė 2012)

$$P_e(D \mid B) = \sum_{j=1}^{N} P(D \mid \boldsymbol{y}_j),$$ (S3)

čia $P(D \mid \boldsymbol{y}_j)$ – pažeidžiamumo funkcijos $P(D \mid \boldsymbol{y})$ reikšmė, apskaičiuota vektoriui $\boldsymbol{y}_j$ (žr. (S2) lygtį). BLEVE poveikių reikšmių $\boldsymbol{y}_j$ imtis taip pat galima taikyti parenkant charakteristines poveikių reikšmes.

Antrame disertacijos skyriuje išspręsti du uždaviniai, kurie iliustruoja, kaip gauti reikšmių $\boldsymbol{y}_j$ imtis. Pavyzdžiuose nagrinėtos dvi skirtingose Lietuvos vietose pastatytos pavojingųjų medžiagų talpyklos. Pirmame pavyzdyje buvo vertinama, kokius skeveldrų poveikius gali patirti projektuojamas saugos barjeras, kurį numatoma išdėstyti išilgai kelio Klaipėdos mieste. Antrame pavyzdyje skaičiuota, kokia šiluminė spinduliuotė gali veikti talpyklas, jei BLEVE sprogimas įvyks kelyje Vilnius–Kaunas.

3. Projektiniai pakelės objektus saugančių barjerų pasiūlymai

Trečiame skyriuje pasiūlyti keli projektiniai saugos barjerų sprendimai. Šie barjerai turėtų padėti apsaugoti pakelės objektus nuo sprogimų BLEVE būdu, galinčių kilti keliuose ir geležinkeliuose. Pirmas pasiūlymas apima saugos barjero išdėstymą turimame statybos plote ir barjero formos parinkimą. Antras pasiūlymas yra preliminarus sunaikinamo plieninio barjero projektas. Barjeras turi apsaugoti pakelės objektus nuo geležinkelio cisternos sprogimo BLEVE būdu. Svarstoma, kaip projektuoti tokį barjerą, derinant konstrukcijų patikimumo ir kiekybinės rizikos analizės metodus. Projektuojama turint mažą sprogimo bangos charakteristikų imtį. Trečias pasiūlymas yra rekomendacijos, kaip projektuoti gelžbetoninį barjerą. Jis turi atlaikyti cisternos sprogimo metu susidariusių skeveldrų smūgius. Visi trys projektiniai pasiūlymai turi išankstinių konstrukcinių sprendimų pobūdį. Detalus barjerų projektavimas nenagrinėjamas. Trečio skyriaus rezultatai pateikti publikacijose Vaidogas ir Linkutė (2012), Linkutė *ir kt.* (2013) ir Vaidogas ir kt. (2013).

Geometriniai veiksniai, kurie labiausiai lemia pakelės objektų terminio ir mechaninio pažeidimo laipsnį yra atstumas nuo sprogimo šaltinio iki pažeidžiamo objekto ir pakelės reljefas. Didėjant atstumui tarp transporto avarijos vietos ir pakelės objekto, mažėja sprogimo bangos energija, šiluminė spinduliuotė, skeveldrų greitis ir aukštis. Tačiau gaisrų ir sprogimų poveikis gali didėti arba mažėti priklausomai nuo to, kurioje vietoje įvyks avarija, ar pakelė lygi, kalvota ar nuožulni.

Pakelės objekto atžvilgiu nesaugią kelio (geležinkelio) atkarpą $\boldsymbol{\omega}$ galima nustatyti nuo objekto link kelio atidedant saugų atstumą $\varDelta$ (S6 pav.). Saugus atstumas $\varDelta$ gali priklausyti (būti kryptiniu) arba ne nuo atidėjimo krypties. Jį gali lemti ir vietovės reljefas. Atidėjus saugų atstumą $\varDelta$, bus suformuota nesaugi zona $\boldsymbol{\Omega}$. Jei transporto priemonės gaisras arba sprogimas įvyks zonoje $\boldsymbol{\Omega}$, pakelės objektas gali būti pažeistas.

Norint pastatyti saugos barjerą tarp kelio (geležinkelio) ir pakelės objekto (pažeidžiamos teritorijos), reikia turėti žemės sklypą, kurio plotas yra A_0. Plotas A_0 sudarys dalį nesaugios zonos $\boldsymbol{\Omega}$ ir bus tarp šalikelės ploto A_1 ir saugomos teritorijos A_2 (S7 pav.). Plotą A_1 lems transporto statinius reglamentuojantys dokumentai, o ploto A_0 dydį ir formą daugiausiai lems žemės nuosavybės padėtis, saugomo ploto A_2 forma,

vietovės reljefas ir geologinės sąlygos. Jei plotas A_0 yra pakankamai didelis, barjerui galima suteikti įvairias formas. Pigiausias ir paprasčiausias bus tiesus barjeras (S7 pav. a). Strėlės ir bastiono pavidalo barjerai bus efektyvesni atspindint sprogimo bangą ir nukreipiant skeveldras (S7 pav. bc). Tačiau tokiems barjerams statyti prireiks didesnio ploto.
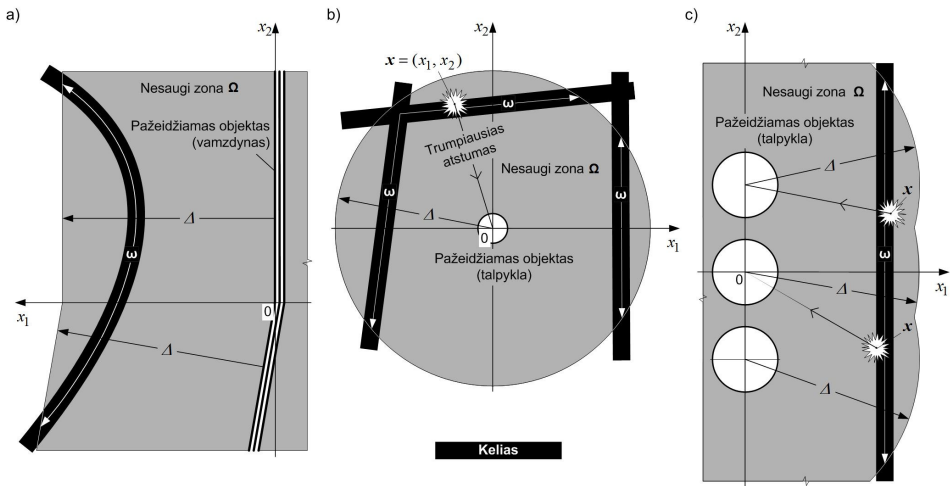
S6 pav. Saugus atstumas Δ ir nesaugi kelio atkarpa skirtingiems objektams: a) dujotiekis; b) apskrita pavienė talpykla; c) eile išdėstytos talpyklos (Vaidogas ir Linkutė 2012)

Trečiajame disertacijos skyriuje aptartos statybinės medžiagos, kurias galima naudoti saugos barjerams įrengti. Jei barjeras bus tvoros pavidalo konstrukcija, jį galima statyti iš gelžbetonio arba plieno. Jei reikia, šias medžiagas galima derinti. Tačiau barjerą galima įrengti sukasant grunto pylimą tarp kelio ir pažeidžiamo pakelės objekto. Gelžbetoninis arba plieninis barjeras gali sustabdyti (nukreipti) BLEVE metu susidarančias skeveldras ir sumažinti sprogimo bangos energiją. Grunto pylimas apsaugos nuo skeveldrų. Tačiau jei jo šlaitai nebus pakankamai statūs, o pylimo aukštis didelis, jis nedaug mažins sprogimo bangos energiją. Nepriklausomai nuo to, kokia medžiaga bus naudojama įrengiant saugos barjerą, jis nebus veiksmingas apsaugant greta kelio arba geležinkelio esantį pakelės objektą nuo šiluminės BLEVE sprogimo ugnies kamuolio spinduliuotės. Čia „barjeru" gali būti didelis atstumas nuo galimo sprogimo epicentro arba šiluminis pakelės objekto ekranavimas.

Projektinis disertacijoje siūlomo plieninio barjero sprendinys pavaizduotas S8 paveiksle. Barjero dalis yra sunaikinama danga iš profiliuotų plieninių lakštų, turinti sugerti BLEVE sprogimo bangą. Šio sprogimo metu susidarančias cisternos skeveldras turi sustabdyti plieninių lynų tinklas, įrengiamas priešingoje pavojui barjero pusėje. Disertacijoje pasiūlytas metodas, kaip projektuoti sunaikinamą dangą turint mažo dydžio statistinę sprogimo bangos charakteristikų imtį. Šiame metode suderinti profiliuoto lakšto skaičiavimas statybinių konstrukcijų patikimumo teorijos principais ir kartotinio statistinio ėmimo (angl. *bootstrap*) procedūra (Linkutė ir *kt*. 2013).
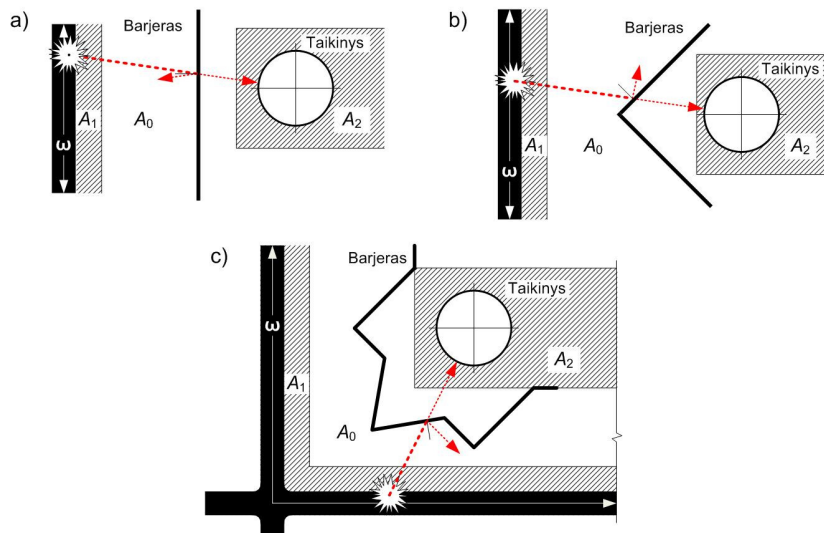
S7 pav. Horizontalus saugos barjero išdėstymas plote A_0: a) tiesi sienos atkarpa; b) strėlės pavidalo barjeras; c) bastiono pavidalo barjeras (Vaidogas ir Linkutė 2012)
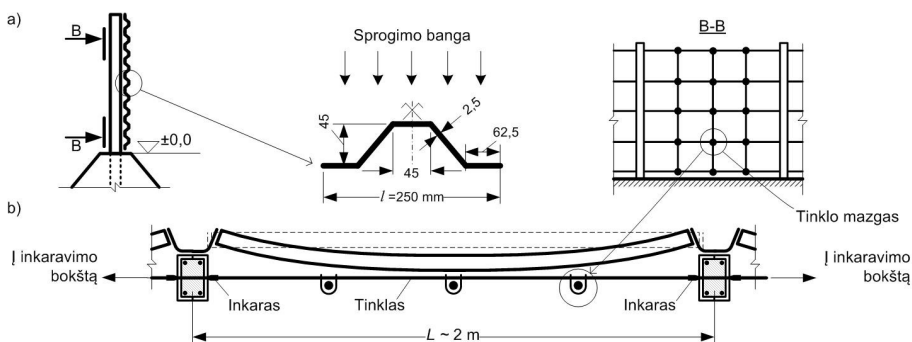
S8 pav. Projektinis plieninio saugos barjero su sunaikinama danga ir apsauginiu tinklu pasiūlymas: a) pjūvis; b) planas (Linkutė *ir kt.* 2013)

Trečiajame disertacijos skyriuje taip pat pateikiamas projektinis gelžbetoninio saugos barjero pasiūlymas. Barjerą galima projektuoti iš surenkamų gelžbetoninių elementų, pavaizduotų S9 paveiksle. Toks barjeras leis sustabdyti BLEVE sprogimo metu susidarančias cisternos skeveldras. Jei barjeras bus pastatytas netoli nuo galimo BLEVE sprogimo epicentro, jis atspindės ir, jei bus specialiai tam projektuotas, sugers namažą dalį sprogimo bangos energijos. Trečiajame skyriuje aptarta, kaip projektuoti gelžbetoninį barjerą, kad jis reaguotų į skeveldrų smūgius kaip plastiška konstrukcija.
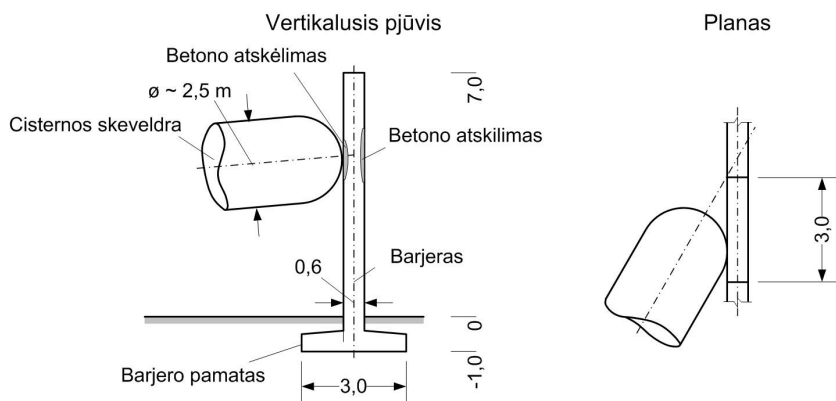
S9 pav. Projektinis gelžbetoninio saugos barjero pasiūlymas

S10 pav. Grunto pylimas (dešinėje), pastatytas apsaugoti degalų saugyklą (kairėje) nuo geležinkelio cisternos sprogimo BLEVE būdu (autorės nuotrauka)

Saugos barjeras gali turėti ir grunto pylimo pavidalą. Pylimas apsaugos pakelės objektą nuo cisternų skeveldrų poveikio su sąlyga, kad jis bus tinkamų matmenų ir išdėstytas labiausiai tikėtinų skeveldrų trajektorijų vietoje. Pylimai gali būti labai pigūs ir supilami per trumpą laiką. Tačiau tam, kad pylimas būtų pakankamai aukštas, jis turi būti labai platus ir užimti didelį plotą tarp saugomo pakelės objekto ir galimos sprogimo vietos. Kai kuriais atvejais gali trūkti vietos tokiam pylimui pastatyti. Be to, pylimo šlaitai gali būti nepakankamai statūs, kad būtų užtikrinta tinkama apsauga nuo sprogimo bangos poveikio. Grunto pylimo, pastatyto apsaugoti degalų saugyklas nuo skeveldrų poveikio, pavyzdys pateiktas S10 ir 3.14 paveiksluose). Šio pylimo statybą paskatino saugos studija, atlikta užsakius „Lietuvos geležinkeliams". (Vaidogas ir kt. 2012c).

Bendrosios išvados

1. Mokslo publikacijų, skirtų transporto rizikai vertinti, apžvalga leido padaryti išvadą, kad daugelis mokslininkų nagrinėja asmeninės ir grupinės rizikos skaičiavimą. Ši rizika tenka pakelės gyventojams. Vyraujantis avarijos scenarijus transporto rizikos vertinimuose yra nuodingosios medžiagos nuotėkis, sukeliantis gyventojų apsinuodijimus. Rizika, kylanti statybiniam pakelės turtui (pastatams, transporto infrastruktūros objektams, pramonės įmonėms), yra minima literatūroje, tačiau detaliai nenagrinėjama.

2. Išanalizavus duomenis apie pavojingųjų medžiagų vežimo avarijas, nustatyta, kad didžiausią žalos statybiniam turtui potencialą turi sprogimai BLEVE būdu ir garų debesų sprogimai. Dažniausiai abiejų rūšių sprogimus sukelia vežami komerciniai angliavandeniliai, ypač propanas. Jo vežimo avarijų nuošimtis kitų medžiagų atžvilgiu yra apie 65 % keliuose ir apie 40 % geležinkeliuose. Sprogimai BLEVE būdu dažnesni už garų debesų sprogimus, todėl pirmieji kelia didžiausią pavojų statybiniam pavojų turtui.

3. Svarstant, kaip galima sumažinti riziką statybiniam pakelės turtui, keliamą BLEVE sprogimų keliuose ir geležinkeliuose, nustatyta, kad tai galima padaryti statant saugos barjerus. Juos galima išdėstyti tarp kelių ir geležinkelių, kuriais vežamos pavojingosios medžiagos, ir pažeidžiamų pakelės objektų. Barjerai gali turėti tvoros pavidalą arba jais gali būti grunto pylimai. Barjeru taip pat gali būti didelis atstumas tarp transporto arterijų ir pakelės objektų.

4. Išanalizavus galimybes vertinti šiluminį ir mechaninį BLEVE sprogimo poveikį pakelės objektams prieita išvados, kad šį uždavinį reikia pradėti spręsti prognozuojant sprogstančios automobilinės arba geležinkelio cisternos padėtį ir orientaciją taikinio atžvilgiu. Toks prognozavimas bus susijęs su dideliais neapibrėžtumais, kuriuos reikia kiekybiškai išreikšti tikimybių skirtiniais. Kai kuriuos iš šių skirstinių galima parinkti remiantis statistiniais duomenimis apie transporto įvykius. Kitus teks užduoti subjektyviai, taikant kiekybinio rizikos vertinimo principus. Duomenys apie automobilinių cisternų avarijas leidžia daryti išvadą, kad avariją patyrusios cisternos centro padėtį skersai kelio reikia aprašyti logistiniu tikimybių skirstiniu su vidurkiu 2,02 m ir standartu 5,62 m. Tokios cisternos pasisukimo kampui kelio ašies atžvilgiu nusakyti tiks empirinis tikimybių skirstinys su vidurkiu 2,83° ir standartu 56,8°.

5. Analizuojant deterministinius modelius, skirtus prognozuoti šiluminį ir mechaninį BLEVE sprogimo poveikį, nustatyta, kad šiais modeliais galima praplėsti cisternos indo padėties ir orientacijos sprogimo metu modeliavimą. Taikant šiuos modelius bus galima įvertinti poveikių neapibrėžtumus pagal kiekybinio rizikos vertinimo principus. Techniškai šiuos neapibrėžtumus galima išreikšti tikimybių skirstiniais ir transformuoti, pasitelkiant stochastinį (Monte Karlo) modeliavimą.

6. Išnagrinėjus galimybes projektuoti saugos barjerus pagal kiekybinio rizikos vertinimo principus, nustatyta, kad tai galima daryti naudojant dviejų rūšių statistines BLEVE poveikių reikšmių imtis: didelę imtį, gautą stochastiškai modeliuojant, ir mažos apimties imtį, gautą eksperimentuojant arba tiriant įvykusias avarijas. Informacija, gaunama su šiomis imtimis, gali būti naudojama vertinant barjero atsako tikimybę. Šios tikimybės įvertis gali būti pagrindinis rodiklis, nusakantis barjero reakciją į BLEVE poveikius.

7. Išnagrinėjus statybines medžiagas, kurias galima naudoti įrengiant saugos barjerus prieita prie išvados, kad iš plieno galima statyti barjerus, kurie suirs absorbuodami sprogimo poveikį. Tokie barjerai vadinami sunaikinamaisiais barjerais. Masyvūs gelžbetoniniai barjerai ir grunto pylimai bus veiksmingi sulaikant skeveldras, susidarančias sprogstant automobilinėms ir geležinkelio cisternoms. Šių skeveldrų masė gali būti iki 10 tonų, o smūgiavimo greitis siekti 400 km/h. Tinkamai įvertinus galimą sprogimo bangą ir tikėtinus cisternos skeveldrų smūgius, plieninių ir gelžbetoninių konstrukcijų skaičiavimą galima atlikti taikant įprastinius konstrukcijų projektavimo metodus.

8. BLEVE sprogimų poveikių tyrimas atskleidė, kad ugnies kamuolys, kylantis sprogstant tipinėms automobilinėms ir geležinkelio cisternoms, bus didelis. Jis gali siekti 300 m aukštį, o jo skersmuo gali būti iki 200 m. Todėl tvoros pavidalo barjerai arba grunto pylimai menkai apsaugos pakelės objektus nuo šiluminio ugnies kamuolio poveikio. Šiuos objektus galima apsaugoti, užtikrinant didelį atstumą tarp kelio (geležinkelio) ir pažeidžiamo taikinio. Pakelės objektai taip pat gali būti apsaugoti šiluminiais ekranais, nes BLEVE sprogimo metu susidarančio ugnies kamuolio trukmė yra santykinai trumpa ir dažnai neviršija 20 sekundžių.

9. Išanalizavus šiame darbe siūlomas metodines procedūras prieita išvados, kad praktinio jų taikymo sėkmė priklausys nuo to, kaip projektuotojas sugebės išspręsti du uždavinius: kaip prognozuoti šiluminius ir mechaninius gaisrų ir sprogimų, galinčių įvykti keliuose ir geležinkeliuose, poveikius (trumpai, uždavinį „A") ir kaip tinkamai išnaudoti šio prognozavimo rezultatus, projektuojant saugos barjerą (trumpai, uždavinį „B"). Saugos barjero, turinčio tvoros, grunto pylimo arba pakankamo saugaus atstumo pavidalą, projektavimas bus santykinai paprastas, turint realistiškus galimų gaisrų ir sprogimų poveikių įverčius.

10. „A" ir „B" uždavinių sprendimas yra tarpdalykinė problema. Uždavinys „A" yra, iš esmės, nestatybinis uždavinys. Jį turėtų spręsti chemijos, mechanikos ir gaisrinės saugos inžinieriai, išmanantys tokius reiškinius, kaip BLEVE ir garų debesies sprogimas. Šie inžinieriai taip pat turėtų sugebėti modeliuoti neapibrėžtumus, susijusius su tokių sprogimų poveikiais.

11. Aukščiau minėtas uždavinys „B" turi būti sprendžiamas statinių konstruktoriaus, kuris projektuos saugos barjerą. Jei gaisrų ir sprogimų poveikiai bus prognozuojami, remiantis tikimybių modeliavimu ir kiekybinio rizikos vertinimo principais, geriausiai šios prognozės rezultatai bus išnaudoti barjerą projektuojant statybinių konstrukcijų patikimumo teorijos metodais.

Saugos barjerą taip pat galima projektuoti, pasitelkiant tradicinius, deterministinius metodus. Taip projektuojant, gaisrų ir sprogimų poveikiai turės būti išreiškiami fiksuotomis skaičiuotinėmis reikšmėmis. Tačiau jos gali būti netikslios arba nepakankamai konservatyvios.

Annexes

Annexes are given in the enclosed compact disc. They include textual information, computation results and data collected for the purposes of the investigation described in this dissertation. Annexes are arranged in six sections entitled as follows:

Annex A. Database on road tank car accidents
Annex B. Kinematic characteristics of fragments
Annex C. Information on the road tanker considered in the case study
Annex D. Results of fragment impact simulation in the case study
Annex E. Results of fragment impact simulation in the case study
Annex F. Results of fragment impact simulation in the case study

Annex A. Database on road tanker accidents

The present annex contains a database with the information on 151 traffic accident in which road tankers and several similar vehicles were involved. The information consists mainly of the data on the final rest position of the tankers as well as material shipped by them. The database was arranged in the form of the Table A1.

Table A1. Database containing information on 151 road tanker accidents

No	Date	Location	Material[1]	y_1 (m)[2]	y_2 (°)[3]	Rest pos.[4]
1	1964/08/09	Louisiana	LPG	19.10	70	A
2	1981/11/02	Kansas City, Missouri	LPG	4.60	-160	B
3	1984/10/25	Jacksonville, Florida	LPG	14.40	-15	B
4	1985/01/24	Jean, Texas	oil	0	0	N
5	1962/08/03	Houston, Texas	gasoline	0	0	N
6	1984/09/03	Norfolk, Texas	gasoline	0	0	N
7	2002/07/12	Masnoa, Syria	fuel	0	0	N
8	2005/08/10	Salt Lake City	explosive	0	0	N
9	2006/04/19	Hubei Province, China	diesel	11.60	10	A
10	2007/02/08	Mahanoy	fuel	17.60	0	C
11	2007/04/27	Houston,	diesel	0	0	C
12	2007/04/30	Oakland	gasoline	0	0	B
13	2007/09/10	Sacramento, Mexico	ammonium nitrate	0	0	A
14	2007/11/16	Lake, Dallas	diesel	0	0	A
15	2007/12/05	Everett	gasoline	9.60	0	A
16	2008/02/14	not reported	hydrogen	0	0	0
17	2008/04/26	Chicago	LPG	0	0	C
18	2009/01/12	Kissimmee, Florida	yogurt	9.10	0	A
19	2009/02/01	Nairobi, Kenya	Petrol	3.10	0	C
20	2009/04/01	Pasadena, California	gasoline	18.10	35	A
21	2009/07/05	Ocraoke	firework	11.10	150	A
22	2009/07/15	Michigan	LPG	18.10	70	C

Table A1. Continued

23	2009/07/15	Detroit	gasoline	0	0	N
24	2009/07/24	Fullerton, California	frozen meat	9.10	0	C
25	2009/07/25	Central Florida	gasoline	11.05	0	C
26	2009/07/25	Oak Park, Michigan	diesel gaso-line	12.35	0	A
27	2009/07/26	New Castle	propane	11.10	0	B
28	2009/08/24	Elmore, Minnesota	fuel	0	-170	C
29	2009/08/26	Rochester, Indiana	LPG	3.85	-20	C
30	2009/09/10	Cedar Rapid, Indiana	Fuel	11.60	0	C
31	2009/09/24	Bakersfield	tequila bot-tles	12.05	-60	C
32	2009/09/25	Bloomfield, Indiana	hot asphalt	16.35	70	A
33	2009/10/17	Tampa, Florida	sulphuric acid	10.10	0	A
34	2009/10/19	Oxford, Indiana	fuel	11.05	85	A
35	2009/10/22	Indianapolis	propane	18.10	85	B
36	2009/10/22	Indiana	propane	0	0	N
37	2009/10/23	Fayetteville	Fuel	11.95	0	C
38	2009/11/16	Orlando, Florida	LPG	13.45	-5	A
39	2009/11/30	Kansas City	hydrochloride acid (HCL)	11.60	-20	A
40	2009/12/10	Paramus, New Jersey	coca cola cans	8.15	0	A
41	2009/12/12	Saylorsburg, Penn-sylvania	fuel	44.60	90	C
42	2009/12/12	Merrill, Indiana	fuel	18.05	45	A
43	2009/12/20	Casper	LPG	9.80	25	C
44	2009/12/22	Warsaw, Indiana	anhydrous ammonia	14.95	-10	A
45	2009/12/30	Tulsa, Oklahoma	diesel	7.15	-30	A
46	2009/12/31	Karunagapally, India	LPG	3.10	170	A

Table A1. Continued

47	2010/01/18	De Witt, New York	crud oil	20.00	-50	C
48	2010/01/20	Williamston, Michigan	boxes or cereal	12.35	10	C
49	2010/01/23	Brooklyn, JAV	gasoline	13.35	-40	A
50	2010/01/23	Melville, New York	fuel	13.30	-20	A
51	2010/01/25	Montpellier, Vermont	propane	3.10	-90	C
52	2010/01/28	Montpellier, Vermont	milk	5.35	80	A
53	2010/02/05	New Stanton, Pennsylvania	candy bars	17.60	0	B
54	2010/02/08	Hoyden, Indiana	LPG	13.05	25	C
55	2010/02/10	Dearborn, Missouri	milk	24.84	0	C
56	2010/02/12	Shuyler, New York	palettes	14.05	0	C
57	2010/02/17	Donald Sonville, Louisiana	sulphuric acid (H2SO4)	14.35	0	C
58	2010/02/22	Grand Hawen Township, Michigan	LNG	6.70	0	C
59	2010/03/05	Phoenix, Arizona	LPG	14.60	10	C
60	2010/03/22	Seminary, Mississippi	grain	4.05	0	C
61	2010/04/02	Sherman, Maine	LPG	11.35	0	C
62	2010/04/01	Chicago, Illinois	LPG	0.10	-100	C
63	2010/04/02	Burverde, Texas	propane	14.60	70	C
64	2010/04/05	Woodbine, New Jersey	Fuel	16.55	5	A
65	2010/04/07	Wamsutter, Wyoming	crude oil	11.55	0	A
66	2010/04/07	Bethpage, New York	fuel	11.35	0	A
67	2010/04/14	Roy, Utah	diesel	8.60	-90	C

Table A1. Continued

68	2010/04/26	Oklahoma City, Oklahoma	flour	16.10	-15	C
69	2010/05/03	Wythe County, Virginia	LPG	21.10	55	C
70	2010/05/05	Weedsport, New York	aliunimum soda cans	6.70	70	A
71	2010/05/05	San Antonio	fuel	0	0	B
72	2010/05/07	Skerwood, Oregon	propane	5.25	-5	A
73	2010/05/08	Scarborough, Maine	empty	12.25	0	C
74	2010/05/10	Madison County, Kentucky	propane	16.35	45	C
75	2010/05/16	Miami Gardens, Florida	fuel oil	11.05	0	A
76	2010/05/18	Walthan, Massachusetts	woodchips	18.85	30	A
77	2010/05/18	Sissonville, Virginia	fuel	17.05	90	A
78	2010/05/19	Brighton, Michigan	monolube 3400	10.05	5	A
79	2010/05/20	Caledonia, Wisconsin	bread	9.60	0	C
80	2010/05/27	Revelstoke	fuel	13.60	180	A
81	2010/05/28	Carona, Los Angeles	gasoline	11.60	0	A
82	2010/05/29	Tynsborough, Massachusetts	aerosol paint	12.40	0	A
83	2010/05/29	Los Angles	gasoline	12.60	0	A
84	2010/05/30	Harrison, Ohio	LPG	10.50	10	C
85	2010/05/31	Tyler, Texas	gas	9.25	0	C
86	2010/06/03	Napa County, California	ceramic pipe	5.25	-20	C
87	2010/06/10	Charlotte, Michigan	LPG	10.55	-90	A
88	2010/06/11	Poulsbo, Washington	Fuel	5.40	85	C
89	2010/06/15	Newport, Virginia	sulphuric acid	18.95	0	A

Table A1. Continued

90	2010/06/16	San Diego, California	gasoline	0	0	C
91	2010/06/18	Henderson, Kentucky	propane	1.55	-90	C
92	2010/06/22	Foxboro, Massachusetts	jet fuel	-2.65	45	A
93	2010/06/26	Broadhead, Wisconsin	milk	5.90	10	C
94	2010/06/28	Hyderabad, Pakistan	thinner	0	0	N
95	2010/06/28	Catskill, New York	hypochlorite	11.35	0	C
96	2010/06/29	Cartez, Florida	LPG	6.70	-50	B
97	2010/07/02	Charlotte, Carolina	ceiled steel	13.30	0	C
98	2010/07/03	Kishnasha, Congo	oil	14.60	-20	A
99	2010/07/04	N. Carolina	fireworks	13.60	130	A
100	2010/07/08	Venice, Florida	propane	9.60	0	C
101	2010/07/08	Fairwax, Virginia	prefabricated mobile house	12.35	-10	A
102	2010/07/14	Kirvin, Kansas	propane	9.60	0	A
103	2010/07/19	San Diego, California	gravel	0.90	-90	A
104	2010/07/24	Waynesboro, Virginia	building lumber	13.45	10	C
105	2010/07/26	Inclive vil., Nevada	building debris	10.93	0	C
106	2010/07/28	Peidmont, S. Carolina	fuel	22.60	15	C
107	2010/08/04	Cedar Rapids, Iowa	sodium hydroxide	16.35	35	A
108	2010/08/09	Highland, Illinois	food	14.60	0	C
109	2010/08/12	Unity, Wisconsin	milk	17.95	-70	C
110	2010/08/13	Clover, South Carolina	yarn	10.60	5	C
111	2010/08/16	Fort Mill, South Carolina	gasoline	13.60	0	A

Table A1. Continued

112	2010/08/16	Charlotte, North Carolinas	fuel	0	0	A
113	2010/08/16	Coloma, Michigan	propane	18.15	-20	C
114	2010/08/18	Salt Lake City, Utah	ham	15.65	95	C
115	2010/08/20	Armold, Maryland	LPG	8.85	-5	A
116	2010/08/21	Arizona	diesel	27.60	50	C
117	2010/08/24	Santa Barbara, California	LPG	15.60	0	C
118	2010/08/26	Montreal, Canada	LPG	11.35	0	A
119	2010/08/27	Gilroy, California	broccoli	5.80	0	C
120	2010/08/28	Utah	diesel	18.10	90	B
121	2010/08/29	Hamshire, Texas	isobutene	19.85	90	B
122	2010/08/31	Falcon Heights, Minnesota	LPG	11.10	10	A
123	2010/09/03	Dearborn County, Indiana	molten phthalic an-hydride	22.85	40	B
124	2010/09/07	Issaquah, Washington	steel con-struction	10.45	0	C
125	2010/09/08	Lake Worth, Florida	PVC pipe	4.35	5	A
126	2010/09/10	Sacramento, Mexico	dynamite	12.60	-20	C
127	2010/09/14	Cache County, Utah	banana	13.35	0	A
128	2010/09/22	Helena, Montana	cattle	14,05	-5	A
129	2010/09/29	Columbia, South Carolina	LPG	4.60	-100	A
130	2010/10/12	New Mexico	diesel	0	0	C
131	2010/10/13	Oldham County	ink	1.85	-90	C
132	2010/10/18	Morgan Hill	molten wax	2.15	-90	A
133	2010/10/23	South Bend, Indiana	mandarins	14.60	0	A
134	2010/10/28	Los Angles, California	LPG	8.10	0	A
135	2010/10/29	Albuquerque, New Mexico	LPG	2.85	-80	A
136	2010/11/01	Foxboro, Massachu-setts	candles	2.90	15	C
137	2010/11/02	Parma, Idaho	empty	7.85	35	A

Table A1. Continued

138	2010/11/05	Ibadan, Nigeria	petrol fuel	0	0	B
139	2010/11/09	California	tar	4.05	15	A
140	2010/11/10	Mt. Juliet, Tennessee	ferric chloride	17.35	-10	C
141	2010/11/26	Rufus, Oregon	LPG	3.65	-30	A
142	2010/12/07	Sent Louis	automotive parts	7.70	-10	A
143	2010/12/10	Bakers Corner, Indiana	propane	22.40	0	C
144	2010/12/12	Maysville, Kentuky	paper	6.75	0	C
145	2010/12/14	Lansing, Michigan	LNG	7.80	0	A
146	2010/12/16	Remington, Indiana	fuel	9.60	0	A
147	2010/12/18	Ningxiang, Japan	fireworks	0	0	B
148	2010/12/20	Utah	bride oil	4.60	-50	A
149	2010/12/21	Canada	oil	11.85		A
150	2011/01/10	Oklahoma	propane	21.10	-90	C
151	2011/01/31	Matttoon, Kentucky	anhydrous ammonia	14.45	-85	B

Notes:

[1] Material = material shipped by the vehicle involved in a traffic accident

[2] y_1 = transverse rest position in the vehicle-based coordinate system $\{0; y_1, y_2, y_3\}$ shown in Fig. 2.5 (Sec. 2.2.1)

[3] y_2 = departure angle in the vehicle-based coordinate system $\{0; y_1, y_2, y_3\}$ shown in Fig. 2.5 (Sec. 2.2.1)

[4] Rest pos. (rest position) = the dominant rest position of the tanker vessel with respect to a horizontal orientation of the principal vessel axis shown in cases a), b) and c) of Fig. 2.17 (Sec. 2.2.3); letters "A","B", and "C" correspond to these three cases; the letter "D" means that the position was different from all three positions indicated in Fig. 2.17; the letter "N" means that the vessel position was not identifiable

Table A2. Worldwide data on 43 BLEVE accidents on road in the period 1959 to 2011 (information was extracted from the FACTS database, FACTS (2014))

Year	Country	Location	Material involved in BLEVE
1959	USA	Road	LPG (propane)
1962	USA	Road	LPG (propane)

Table A2. Continued

1963	Netherlands	Level crossing	LPG (butane, propane)
1967	Belgium	Road	Propylene
1970	USA	Built-up-area	Oxygen (liquid)/lox
1970	USA	Engineering-works	LPG (propane)
1972	USA	Road	Propylene
1973	France	Road	LPG (propane)
1975	USA	Road	LPG (butane, propane)
1976	USA	Road	LPG (propane)
1977	USA	Unknown	LP LPG (propane)G
1977	Netherlands	Road	LPG (propane)
1978	Netherlands	Road	Inflammable liquid gas
1978	Denmark	Road	Benzene
1979	Canada	Level crossing	LPG (propane)
1979	Netherlands	Road	LPG (propane)
1980	USA	Road	Benzene
1980	Netherlands	Road	Hydraulic oil
1980	Netherlands	Road	LPG (propane)
1981	Netherlands	Road	LPG (propane)
1981	USA	Road	LPG (propane)
1981	Netherlands	Road	LPG (propane)
1982	India	Road	LPG (propane)
1982	Netherlands	Road	Freon
1984	Netherlands	Road	LPG (propane)
1984	Netherlands	Road	LPG (propane)
1990	Estonia	Road	LPG (propane)
1995	USA	Road	LPG (propane)
1996	India	Tunnel	LPG (propane)
1997	Malaysia	Road	LPG (propane)
1997	France	Road	LPG (propane)
1998	France	Road	LPG (propane)

Table A2. Continued

1998	India	Parking	LPG (propane)
1998	USA	Road	Diesel oil/Fuel
1999	Greece	Road	LPG (propane)
2001	Netherlands	Road	Diesel oil
2001	India	Road	Inflammable liquefied gas
2002	Estonia	Road	Diesel oil
2003	France	Road	LPG (propane)
2006	Zambia	Road	Methanol
2007	France	Parking	LPG (propane)
2007	Greece	Road	LPG (propane)
2011	Spain	Road	LPG (propane)

Table A3. Data on 38 BLEVE accidents on rail in the years 1958 to 2003 (extracted from the FACTS database, FACTS (2014))

Year	Country	Location	Material involved in BLEVE
1958	Denmark	Rail yard	LPG (propane)
1968	USA	Railway	Vinyl chloride
1969	USA	Railway	LPG (propane)
1969	USA	Railway	LPG (propane)
1970	USA	City	LPG (propane)
1971	USA	Rail yard	Vinyl chloride
1974	USA	Railway	LPG (propane)
1975	USA	Railway	LPG (propane)
1976	USA	City	Benzene
1977	USA	Railway	Isobutene
1977	USA	Depot	LPG (propane)
1978	USA	Engineering-works	Butadiene
1978	USA	Railway	LPG (propane)
1978	USA	Railway	LPG (propane)
1979	Netherlands	Railway	Methane

Table A3. Continued

1979	Canada	Level crossing	LPG (propane)
1979	USA	Railway	Butadiene
1982	Canada	Railway	Ammonium phosphate
1982	USA	Railway	Vinyl chloride
1982	Canada	Level crossing	Sodium sulphide
1983	USA	Railway	Ammonia
1985	USA	Engineering-works	Butyl acrylate
1985	Denmark	Railway	Benzene
1986	Sudan	Railway	Benzene
1989	Russia	Railway station	LPG (propane)
1990	Belgium	Railway station	Dimethyl ether
1983	USA	Railway	Sulphuric acid
1996	USA	Railway	LPG (propane)
1996	USA	Rail yard	LPG (propane)
1999	Canada	Railway	Ammonia
1999	USA	Factory	Diesel oil/Fuel
1999	Canada	Railway	Benzene
1999	Finland	Rail yard	Crude oil
2000	Netherlands	Railway station	LPG (propane)
2000	USA	Engineering-works	Acrylic acid
2001	USA	Tunnel	Acetic acid
2002	Ethiopia	Railway	Butane
2003	Canada	Railway	Ammonia

Annex B. Kinematic characteristics of fragments

The departure velocity of the generated fragnment can be derived from its kinetic energy, E_c and its mass, m_p:

$$v_p = \sqrt{\frac{2 \cdot E_c}{m_p}} \tag{B1}$$

where total energy, E, that causes the expansion, the rupture and the vessel explosion can be calculated by comparing the pressures onside and outside the vessel, (Baum1988):

$$E = \left[1 - \left(\frac{p_e}{p_0} \right)^{\frac{\gamma-1}{\gamma}} + (\gamma-1)\frac{p_e}{p_0}\left(1 - \left(\frac{p_e}{p_0} \right)^{-\frac{1}{\gamma}} \right) \right] \frac{p_0}{\gamma-1} V \tag{B2}$$

where V is the vessel volume; p_0 is the failure pressure; p_e is the atmospheric pressure (i.e. the external pressure); γ is the specific heat ratio.

Table B1. Probability density of fragment velocity

No.	Interval	Number of test	Experimental frenquency	Theoretical frequency
1	[0.00, 0.02]	23	0.1966	0.2272
2	[0.02, 0.04]	34	0.2906	0.2336
3	[0.04, 0.06]	22	0.1880	0.1812
4	[0.06, 0.08]	12	0.1026	0.1293
5	[0.08, 0.10]	7	0.0598	0.0886
6	[0.10, 0.12]	6	0.0513	0.0592
7	[0.12, 0.14]	3	0.0256	0.0389
8	[0.14, 0.16]	2	0.0171	0.0253
9	[0.16, 0.18]	2	0.0171	0.0163
10	[0.18, 0.20]	2	0.0171	0.0105
11	[0.20, 0.22]	3	0.0256	0.0067
12	[0.22, 0.24]	1	0.0085	0.0047

The fragment kinematic energy, E_c, is then derived from the total energy, E (Hauptmanns, 2001b):

$$E_c = \alpha \cdot E \tag{B3}$$

where α is a multiplying factor.

One the base of the available data (Baum 1988, 1995, 2001), the experimental values for the factor, α, derived from equations B1–B2, are summarized in Table B1.

Mébarki *et al.* (2009) investigate,an adequate probabilistic distribution for the multiplying factor, α. Actually, considering this factor asa random variable, its adequate p.d.f. can be derived from the maximum entropy principle (Kapur 1989; Mébarki *et al.* 2008):

$$p_\alpha(\alpha) = \alpha; \ g_2(\alpha) = \ln(\alpha) \tag{B4}$$

where $p_\alpha(\alpha)$ is the p.d.f. of thr factor α).

The available information used herein is:

$$g_1(\alpha) = \alpha; \ g_2(\alpha) = ln(\alpha) \tag{B5}$$

Their mean values can be, therefore expressed as mathematical expectation value of order 1 (the mean value), E_1:

$$E_1 = \int\limits_{Support=D} \alpha \cdot e^{-\lambda_0 - \lambda_1 \cdot \alpha - \lambda_2 \cdot ln(\alpha)} d\alpha \tag{B6}$$

where the support:

$$D = [\,0 \ up \ to \ 24\,] \tag{B7}$$

$$E_1 \approx \sum_{i=1}^{12} 0.02\alpha \cdot e^{-\lambda_0 - \lambda_1 \cdot \alpha - \lambda_2 \cdot ln(\alpha)} \tag{B8}$$

with $\alpha = 0.02(i-1) + 0.01$ and $\Delta\alpha = 0.02$.

Mathematical expectation value for the logarithm of α, $E(\ln(\alpha))$:

$$E(ln(\alpha)) = \int\limits_{Support=d} ln(\alpha) \cdot e^{-\lambda_0 - \lambda_1 \cdot \alpha - \lambda_2 \cdot ln(\alpha)} d\alpha \tag{B9}$$

so that:

$$E(ln(\alpha)) \approx \sum_{i=1}^{12} 0.02\,ln(\alpha) \cdot e^{-\lambda_0 - \lambda_1 \cdot \alpha - \lambda_2 \cdot ln(\alpha)} \tag{B10}$$

with $\alpha = 0.02(i-1) + 0.01$ and $\Delta\alpha = 0.02$.

The multipliers values are therefore obtained by solving the following system:

$$
\begin{cases}
\int\limits_{Support=D} exp(-\lambda_0 - \lambda_1 \cdot \alpha - \lambda_2 \cdot ln(\alpha)) \cdot d\alpha = 1 \\[2mm]
\int\limits_{Support=D} \alpha \cdot exp(-\lambda_0 - \lambda_1 \cdot \alpha - \lambda_2 \cdot ln(\alpha)) \cdot d\alpha = E_1 \\[2mm]
\int\limits_{Support=D} ln(\alpha) \cdot exp(-\lambda_0 - \lambda_1 \cdot \alpha - \lambda_2 \cdot ln(\alpha)) \cdot d\alpha = E(ln(\alpha))
\end{cases}
\quad \text{(B11)}
$$

$$
\Rightarrow \lambda_0 = -4.8869,\ \lambda_1 = 24.9431\ and\ \lambda_2 = -0.4793 \quad \text{(B12)}
$$

The good acoordance between theoretical and experimental histograms for the factor α. Therefore, the multiplying factor α is assumed to follow continuous exponential distribution.

As discussed in Mébarki *et al.* (2007; 2008; 2009ab); and Nguyen *et al.* (2009), the total energy E can be calculated using eq. B12 from Baum (1988) when the explosion of a tank occurs. Afterward, the kinetic energy E_k of the fragments can be derived using Eq. B14. the initial velocity of general fragments v_0, can be derived from their kinetic energy E_k and mass m Eq. B13.

$$
E = \left[1 - \left(\frac{p_e}{p_0} \right)^{\frac{\gamma-1}{\gamma}} + (\gamma-1)\frac{p_e}{p_0} \right] \frac{p_0}{\gamma-1} fV \quad \text{(B13)}
$$

$$
E_k = cE \quad \text{(B14)}
$$

$$
v_{dep} = \frac{\sqrt{2E_k}}{m} \quad \text{(B15)}
$$

where p_e is the atmosheric pressure, p_0 is the failure pressure of the source vessel, γ is the specific heat ratio, f is the degree of filling of the source vessel, V is the volume of source vessel, c is a multipliecative factor relating total expansion energy in the vessel and kinetic energy of the fragment.

The generated fragments may impact potential targets on their trajectory, being therefore a mechanical threat for these targets, as it may damage them seriously. The trajectory of the projectiles has then to be exactly known. This kind of problem has already been studied in order to investigate the possible collision between a fragments (the projectile) and tank (the target) in its vicinity (Hauptmanns 2011 ab). The movement of the fragment has been analysed in

bidimensional (2D). The simplified form of the possible impct analysis supposes that the fragment trajectory can be described by trajectory of a point (its barycentre). For this purpose Gubinneli *et al.* (2004) presents also the model known as "minimal distances". The simplified forms are the following: rectangular from in *xy* plane and circular form on *xz* plane.

The present study details with the possible impact and requires also the detailed information in order to evaluate the mechanical damage caused to the target by the impact. A three dimensional analysis is therefore considered. However, for simplification purposes at the step, the rotation effect of the fragment during the movement is neglected. The equations of motion for fragment centre are as follows:

$$
\begin{cases}
\left(k_D - (-1)^q \cdot k_L\right) \cdot \dot{x}^2 + \ddot{x} = 0 \\
\left((-1)^q \cdot k_D + k_L\right) \cdot \dot{y}^2 + \ddot{y} + g = 0 \\
\left(k_D - (-1)^q \cdot k_L\right) \cdot \dot{z}^2 + \ddot{z} = 0
\end{cases}
\tag{B16}
$$

where:
$$
k_D = \frac{1}{2}\frac{\rho_{air} \cdot C_D \cdot A_D}{m_p}; \; k_L = \frac{1}{2}\frac{\rho_{air} \cdot C_L \cdot A_L}{m_p};
\tag{B17}
$$
$$
(k_D - k_L) = k_m; \; (k_D + k_L) = k_p
$$

where $q = 1$ at descending part; $q = 2$ at ascending part; g is gravity; m_p is fragment mass; A_D is drag area and A_L is lift area.

The detailed equation are described in the Appendix A where the analytical solution of the nonlinear differential equations system of fragment a presented. With the coordinates, the size and dimensions of a given target, Nguyen *et al.* 2009develop an additional equation system in order to modelize target shape. The impact occurs when it exists a possible intersection between the fragment and the considered target , i.e. any point on the fragment trajectory meets the target. If an impact is possible, the coordinates of the intersection point (*I*), the velocities and the angles at the impact are calculated. The probability of impact P_{imp} might then be defined:

$$
P_{imp} = \sum_{k=1}^{N_{sim}} \frac{1\left(V_{t\,arg\,et} \cap V_{fragment}(t) \neq \phi\right)^{(k)}}{N_{sim}}
\tag{B18}
$$

$$
1\left(v_{t\,arg\,et} \cap v_{fragment}(t) \neq \phi\right)^{(k)}
$$
$$
= \begin{cases} 1\;if\left(v_{t\,arg\,et} \cap v_{fragment}(t) \neq \phi\right)at\;the\;kth\;simulation \\ \qquad\qquad 0\;otherwise \end{cases}
\tag{B19}
$$

where N_{sim} the number of Monte Carlo simulations; $1\left(v_{t\,arg\,et} \cap v_{fragment}(t) \neq \phi\right)^{(k)}$: the indicator function that indicates whether the projectile meets and impacts the target under study or not; V_{target}: the volume of target with a given location, dimensions and shape; $V_{fragment\,(t)}$: the volume of fragment at hte kth simulation depending on the dimensions, the shape and the location on trajectory that depends on the time t (with $t > 0$).

The trajectory of fragments projected from the exploded vessels results from the combined effects of inertia, gravitation and aerodynamics (drag and lift). Let (O, X, Y, Z) be the set of system axes used for the trajectory description and let O be the departure point for a generated fragment. The fragment trajectory can be described as as shown in Mébarki *et al.* (2009b). After the fragment has been projected, an impact is possible with any potential target that crosses its trajectory.

For fragments, the complete movement approach is used (Mébarki *et al.* (2007; 2008; 2009ab and Nguyen *et al.* 2009):

$$
\left\{
\begin{aligned}
&\left(-k_D \cdot cos(\varphi) \cdot cos(\theta) - (-1)^q \cdot k_L \cdot sin(\varphi) \cdot cos(\theta)\right) \cdot \\
&\qquad\qquad\qquad \cdot \left(\dot{x}^2 + \dot{y}^2 + \dot{z}^2\right) - \ddot{x} = 0 \\
&\left(-k_D \cdot cos(\varphi) \cdot sin(\theta) - (-1)^q \cdot k_L \cdot sin(\varphi) \cdot sin(\theta)\right) \cdot \\
&\qquad\qquad\qquad \cdot \left(\dot{x}^2 + \dot{y}^2 + \dot{z}^2\right) - \ddot{y} = 0 \\
&\left(-(-1)^q \cdot k_D \cdot sin(\varphi) + k_D \cdot cos(\varphi)\right) \\
&\qquad\qquad \cdot \left(\dot{x}^2 + \dot{y}^2 + \dot{z}^2\right) - \ddot{z} - g = 0
\end{aligned}
\right.
\qquad (B20)
$$

where $q = 1$ at descending part; $q = 2$ at ascending part; g is gravity; x, y, z are the fragment center coordinates; k_D is the drag factor $k_D = \dfrac{1}{2}\dfrac{\rho_{air} \cdot C_D \cdot A_D}{m_p}$ (Eq. B16), k_L is the lift factor $k_L = \dfrac{1}{2}\dfrac{\rho_{air} \cdot C_L \cdot A_L}{m_p}$ (Eq. B16), ρ_{air} is the dencity of air.

The solution of the fragment motion equations can be derived under the following set of hypotheses porposed by Mébarki *et al.* (2007; 2008; 2009ab) and Nguyen *et al.* (2009):

- Initial conditions: at departure, the fragment is located at the system origin (poit *O*). The pulse produced by the blast (vessel explosion) produces the initial velocity of fragment ($v_{Ox}, v_{Oy} v_{Oz}$).
- When the projectile reaches its trajectory upper position (top point), its vertical velocity becomes zero.
- Final conditions: when the fragment craches on the ground , in the descending part of its trajectory, its vertical coordinate becomes zero.

Hereafter, the distribution of the fragments craching on the ground will be evaluated by means of Monte – Carlo simulation using the complete movement approach.

Annex C. Information on the road tanker considered in the case study

The case study presented in Sec. 2.2.4 includes prediction an impact of fragments (projectiles) on a potential safety barrier. The impact can be caused by a fragmentation of pressure vessel in the course of a BLEVE. The vessel is a part of a HLQ 3-axle LPG tank semi-trailer (Fig. C1). It is produced by the Hubei Heli Special Automobile Manufacturing Company (http://hltruck.en.china.cn/).

This vessel was chosen only as an example. If the safety barrier considered in Sec. 2.2.4 will be threatened by a BLEVE of a pressure vessel of another type or a vessel having another characterisics, the prediction of impact effects should be done anew.
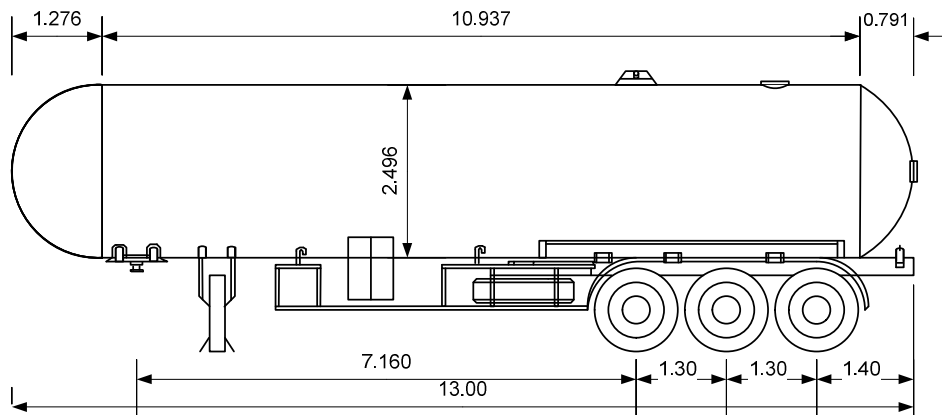
Fig. C1. HQL LPG tank 3-axe semi trailer

The tank volume of the HLQ 3-axle LPG tank semi-trailer shown in Fig. C1 are 52 m^3. The tank material is Q345R (Chinese standard). The semi-tailer was designed to ship LPG only. The nominal pressure of the safety valve are 2.5 MPa. The main specifications of the semi trailer are given in Table C1.

The case study presented in Sec. 2.2.4 describes a simulation-based prediction of fragmentation, trajectories and impact characteristics of the tank semi-trailer shown in Fig. C1. Mathematical models used for this prediction are presented in Sec. 2.2.4 and Annex B. Some input variables of these models are eterministic and some are random. Values of deterministic input variables related to the tank trailer are listed in Table C2, wereas probability distributions of the random input variables are given in Table C3.

Table C1. The main specification of the HLQ LPG tank semi trailer

LPG TANK SEMI TRAILER SPECIFICATION			
Product model	HLQ LPG tank 3 axle semi trailer	Design the limited ve-lovity	Straight road 80 km/h
G.V.W.	Approx 40000 kg		Turning 20 km/h
Net weght	Approx 17600 kg	F/R track base	-/ 1840/ 1840/ 1840
Axle	12 T BPW *3 pcs	Wheel base	6800+1310+1310 mm
Axle load	15200/ 24800 kg (triaxle)	Overall Dimensions	12740*2500*3950 mm
Tire specification	12.00-20*12 pcs	Max vehicle roll angle	> 35 o
LPG TANK SPECIFICATION		EMERGENCY CUT OFF DEVICE	
Tank dimensions (diameter*thickness*L)	DN 2320*14*12360 mm	Type	QGJ43F-2.5 or FISHER internal valve C427-16-25 / C427-24-50
Net weight	Approx 13000 kg	Nominal pressure	PN2.5 MPa
Vessel type	III	Nominal diameter	Gas Valve: DN 25 Liquid valve: DN50
Designing pressure	1.77 MPa	Control method	Manual machinery
Working pressure	≤1.61 MPa	Closing time	≤ 10 s
Melting switch temperature	70± 5 0 C	Melting close temperature	70± 5 0 C
Designing temperature	-19 ~+ 50 0 C	Emergency cut off type	Emergemcy shut-off valve and valve combination of over-current limit
Loading material	Liquified petroleum gas (propane)	LIQUID INDICATOR	
Corrosion margin	1.00 mm	Model	UHZ- 518C14
Volume (water capacity)	52 m3	Nomial pressure	PN 2.5 MPA
Tank &Pressure material	Q345R	Precision	2.5 Grade
Hydraulic pressure test	2.22 MPa	SAFETY VALVE	
Gas tight pressure test	1.77 MPa	Model	A42F-2.5-80

Table C1. Continued

Cylinder thickness	13.56 mm	Version	Inner full lift
Head thickness	13.53 mm	Nominal pressure	2.5 MPa
Service life	10 years	Nominal radius	DN 80
LOADING AND UNLOADING		Opening pressure	1.68~1.76 MPa
Valve type	Q41F-2.5 P/ CQA41F-25 P	Reseating pressure	≥ 0.8 MPa
Model	Qiuck tie -in	Closing pressure	> 1.54 MPa
Nominal Diameter	Gas phase DN25 mm	Complete opening pressure	< 2.19 MPa
	Liquid phase DN50 mm	Design standart meet ASME, SGS, etc	

Table C2. Deterministic input variables used for the simulation of LPG tank fragmentation

Variable	Symbol	Value
The length mass of the cylindrical part	l_{cyl}	10.94 m
The linear (1 m) mass of the cylindrical part	$m_{cyl,\,1}$	882 kg
Mass of front end-cap	$m_{e-c,\,front}$	1103 kg
Mass of rear end-cap	$m_{e-c,\,rear}$	681 kg
Volume of the tank	V	52 m^3
The specific heat ratio for propane at 15 °C	γ	1.13

Table C3. Random input variables used for the simulation of LPG tank fragmentation

Variable	Symbol	Probability distribution
Length of the cylindrical part between the end-cap and circumferential crack	ξcyl	Uniform over [0, lcyl]
The length of the cylindrical part of the front oblong end-cap	ξfront	Beta Be(2, 4) adjusted to the half-length lcyl/2
The length of the cylindrical part of the rear oblong end-cap	ξrear	Beta Be(4, 2) adjusted to the half-length lcyl/2
The failure pressure	p0	Normal N(2.5 MPa, 0.125 MPa)
The atmospheric (external) pressure	pe	Normal N(0.1013 MPa, 0.0051 MPa)

Table C3. Continued

The degree of filling of the source vessel	f	Uniform over [0.2 %, 0.8 %]
The factor relating the expansion energy in the vessel and kinetic energy of a fragment	c	Exponential with the mean of 0.04

Annex D. Results of fragment impact simulation in the case study

Two models were used to predict characteristics of road tanker vessel fragmentation:

- The model of vessel fragmentation presented in Sec. 2.2.3 and used for predicting the masses of the front and rear fragments, $\xi_{frg,\,front}$ and $\xi_{frg,\,rear}$.
- The model described and used for an assessment of fragment departure velocities $v_{dep,\,front}$ and $v_{dep,\,rear}$.

A stochastic simulation was carried out by applying the models just listed and the input data given in Tables C2 and C3. A total of 10 000 simulations were carried out to assess the variability of the fragment masses and departure velocities. The simulation yielded four samples of the simulated values $\xi_{frg,\,front,\,j}$, $\xi_{frg,\,rear,\,j}$, $v_{dep,\,front,\,j}$ and $v_{dep,\,rear,\,j}$ (j = 1, 2, … , 10 000). Desciptive statistics and correlation matrix of these values is presented in Tables D1 and D2.

Table D1. Descriptive statistics of the simulated characterising of the road tanker vessel fragmentation, $\xi_{frg,\,front,\,j}$, $\xi_{frg,\,rear,\,j}$, $v_{dep,\,front,\,j}$ and $v_{dep,\,rear,\,j}$ (j = 1, 2, … , 10 000)

Departure characteristic	Mean	Min.	Max.	Std. dev.	Skew.	Kurt.
Front fragment mass (kg)	4230	1103	10713	2579	1.01	–0.167
Rear fragment mass (kg)	3804	685.2	10294	2569	1.03	–0.108
Departure velocity (front) (km/h)	193.4	1.47	931	124.37	1.21	1.84
Departure velocity (rear) (km/h)	211.2	1.74	1141	141.98	1.41	2.86

Table D2. The correlation matrix of the simulated characterising of the road tanker vessel fragmentation, $\xi_{frg,\,front,\,j}$, $\xi_{frg,\,rear,\,j}$, $v_{dep,\,front,\,j}$ and $v_{dep,\,rear,\,j}$ (j = 1, 2, … , 10 000)

	1.	2.	3.	4.
1. Front fragment mass (kg)	1	–0.17	–0.40	0.06
2. Rear fragment mass (kg)	–0.17	1	0.06	–0.43
3. Departure velocity (front) (km/h)	–0.40	0.06	1	0.72
4. Departure velocity (rear) (km/h)	0.06	–0.43	0.72	1
* All correlations are significant at p < 0.05				

The histograms of $\xi_{frg, front, j}$, $\xi_{frg, rear, j}$, $v_{dep, front, j}$ and $v_{dep, rear, j}$ are given in Fig. D.1 and D2. The scaterplots of the pairs of $\xi_{frg, front, j}$, $\xi_{frg, rear, j}$, $v_{dep, front, j}$ are presented in Fig. D3, Fig. D4 and D5.

Histograms of the simulated values $\xi_{frg, front, j}$, $\xi_{frg, rear, j}$, $v_{dep, front, j}$ and $v_{dep, rear, j}$ ($j = 1, 2, \ldots, 10\,000$) are shown in Fig. D1 and D2. The scatter diagrams of the pairs $(\xi_{frg, front, j}, \xi_{frg, rear, j})$, $(\xi_{frg, front, j}, v_{dep, front, j})$, $(\xi_{frg, front, j}, v_{dep, rear, j})$, $(\xi_{frg, rear, j}, v_{dep, front, j})$, $(\xi_{frg, rear, j}, v_{dep, rear, j})$ and $(v_{dep, front, j}, v_{dep, rear, j})$ are presented in Fig. D3, Fig. D4 and D5.
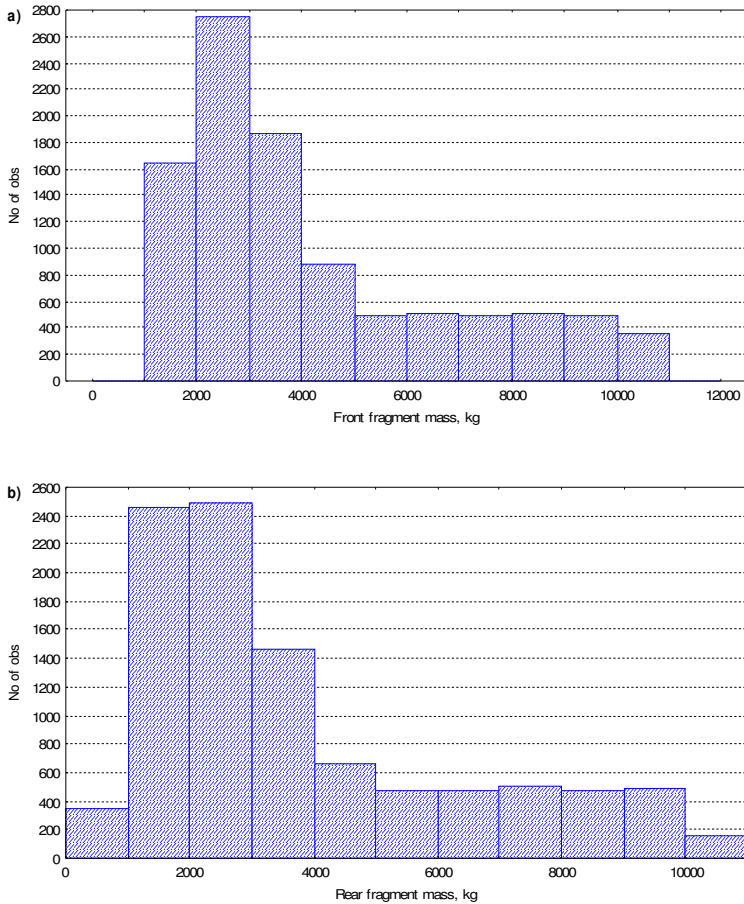
Fig. D1. Histograms of the simulated values $\xi_{frg, front, j}$, $\xi_{frg, rear, j}$ ($j = 1, 2, \ldots, 10\,000$)
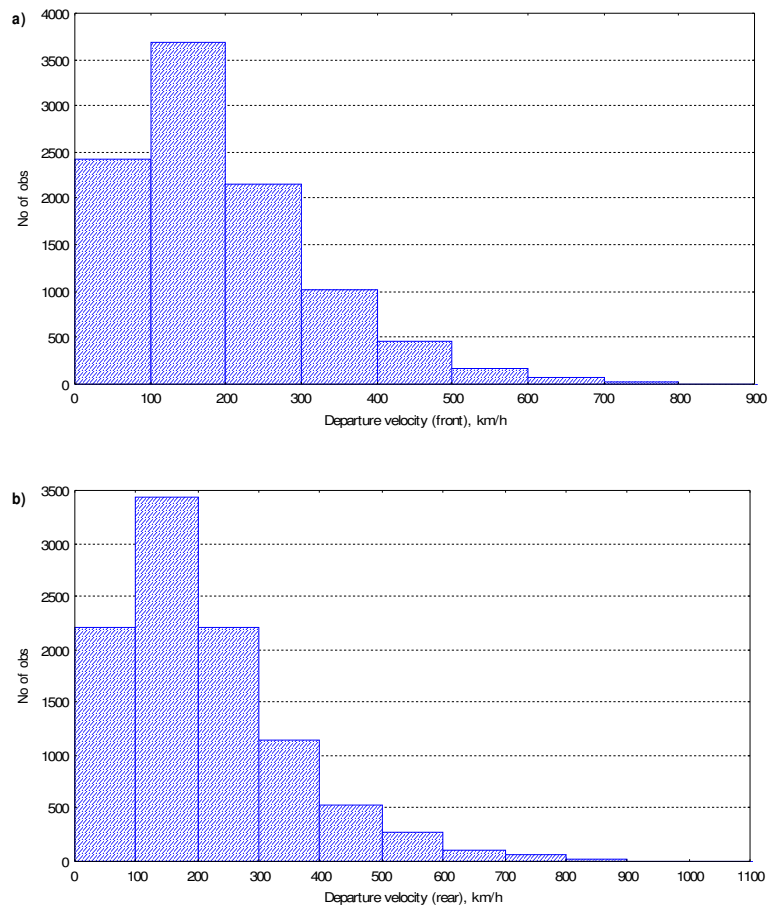
Fig. D.2. Histograms of the simulated values $v_{dep, front, j}$ and $v_{dep, rear, j}$ ($j = 1, 2, \dots$, 10 000)
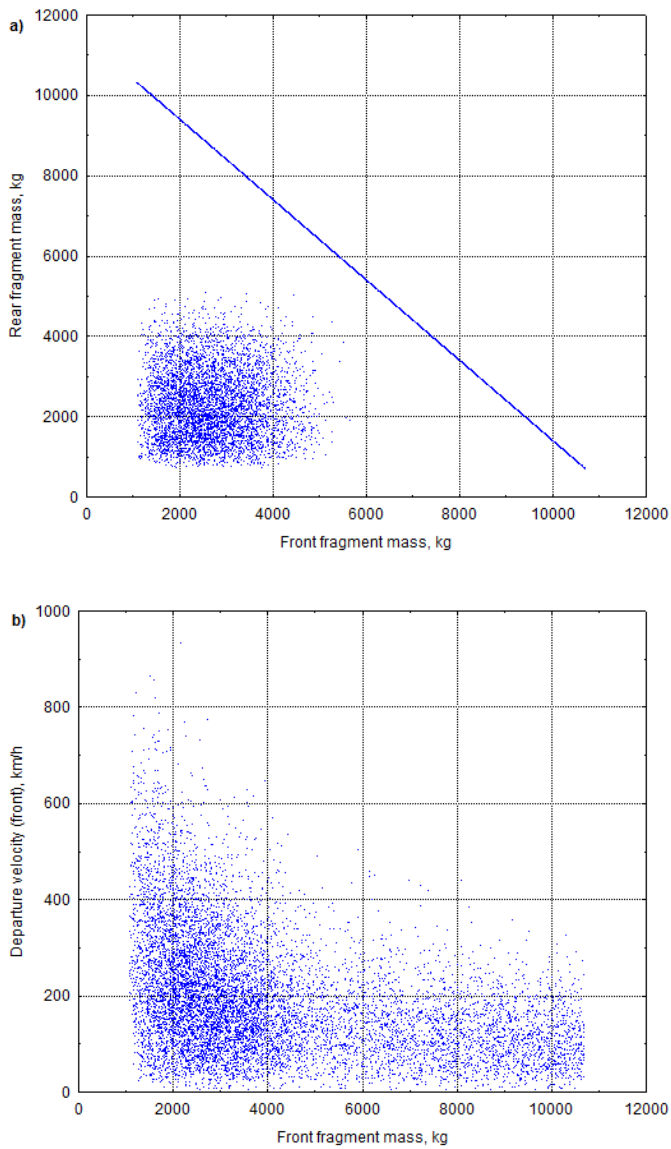
Fig. D3. Scatter diagrams of the pairs ($\xi_{frg,\,front,\,j}$, $\xi_{frg,\,rear,\,j}$) and ($\xi_{frg,\,front,\,j}$, $v_{dep,\,front,\,j}$) ($j = $ 1, 2, … , 10 000)
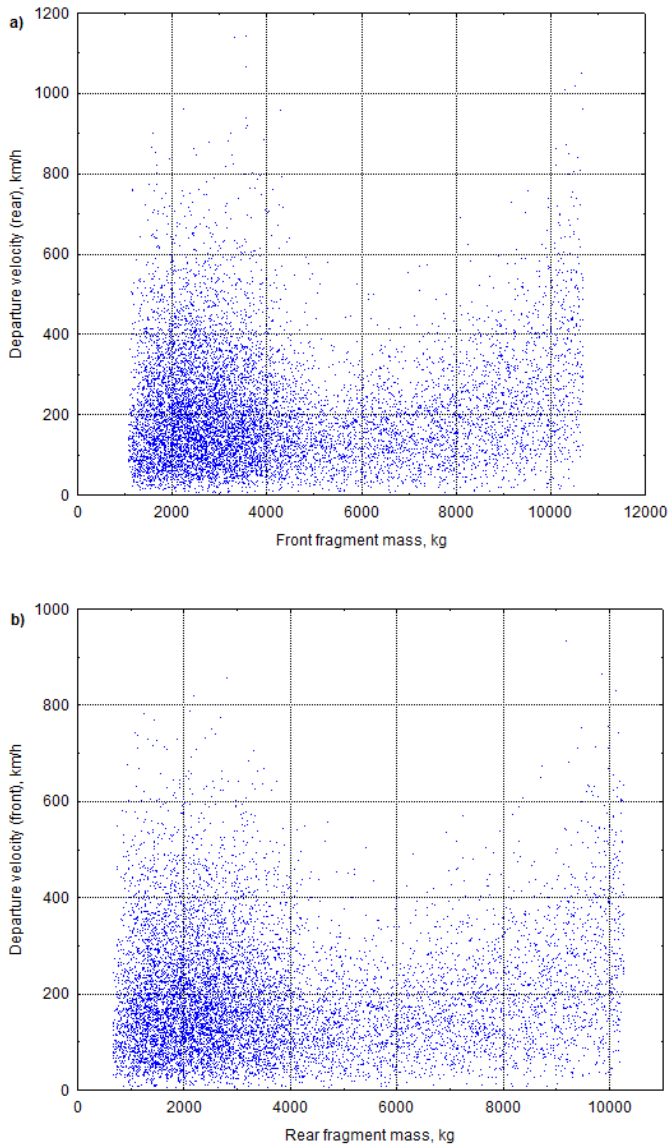
Fig. D4. Scatter diagrams of the pairs ($\xi_{frg,\,front,\,j}$, $v_{dep,\,rear,\,j}$) and ($\xi_{frg,\,rear,\,j}$, $v_{dep,\,front,\,j}$) ($j =$ 1, 2, … , 10 000)
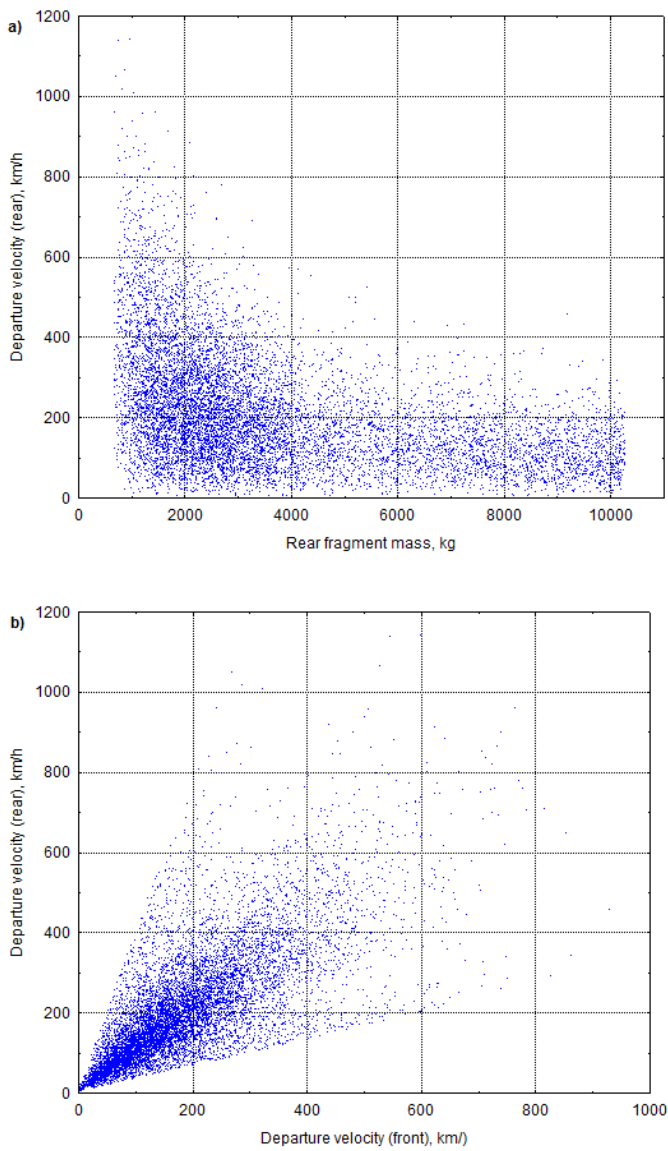
Fig. D5. Scatter diagrams of the pairs $(\xi_{frg, rear, j},\, v_{dep, rear, j})$ and $(v_{dep, front, j},\, v_{dep, rear, j})$ $(j = 1, 2, \ldots , 10\,000)$

The simulated impact characterisitcs were obtained by means of three simulation runs with different simulation numbers:

1. 1×10^6 of simulations were were used to calculate frequencies of fragment impacts on four individual barrier segments $B_1 - B_2$, $B_2 - B_3$, $B_3 - B_4$ and $B_4 - B_5$ (Fig. 2.29); these frequencies are presented in Table 2.12.

2. 100 000 simulations were used to compute descriptive measures of samples consisting of the simulated impact characteristics $\xi_{frg,j}$, $v_{arv,j}$, φ_j and $h_{arv,j}$; the samples were obtained for each of the barrier segments $B_1 - B_2$, $B_2 - B_3$, $B_3 - B_4$ and $B_4 - B_5$; in total 16 samples of individual impact characteristics were analysed; frequencies of fragment impacts into the segments at 100 000 simulations are presented in Table D3.

3. 10 000 simulations were applied to visualise 16 samples consisting of the characteristics $\xi_{frg,j}$, $v_{arv,j}$, φ_j and $h_{arv,j}$ and related to the aforementioned barrier segments.

Table D3. Absolute and relative frequencies of fragment impacts on the segment of the barrier (results were obtained with 1×10^5 simulations of vessel fragmentation and flights of fragments)

Freaquency	B1–B2	B2–B3	B3–B4	B4–B5	The whole barrier
Absolute	5014	5423	16 796	20 899	48 132
Relative	0.05014	0.05423	0,16796	0.20899	0.48132

The present section contains results of processing the simulated impact characterisitcs of the tanker vessel fragments which crossed the vertical plane running along the barrier segment B_1–B_2. The numerical results consists of the descriptive measures of the samples formed from the values $\xi_{frg,j}$, $v_{arv,j}$, φ_j and $h_{arv,j}$ (Table D4). In addition, coefficients of correlation between these four samples were computed (Table D5).

The properties of samples consisting of the values $\xi_{frg,j}$, $v_{arv,j}$, φ_j and $h_{arv,j}$ were visualised using three types of graphs: the scatterplot of the points, where fragments crossed the vertical plane of the barrier segment B_1–B_2 (Fig. D6); the histograms of the four individual samples of $\xi_{frg,j}$, $v_{arv,j}$, φ_j and $h_{arv,j}$ (Fig. D7 and D8); and the scatterplots of pairs of $\xi_{frg,j}$, $v_{arv,j}$, φ_j and $h_{arv,j}$ (Fig. D9, Fig. D10 and D11).

Table D.4. Characteristics of impact on the barrier segment B_1–B_2

Component of the simulated sample	Mean	Min	Max	Std.dev.
Ricochet angle φ_j (degs)	49.3	0.741	90.0	18.5
Angle of obliquity θ_j (degs)	40.7	0.004	89.3	18.5
Horizontal flight distance $d_{hor,j}$ (m)	23.4	0.026	95.0	17.3
Impact altitude $h_{imp,j}$ (m)	13.1	0.002	66.1	11.3
Fragment mass $\xi_{frg,j}$ (kg)	3930.9	698.0	10714.2	2584.8
Impact velocity $v_{arv,j}$ (km/h)	208.1	0.835	973.0	139.0

Table D5. Correlation matrix of the simulated samples of fragment impact charakteristics related to barrier segment B_1–B_2 (see Fig. 2.29)*

	φ	h_{imp}	ξ_{frg}	v_{arv}
φ	1.00	0.01	0.01	-0.01
h_{imp}	0.01	1.00	0.02	0.00
ξ_{frg}	0.01	0.02	1.00	**-0.43**
v_{arv}	-0.01	0.00	**-0.43**	1.00

* The bold numbers indicate statisticaly significant correlation coeficients
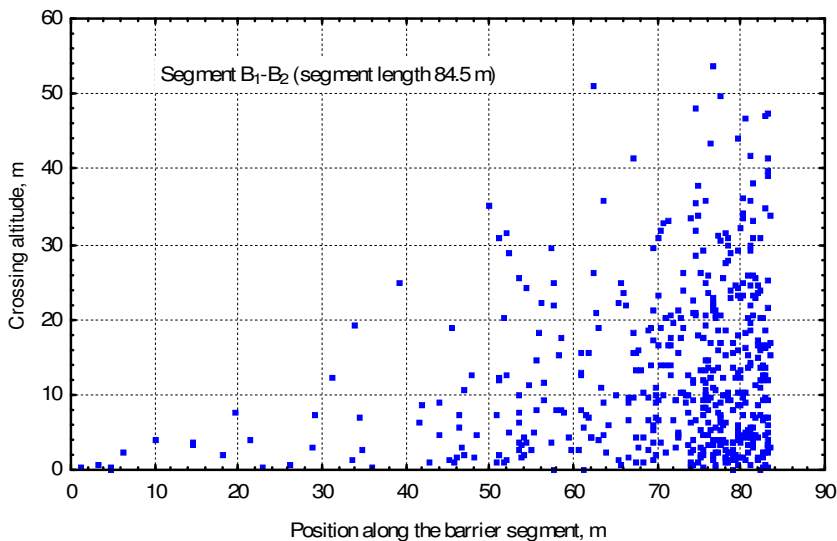
Fig. D6. Scatter diagrams of the points where fragments crossed the vertical plane of the barrier segments B_1–B_2 (10 000 simulated values)
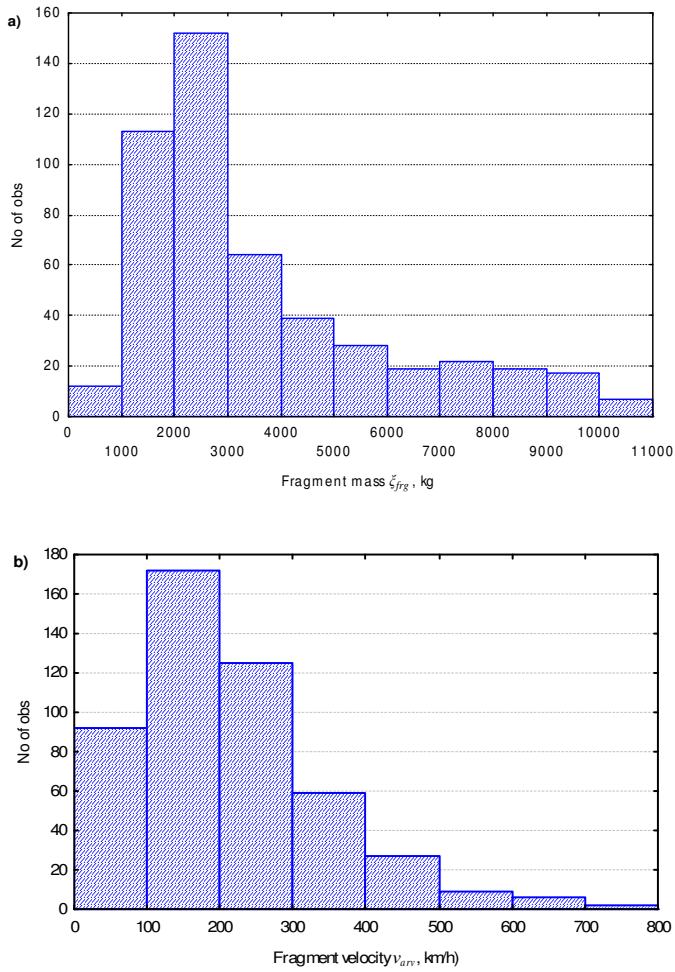
Fig. D7. Histograms of the simulated values of $\xi_{frg,j}$, $v_{arv,j}$, related to the barrier segments B_1–B_2 ($j = 1, 2, \dots, 10\,000$)
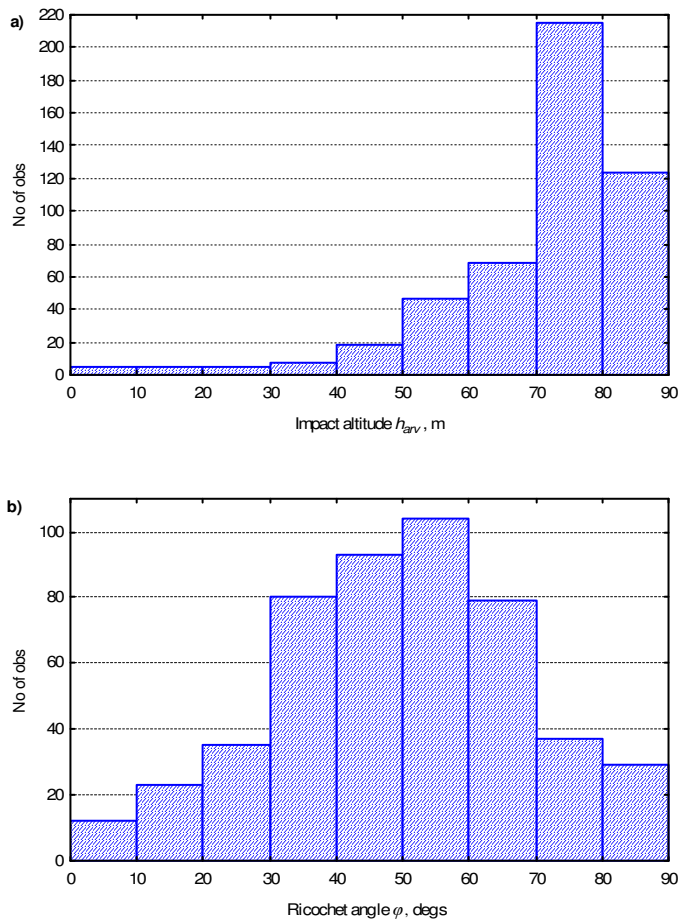
Fig. D8. Histograms of the simulated values of φ_j and $h_{arv,j}$ related to the barrier segments B_1–B_2 ($j = 1, 2, \ldots , 10\,000$)
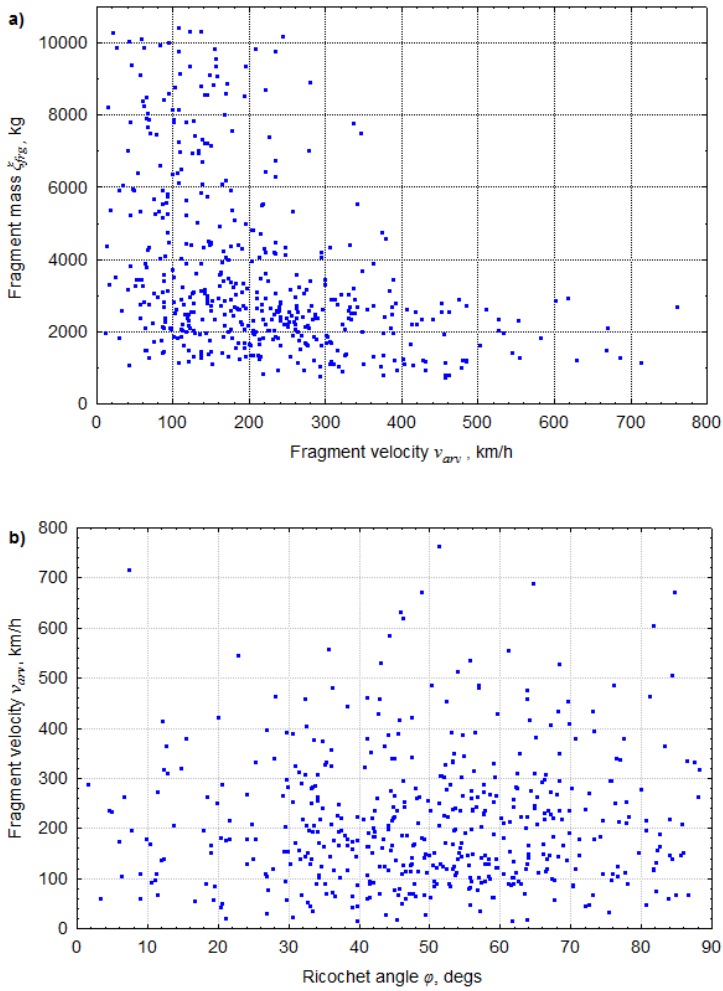
Fig. D9 The scatterplots of pairs of $\xi_{frg,j}$, $v_{arv,j}$, φ_j and $h_{arv,j}$ related to the barrier segments B_1–B_2 ($j = 1, 2, \ldots, 10\,000$)
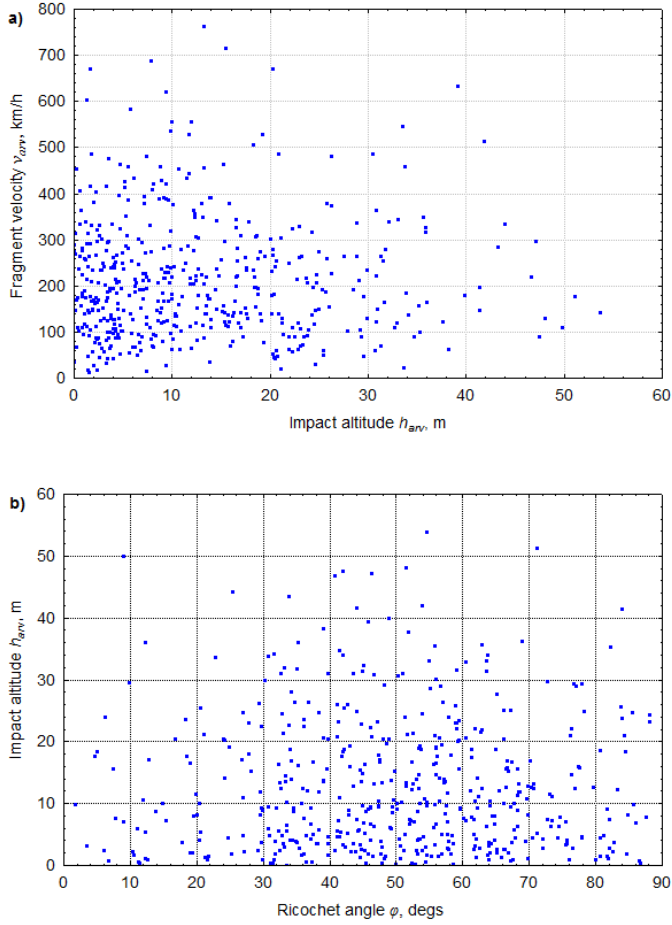
Fig. D10. The scatterplots of pairs of $v_{arv,j}$, φ_j and $h_{arv,j}$ related to the barrier segments B_1-B_2 ($j = 1, 2, \ldots, 10\,000$)
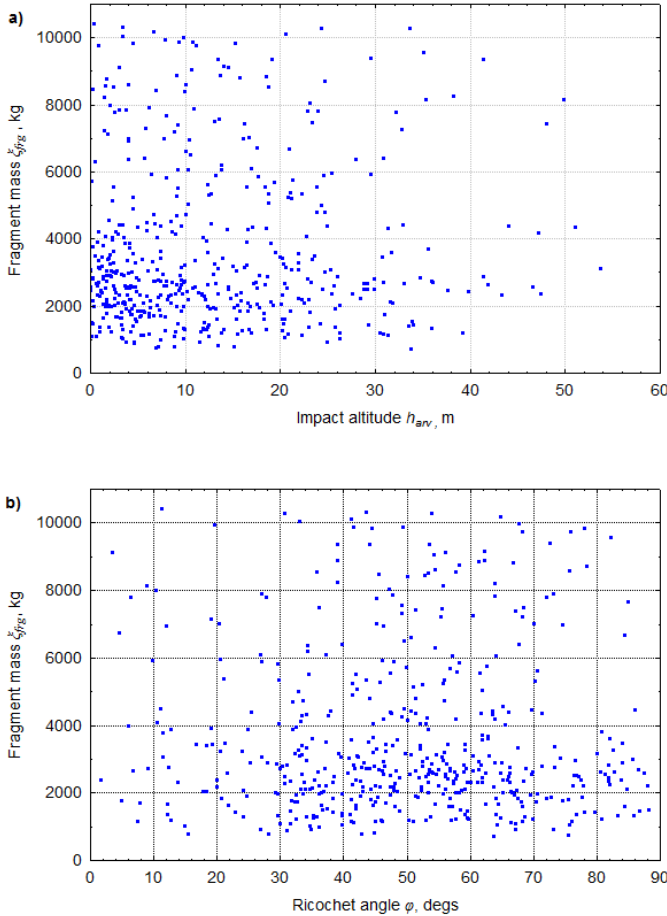
Fig. D11. The scatterplots of pairs of $\xi_{frg,j}$, φ_j and $h_{arv,j}$ related to the barrier segments B_1-B_2 ($j = 1, 2, \ldots , 10\,000$)

The present section contains results of processing the simulated impact characterisitcs of the tanker vessel fragments which crossed the vertical plane running along the barrier segment B_2-B_3. The numerical results consists of the descriptive measures of the samples formed from the values $\xi_{frg,j}$, $v_{arv,j}$, φ_j and $h_{arv,j}$ (Table D6). In addition, coefficients of correlation between these four samples were computed (Table D7).

The properties of samples consisting of the values $\xi_{frg,j}$, $v_{arv,j}$, φ_j and $h_{arv,j}$ were visualised using three types of graphs: the scatterplot of the points, where fragments crossed the vertical plane of the barrier segment B_2-B_3 (Fig. D12); the histograms of the four individual samples of $\xi_{frg,j}$, $v_{arv,j}$, φ_j and $h_{arv,j}$ (Fig. D13 and

D14); and the scatterplots of pairs of $\xi_{frg,j}$, $v_{arv,j}$, φ_j and $h_{arv,j}$ (Fig. D15, Fig. D16 and 17).

Table D6. Characteristics of impact on the barrier segment B_2–B_3 (see Fig. 2.29)

Component of the simulated sample	Mean	Min	Max	Std.dev.
Ricochet angle φ_j (degs)	24.1	0.20	89.9	15.96
Angle of obliquity θ_j (degs)	65.9	0.09	89.8	15.96
Horizontal flight distance $d_{hor,\,j}$ (m)	16.3	1.82	98.6	10.38
Impact altitude $h_{imp,\,j}$ (m)	2.2	0.00	17.6	2.53
Fragment mass $\xi_{frg,\,j}$ (kg)	4072.9	689.29	10705.7	2585.94
Impact velocity $v_{arv,\,j}$ (km/h)	201.7	1.75	1362.9	134.73

Table D7. Correlation matrix of the simulated samples of fragment impact charakteristics related to barrier segment B_2–B_3 (see Fig. 2.29)*

	φ	h_{imp}	ξ_{frg}	v_{arv}
φ	1.00	**0.06**	-0.02	0.00
h_{imp}	**0.06**	1.00	-0.02	0.01
ξ_{frg}	-0.02	-0.02	1.00	**-0.42**
v_{arv}	0.00	0.01	**-0.42**	1.00
* The bold numbers indicate statisticaly significant correlation coeficients				
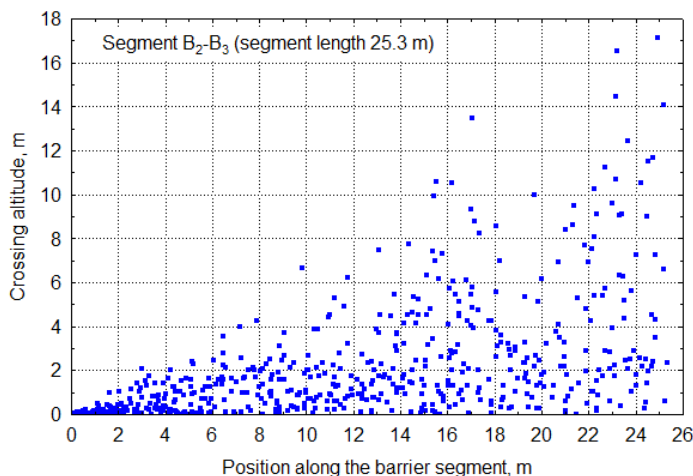
Fig. D12. Scatter diagrams of the points where fragments crossed the vertical plane of the barrier segments B_2–B_3 (10 000 simulated values)
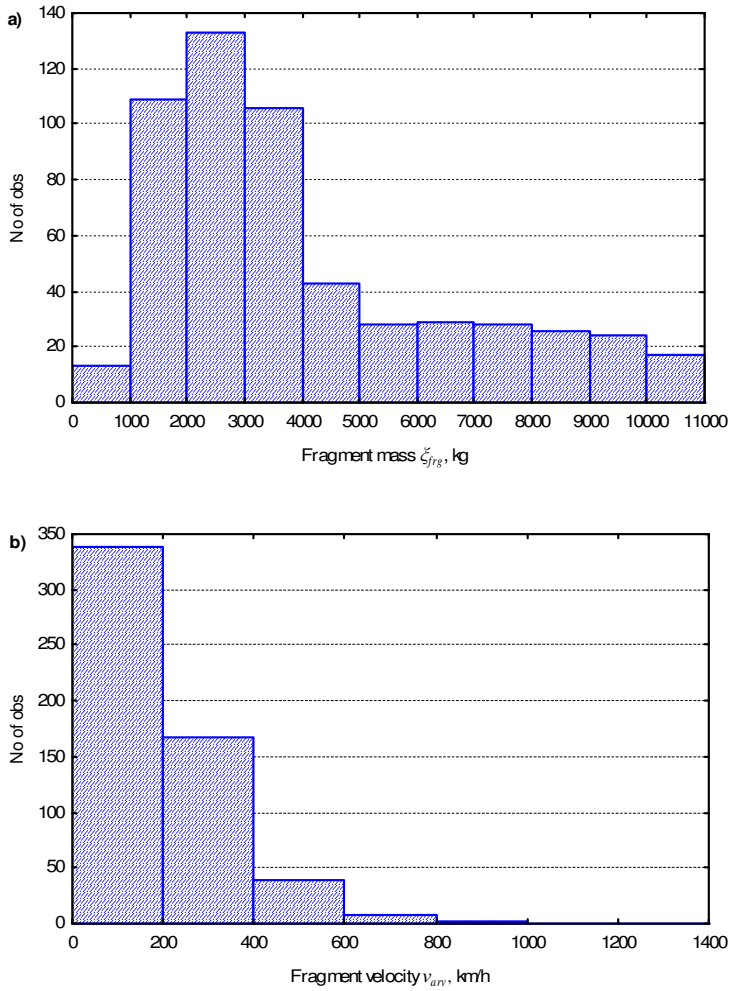
Fig. D13. Histograms of the simulated values of $\xi_{frg,j}$, $v_{arv,j}$, related to the barrier segments B_2–B_3 ($j = 1, 2, \ldots , 10\,000$)
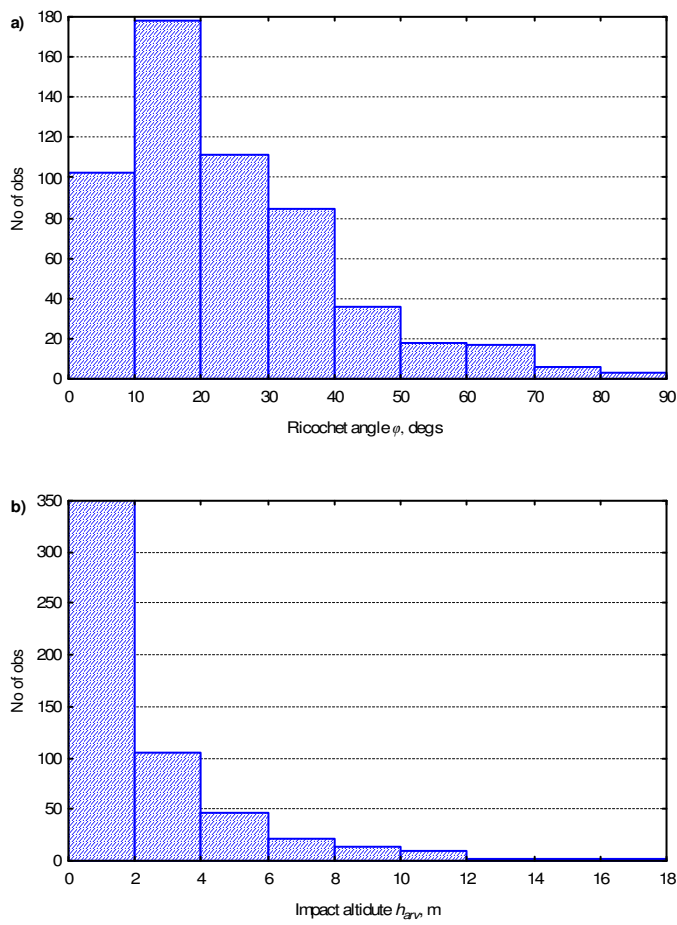
Fig. D14. Histograms of the simulated values of φ_j and $h_{arv,j}$ related to the barrier segments B_2–B_3 ($j = 1, 2, \ldots , 10\ 000$)
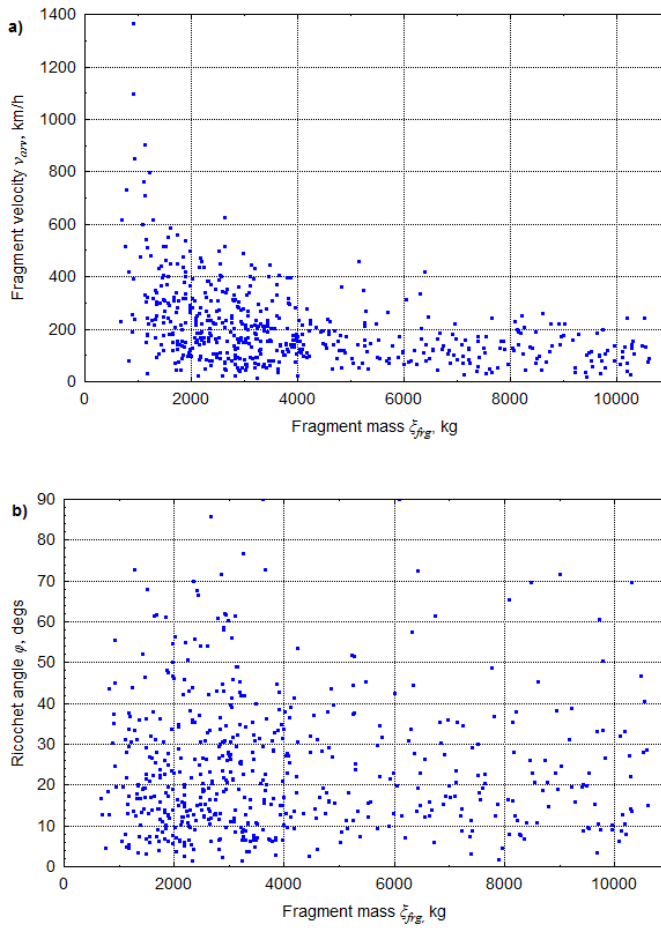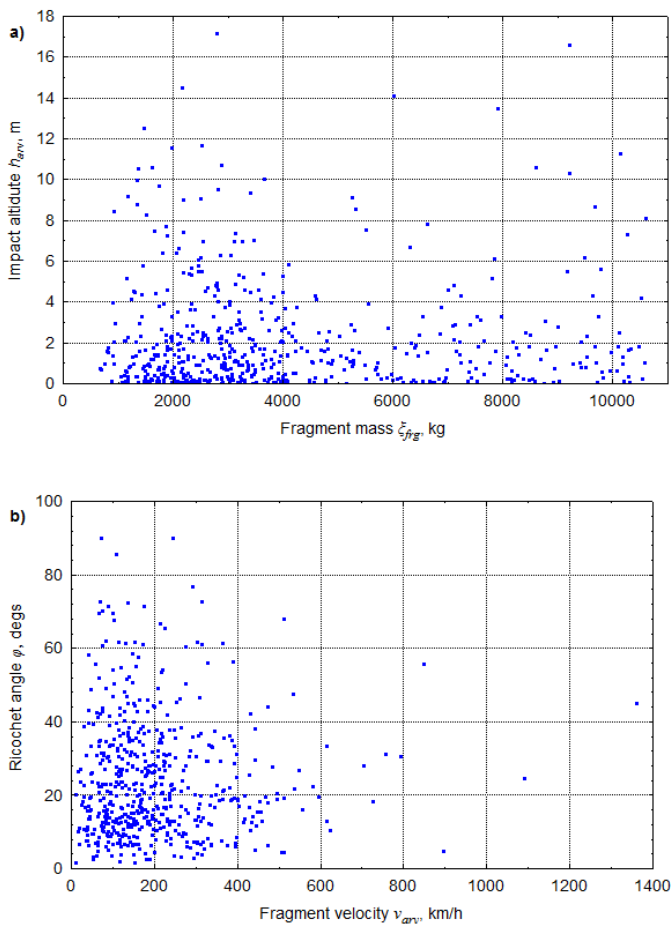
Fig. D15 The scatterplots of pairs of $\xi_{frg,j}$, $v_{arv,j}$, φ_j related to the barrier segments B$_2$–B$_3$
($j = 1, 2, \ldots , 10\,000$)

Fig. D16 The scatterplots of pairs of $\xi_{frg,j}$, $v_{arv,j}$, φ_j and $h_{arv,j}$ related to the barrier segments B_2–B_3 ($j = 1, 2, \ldots, 10\,000$)
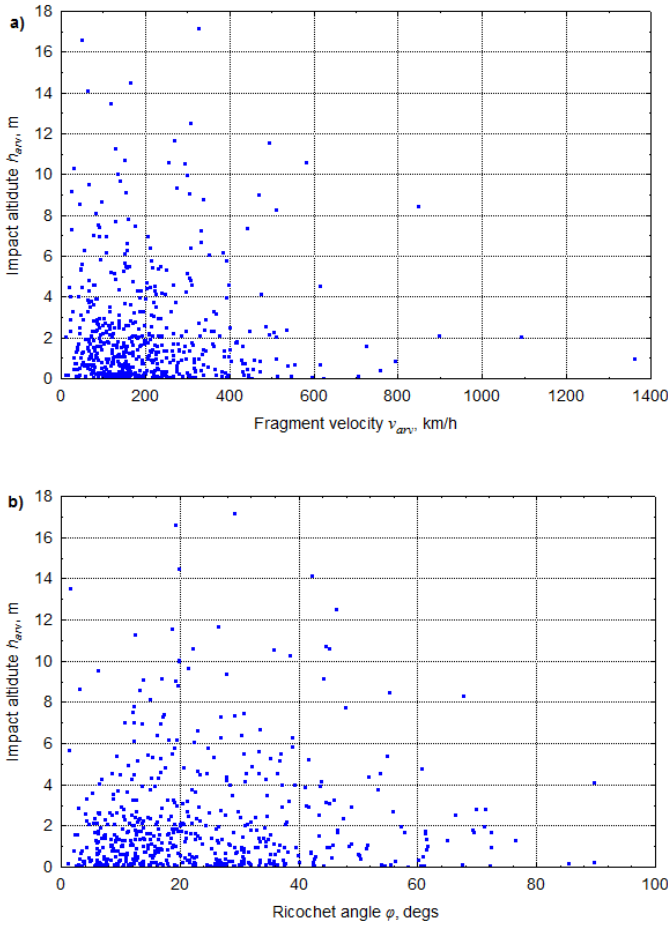
Fig. D17 The scatterplots of pairs of $v_{arv,j}$, φ_j and $h_{arv,j}$ related to the barrier segments
B_2–B_3 ($j = 1, 2, \ldots , 10\,000$)

The present section contains results of processing the simulated impact characterisitcs of the tanker vessel fragments which crossed the vertical plane running along the barrier segment B_3–B_4. The numerical results consists of the descriptive measures of the samples formed from the values $\xi_{frg,j}$, $v_{arv,j}$, φ_j and $h_{arv,j}$ (Table D8). In addition, coefficients of correlation between these four samples were computed (Table D9).

The properties of samples consisting of the values $\xi_{frg,j}$, $v_{arv,j}$, φ_j and $h_{arv,j}$ were visualised using three types of graphs: the scatterplot of the points, where fragments crossed the vertical plane of the barrier segment B_3–B_4 (Fig. D18); the histograms of the four individual samples of $\xi_{frg,j}$, $v_{arv,j}$, φ_j and $h_{arv,j}$ (Fig. D19 and

D20); and the scatterplots of pairs of $\xi_{frg,j}$, $v_{arv,j}$, φ_j and $h_{arv,j}$ (Fig. D21, Fig. D22 and D23).

Table D8. Characteristics of impact on the barrier segment B_3–B_4 (see Fig. 2.29)

Component of the simulated sample	Mean	Min	Max	Std.dev.
Ricochet angle φ_j (degs)	30.4	1.24	135.6	14.83
Angle of obliquity θ_j (degs)	59.6	-45.64	88.8	14.83
Horizontal flight distance $d_{hor,j}$ (m)	46.7	2.92	177.1	49.45
Impact altitude $h_{imp,j}$ (m)	3.17	0.00	27.0	3.70
Fragment mass $\xi_{frg,j}$ (kg)	4136.5	683.81	10716.3	2591.7
Impact velocity $v_{arv,j}$ (km/h)	200.3	1.61	1071.1	132.24

Table D9. Correlation matrix of the simulated samples of fragment impact charakteristics related to barrier segment B_3–B_4 (see Fig. 2.29)*

	φ	h_{imp}	ξ_{frg}	v_{arv}
φ	1.00	**0.08**	-0.01	-0.00
h_{imp}	**0.08**	1.00	-0.01	0.00
ξ_{frg}	-0.01	-0.01	1.00	**-0.41**
v_{arv}	-0.00	0.00	**-0.41**	1.00
* The bold numbers indicate statisticaly significant correlation coeficients				
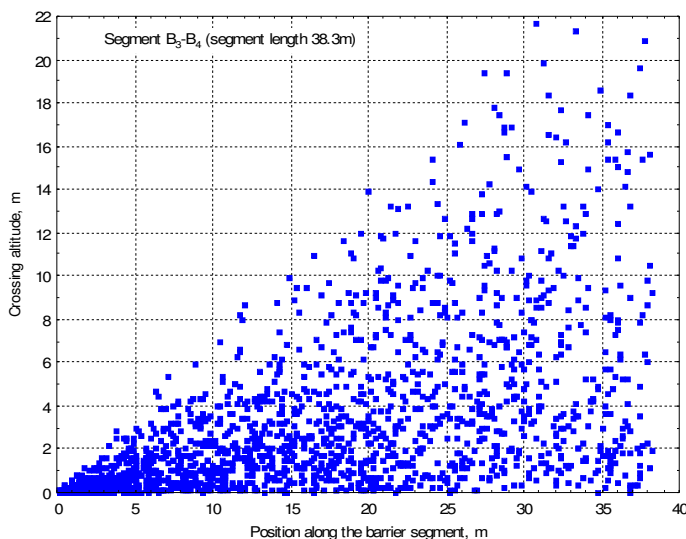
Fig. D18. Scatter diagrams of the points where fragments crossed the vertical plane of the barrier segments B_3–B_4 (10 000 simulated values)
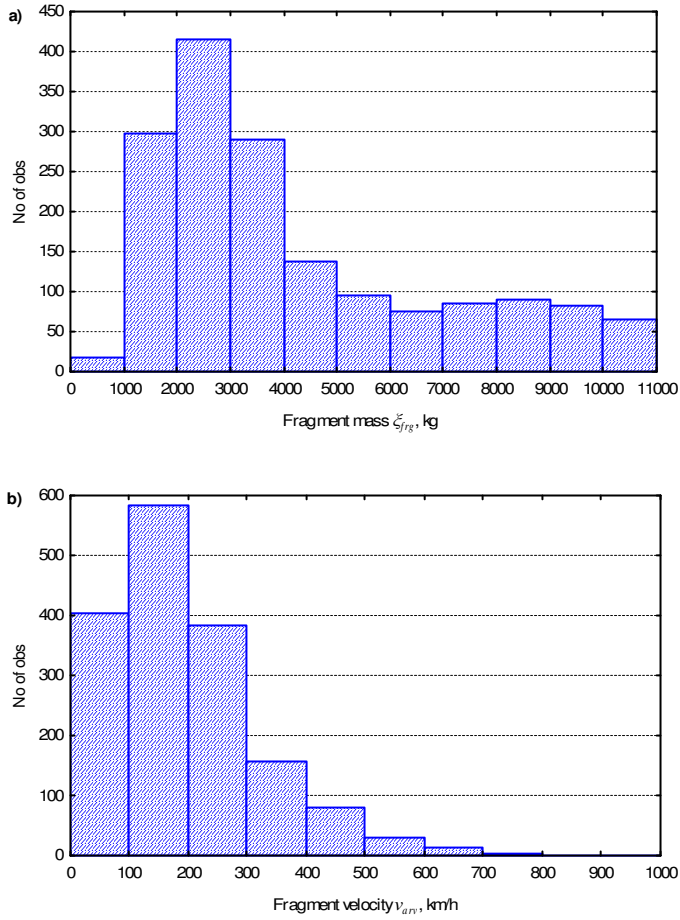
Fig. D19. Histograms of the simulated values of $\xi_{frg,j}$, $v_{arv,j}$, related to the barrier segments B_3–B_4 ($j = 1, 2, \ldots , 10\,000$)
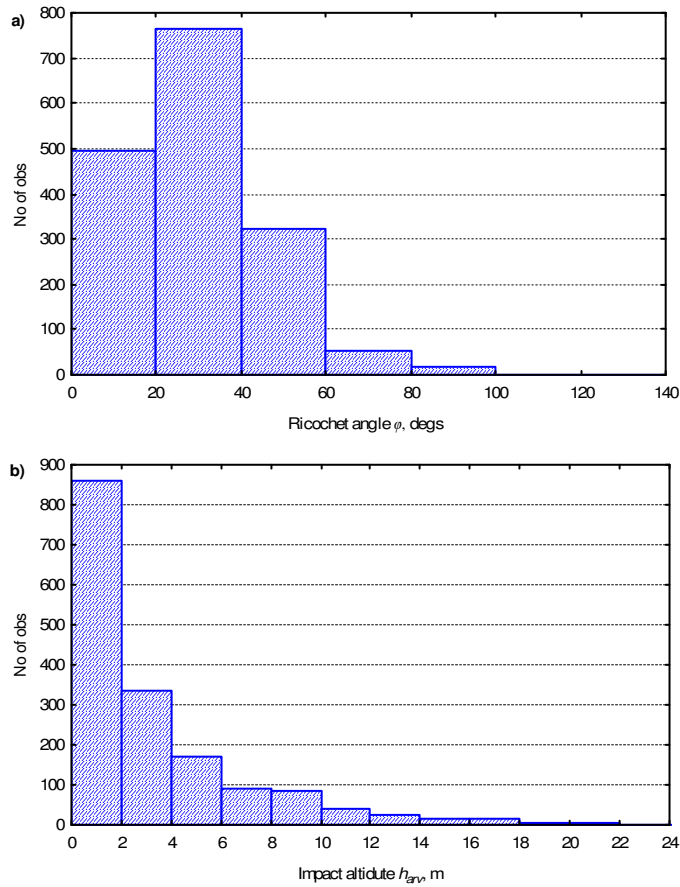
Fig. D20. Histograms of the simulated values of φ_j and $h_{arv,j}$ related to the barrier segments B$_3$–B$_4$ ($j = 1, 2, \dots , 10\,000$)
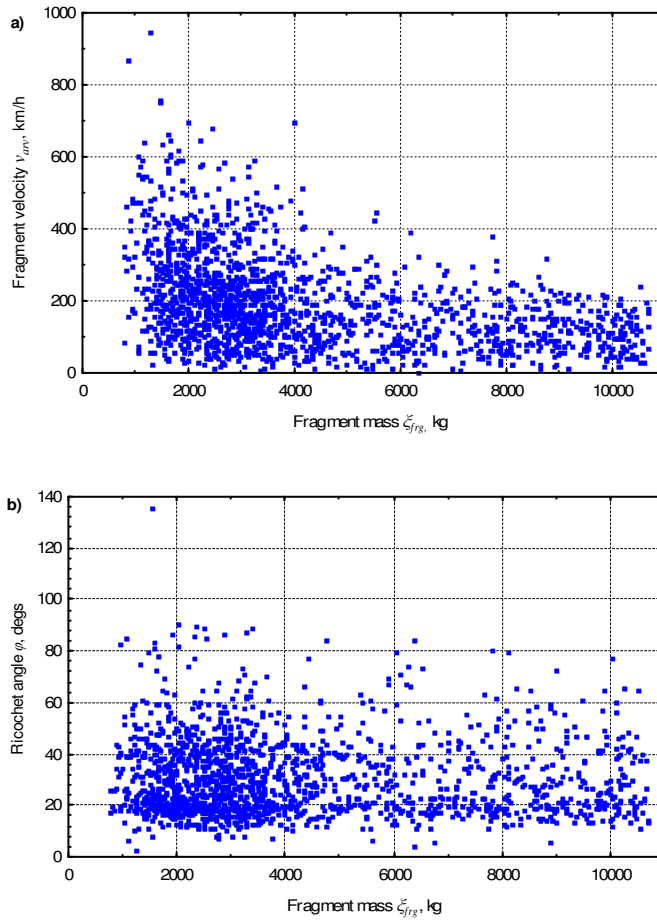
Fig. D21. The scatterplots of pairs of $\xi_{frg,j}$, $v_{arv,j}$, φ_j and related to the barrier segments B_3–B_4 ($j = 1, 2, \dots, 10\,000$)
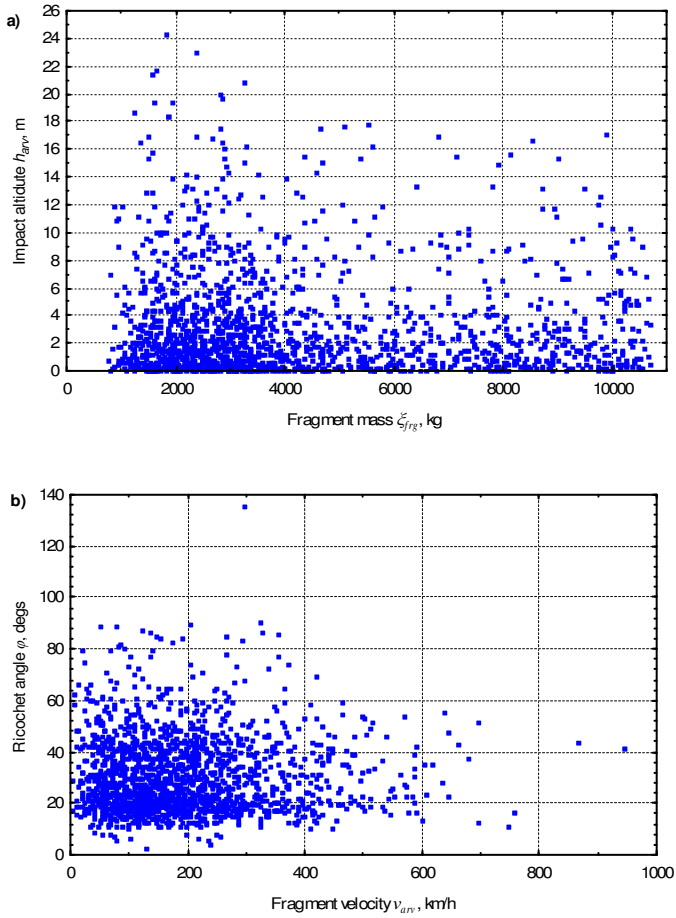
Fig. D22. The scatterplots of pairs of $\xi_{frg,j}$, $v_{arv,j}$, φ_j and $h_{arv,j}$ related to the barrier segments B_3–B_4 $(j = 1, 2, \ldots , 10\,000)$
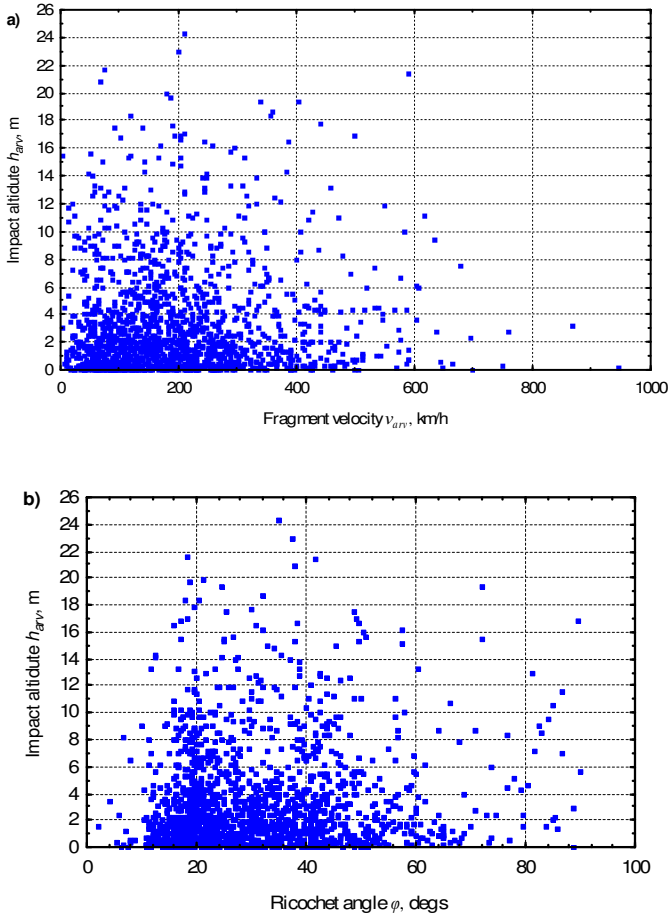
Fig. D23. The scatterplots of pairs of $v_{arv,j}$, φ_j and $h_{arv,j}$ related to the barrier segments
B$_3$–B$_4$ ($j = 1, 2, \ldots , 10\,000$)

The present section contains results of processing the simulated impact characterisitcs of the tanker vessel fragments which crossed the vertical plane running along the barrier segment B$_4$–B$_5$. The numerical results consists of the descriptive measures of the samples formed from the values $\xi_{frg,j}$, $v_{arv,j}$, φ_j and $h_{arv,j}$ (Table D10). In addition, coefficients of correlation between these four samples were computed (Table D11).

The properties of samples consisting of the values $\xi_{frg,j}$, $v_{arv,j}$, φ_j and $h_{arv,j}$ were visualised using three types of graphs: the scatterplot of the points, where fragments crossed the vertical plane of the barrier segment B$_4$–B$_5$ (Fig. D24); the histograms of the four individual samples of $\xi_{frg,j}$, $v_{arv,j}$, φ_j and $h_{arv,j}$ (Fig. D25 and

26); and the scatterplots of pairs of $\xi_{frg,j}$, $v_{arv,j}$, φ_j and $h_{arv,j}$ (Fig. D27, Fig. D28 and D29).

Table D10. Characteristics of impact on the barrier segment B_4–B_5 (see Fig. 2.29)

Component of the simulated sample	Mean	Min	Max	Std.dev.
Ricochet angle φ_j (degs)	38.0	0.446	90.0	17.46
Angle of obliquity θ_j (degs)	52.0	0.0280	89.6	17.46
Horizontal flight distance $d_{hor,j}$ (m)	75.0	6.76	184.7	29.6
Impact altitude $h_{imp,j}$ (m)	9.00	0.0	104.2	10.99
Fragment mass $\xi_{frg,j}$ (kg)	4116.9	681.6	10714.9	2596
Impact velocity $v_{arv,j}$ (km/h)	198.9	1.044	1261.5	130.3

Table D11. Correlation matrix of the simulated samples of fragment impact charakteristics related to barrier segment B_4–B_5 (see Fig. 2.29)*

	φ	h_{imp}	ξ_{frg}	v_{arv}
φ	1.00	**0.17**	**0.02**	-0.01
h_{imp}	**0.17**	1.00	-0.01	-0.01
ξ_{frg}	**0.02**	-0.01	1.00	**-0.41**
v_{arv}	-0.01	-0.01	**-0.41**	1.00

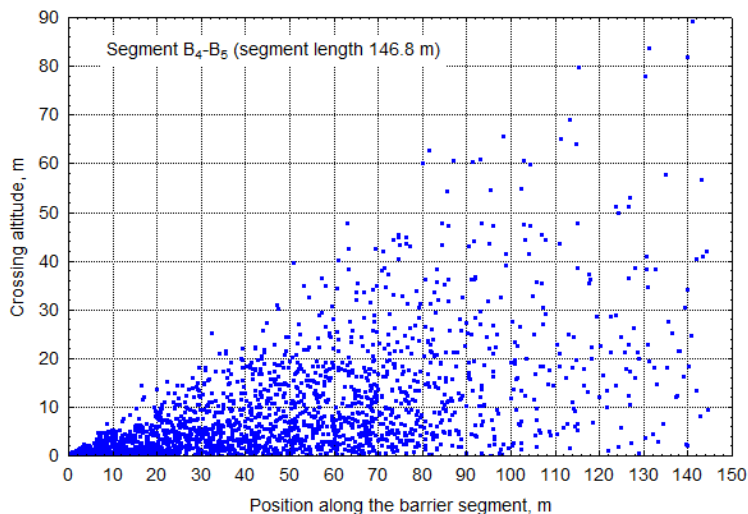* The bold numbers indicate statisticaly significant correlation coeficients

Fig. D24. Scatter diagrams of the points where fragments crossed the vertical plane of the barrier segments B_4–B_5 (10 000 simulated values)
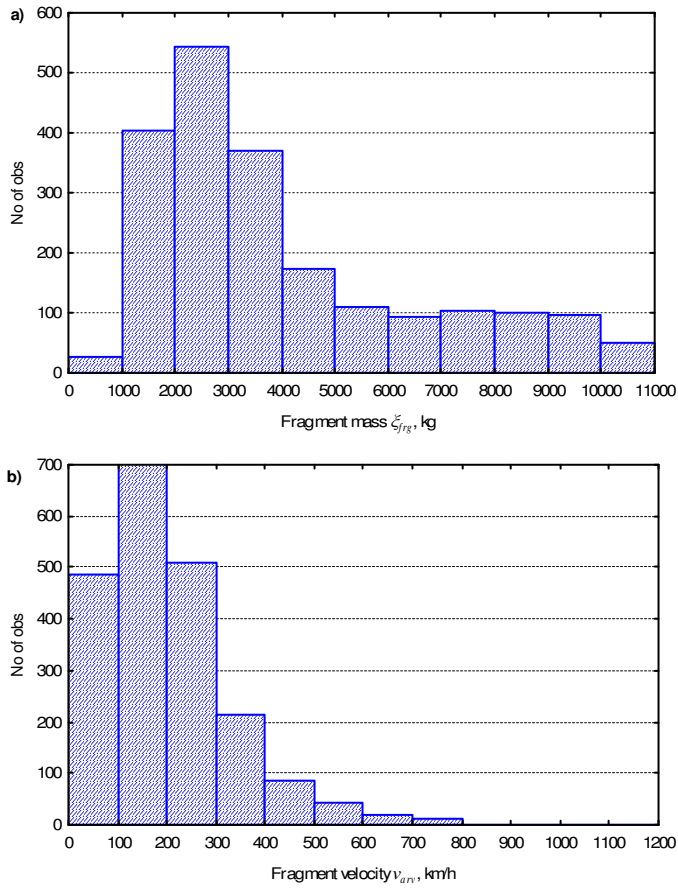
Fig. D25. Histograms of the simulated values of $\xi_{frg,j}$, $v_{arv,j}$, related to the barrier segments B$_4$–B$_5$ (j = 1, 2, … , 10 000)
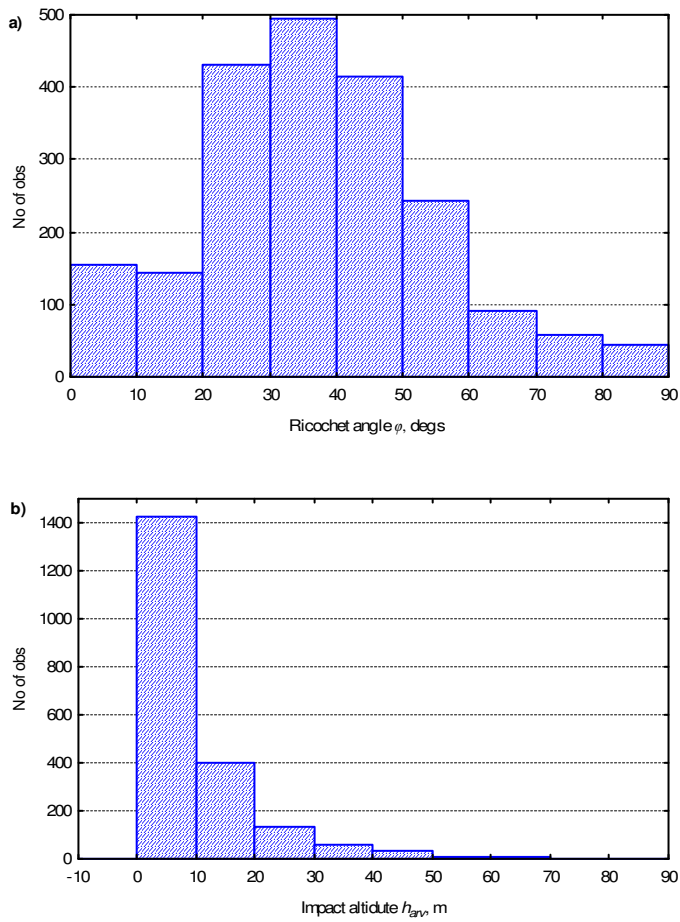
Fig. D26. Histograms of the simulated values of φ_j and $h_{arv,j}$ related to the barrier segments B_4–B_5 ($j = 1, 2, \ldots , 10\,000$)
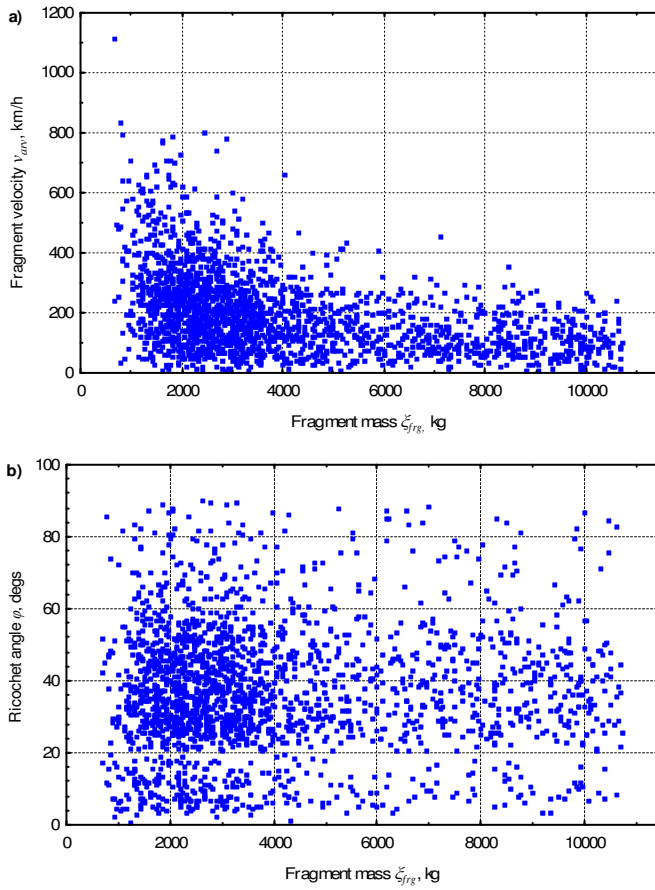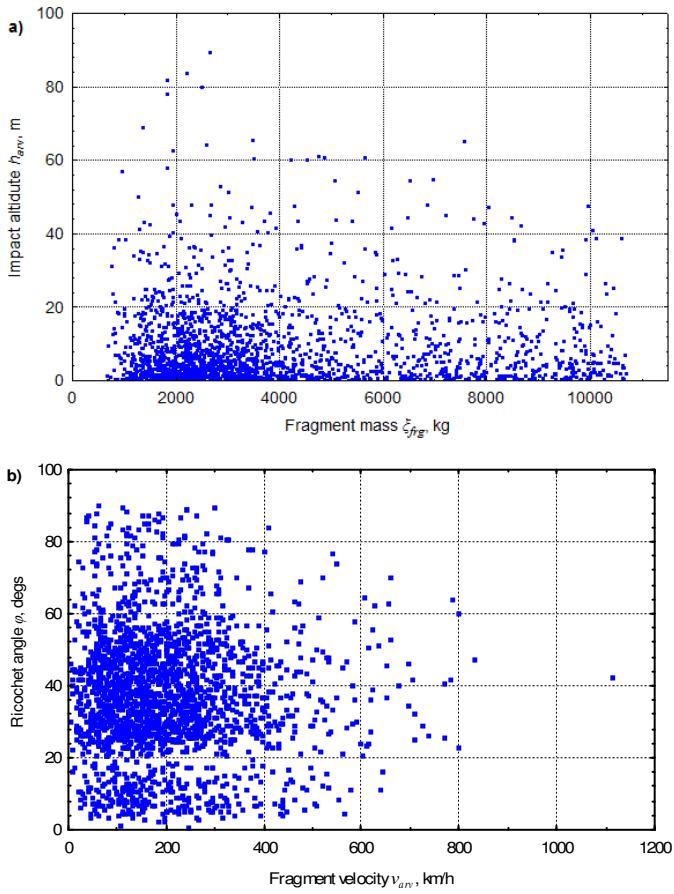
Fig. D27. The scatterplots of pairs of $\xi_{frg,j}$, $v_{arv,j}$, φ_j related to the barrier segments B_4–B_5 ($j = 1, 2, \dots , 10\,000$)
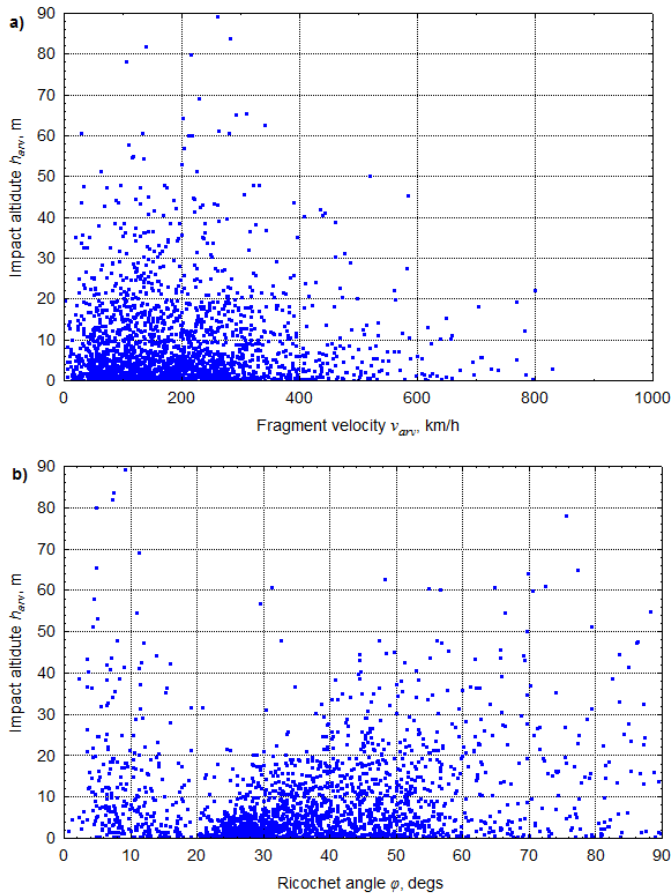
Fig. D28. The scatterplots of pairs of $\xi_{frg,j}$, $v_{arv,j}$, φ_j and $h_{arv,j}$ related to the barrier segments B_4–B_5 ($j = 1, 2, \ldots, 10\,000$)

Fig. D29. The scatterplots of pairs of $v_{arv,j}$, φ_j and $h_{arv,j}$ related to the barrier segments B_4–B_5 ($j = 1, 2, \ldots , 10\,000$)

Lina KISEŽAUSKIENĖ

EPLORING THE POSSIBILITY TO ASSESS AND REDUCE THE RISK
DUE TO HAZARDOUS MATERIALS TRANSPORTATION
BY DEPLOYING ROADSIDE SAFETY BARRIERS

Doctoral Dissertation
Technological Sciences,
Civil Engineering (02T)

TRANSPORTUOJAMŲ PAVOJINGŲJŲ MEDŽIAGŲ KELIAMOS
RIZIKOS TYRIMAS TYRIMAS IR MAŽINIMAS
ĮRENGIANT SAUGOS BARJERUS

Daktaro disertacija
Technologijos mokslai,
statybos inžinerija (02T)